

Self-Organized Dynamics of Power Grids: Smart Grids, Fluctuations and Cascades

Dissertation
(Cumulative Thesis)

for the award of the degree
“Doctor rerum naturalium”
of the Georg-August-Universität Göttingen
within the doctoral program Physics of Biological and Complex Systems (PBCS) of
the Georg-August University School of Science (GAUSS)

submitted by

Benjamin Schäfer
from Schönebeck (Elbe)

Göttingen 2017

Thesis Committee

Prof. Dr. Marc Timme

Institute for Nonlinear Dynamics, Georg-August University of Göttingen, Göttingen, Germany
Network Dynamics, Max Planck Institute for Dynamics and Self-Organization, Göttingen, Germany
Chair for Network Dynamics, Center for Advancing Electronics Dresden (cfaed) and Institute for Theoretical Physics, Technical University of Dresden, Dresden, Germany

Prof. Dr. Annette Zippelius

Institute of Theoretical Physics, Georg-August University of Göttingen, Göttingen, Germany

Jun.-Prof. Dr. Dirk Witthaut

Forschungszentrum Jülich, Institute for Energy and Climate Research - Systems Analysis and Technology Evaluation (IEK-STE), Jülich, Germany
Institute for Theoretical Physics, University of Cologne, Köln, Germany

Members of the Examination Board

First reviewer:

Prof. Dr. Marc Timme

Institute for Nonlinear Dynamics, Georg-August University of Göttingen, Göttingen, Germany
Network Dynamics, Max Planck Institute for Dynamics and Self-Organization, Göttingen, Germany
Chair for Network Dynamics, Center for Advancing Electronics Dresden (cfaed) and Institute for Theoretical Physics, Technical University of Dresden, Dresden, Germany

Second Reviewer:

Prof. Dr. Annette Zippelius

Institute of Theoretical Physics, Georg-August University of Göttingen, Göttingen, Germany

Further members of the Examination Board

Jun.-Prof. Dr. Dirk Witthaut

Forschungszentrum Jülich, Institute for Energy and Climate Research - Systems Analysis and Technology Evaluation (IEK-STE), Jülich, Germany
Institute for Theoretical Physics, University of Cologne, Köln, Germany

Prof. Dr. Ulrich Parlitz

Max Planck Institute for Dynamics and Self-Organization, Göttingen, Germany
Institute for Nonlinear Dynamics, Georg-August University of Göttingen, Göttingen, Germany

Prof. Dr. Reiner Kree

Institute of Theoretical Physics, Georg-August University of Göttingen, Göttingen, Germany

Prof. Dr. Stefan Klumpp

Institute for Nonlinear Dynamics, Georg-August University of Göttingen, Göttingen, Germany

Date of oral examination:

16th of November, 2017

Declaration

I confirm that I have written this thesis independently and with no other sources and aids than quoted. At the beginning of each chapter in *Part II Results - Original Manuscripts*, I clarify my contributions in detail.

Göttingen, September 2017

(Benjamin Schäfer)

List of publications

[1] D. Manik, D. Witthaut, **B. Schäfer**, M. Matthiae, A. Sorge, M. Rohden, E. Katifori and M. Timme, Supply Networks: Instabilities without Overload, European Physical Journal Special Topics 223: 2527, October 2014

[2]* **B. Schäfer**, M. Matthiae, M. Timme and D. Witthaut, Decentral Smart Grid Control, New Journal of Physics 17 015002, January 2015

(for reprint, see Chapter 3)

[3]* **B. Schäfer**, C. Grabow, S. Auer, J. Kurths, D. Witthaut and M. Timme, Taming Instabilities in Power Grid Networks by Decentralized Control, European Physical Journal Special Topics 225: 569, May 2016

(for reprint, see Chapter 4)

[4]* **B. Schäfer**, M. Matthiae, X. Zhang, M. Rohden, M. Timme and D. Witthaut, Escape Routes, Weak Links, and Desynchronization in Fluctuation-driven Networks. Physical Review E 95, 060203(R), November 2016.

(for reprint, see Chapter 5)

[5]* **B. Schäfer**, C. Beck, K. Aihara, D. Witthaut and M. Timme, Non-Gaussian Power Grid Frequency Fluctuations Characterized by Lévy-stable Laws and Superstatistics, Nature Energy, accepted

(for reprint, see Chapter 6)

[6]* **B. Schäfer**, D. Witthaut, and M. Timme and V. Latora, Dynamically Induced Cascading Failures in Supply Networks, under review, arXiv:1707.08018

(for reprint, see Chapter 7)

* manuscripts included in the main part of this thesis; a signed statement of own contribution is given in the beginning of the corresponding Chapters 3 - 7

Abstract

Climate change is one of the most pressing issues of our time and mitigating it requires a reduction of CO_2 emissions. A big step towards achieving this goal is increasing the share of renewable energy sources, as the energy sector currently contributes 35% to all greenhouse gas emissions. However, integrating these renewable energy sources challenges the current power system in two major ways. Firstly, renewable generation consists of more spatially distributed and smaller power plants than conventional generation by nuclear or coal plants, questioning the established hierarchical structures and demanding a new grid design. Restructuring becomes necessary because wind and solar plants have to be placed at favorable sites, e.g., close to coasts in the case of wind. Secondly, renewables do not provide a deterministic and controllable power output but introduce power fluctuations that have to be controlled adequately. Many solutions to these challenges are build on the concept of *smart grids*, which require an extensive information technology (IT) infrastructure communicating between consumers and generators to coordinate efficient actions. However, an intertwined power and IT system raises great privacy and security concerns.

Is it possible to forgo a large IT infrastructure in future power grids and instead operate them purely based on local information? How would such a decentrally organized system work? What is the impact of fluctuation on short time scales on the dynamical stability? Which grid topologies are robust against random failures or targeted attacks? This thesis aims to establish a framework of such a self-organized dynamics of a power grid, analyzing its benefits and limitations with respect to fluctuations and discrete events.

Instead of a centrally monitored and controlled smart grid, we propose the concept of *Decentral Smart Grid Control*, translating local power grid frequency information into actions to stabilize the grid. This is not limited to power generators but applies equally to consumers, naturally introducing a demand response. We analyze the dynamical stability properties of this framework using linear stability methods as well as applying numerical simulations to determine the size of the basin of attraction. To do so, we investigate general stability effects and sample network motifs to find that this self-organized grid dynamics is stable for large parameter regimes. However, when the actors of the power grid react to a frequency signal, this reaction has to be sufficiently fast since reaction delays are shown to destabilize the grid. We derive expressions for a maximum delay, which always desynchronizes the system based on a rebound effect, and for destabilizing delays based on resonance effects. These resonance instabilities are cured when the frequency signal is averaged over a few seconds (low-pass filter). Overall, we propose an alternative smart grid model without any IT infrastructure and analyze its stable operating space.

Furthermore, we analyze the impact of fluctuations on the power grid. First, we determine the escape time of the grid, i.e., the time until the grid desynchronizes when subject to stochastic perturbations. We simulate these events and derive an analytical expression using Kramer's method, obtaining the scaling of the escape time as a function of the grid inertia, transmitted power, damping etc. Thereby, we identify weak links in networks, which have to be enhanced to guarantee a stable operation. Second, we collect power grid frequency measurements from different regions across the world and evaluate their statistical properties. Distributions are found to be heavy-tailed so that large disturbances are more common than predicted by Gaussian statistics. We model the grid dynamics

using a stochastic differential equation to derive the scaling of the fluctuations based on power grid parameters, identifying effective damping as essential in reducing fluctuation risks. This damping may be provided by increased demand control as proposed by *Decentral Smart Grid Control*.

Finally, we investigate discrete events, in particular the failure of a single transmission line, as a complementary form of disturbances. An initial failure of a transmission line leads to additional load on other lines, potentially overloading them and thereby causing secondary outages. Hence, a cascade of failures is induced that propagated through the network, resulting in a large-scale blackout. We investigate these cascades in a combined dynamical and event-driven framework, which includes transient dynamics, in contrast to the often used steady state analysis that only solves static flows in the grid while neglecting any dynamics. Concluding, we identify critical lines, prone to cause cascades when failing, and observe a nearly constant speed of the propagation of the cascade in an appropriate metric.

Overall, we investigate the self-organized dynamics of power grids, demonstrating its benefits and limitations. We provide tools to improve current grid operation and outline a smart grid solution that is not reliant on IT. Thereby, we support establishing a 100% renewable energy system.

Contents

I	Introduction	7
1	Motivation	8
2	Fundamentals	15
2.1	Networks	15
2.2	Power Grids	22
2.3	Stochastic Equations	37
2.4	Distributions	40
2.5	Simulations	45
II	Results - Original Manuscripts	50
3	Decentral Smart Grid Control	51
4	Taming Instabilities in Power Grid Networks by Decentralized Control	68
5	Escape Routes, Weak Links, and Desynchronization in Fluctuation-driven Networks	90
6	Heavy Tails, Superstatistics and Scaling of Power Grid Frequency Fluctuations	101
7	Dynamically Induced Cascading Failures in Supply Networks	127
III	Conclusion	155
8	Summary & Discussion	156
	Bibliography	163

Part I

Introduction

Chapter 1

Motivation

Climate change, energy transition and the role of electricity

One of today's greatest challenges to humankind is to mitigate climate change and its effects [65]. To cope with this challenge, the Paris conference 2015 saw leaders of nearly all countries agree to limit global warming to 1.5°C [153]. However, reaching this ambitious goal requires a significant reduction of greenhouse gas emissions, especially CO_2 , which is, for example, released in large quantities to satisfy energy demands [42]. These demands arise in several, mainly disconnected consumption areas. Electrical energy, for example, is directly used by numerous devices and machines in private and industrial contexts to light up buildings, power engines, run computers and much more. In addition, energy provided by burning oil or gas is used in cars, trucks and trains for transportation purposes as well as in the heating sector. While these three sectors of energy consumption are mainly independent today, we expect that heating and transportation sectors will rely more on electricity in the future [10]. For instance, the introduction of electrical cars makes the transport sector more depended on the electricity generation. Similarly, the usage of heat pumps to heat up or cool down buildings couples the heating sector to the electric one [35], in addition to already common solar or electrical district heating [84]. Therefore, reducing CO_2 emissions and switching to a sustainable energy supply, crucially depends on reforming and restructuring the power grid to supply enough energy for all sectors while avoiding greenhouse gas emissions. To achieve this, it is central to incorporate as much renewable energy generation into the grid as possible [42,147] with wind and solar power being the most promising contributors to reach a sustainable energy supply [32,67].

However, integrating these sources into the existing grid raises many challenges [21,158,159], ranging from the design of the grid to the necessity of new control frameworks due to sources being distributed, far away and fluctuating. Furthermore, the power grid has become a large and complex system, intertwining countries and crossing borders [44], making an isolated analysis of a single country almost impossible (see also Fig. 1.1).



Figure 1.1: Europe at night observed by a satellite. The map shows no borders, as light is not stopped at the border of a country. Similarly, the electricity powering the light is transmitted across borders. In recent years, previous national power grids got coupled into one very complex Continental European power grid. The picture is assembled from recordings of the Suomi NPP satellite from April 2012 and October 2012, displaying the light emitted from settlements. Reproduced from [100], published under CC-BY-2.0.

Power grid research as a physicist

The current power grid, especially in Western states, is very reliable and stable. Recent reports by grid operators proudly state how the grid service is lost for less than a couple of hours per year [24, 43, 47]. So why do we need additional basic research on this topic when the ongoing energy transition has been handled very well so far?

First, more subtle measures than outages indicate increasing stress on the grid. For example, the total power re-dispatch, i.e., the redistribution of power within the network to avoid overload, increased significantly within the last years [1, 174]. Furthermore, a recent study points out that currently no framework exists that operates with 100% renewable energy generation and reliably meets demand criteria using realistic demand forecast while being resilient [60]. In addition, the power grid operators themselves do not seem ready to implement a fully renewable system, as the scientific director for research and development at EDF (Électricité de France S.A.), one of the largest energy companies world-wide, said in July 2016: “[Today, a] 100% renewable energy system is still hard to manage. It is technically impossible and economically unsustainable.” [152].

Facing increasing loads and without a plan for implementing a 100% renewable power grid, we believe that basic research is necessary to pave the way towards such a sustainable system [23, 116, 154].

So far, the technical adaptations made by the grid operators have been mostly sufficient to adapt the power grid to the changing needs. Nevertheless, some conceptional steps are missing before a sustainable energy system can be established. As physicists, we do not intend to instruct operators on how to precisely operate the grid using specific scenarios, instead we aim to provide fundamental insights into options and constraints of the system, using a powerful and versatile analytical toolbox.

Research in this area is not only of direct interest for applications to power grid systems but is also relevant from a basic science point of view. Power grids are very interesting complex dynamical systems displaying collective nonlinear dynamics, including oscillation and synchronization phenomena that are observed and studied in numerous other fields [114]. For example, the well-known Kuramoto model [77, 78], explaining essential mechanisms underlying synchronization, is very similar to the power grid dynamics when neglecting inertia.

The broad interest of physicists to work on questions regarding power grids arose within the last 10 to 15 years, likely driven by progress in computation power and general political interest in the topic. A few early works on power grids by physicists are by Cruicitti et al. [34] in 2004, Kinney et al. in 2005 [71] and Anghel et al. in 2007 [8], which mainly focused on the topological properties of power grids. However, the topic became of widespread interest in the physics community based on Filatrella et al. in 2008 [55], introducing small systems and simulations, Rohden et al. in 2012 [121], investigating the role of network topology, Motter et al. [98] and Dörfler et al. [39], both 2013, providing synchronization and stability conditions, which were followed by numerous articles, see e.g., [38, 39, 79, 87, 88, 89, 91, 92, 98, 103, 122, 123, 129, 130, 131, 132, 133, 170, 171, 172, 173, 179] demonstrating the interest in the field and the large amount of open questions.

Challenges facing the power grid

Let us review some of the challenges facing the power grid when including a high share of renewable power generation. We will not be able to cover all aspects within this thesis so that we will mostly neglect economic aspects concerning the reformation of the energy market [52, 59] and very long time scales, e.g., seasonal effects [61]. Instead, we focus on effects on the short time scale, where fluctuations, discrete events, e.g., line failures, lead to a desynchronization and thereby outage of the grid. In addition, we study how supply and demand may be matched all time, using demand control in smart grids.

Fluctuations. Traditional coal or gas fired power plants have a deterministic and controllable power output, so that the output can be increased during an energy shortage and decreased during phases of excess energy [62, 86]. In contrast, the power output by renewables is often not deterministic but depends, for instance, on solar irradiation, wind and cloud conditions. Therefore, the power fluctuates on different time scales from several days [61] to less than a second [93]. Each time scale poses its individual challenges. Several days without wind and solar generation (due to cloudy weather conditions) require long-term storage [3], while a sudden increase of energy within a second has to be balanced by a fast control [20]. Beyond acting on multiple time scales, fluctuations by renewables also display highly non-Gaussian statistics. This includes jump noise in solar power generation, due to gaps in the clouds [9], and heavy tails in wind power generation, partially due to the turbulent nature of wind itself [93, 94].

In this thesis, we focus on short time fluctuations using a dynamical model for the power grid on the time scale of sub-seconds to a few seconds. We consider two main questions posed by fluctuations to the grid: Can fluctuations destabilize the dynamics of the grid and thereby lead to a blackout? And secondly: How do fluctuations impact the bulk (average) power grid frequency?

The first question concerns the capability of fluctuations to desynchronize a heavily loaded grid [75] by driving it out of its steady state after a finite escape time. The second question concerns regulations by grid operators that state that voltages and frequencies have to stay within strict bounds to protect machines [45]. Therefore, we investigate how fluctuations of renewables impact the statistics of the power grid frequency.

Discrete events. In contrast to continuous fluctuations, singular discrete events, like the tripping of an important transmission line or the shutdown of a large power plant, are much rarer but might have severe impacts on the dynamical stability of the grid. In extreme cases, an initial failure of one line increases the load on the remaining grid and causes multiple secondary failures and finally a wide area blackout [108]. We expect the frequency of these events to increase with increasing load of the network due to large distances between power generation and consumption areas, e.g., with wind generation at the coasts and demand in urban areas [1,2]. Major blackouts due to discrete failures include the often cited Italian blackout in 2003, as well as more recently, the Indian blackout in 2012 and the South Australian blackout in 2016.

In September 2003, the Italian power grid and Internet communication network demonstrated their essential interdependence. The shutdown of a power plant unpowered a communication node, which in turn disconnected the communication grid, causing additional shutdowns of power plants and failures of more communication nodes. Eventually, a large cascade of these events unpowered most of the Italian grid, affecting a total of about 56 million people, due to power grid and information technology (IT) infrastructure failing interdependently [25].

On the 30th and 31st of July 2012, the largest blackouts in the history of mankind took place in India, affecting about 600 to 700 million people [113]. Before the failure, the grid was highly loaded and instead of heavy rain falls, the monsoon season to this point of time had been drier than expected, resulting in less power generated in hydro plants [28]. Similar to many other blackouts, the failure was traced back to the failure of a single element, typically a transmission line or power plant, which resulted in the subsequent failure of additional lines within a short time frame due to automatic disconnections [28]. As a consequence of the blackout, trains were stopped, causing millions of stranded passengers. Hospitals had to rely on nurses operating life-saving equipment manually while surgeries were canceled [113]. Production halted, while major cities suffered from failing air conditioning and traffic jams, e.g., in New Delhi and Kolkata [80,113].

Finally, on September 28 in 2016, the whole grid of South Australia went down when a severe storm knocked out a large number of high voltage pylons leading to additional automatic shutdowns and finally a blackout of the whole state of South Australia. In total about 1.7 million people [13] were without electricity and the grid needed a black start, i.e., start without using power from any running power plant [148].

Such large scale blackouts have huge economical and societal costs [19,138] and might even be worse in the future [112] because our societies increasingly rely on the well-functioning of the electricity supply. Hence, it is of utmost importance to understand how cascading failures take place, how they propagate through the grid and how they might be stopped to protect the “*uniquely critical*” energy system [104].

Although many cascading failures took place within a short time frame of seconds [26,28,101],

existing studies on cascades [33, 34, 68, 71, 115, 120, 173] mainly used static flow analysis, which is suitable on time scales of minutes to hours, demanding a dynamical description.

Demand control and smart grids. Power grids were designed to generate electric power at a high voltage, feed it into the high voltage transmission grid to then distribute the power to customers at lower voltage levels, see Chapter 2 and [62, 76]. However, solar and wind plants cannot be located close to the demand locations but require favorable weather conditions to achieve a high average generation. Due to the large distance between generation and consumption, additional transmission lines become necessary to deliver the power to the consumption sites [2]. Furthermore, the power supplied by the numerous distributed solar and wind plants put on roofs or in backyards already results in a power flow from former consumer grids, i.e., distribution grids, at low voltage into the high voltage transmission grid [66]. This direction of power flow poses a substantial challenge to the control of the grid as most regulations target the high voltage transmission grid and not the low voltage distribution grid, where additional control will be needed [45]. Finally, the conventional framework for power grids assumes that consumers have no restrictions and may modify their demand as they see fit, so that the generators have to mirror consumption behavior and increase supply when demand rises [177]. However, renewable sources cannot supply a constant or 100% controllable power output [9, 61, 93]. Therefore, to balance supply and demand it was proposed to make consumption more flexible and let consumers follow the generation of renewables using *demand response* or *demand control* [109].

To cope with distributed and fluctuating generation on low voltage levels, further coordination of generation as well as consumption on the lower voltage distribution grid becomes necessary, in addition to existing control on the high voltage transmission grid. Additional control and communication is often proposed to be handled by a *Smart Grid* that integrates consumers and distributed generators into the system manageable by the grid operators [6]. Such a system relies on an extensive IT infrastructure to read off demand data, predict generation by renewables and communicate the desired strategy for consumption and generation [54, 66].

However, from our point of view, reading and communicating demand data raises severe privacy concerns. In addition, any IT infrastructure has to withstand random failure of components, which already lead to the large scale blackout in Italy [25], see also above. In addition, recent cyber attacks [106, 111] demonstrated that even large companies (e.g. banks and logistic enterprises) are vulnerable to hacking attempts. Therefore, we question the idea of basing the critical electricity supply [76] even more on the functioning of potentially hackable IT and consequently consider alternatives.

Synopsis and structure of this thesis

In this thesis, we investigate various aspects of self-organized dynamics of power grids by omitting external or global control actions. Instead, we assume a purely local reaction of each actor in the grid. The chapters cover topics ranging from smart grids to continuous fluctuations and discrete perturbation events, based on individual manuscripts.

In **Chapter 2**, we provide additional information on network science and the basics of power grid organization and modeling, extending this introduction. This is mainly intended to provide a framework for the following chapters, not a thorough treatment of the topics it touches upon. In addition, we review some often used tools treating ordinary differential, delay differential and stochastic equations complementing the brevity of the following original manuscripts.

In **Chapter 3**, we introduce the concept of *Decentral Smart Grid Control* as a self-organized control scheme for power grids, without the need for a central IT infrastructure. The control uses power grid frequency measurements at each network node to adapt the power generation or consumption, thereby providing a concrete proposal for self-organized smart grids applicable to consumers and generators alike. We analyze the dynamical stability properties of this system, considering both instantaneous reaction, which improves the grid's stability, and delayed reaction to the signal, which results in resonance risks. Finally, we introduce an averaging mechanism for the frequency signal to stabilize the system against resonance instabilities. The dynamical analysis is restricted to small networks of $N = 2 \dots 4$ nodes.

Chapter 4 extends results obtained in Chapter 3 by applying Decentral Smart Grid Control to a few additional network motifs with $N = 4 \dots 9$ nodes. In addition, we explore a destabilizing effect for large delays on any potential network topology using analytical methods only. Furthermore, we study larger networks using numerical tools. Thereby, we detect a transition from the system being multistable to one globally stable attractor.

In **Chapter 5**, we characterize the power grid stability when subject to uncorrelated Gaussian noise, which leads to a desynchronization of the grid after a finite time, i.e., to a blackout. We investigate this escape time both numerically and analytically using Kramer's escape rate mapped to the network problem. By doing so, we identify critical lines in the network that are most prone to be overloaded and provide the scaling of the escape time as a function of the grid's parameters like inertia, transmitted power, damping etc.

Chapter 6 also investigates fluctuations in power grids, focusing on daily fluctuations instead of blackouts. To this end, we investigate power quality, i.e., we determine how much the grid frequency deviates from $f = 50$ Hz or $f = 60$ Hz. We do so by analyzing power grid frequency measurements from around the world, highlighting heavy tails in their distributions. Applying a dynamical power grid model, we derive a Fokker-Planck equation of the grid frequency. By solving it, we derive the scaling of the frequency fluctuations as a function of the inertia, the size of the grid and the effective damping (e.g., as provided by decentralized control). Finally, we apply superstatistics to frequency fluctuations, providing an alternative explanation for heavy tails in the distributions.

In **Chapter 7**, we investigate another type of disturbances to power grids, namely discrete events like the failure of a single transmission line, leading to potentially large cascading failures. Compared to the majority of the existing literature, we do not apply a static flow approach but consider cascades using a dynamical framework, thereby revealing important effects, which are often missed. Investigating different network topologies, we develop a predictor identifying critical links for the dynamical stability of the grid and observe a propagation of the cascade within the grid.

Chapter 8 closes this thesis with a summary and discussion of the obtained results, putting them into context of existing work.

Chapters 3-7 constitute independent publications and all contain a separate bibliography. Another list of references for Chapters 1, 2 and 8 is given at the end of the thesis.

Chapter 2

Fundamentals

This chapter provides a brief introduction to basic concepts used in later chapters. We cover all necessary terminology and theory to enable the reader to follow the occasional brief calculation in the original manuscripts. However, we do not provide a thorough coverage of any of the fields we touch on, so readers are encouraged to check the cited literature for further information.

2.1 Networks

The primary focus of this thesis is on power grids, which are best described as complex networks constituted of generators, consumers, transmission lines, transformers etc. Here, we introduce the basic concepts of network theory mainly following [102].

First, we note that network science has been and continues to be a highly interdisciplinary topic. Social scientists are interested in social interaction networks, while biologists describe networks as different as food webs, gene regulatory networks or the brain. Infrastructure like train and street networks are essential for today's society. And in recent years, computer science became more important than ever for our daily lives in the form of the internet, a huge and complex network, see also Fig. 2.1. Hence, network science is of great importance for many fields resulting often in non-unique terminology since different fields introduced different terms to describe the same concept. We restrict ourselves to a couple of synonyms throughout this thesis.

A *network* (also graph/(power) grid) is a collection of *nodes* (also vertices/actors) that are connected via *edges* (also links/lines). We count the nodes of a network with indices $i = 1, 2, \dots, N$ and denote the edges as $i - j$ or (i, j) with a total of $|E|$ edges. Concepts like self-edges, i.e., a node connected to itself, or multi-edges, i.e., more than one edge between two nodes, are not explicitly used in this thesis.

Adjacency matrix. The connectivity of a network is easily described by the *adjacency matrix* $\mathbf{A} \in \mathbb{R}^{N \times N}$ that is defined as

$$A_{ij} = \begin{cases} 1 & \text{if } i \text{ and } j \text{ are connected via an edge,} \\ 0 & \text{else.} \end{cases} \quad (2.1)$$

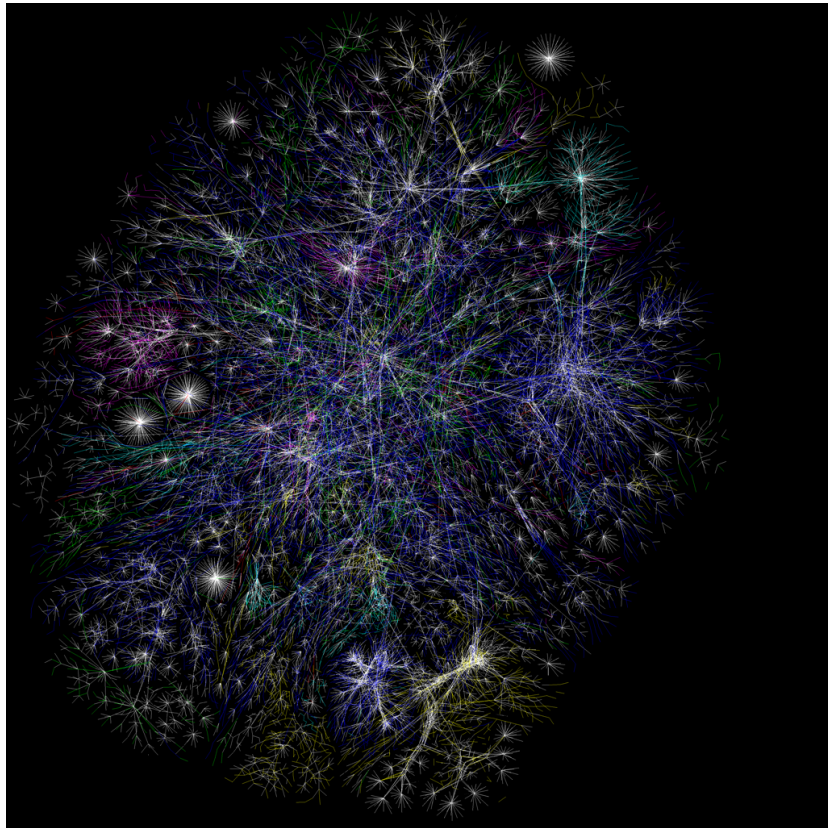


Figure 2.1: The internet is a complex network. Shown is the Internet structure where vertices represent similar IP addresses and connections represent typical paths of data packages on this network. Reproduced from [107], published under the CC-BY-NC-4.0.

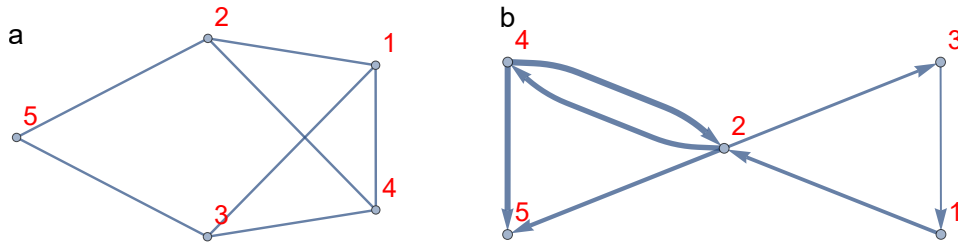


Figure 2.2: Small sample networks. **a**: A five node unweighted graph with a total of seven edges is shown. **b**: A five node network with seven directed and weighted edges is depicted, where thicker edges have higher weights and arrows indicate the direction of the edge.

For a network formed of N nodes, the adjacency matrix is hence a $N \times N$ matrix, which is typically very sparse for sufficiently large networks [5]. Fig. 2.2a shows a small sample network with adjacency matrix

$$A = \begin{pmatrix} 0 & 1 & 1 & 1 & 0 \\ 1 & 0 & 0 & 1 & 1 \\ 1 & 0 & 0 & 1 & 1 \\ 1 & 1 & 1 & 0 & 0 \\ 0 & 1 & 1 & 0 & 0 \end{pmatrix}. \quad (2.2)$$

This adjacency matrix is unweighted, i.e., all edges described in the network are equal. Instead, an edge could be weighted, e.g., to differentiate between a highway and a small lane or a thick and thin transmission cable. A weighted adjacency matrix still has entries that are zero, implying no connection, and general non-zero entries where the entry of the matrix is the weight of the link. Furthermore, we can also introduce directed links that start at one node and end at another symbolizing, e.g., a one way street, by setting $a_{ij} > 0$ but $a_{ji} = 0$, for example

$$A = \begin{pmatrix} 0 & 8.73 & 0 & 0 & 0 \\ 0 & 0 & 6.27 & 14.07 & 10.33 \\ 2.89 & 0 & 0 & 0 & 0 \\ 0 & 16.86 & 0 & 0 & 16.14 \\ 0 & 0 & 0 & 0 & 0 \end{pmatrix}, \quad (2.3)$$

see Fig. 2.2b.

One alternative to the adjacency matrix is an edge list, i.e., edges are listed in the form 1 – 2, 2 – 3, 2 – 4, 2 – 5, 3 – 1, 4 – 2, 4 – 5 for the graph in Figure 2.2a, where the weight needs to be stored for each edge in case of weighted graphs. Edge lists are often used for memory-efficiency in computer calculations, especially when networks are sparse, i.e., have few links [176].

Graph measures. The adjacency matrix allows easy calculation of many important graph metrics, including degree, centrality and node distances. Consider an unweighted and undirected network of N nodes and $|E|$ edges. Each node has a *degree* k_i , which is defined as the number of edges connected to

it:

$$k_i = \sum_{j=1}^N A_{ij}. \quad (2.4)$$

In case of an unweighted but directed network we have to distinguish between in-degree $k_i^{\text{in}} = \sum_{j=1}^N A_{ji}$ and out-degree $k_i^{\text{out}} = \sum_{j=1}^N A_{ij}$. In addition, the *degree distribution* $p(k)$ gives the probability to find a node with degree k in the network. It is in particular interesting when comparing different network ensembles.

Next, we define a *path* in the network between nodes a and b as the sequence of nodes visited to get from a to b . Using Fig. 2.2b as an example graph, one path from node 1 to node 5 would be $p = (1, 2, 4, 5)$ and an alternative is given by $\tilde{p} = (1, 2, 5)$. The second path seems more intuitive and “shorter”. We quantify the *length of a path* as $l(p) = \sum_i A_{p_i p_{i+1}}$ where i goes from 1 to number of vertices -1 in p , i.e., for our example this results in $l(p) = A_{12} + A_{24} + A_{45}$ and $l(\tilde{p}) = A_{12} + A_{25}$. Traveling in a street network or sending packages through the Internet should often be as fast as possible, i.e., one is interested in finding the *shortest path*, also known as geodesic path or distance. All paths between nodes a and b that have the smallest length are shortest paths, see also Fig. 2.3.

Ranking the importance of nodes is often done using the concept of centrality. Two simple concepts of centrality include degree centrality and betweenness centrality. The *degree centrality* uses the degree k of each node as a centrality measure, i.e., nodes that have many edges are considered to be very central. Conversely, the betweenness centrality counts how often each vertex is used when considering all possible shortest paths in the network. Thereby, nodes with few edges that connect two large sub-networks are very central in this sense, see Fig. 2.4.

Finally, we will also use the concept of a *clustering coefficient*, which captures the share of connected triangles. In a social network this is the probability that two friends of mine are also friends. One way to define the clustering coefficient is to compute

$$C = \frac{3 \text{ (number of triangles)}}{\text{(number of connected triples)}}, \quad (2.5)$$

where a triangle is a set of three fully connected vertices (a, b, c) with edges $a - b$, $b - c$, $c - a$ present while a triple only requires edges $a - b$ and $b - c$ (permuting indices is allowed), see [102] for details.

Alternative distance measure. We introduced the concept of shortest paths above, which define a graph distance using the adjacency matrix \mathbf{A} . When describing cascades in Chapter 7, we will need the concept of *effective distances* introduced by Brockman and Helbing [22] for epidemic spreading. We define effective distances between two vertices i and j as

$$d_{ij} = 1 - \log \left(\frac{A_{ij}}{\sum_{k=1}^N A_{ik}} \right), \quad (2.6)$$

and all nodes that do not share an edge, i.e., $A_{ij} = 0$, have effective distance $d_{ij} = \infty$. To compute the length of paths, we again use the concept of shortest paths but use d_{ij} instead of A_{ij} . Using highly weighted edges in the original graph description \mathbf{A} resulted in very high distances. In contrast, the effective distance defined in Eq. (2.6) is small between highly connected nodes and large, if the

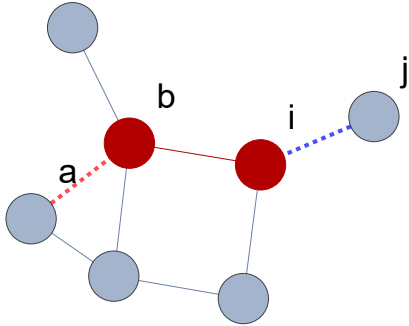


Figure 2.3: Illustration of shortest paths on a sample network. The highlighted path is the shortest path between nodes a and j with a distance of $d = 3$ (unweighted). Furthermore, this illustrates the basic idea of edge distances. The edges $a - b$ and $i - j$ have the distance based on all possible shortest paths between all involved nodes, see Eq. (2.7). Here the distance is $d_{a-b,i-j} = d_{bi} + d_{ab}$.

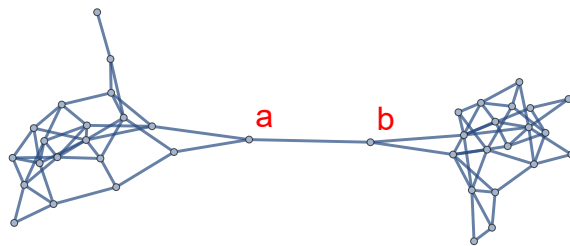


Figure 2.4: Example graph with two nodes showing high betweenness centrality. The nodes a and b are part of a 20 node sub-graph each, both having degree $k = 2$ within their respective graph. However, the edge connecting both nodes is the only connection between the two subgraphs. Therefore, the nodes a and b and the edge $a - b$ is highly central, as also quantified by a high betweenness.

weights are comparatively small. Note further that the effective distance is an asymmetric measure with $d_{ij} \neq d_{ji}$ in general.

In addition, we need to define the *distance of two edges* for this weighted graph. Let d_{ij} be the distance measure between two vertices. We then define the distance between edge $a - b$ and edge $i - j$ as

$$d_{a-b,i-j} = \min_{v_1 \in \{a,b\}, v_2 \in \{i,j\}} d_{v_1 v_2} + d_{ab}, \quad (2.7)$$

i.e., it is the minimum of the shortest path lengths of the paths $a \rightarrow i$, $a \rightarrow j$, $b \rightarrow i$ and $b \rightarrow j$ plus the effective distance between the vertices a and b , see Fig. 2.3 for an illustration and Chapter 7 for the application.

Network Models. When investigating the properties of networks we would like to derive general statements that are not only true for one specific simulation [143] but hold for every network or at least a large class of potential networks. However, if a fully analytical approach is not available, one can simulate multiple realizations of a specific network ensemble for comparison and some insight [122]. But what is an appropriate way to generate a random network?

There exist numerous network models. To name just a few: The *Erdős-Rényi model* uses a fixed number of nodes N and assigns either a fixed number of links $|E|$ connecting nodes at random or each potential link is realized with a fixed probability p [49]. The *Watts-Strogatz model* starts with a regular graph where for example every node on a ring is connected to its next neighbors and continues by re-wiring each link with a fixed probability [165] leading to the *small world effect*. In these network every node is at a small distance from any other node in the grid due to non-local shortcuts in the connectivity, see Fig. 2.5. In addition, the clustering coefficient in these networks is large. Even more prominent might be the *Barabasi-Albert model*, which starts with one node, then adds one node at a time and connects them preferentially to nodes with already many connections, leading to a “rich-get-richer” phenomenon [14]. Finally, there exist specific power-grid related network ensembles, which aim to construct a network with network measures similar to real power grids [139].

Note however, that the differences of these various network ensembles are much more pronounced when comparing large networks with thousands of nodes $N \sim 10^3 - 10^5$ while this thesis mainly considers smaller networks of $N \sim 10$ for illustration purposes and $N \sim 100$ to model national grids in Europe. Therefore, we typically do not focus as much on different graph ensembles as, e.g. [122].

Dynamics on networks. So far, we have covered only structural properties of networks like degrees, distances and network ensembles. Here, we extend the treatment of networks by the dynamics of variables on the network itself.

Consider a network of N nodes with adjacency matrix \mathbf{A} . Furthermore, let each node i in the network be characterized by the state \mathbf{x}_i , which may be multi-dimensional, i.e., each node might have D different variables $\mathbf{x}_i = (x_i^1, x_i^2, \dots, x_i^D)$. A single state component is noted as x_i^μ with the superscript μ describing the different variables of a node ($\mu = 1, \dots, D$, Dimension D) and the subscript i denoting the different nodes ($i = 1, \dots, N$). A general dynamical system (allowing at most pairwise interactions)

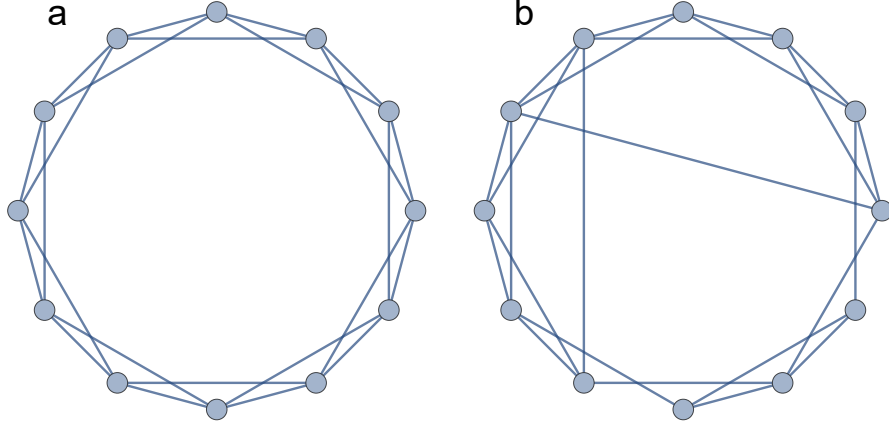


Figure 2.5: Small world networks introduce shortcuts in regular networks. **a**: A regular twelve node network is shown where each node is coupled to its four nearest neighbors. **b**: The regular network from **a** is transformed into a small world network by re-wiring each link with probability $p = 0.15$, introducing shortcuts into the network leading to the *small world effect*.

on such network is then written as

$$\frac{d}{dt}\mathbf{x}_i = \mathbf{f}_i(\mathbf{x}_i) + \sum_{j=1}^N A_{ij}\mathbf{g}_{ij}(\mathbf{x}_i, \mathbf{x}_j), \quad (2.8)$$

where \mathbf{f}_i is the intrinsic dynamics of the node while \mathbf{g}_{ij} gives the interaction dynamics. In many cases, we assume that the functional form of both intrinsic and interaction dynamics are identical for all nodes, leading to the simplified form

$$\frac{d}{dt}\mathbf{x}_i = \mathbf{f}(\mathbf{x}_i) + \sum_{j=1}^N A_{ij}\mathbf{g}(\mathbf{x}_i, \mathbf{x}_j). \quad (2.9)$$

A fixed point \mathbf{x}_i^* of this system is defined by

$$0 = \mathbf{f}(\mathbf{x}_i^*) + \sum_{j=1}^N A_{ij}\mathbf{g}(\mathbf{x}_i^*, \mathbf{x}_j^*). \quad (2.10)$$

To obtain the stability of such a fixed point with respect to small perturbations we linearize the dynamics of \mathbf{x}_i around \mathbf{x}_i^* :

$$\mathbf{x}_i \approx \mathbf{x}_i^* + \delta\mathbf{x}_i, \quad (2.11)$$

resulting in the linear dynamics of the small perturbations $\delta\mathbf{x}_i$:

$$\frac{d}{dt}\delta\mathbf{x}_i = \mathbf{J}\delta\mathbf{x}_i, \quad (2.12)$$

with Jacobian matrix \mathbf{J} , which for our dynamical system is given as [150]

$$\mathbf{J} = \begin{pmatrix} \frac{\partial}{\partial x_1^1} \left(\frac{d}{dt} x_1^1 \right) & \cdots & \frac{\partial}{\partial x_1^D} \left(\frac{d}{dt} x_1^1 \right) & \frac{\partial}{\partial x_2^1} \left(\frac{d}{dt} x_1^1 \right) & \cdots & \frac{\partial}{\partial x_N^D} \left(\frac{d}{dt} x_1^1 \right) \\ \vdots & \ddots & & & & \vdots \\ \frac{\partial}{\partial x_1^1} \left(\frac{d}{dt} x_N^1 \right) & & \cdots & & & \frac{\partial}{\partial x_N^D} \left(\frac{d}{dt} x_N^1 \right) \\ \frac{\partial}{\partial x_1^1} \left(\frac{d}{dt} x_1^2 \right) & & & \cdots & & \frac{\partial}{\partial x_N^D} \left(\frac{d}{dt} x_1^2 \right) \\ \vdots & & & & \ddots & \vdots \\ \frac{\partial}{\partial x_1^1} \left(\frac{d}{dt} x_N^D \right) & \cdots & \frac{\partial}{\partial x_1^D} \left(\frac{d}{dt} x_N^D \right) & \frac{\partial}{\partial x_2^1} \left(\frac{d}{dt} x_N^D \right) & \cdots & \frac{\partial}{\partial x_N^D} \left(\frac{d}{dt} x_N^D \right) \end{pmatrix}. \quad (2.13)$$

We set the variables to their fixed point values $\mathbf{x}_i = \mathbf{x}_i^*$, so that all entries in \mathbf{J} are numerical. Then, we compute the eigenvalues of \mathbf{J} as $\lambda_1, \lambda_2, \dots, \lambda_{N \cdot D}$. If any of these eigenvalues have a positive real part, the fixed point is linearly unstable and the system diverges from it. If however, the real parts of all eigenvalues are negative, the system is linearly stable and decays back to the fixed point after small perturbations.

2.2 Power Grids

How is the power grid organized? Why do we use AC power equipment instead of DC equipment? What are appropriate models to describe the power grid's dynamics? We review these questions together with a general introduction to power grids here. Furthermore, we give a derivation of a dynamical and static model describing the grid with and without voltage dynamics.

2.2.1 General Properties of Power Grids

Here, we briefly review some important elements and properties of the power grid system with a focus on the elements crucial for this thesis and refer the interested reader to specialized books on control [76], markets [52, 59] or power grid models [86, 103] for further details.

Brief history. AC vs. DC transmission

About 150 years ago Thomas Edison invented the first practical electric light bulb illuminating buildings with electricity [137]. Edison was committed to use electricity based on the principle of a directed current (DC). However, DC lines typically only used one voltage since transformation to different voltage levels was not easy. This led to numerous electric lines being needed, one for each voltage, see Fig. 2.6 for the situation in New York in 1890.

In contrast, the entrepreneur Westinghouse developed an electricity system based on alternating current (AC) together with the help of Nikola Tesla at the end of the 19th century [29]. Transformation of AC power to different voltage levels was much easier than it was the case with DC. The conflict of the two opposing concepts led to the *war of currents* [29] during which DC was advertised by Edison as a safe solution while the high voltage transmission of the alternating current was proclaimed to be too dangerous. In the end, the potential to transport power over large distances at high voltage to the

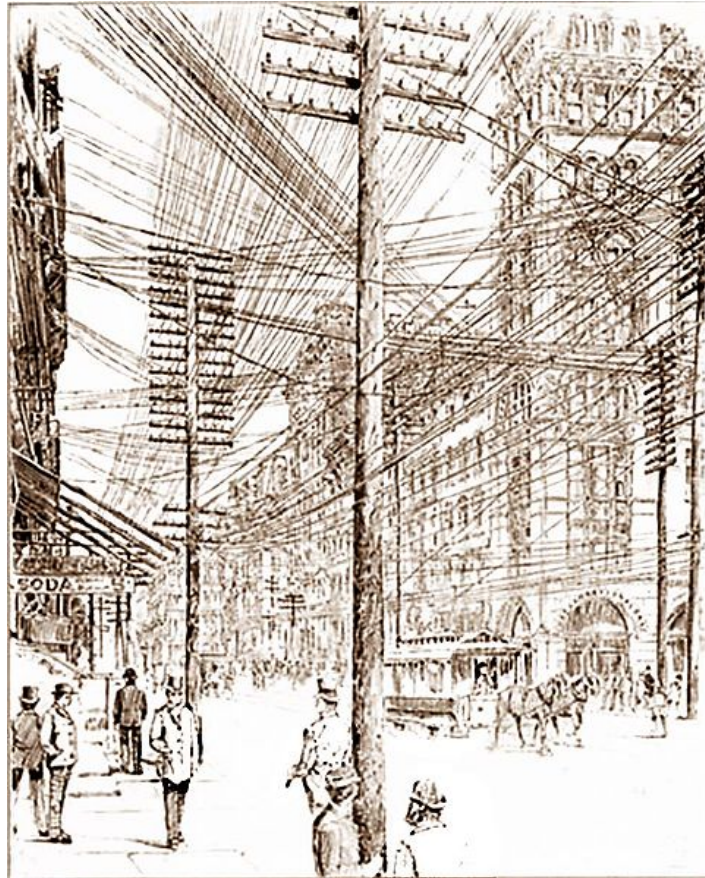


Figure 2.6: In 1890, New York needed many power transmission lines. At this time at least one line was needed for each voltage and household. Since the applied DC was not easy to transform, many lines were build. Reproduced from [167], published under public domain.

cities and using transformers to convert it to lower voltages for consumption prevailed, leading to the AC design to be widely adapted [29].

Today, we combine AC and DC approaches seeing them as complimentary instead of competitive due to huge advancements in power electronics [96]. While large parts of the transmission power grid use AC, high voltage directed current (HVDC) transmission lines are used for long-range transport or to couple different synchronous regions like Continental Europe and Great Britain [70]. Furthermore, solar and wind power are often supplied as DC and then converted to AC to be fed into the grid [18].

Power grid organization

Power generation. Our modern power generation still relies on the same principle as used by Tesla in the 1890th, namely Faraday's law [29]. It states that a changing magnetic field introduces a electromotive force, i.e., electric currents in a wire [126]. Given this observation, there are different options of how the magnetic field may change. One option is to place a static conductor in the field of an electromagnet and vary the magnetic field strength without any movement. Alternatively, the magnetic field is held constant and instead the conductor is moved, e.g. rotated, within the field.

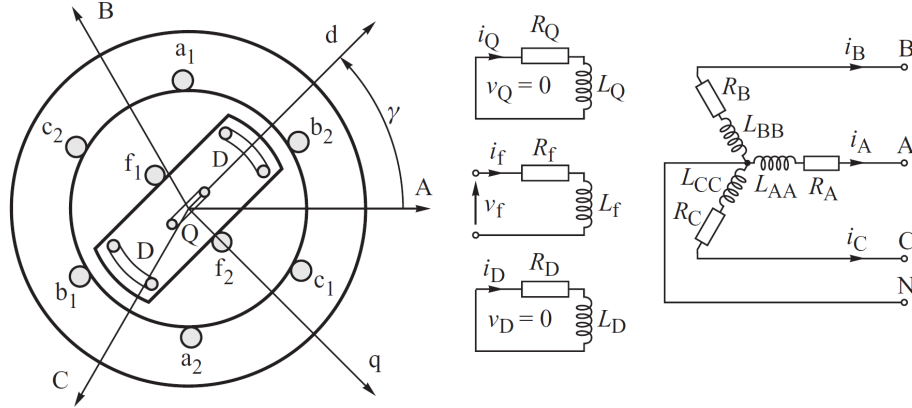


Figure 2.7: Schematic of a three phase generator displaying the two axes of the rotor (d and q) and the three axes of the stator (A,B,C). Reproduced from [86] with permission.

Conversely, it is also possible to move the magnet and keep the conductor static. The last approach is used in modern synchronous generators, which often use three poles, as shown in Fig. 2.7 [86].

A three pole synchronous generator consists of a stator and a rotor driven by mechanical forces, e.g., water flow in a hydro plant or steam in a combustion plant. The rotor is equipped with windings along its main direction, which is called direct axis or d-axis. Conversely, the axis perpendicular to it, more specifically, 90° later in the rotation, is the quadrature axis or q-axis. The stator has three pairs of windings giving rise to the three axes A,B,C. The rotor windings are powered with a DC field to induce a magnetic field (flux), which penetrates the stator windings. The rotation of the magnetic field of the rotor changes periodically in the stator windings and thereby induces an AC current in the stator [86].

For our purposes, we do not need to specify all fluxes and fields in the rotor and stator respectively. Instead, we focus on some key variables and parameters to characterize a given machine: For a spinning machine, the mechanical frequency ω of the rotor is very important because it is closely linked to the frequency of the induced alternating current (AC) in the stator. More precisely, we assume here that the voltage phase angle in complex notation and the mechanical angle γ depicted in Fig. 2.7 are identical, as justified for the equilibrium state with small disturbances [7,86]. Voltage phase angle and frequency are linked via the time derivative

$$\frac{d}{dt}\gamma = \omega. \quad (2.14)$$

During steady-state operation voltages, currents and fluxes in the machine are almost periodic and small disturbances from the steady state are modeled via the *swing equation*, see below. The grid frequency is then close to its reference value of $f = 60$ Hz (North America, Parts of South America, Parts of Asia) or $f = 50$ Hz (other countries). On the contrary, when large disturbances, e.g. short-circuits, are considered, the voltages are dynamically changing over time and the reactances between the different axes also play an important role, especially on the q and f axes. We assume most of these quantities to be constants and at most consider a model where the voltage in the q-axis is allowed to

vary over time, see *3rd order model* below.

The electric energy provided by spinning generators has to be consumed immediately or needs to flow into batteries or hydro storage. The only storage that the generators themselves provide is the stored kinetic energy of their rotation, which is proportional to their respective inertia I . To keep the frequency close to its reference values, a sophisticated control architecture and specialized reserve power markets have been established, which also use the *spinning reserve* of connected machines [86].

Alternatives to synchronous machines. Classical mechanical synchronous machines, as mentioned above, provide substantial inertia for the grid. This was long seen as an obvious contribution. However, integrating renewable generation into the power grid changes the situation significantly. Current technology to couple solar or wind power into the power grid relies on inverters, i.e., even the rotation of the wind turbine is first converted to a DC, transmitted to a converter and then fed as AC into the grid [62]. Thereby, replacing synchronous machines with inverters, i.e., power electronics without any mechanical rotor, that are connected to a DC power source, like a battery or solar cell, keeps the total power in the grid constant while decreasing the inertia. Unfortunately, inertia is generally beneficial for the system stability so that we have to find an solution to the decreasing inertia [160].

One solution is to use inverters in the *grid-following* mode, given there is a grid frequency to follow in the first place [134]. Alternatively, inverters operate as *grid-forming*, i.e., they are used to establish a frequency, which other inverters can then follow [134]. The downside of the second kind is that they need very large amounts of energy very fast in order to keep the grid stable [27]. Furthermore, there are critics pointing to the finite measuring times of inverters posing a problem for stability [40].

In addition to inverters forming or following a frequency, there are also attempts in building a virtual synchronous machine with non-zero inertia that acts towards the grid as if it was a mechanical synchronous machine but is driven by power electronics and uses batteries or solar panels as power sources [18]. This research area is very important for today's power engineering and control community [160].

Based on these approaches, we model the grid focusing on AC mechanics (today's standard) and investigate how a decreasing inertia and potential delays of the control may affect the grid stability.

Voltage levels. When consuming energy on a local level, e.g., by turning on the light, using the fridge or connecting a laptop to a power plug, we are drawing energy from the system that has to be generated somewhere. Traditionally, most of the power generation is performed at the extra high voltage level so that losses during long-distance transport are minimized [62, 86, 177]. To connect this extra high voltage to the local low voltage grid and finally our power plugs, a hierarchical structure is used, as shown in Fig. 2.8. Most conventional generators, like nuclear power plants and combustion plants, are connected to the extra high voltage and high voltage levels, which also connect neighboring regions and a few very large costumers using large amounts of electricity. Since these extra high voltages (typically 220 kV or 380 kV in Europe) cannot be connected to most consumers, domestic or industrial, the voltage is reduced at transformers feeding into the sub-transmission or supra-regional distribution grid (of about 36 to 150 kV), which is connected to some generators and large consumers but does typically not transmit energy over long distances or across borders. Additional transformers convert the voltage down to about 1 to 36 kV in regional distribution systems, finally leading to the

local distribution grid, which connects, e.g., to private households [151]. Since the liberalization of the energy market [177], the generation, transmission and distribution are all handled by different companies. Relevant for this thesis is the role of the Transmission System Operator (TSO) who is in charge of controlling the transmission grid, ensuring its stability and providing a certain power quality, i.e., keeping frequency and voltage within certain bounds [86].

Note also that this traditional design works top-down, assuming that most of the energy is generated at higher voltage levels, then transmitted and transformed to lower voltage levels where it is consumed. This effectively leads to a power flow from high voltage levels to low voltage levels. In contrast, installing large amounts of distributed solar and wind generators that are coupled to the low voltage (distribution) grid, leads already today to occasional power flow from lower voltage levels to higher ones [66]. Hence, controlling and regulating the grid completely based on a top-down scheme becomes less feasible.

In the context of distribution grids, the term *microgrid* is also often used when discussing future grid design. It describes a group of electric devices, both generators and consumers, that form their own small grid that has the option to completely disconnect from the large trans-regional transmission grid [40, 81]. Compared to the current hierarchical structure of the grid, microgrids emphasize a local balance of supply and demand, to prevent a disruption of the power grid to affect the whole system [81].

Synchronous zones. When we connect our laptop to a local power plug the energy we receive is not necessarily provided by the closest power plant but by the whole grid we are connected to. But where does this grid start and where does it end? During the last decades, power grids became more connected, i.e., while initially each state had its own power grid they are getting more intertwined [62, 177]. This is exemplified in Figures 2.9 and 2.10 that display the European and North American power grid zones respectively. Each zone is characterized by its own grid frequency, which is kept close to its reference value of $f = 50$ Hz or $f = 60$ Hz by the Transmission System Operators (TSOs) [45, 46]. In Europe, all TSOs are organized in the European Network of Transmission System Operators (ENTSO-E), developing and implementing network codes, coordinating TSO activities, grid extensions and more.

In normal operation, all nodes within a synchronous zone have exactly the same frequency. However, disturbances can induce oscillating deviations from the steady state with frequencies in the sub-second regime called inter-area oscillations [72]. Coupling between two connected synchronous zones, e.g. between Continental Europe and Great Britain, is typically realized via high voltage directed current (HVDC) power transmission so that both zones can have different grid frequencies during the transmission. Contrary, transmission within a synchronous region is mainly done via AC lines. The extent of transmitted power is easily illustrated by a few figures: In 2014, the ENTSO-E members consumed a total of $E_{\text{total}} \approx 3174$ TWh and exchanged a total of $E_{\text{exchange}} \approx 432.5$ TWh [44], i.e., about 13.6 % worth of the total consumption was exchanged between different countries. Returning to our laptop this means, connecting it in Germany may very well result in additional electrical energy to flow from Spain via France to Germany through the ENTSO-E grid to provide the necessary power.

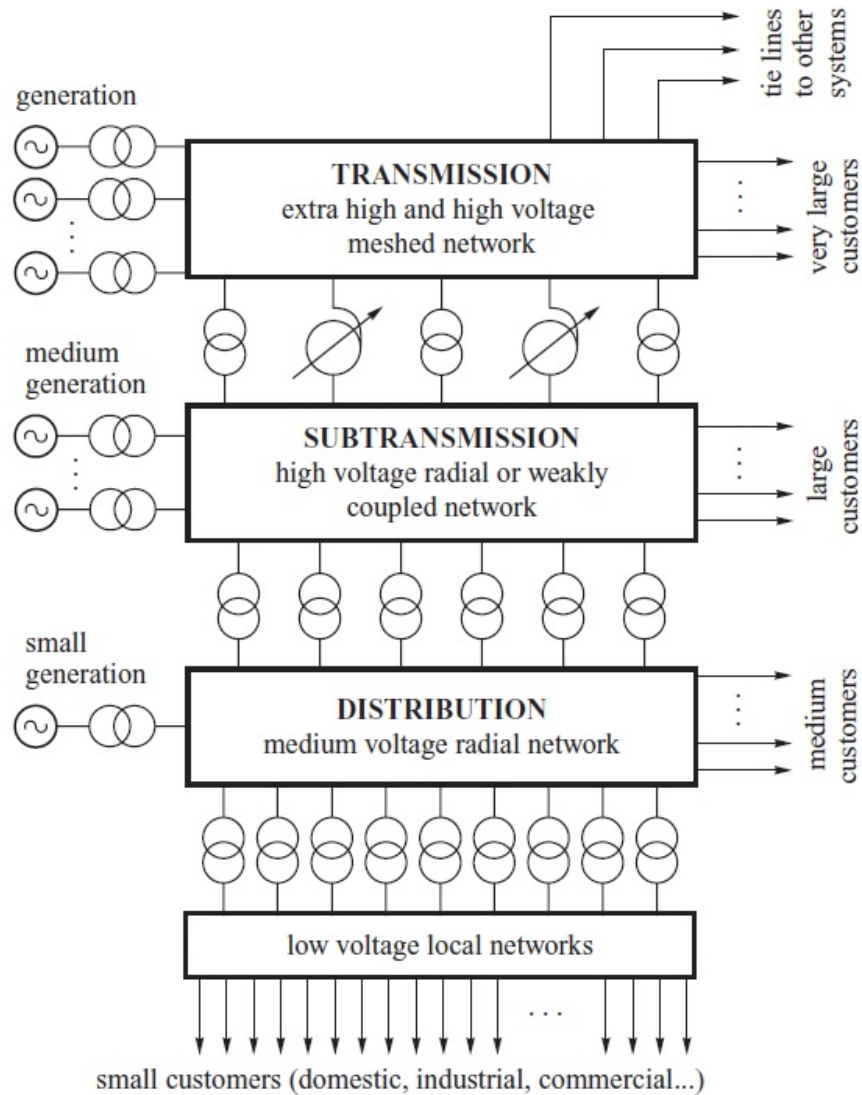


Figure 2.8: The power grid is organized in levels of decreasing voltage. Higher voltages are used for transmission within and across countries while lower voltages connect domestic consumers to the grid. Each level, in particular the transmission level, has synchronous generators feeding power via converters into the grid. The levels are connected via additional fixed and tunable converters. Reproduced from [86] with permission.

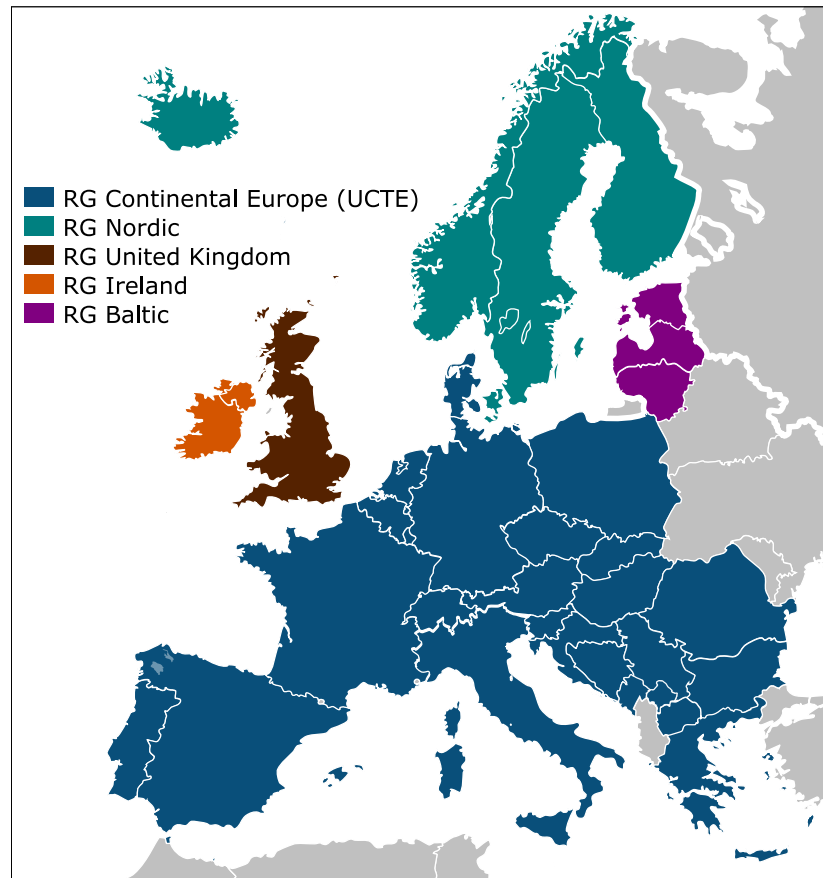


Figure 2.9: The European grid consist of a few large synchronous regions, which are organized by regional groups (RG). The largest synchronous zone is the one of Continental Europe, followed by the grid of the United Kingdom and the Nordic grid. Although part of the Nordic regional group, Iceland has its own synchronous grid, as do several small islands. Reproduced from [168], published under CC-BY-SA-3.0.

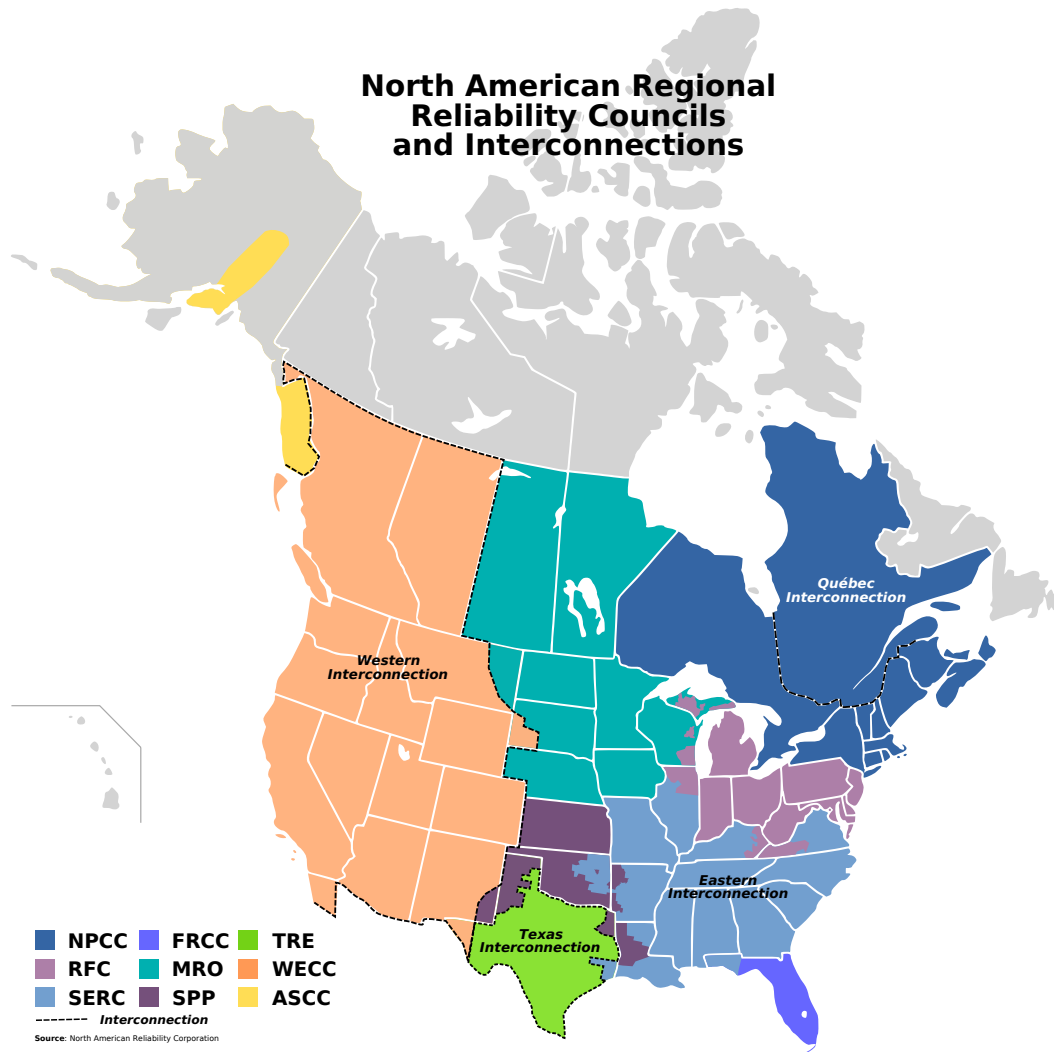


Figure 2.10: North America is organized into four major synchronous zones: The Western Interconnection (light orange), the Texas Interconnection (green), the Québec Interconnection (dark blue) and the Eastern Interconnection (rest). The Eastern Interconnection is by far the largest, similarly sized to the Continental European one [161]. Reproduced from [169], published under CC-BY-SA-3.0.

Control and trading. Electric energy in an AC grid cannot be easily stored in the grid itself so that demand and supply have to match at all times. Establishing large synchronous regions helps because the balancing power does not need to be provided locally but can be drawn from some point in the inter-connected grid [86]. To ensure balance, we need to consider different time scales: On the time scale of 1 day there is a forecast of the expected demand, e.g., based on previous statistics for workdays vs. weekends. Power providers then bid on a *day-ahead* spot market to supply their power to the lowest price possible for the grid [74]. During the day of operation power is also traded to adjust to the actual demand using an *intra-day* spot market acting on a time scale of few hours to several minutes [74]. In addition to market constraints, the power network needs to be able to carry these currents, introducing constraints based on the capacity. Finally, grid operators enforce the *N-1* criterion, which means that the grid has to be able to operate stably even if any single element (of its total N elements) fails. This introduces security constraints to the previously mentioned cost optimization problem [177]. To fulfill all these economic, network and security constraints typically an Optimal Power Flow problem is solved, which solves the optimization under constraints, leading to slightly larger prices compared to the case without security constraints [177]. Alternatively, the power is dispatched following purely economic rules and the constraints are implemented via a re-dispatch by the grid operator [1].

Suppose there is a large fault, e.g., a large power plant suddenly disconnects from the grid, leading to a rapidly decreasing frequency. In such a case, the trading mechanisms discussed so far are too slow to react because blackouts take place on time scales of seconds compared to the minutes or hours that trading needs [19]. Therefore, additional measures are needed to stabilize the grid. After any fault there is no active control yet for about 1 second but the inertia of the rotating machines keeps the frequency close to its reference value [86]. During the following seconds, *primary control* activates in dedicated power plants. Its purpose is to prevent a too abrupt change of frequency, i.e., stop the frequency decrease by supplying additional energy. The frequency then approaches a new steady state, which is not necessarily the reference frequency. To restore the grid to the reference frequency, the *secondary control* is activated a few minutes after the fault. Finally, *tertiary control* also exists in some schemes acting on even slower time scales as a long-term reserve [86], see also Fig. 2.11 for an illustration of the control mechanisms.

During the course of this thesis, we do not model explicit effects of long-term trading and only consider primary control (and real-time prices in Chapter 3) since we are mainly interested in the self-organized, i.e., uncontrolled, response of the complex system power grid. In addition, we are primarily modeling short time scales of typically seconds during which there is no trading and little to no control actions are taken aside from primary control.

2.2.2 Power Grid Models

Power injected in a node

Let us derive the equations determining the power flows and dynamics in a power grid.

Consider two nodes a and b . Let U_a be the voltage at node a , written in polar decomposition as

$$U_a = E_a e^{i\theta_a}, \quad (2.15)$$

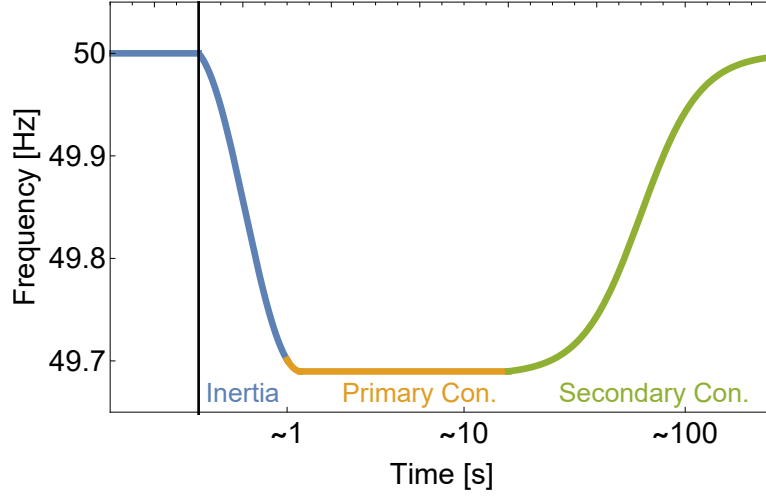


Figure 2.11: Power grid control is divided into different time scales [64]. We display a typical response of the bulk frequency after a large power plant is disconnected (e.g., due to an outage): The first few seconds are uncontrolled and only the inertia prevents large changes. Within the next seconds, the primary control stabilizes the frequency drop to a new equilibrium value. Finally, the secondary control restores the frequency back to its reference value during the following minutes.

with voltage phase angle θ_a , complex unit i and voltage amplitude E_a . The current I_{ab} from b to a is simply given by Ohm's law as

$$I_{ab} = -y_{ab}(U_a - U_b), \quad (2.16)$$

with admittance (inverse impedance) y_{ab} of the line (a, b) . Instead of admittance, the nodal admittance matrix \mathbf{Y} is often used, which is defined as the Laplacian of the admittance \mathbf{y} [86]:

$$y_{ab} = G_{ab} + iB_{ab} = \begin{cases} -Y_{ab} & \text{if } a \neq b \\ \sum_b Y_{ab} & \text{if } a = b \end{cases}, \quad (2.17)$$

with conductance \mathbf{G} and susceptance \mathbf{B} . In terms of the nodal admittance matrix \mathbf{Y} , the current is expressed as

$$I_{ab} = Y_{ab}(U_a - U_b). \quad (2.18)$$

The complex power S_{ab} from b to a is then given as [89]:

$$S_{ab} = U_a I_{ab}^* \quad (2.19)$$

$$= U_a Y_{ab}^* (U_a^* - U_b^*) \quad (2.20)$$

$$= E_a e^{i\theta_a} Y_{ab}^* (E_a e^{-i\theta_a} - E_b e^{-i\theta_b}) \quad (2.21)$$

$$= Y_{ab}^* (E_a^2 - E_a E_b e^{i(\theta_a - \theta_b)}) \quad (2.22)$$

$$= Y_{ab}^* (E_a^2 - E_a E_b [\cos(\theta_a - \theta_b) + i \sin(\theta_a - \theta_b)]). \quad (2.23)$$

Due to energy conservation (Tellegen's theorem), we get the power injected into node a by summing

over all potentially neighboring nodes b

$$S_a = \sum_{b=1}^N S_{ab} = \sum_{b=1}^N Y_{ab}^* (E_a^2 - E_a E_b [\cos(\theta_a - \theta_b) + i \sin(\theta_a - \theta_b)]). \quad (2.24)$$

Applying this and splitting the apparent power into its real part, i.e., active power P and its imaginary part, i.e., reactive power Q gives

$$S_a = P_a + iQ_a \quad (2.25)$$

$$= \sum_{b=1}^N [G_{ab} E_a E_b \cos(\theta_a - \theta_b) + B_{ab} E_a E_b \sin(\theta_a - \theta_b)] \quad (2.26)$$

$$+ i \sum_{b=1}^N [G_{ab} E_a E_b \sin(\theta_a - \theta_b) - B_{ab} E_a E_b \cos(\theta_a - \theta_b)]. \quad (2.27)$$

Switching indices $a \rightarrow i$ and $b \rightarrow j$ to be comparable with the following publications¹, the active (real) and reactive (imaginary) transmitted powers incoming to node i read

$$P_i = \sum_{j=1}^N E_i E_j [G_{ij} \cos(\theta_i - \theta_j) + B_{ij} \sin(\theta_i - \theta_j)], \quad (2.28)$$

$$Q_i = \sum_{j=1}^N E_i E_j [G_{ij} \sin(\theta_i - \theta_j) - B_{ij} \cos(\theta_i - \theta_j)]. \quad (2.29)$$

Finally, we note that conductances \mathbf{G} are typically smaller than susceptances \mathbf{B} by a factor of $B/G \approx 5 \dots 10$ [177].

Power flow equations

The power flow equations are often used in engineering literature to determine the flows on the lines, especially for security purposes [76, 177]. Active and reactive power are modeled using Eqs. (2.28) and (2.29). The left hand side of each equation is the active/reactive power effectively generated at this node. In total each node (or *bus*) of the power grid is characterized by four quantities: active power P_i , reactive power Q_i , voltage amplitude E_i and voltage phase angle θ_i . However, with only two equations per node, two of those four have to be fixed for each node, leading to different bus types:

At the *slack (swing) bus* the voltage amplitude E_i and voltage phase angle θ_i are specified, while P_i and Q_i are unspecified to compensate power loss in the system. Typically, this bus is one of the generators, stabilizing the grid. In addition, there are *voltage-controlled buses (PV)*, which are usually generator nodes for which active power P_i and voltage amplitude E_i are fixed while the equations are solved for Q_i and θ_i . Finally, there exist *load buses (PQ)* with given active power P_i and reactive power Q_i , but unknown voltage amplitude E_i and voltage phase angle θ_i [177].

¹We wanted to avoid confusion of index and imaginary unit i in this derivation.

Dynamical equations

In contrast to the power flow equations, the swing equation only considers the long-distance transmittable power, i.e., the active power given by Eq. (2.28), neglecting any reactive powers, which is often compensated locally [76]:

$$P_i^{\text{trans}} = \sum_{j=1}^N E_i E_j [G_{ij} \cos(\theta_i - \theta_j) + B_{ij} \sin(\theta_i - \theta_j)]. \quad (2.30)$$

Furthermore, let us derive an equation of motion for each node i , which we characterize by its angular velocity ω_i and its voltage phase angle θ_i . The law of energy conservation at each generator i reads:

$$P_i^{\text{mech}} = P_i^{\text{diss}} + P_i^{\text{acc}} + P_i^{\text{trans}}, \quad (2.31)$$

i.e., the mechanical power driving a generator P_i^{mech} has to equal the dissipated power P_i^{diss} plus the accumulated kinetic power P_i^{acc} plus the transmitted power. Let us describe the angular motion of generator i by

$$\phi_i(t) = \Omega t + \theta_i \quad (2.32)$$

with reference angular velocity $\Omega = 2\pi \times 50$ Hz or $\Omega = 2\pi \times 60$ Hz and relative machine angle θ_i . The energy dissipated at this generator is then

$$P_i^{\text{diss}} = D_i \left(\frac{d\phi_i}{dt} \right)^2, \quad (2.33)$$

with damping D_i [55, 86, 89]. A simple argument for this form is that friction forces F^{diss} are proportional to velocities and powers are proportional to velocity times force

$$F^{\text{diss}} \sim \frac{d\phi}{dt}, \quad (2.34)$$

$$P^{\text{diss}} \sim F^{\text{diss}} \frac{d\phi}{dt}, \quad (2.35)$$

$$P^{\text{diss}} \sim \left(\frac{d\phi}{dt} \right)^2. \quad (2.36)$$

Next, the energy stored in the rotation of the inertial machine is given by

$$P_i^{\text{acc}} = \frac{d}{dt} E_i^{\text{kin}} = \frac{1}{2} M_i \frac{d}{dt} \left(\frac{d\phi_i}{dt} \right)^2, \quad (2.37)$$

with moment of inertia M_i . Let us assume that deviations from the reference frequency are small compared to the reference $|\dot{\theta}| \ll \Omega$, i.e., the grid operates close to its steady state. Then, plugging Eq.

(2.32) into the damping Eq. (2.33) yields

$$P_i^{\text{diss}} = D_i \left(\Omega + \left(\frac{d\theta_i}{dt} \right) \right)^2 \quad (2.38)$$

$$\approx D_i \Omega^2 + 2D_i \Omega \left(\frac{d\theta}{dt} \right). \quad (2.39)$$

Doing the same for the inertial power of Eq. (2.37) yields

$$P_i^{\text{acc}} = \frac{1}{2} M_i \frac{d}{dt} \left(\Omega + \left(\frac{d\theta_i}{dt} \right) \right)^2 \quad (2.40)$$

$$= \frac{M_i}{2} \left(2\Omega \frac{d^2\theta_i}{dt^2} + 2 \frac{d\theta_i}{dt} \frac{d^2\theta_i}{dt^2} \right) \quad (2.41)$$

$$\approx M_i \Omega \frac{d^2\theta_i}{dt^2}. \quad (2.42)$$

Substituting all power terms into the energy conservation law (2.31) gives the equation of motion

$$M_i \Omega \frac{d^2\theta_i}{dt^2} = P_i^{\text{mech}} - D_i \Omega^2 - 2D_i \Omega \frac{d\theta_i}{dt} - P_i^{\text{trans}}, \quad (2.43)$$

which is the *swing equation*. Plugging in the transmitted power gives

$$\begin{aligned} M_i \Omega \frac{d^2\theta_i}{dt^2} &= P_i^{\text{mech}} - D_i \Omega^2 - 2D_i \Omega \frac{d\theta_i}{dt} \\ &\quad - \sum_{j=1}^N E_i E_j [G_{ij} \cos(\theta_i - \theta_j) + B_{ij} \sin(\theta_i - \theta_j)]. \end{aligned} \quad (2.44)$$

This thesis focuses on effects of the transmission grid for which ohmic losses are negligible [7]. Using this simplification, we set $G_{ij} = 0$ in Eq. (2.44) and define the following abbreviations:

$$P_i = \frac{P_i^{\text{mech}} - D_i \Omega^2}{M_i \Omega}, \quad (2.45)$$

$$\gamma_i = 2 \frac{D_i}{M_i}, \quad (2.46)$$

$$A_{ij} = \frac{B_{ij}}{M_i \Omega}. \quad (2.47)$$

Thereby, the equations of motion simplify to

$$\frac{d}{dt} \theta_i = \omega_i, \quad (2.48)$$

$$\frac{d}{dt} \omega_i = P_i - \gamma_i \omega_i + \sum_{j=1}^N A_{ij} E_i E_j \sin(\theta_j - \theta_i). \quad (2.49)$$

In the following, we consider two explicit dynamical models often used in this thesis, which are based on this simplified swing equation.

2nd order model. So far, our variables include the voltage phase angle θ and angular velocity ω . While the voltage amplitude E_i could also change over time, this is typically not the case for extra high voltage transmission grids [76] so that we assume constant and identical voltage amplitudes throughout the grid $E_i = E_0 \forall i \in \{1, \dots, N\}$. Using this simplification leads to the 2nd order swing equation in the following form

$$\frac{d}{dt}\theta_i(t) = \omega_i(t), \quad (2.50)$$

$$\frac{d}{dt}\omega_i(t) = P_i - \gamma_i\omega_i(t) + \sum_{j=1}^N K_{ij} \sin(\theta_j(t) - \theta_i(t)), \quad (2.51)$$

with coupling constant

$$K_{ij} = A_{ij}E_0^2 = \frac{B_{ij}E_0^2}{M_i\Omega}. \quad (2.52)$$

Note that the susceptance matrix \mathbf{B} is symmetric since the current is free to flow in both directions along a transmission line. Furthermore, we typically assume similar inertia values M_i through the grid leading to also symmetric coupling K_{ij} .

3rd order model. Now let us consider that the voltage amplitudes E_i are not constant but change over time. Then, the system is characterized by the following equations of motion after renormalization of E [11, 85, 86, 135]:

$$\begin{aligned} \frac{d}{dt}\theta_i(t) &= \omega_i(t), \\ \frac{d}{dt}\omega_i(t) &= P_i - \gamma_i\omega_i(t) + \sum_{j=1}^N E_i(t) E_j(t) B_{ij} \sin(\theta_j(t) - \theta_i(t)), \\ \frac{d}{dt}E_i(t) &= \frac{1}{T_E} \cdot \left(E_f(t) - E_i(t) + X_i \sum_{j=1}^N E_j(t) B_{ij} \cos(\theta_j(t) - \theta_i(t)) \right), \end{aligned} \quad (2.53)$$

with the voltage time scale $T_E < 1$ s, the susceptance matrix B_{ij} including self-coupling terms B_{ii} , voltage set-point $E_f = 1$ and the voltage droop X , which is the difference of the static and transient reactance along the d-axis $X_i = X_i^{(d)} - X_i^{(d)'}$. For $X_i = 0$ and $E_i(0) = 1$ the voltage remains at the fixed point $E_i^* = 1$ at all times and reproduces the second order model. In contrast, for $X_i > 0$ deviations from the second order model are observed. Note also that the voltage dynamics is typically slower than the angle and angular velocity dynamics, allowing to neglect it for short time scales.

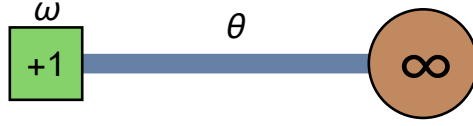


Figure 2.12: Illustration of one generator coupled to the infinite grid. The generator has power $P = 1/s^2$, angle θ relative to the bulk and angular velocity ω .

2.2.3 Infinite Grid

Let us apply the basics of power grid models and methods reviewed so far on a simple test case, the infinite grid model [86, 92]. There, we assume that one generator with power $P = 1/s^2$ is connected to the bulk grid, which is assumed to be so large that its angle and frequency are fixed, see Fig. 2.12. Following the simplified second order swing equation, its equation of motion is

$$\frac{d}{dt}\theta = \omega, \quad (2.54)$$

$$\frac{d}{dt}\omega = P - \gamma\omega - K \sin(\theta), \quad (2.55)$$

with voltage angle θ relative to the (infinite) bulk grid, angular velocity ω , coupling constant K , mechanical power P and damping γ . For this example, we set these parameters to $K = 8/s^2$, $P = 1/s^2$, $\gamma = 0.1/s$.

We obtain the fixed point of this system by setting $\frac{d}{dt}\theta = 0$ and $\frac{d}{dt}\omega = 0$ in Eqs. (2.54) and (2.55). This leads to

$$\omega^* = 0, \quad (2.56)$$

$$\theta_1^* = \arcsin\left(\frac{P}{K}\right), \quad (2.57)$$

$$\theta_2^* = \pi - \arcsin\left(\frac{P}{K}\right), \quad (2.58)$$

with two solutions for the angle θ . We note that for $K < P$ there is no fixed point as the capacity between the generator and the bulk is too small to transmit the generated power.

Next, we perform a linear stability analysis of the two fixed points (ω^*, θ_1^*) and (ω^*, θ_2^*) . Computing the Jacobian for the system yields

$$J = \begin{pmatrix} 0 & 1 \\ -K \cos(\theta^*) & -\gamma \end{pmatrix}. \quad (2.59)$$

The characteristic equation for the Jacobian is

$$p(\lambda) = \lambda^2 + \gamma\lambda + K \cos(\theta^*), \quad (2.60)$$

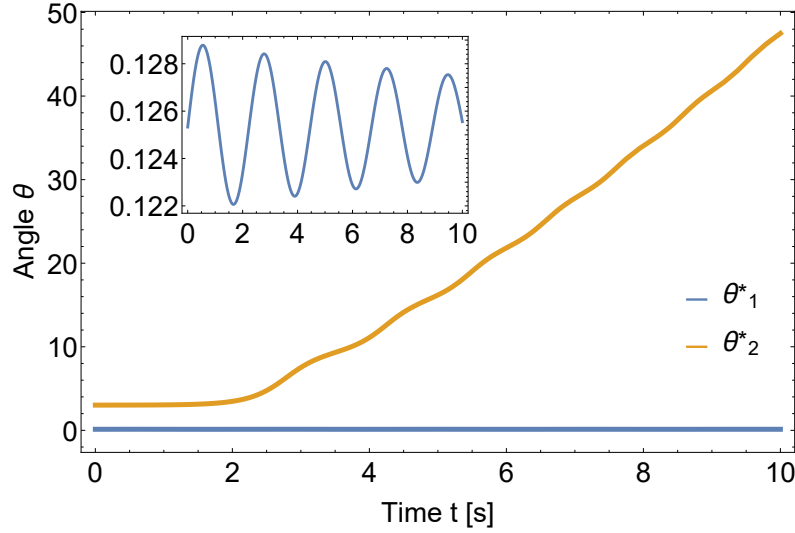


Figure 2.13: Trajectories of the infinite grid system close to the two fixed points. We initialize the system close to its two fixed points with $(\omega_1(0) = 0.01/s, \theta_1(0) = \arcsin(\frac{P}{K}))$ (blue curves) and $(\omega_2(0) = 0.01/s, \theta_2(0) = \pi - \arcsin(\frac{P}{K}))$ (orange curves) and observe that the first fixed point is stable while the second is not. The inset shows that the system returns to the fixed point angle θ_1^* with small oscillations. Parameters are $K = 8/s^2$, $P = 1/s^2$, $\gamma = 0.1/s$.

which is solved to give the eigenvalues

$$\lambda_{1/2} = -\frac{\gamma}{2} \pm \sqrt{\frac{\gamma^2}{4} - K \cos(\theta^*)}. \quad (2.61)$$

The fixed point is stable if both eigenvalues have a negative real part, i.e., if $K \cos(\theta) > 0$. Using parameters $K = 8/s^2$, $P = 1/s^2$, $\gamma = 0.1/s$, the eigenvalue expressions read for both fixed points

$$K \cos(\theta_1^*) \approx 7.94/s^2, \quad (2.62)$$

$$K \cos(\theta_2^*) \approx -7.94/s^2, \quad (2.63)$$

$$\lambda_{1/2}^{\theta_1^*} \approx -0.05 \pm 2.82i, \quad (2.64)$$

$$\lambda_{1/2}^{\theta_2^*} \approx \pm 2.87, \quad (2.65)$$

i.e., fixed point (ω^*, θ_1^*) is stable, while fixed point (ω^*, θ_2^*) is unstable. We illustrate the dynamics of the grid close to each fixed point in Fig. 2.13, where we observe the stability of the first and the instability of the second fixed point.

2.3 Stochastic Equations

In Chapters 5 and 6, we investigate the power grid when subject to random noise. We use stochastic differential equations, which give the equation of motion for the state $x(t)$, and Fokker-Planck equations, i.e., equations of motion for the probability density function $p(x)$ of the stochastic state $x(t)$.

Here, we present some basics on stochastic calculus.

Let us consider the one-dimensional equation of motion

$$\frac{dx}{dt} = a(x, t) + b(x, t) \xi(t), \quad (2.66)$$

where ξ is a random variable, which satisfies

$$\langle \xi(t) \rangle = 0, \quad (2.67)$$

$$\langle \xi(t) \xi(t') \rangle = \delta(t - t'), \quad (2.68)$$

i.e., its mean value is zero and it is uncorrelated unless measured at identical times. ξ is then called white noise [56, 118].

Equation (2.66) is a Langevin equation and intuitively extends (deterministic) ordinary differential equations (ODEs) into stochastic differential equations (SDEs). First, we note that no real process exactly fulfills the conditions for the noise ξ . Having mean zero is possible but realistic processes have a finite correlation time, instead of a delta peak. Next, we have to think how a trajectory of $x(t)$ would look like. For ODEs, we would simply integrate the differential

$$x(t) - x(0) = \int_0^t \frac{dx}{ds}(s) ds. \quad (2.69)$$

However, to compute this integral, we need to compute

$$y(t) = \int_0^t \xi(s) ds, \quad (2.70)$$

which turns out to be the Wiener process $y(t) = W(t)$ [56]. Hence, $\xi(t)$ is the derivative of the Wiener process. However, the Wiener process does not have a time-derivative and the Langevin equation (2.66) is strictly speaking only defined when integrating both sides, as in (2.69). Treating expressions like (2.66) and (2.69) mathematically rigorously, requires the definition of stochastic integrals and the introduction of the Itô calculus, for which we refer to [31, 56, 119]. During this thesis, we use the Langevin equation due to its intuitive notation, keeping in mind that it should be interpreted as an integral equation or connected to a Fokker-Planck equation as described below. Finally, we note that there are two main interpretations for stochastic equations and integrals, one by Stratonovich and one by Itô [162]. In case of additive noise, i.e. $b(x) \equiv b_0$, which is the case for all our calculations, both interpretations yield exactly the same results. For any equations that are more general, we adopt the notation following Itô.

2.3.1 Fokker-Planck Equations

The Langevin equation (2.66) can be connected to a partial differential equation of the probability density function of the random variable $x(t)$, called a Fokker-Planck equation [56, 118]:

$$\frac{\partial p}{\partial t}(x, t) = -\frac{\partial}{\partial x} [a(x, t) p(x, t)] + \frac{1}{2} \frac{\partial^2}{\partial x^2} [b(x, t)^2 p(x, t)]. \quad (2.71)$$

In general, multidimensional problems use a state vector \mathbf{x} , changing the constants a and b to a vector \mathbf{a} , with components a_i , and matrix \mathbf{B} , with components B_{ij} , respectively. The equation of motion is then given by

$$\frac{d\mathbf{x}}{dt} = \mathbf{a}(\mathbf{x}, t) + \mathbf{B}(\mathbf{x}, t) \boldsymbol{\xi}(t), \quad (2.72)$$

or written in component form

$$\frac{dx_i}{dt} = a_i(\mathbf{x}, t) + \sum_{j=1}^N B_{ij}(\mathbf{x}, t) \xi_j(t) \quad i \in \{1, \dots, N\}, \quad (2.73)$$

and gives the following Fokker-Planck equation [56]:

$$\frac{\partial p}{\partial t}(\mathbf{x}, t) = - \sum_{i=1}^N \frac{\partial}{\partial x_i} [a_i(\mathbf{x}, t) p(\mathbf{x}, t)] + \frac{1}{2} \sum_{i,j=1}^N \frac{\partial}{\partial x_i} \frac{\partial}{\partial x_j} [\mathbf{B}(\mathbf{x}, t) \mathbf{B}^T(\mathbf{x}, t) p(\mathbf{x}, t)], \quad (2.74)$$

which is written in component form as

$$\frac{\partial p}{\partial t}(\mathbf{x}, t) = - \sum_{i=1}^N \frac{\partial}{\partial x_i} [a_i(\mathbf{x}, t) p(\mathbf{x}, t)] + \frac{1}{2} \sum_{i,j=1}^N \frac{\partial}{\partial x_i} \frac{\partial}{\partial x_j} \left[\left(\sum_{k=1}^N B_{jk}(\mathbf{x}, t) B_{ik}(\mathbf{x}, t) \right) p(\mathbf{x}, t) \right]. \quad (2.75)$$

2.3.2 Ornstein-Uhlenbeck Process

One especially important process is the *Ornstein-Uhlenbeck process* for which we provide the general solution here. Consider an overdamped particle moving in a quadratic potential $V(x) = \frac{a}{2}x^2$ with positive constant $a > 0$. We neglect inertial forces so that the equation of motion reads

$$\frac{dx}{dt}(t) = -\frac{\partial V}{\partial x}(x) = -ax(t).$$

When this particle is subject to Gaussian noise ξ with amplitude ϵ , the stochastic equation of motion becomes

$$\frac{dx}{dt}(t) = -ax(t) + \epsilon \xi(t),$$

which is the Ornstein-Uhlenbeck process. Following [56, 118], the Fokker-Planck equation for this process is

$$\frac{\partial p}{\partial t}(x, t) = \frac{\partial}{\partial x} (a \cdot x \cdot p(x, t)) + \epsilon^2 \frac{\partial^2 p}{\partial x^2}(x, t) \quad (2.76)$$

and the general dynamical solution to the Ornstein-Uhlenbeck process is given by

$$p(x, t) = \sum_{n=0}^{\infty} \sqrt{\frac{a}{2^n n! \pi \sqrt{\epsilon}}} e^{-\frac{a}{\sqrt{\epsilon}} x^2} H_n \left(x \sqrt{\frac{a}{\sqrt{\epsilon}}} \right) e^{-nat} A_n, \quad (2.77)$$

with amplitudes

$$A_n = \int_{-\infty}^{\infty} p(x, 0) H_n \left(x \sqrt{\frac{a}{\sqrt{\epsilon}}} \right) (2^n n!)^{-\frac{1}{2}} dx, \quad (2.78)$$

where H_n is the Hermite polynomial of n th order. As usual, boundary conditions are chosen so that the probability density function and its spatial derivative vanish at infinity

$$\lim_{|x| \rightarrow \infty} p(x, t) = 0, \quad (2.79)$$

$$\lim_{|x| \rightarrow \infty} \frac{\partial}{\partial x} p(x, t) = 0. \quad (2.80)$$

Often, we will only be interested in the simpler, stationary solution

$$p_{\text{stationary}}(x) = \sqrt{\frac{a}{2\pi\epsilon^2}} e^{-\frac{a}{2\epsilon^2}x^2}, \quad (2.81)$$

obtained via the limit $t \rightarrow \infty$. Furthermore, the non-normalized auto-correlation is given by an exponentially decaying function [56]

$$\langle x(t) x(t + \Delta t) \rangle = \frac{\epsilon}{2a} \exp[-a\Delta t]. \quad (2.82)$$

2.4 Distributions

In Chapter 6, we investigate different probability distributions to represent the statistics of the power grid frequency. Here, we briefly review two of the most important distributions, Lévy-stable and q-Gaussian distributions and begin by quantifying some moments of distributions.

2.4.1 Moments

The power grid frequency data that we recorded is often skewed or displays heavy tails, see also Chapter 6. To quantify this statement, we define the first four (normalized) moments of a distribution [58,166].

Given M measurements of a discrete stochastic variable x , as x_1, x_2, \dots, x_M , its n -th moment is defined as

$$\mu_n := \frac{1}{M} \sum_{i=1}^M x_i^n. \quad (2.83)$$

The first moment of a distribution is the mean $\mu_1 \equiv \mu$. Instead of the second moment, we often use the square root of the centralized second moment, i.e., the standard deviation σ , which is defined as

$$\sigma := \sqrt{\frac{1}{M} \sum_{i=1}^M (x_i - \mu)^2}. \quad (2.84)$$

These two quantities are common when characterizing Gaussian distributions. In addition, we use the normalized third and fourth moments, the skewness β and kurtosis κ , respectively, which are defined

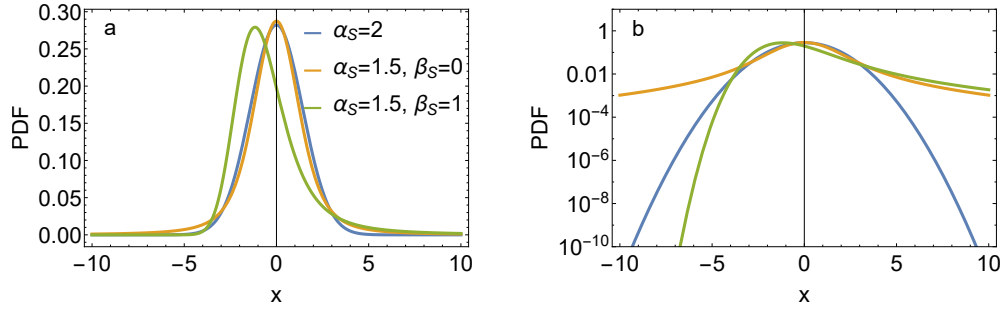


Figure 2.14: Probability density function (PDF) of stable distributions. **a**: Linear scale of the PDF. **b**: Log-Scale of the PDF. For $\alpha_S = 2$, the distribution is a Gaussian distribution, regardless of β_S . For $\alpha_S < 2$, the distribution has heavy tails (see especially the log-scale) and is skewed if $\beta \neq 0$ (positive skewness in the case of $\beta_S = 1$). Other parameters are $\mu_S = 0$ and $\sigma_S = 1$.

as

$$\beta := \frac{1}{M} \sum_{i=1}^M \left(\frac{x_i - \mu}{\sigma} \right)^3, \quad (2.85)$$

$$\kappa := \frac{1}{M} \sum_{i=1}^M \left(\frac{x_i - \mu}{\sigma} \right)^4. \quad (2.86)$$

A Gaussian distribution is symmetric and hence the skewness β equals zero. A non-zero skewness implies a distribution that is not symmetric around the mean but is more pronounced in one direction, see e.g. Fig. 2.14. The kurtosis meanwhile quantifies how much of the distribution is found in its tails. A Gaussian distribution has $\kappa_{\text{Gauss}} = 3$ while a higher value of the kurtosis indicates an increased likelihood of large deviations, leading to a higher probability density in the tails, i.e., heavy tails.

2.4.2 Lévy-stable Distributions

Lévy-stable, α -stable or just stable distributions are often observed in nature [93, 110], displaying heavy tails and skewness. We introduce them mainly following [128]. First, we note that Gaussian distributions are a special case of stable distributions.

Let X be a random variable. It follows a stable distribution, if there exists a positive C_n and real D_n for each $n \geq 2$ such that

$$X_1 + X_2 + \dots + X_n \sim C_n X + D_n, \quad (2.87)$$

where X_1, X_2, \dots, X_n are independent copies of X and $X \sim Y$ denotes that X and Y follow the same distribution. If X is following a stable distribution, then $C_n = n^{1/\alpha_S}$ [128].

We list some key properties, where we often omit the special case $\alpha_S = 1$ because it is of no special interest for us. The interested reader is directed to [128] or literature on Cauchy distributions.

The characteristic function of a stable distribution is given as

$$S_k(\alpha_S, \beta_S, \sigma_S, \mu_S) = \begin{cases} \exp[-\sigma^{\alpha_S} |k|^{\alpha_S} (1 - i\beta_S \text{sign}(k) \tan(\frac{\pi\alpha_S}{2}) + i\mu k)], & \text{if } \alpha \neq 1, \\ \exp[-\sigma |k| (1 + i\beta_S \text{sign}(k) \tan(\frac{\pi\alpha_S}{2}) + i\mu k)], & \text{if } \alpha_S = 1. \end{cases} \quad (2.88)$$

A univariate (single variable) stable distribution is described by four parameters. The stability parameter $\alpha_S \in (0, 2]$ determines the tails of the distribution. For $\alpha_S < 2$, the distributions do not have a defined variance and for $\alpha_S \leq 1$ they do not have a mean since the corresponding integrals do not converge. Furthermore, the tails of the probability density function follow a power law $p(x) \propto |x|^{-\alpha_S-1}$. Finally, a stable distribution resembles a Gaussian distribution for $\alpha_S = 2$ and a Cauchy distribution for $\alpha_S = 1$. The remaining parameters are the skewness parameter $\beta_S \in [-1, 1]$, the scale parameter $\sigma_S \in (0, \infty)$ and the location parameter $\mu_S \in (-\infty, \infty)$. For $\alpha_S > 1$, the location parameter μ_S gives the mean of the distribution. We will often set it to zero. For $\alpha_S = 2$, i.e., the Gaussian case, the standard deviation of the distribution is determined by the scale parameter as $\sigma = \sqrt{2}\sigma_S$. We always express stable distributions in terms of their characteristic function since the probability density function does not have a closed form, see Fig. 2.14 for examples.

Consider two independent random stable variables $X_i \sim S_k(\alpha_S^i, \beta_S^i, \sigma_S^i, \mu_S^i)$, $i = 1, 2$. Their sum is again a stable distribution, if $\alpha_S^1 = \alpha_S^2 = \alpha_S$. Their sum is distributed according to $X_1 + X_2 \sim S_k(\alpha_S, \beta_S, \sigma_S, \mu_S)$ [128], with

$$\sigma_S = \left((\sigma_S^1)^{\alpha_S} + (\sigma_S^2)^{\alpha_S} \right)^{1/\alpha_S}, \quad \beta_S = \frac{\beta_S^1 (\sigma_S^1)^{\alpha_S} + \beta_S^2 (\sigma_S^2)^{\alpha_S}}{(\sigma_S^1)^{\alpha_S} + (\sigma_S^2)^{\alpha_S}}, \quad \mu_S = \mu_S^1 + \mu_S^2. \quad (2.89)$$

Let X be a stable distribution $X \sim S_k(\alpha_S, \beta_S, \sigma_S, \mu_S)$ and a be a non-zero real constant. Then

$$aX \sim S_k(\alpha_S, \text{sign}(a)\beta_S, |a|\sigma_S, a\mu_S), \text{ if } \alpha_S \neq 1. \quad (2.90)$$

With these properties, we can calculate the distribution of a large sum of stable distributions X_i :

$$\sum_{i=1}^N \epsilon_i X_i. \quad (2.91)$$

First, we note that the factor ϵ can be easily absorbed in the scale parameter: $X_i \sim S_k(\alpha_S^i, \beta_S^i, \sigma_S^i, \mu_S^i) \Rightarrow \epsilon_i X_i \sim S_k(\alpha_S^i, \beta_S^i, \epsilon_i \sigma_S^i, \epsilon_i \mu_S^i)$, where we assume that the constant $\epsilon_i > 0$. To shorten notation, we set $\sigma_S^i = 1$. Let us start with two variables, which are identically distributed but multiplied by a different factor $\epsilon_1 X_1 \sim S_k(\alpha_S, \beta_S, \epsilon_1, \epsilon_1 \mu_S)$ and $\epsilon_2 X_2 \sim S_k(\alpha_S, \beta_S, \epsilon_2, \epsilon_2 \mu_S)$ and whose sum is distributed as (using Eq. (2.89))

$$X_1 + X_2 \sim S_k\left(\alpha_S, [\epsilon_1^{\alpha_S} + \epsilon_2^{\alpha_S}]^{1/\alpha_S}, \beta_S, (\epsilon_1 + \epsilon_2) \mu_S\right). \quad (2.92)$$

Using this as our induction basis, we formulate our induction hypothesis to be

$$\sum_{i=1}^N \epsilon_i X_i \sim S_k\left(\alpha_S, \left[\sum_{i=1}^N \epsilon_i^{\alpha_S}\right]^{1/\alpha_S}, \beta_S, \sum_{i=1}^N \epsilon_i \mu_S\right), \quad (2.93)$$

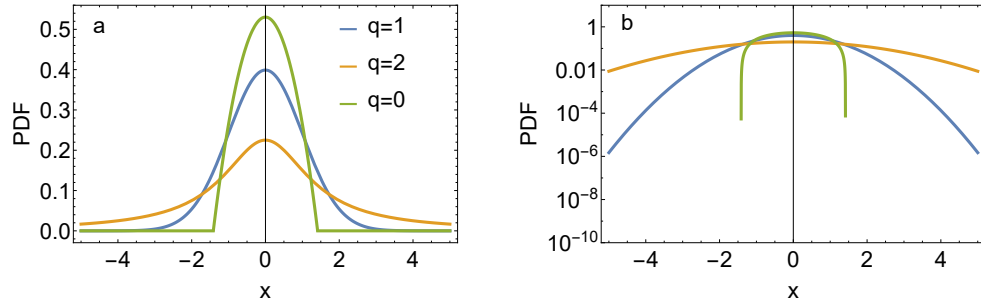


Figure 2.15: Probability density function (PDF) of q -Gaussian distributions. **a:** Linear scale of the PDF. **b:** Log-Scale of the PDF. For $q = 1$, the distribution is a Gaussian distribution, while it has heavy tails for $q > 1$ and only bounded support for $q < 1$. We use the parameter $\beta = 1$.

where $\epsilon_i X_i \sim S_k(\alpha_S, \beta_S, \epsilon_i, \epsilon_i \mu_S)$. We proof this by performing the inductive step, defining $\sum_{i=1}^N \epsilon_i X_i =: Y \sim S_k(\alpha_S, \beta_S, \epsilon_Y, \mu_S^Y)$:

$$\sum_{i=1}^N \epsilon_i X_i + \epsilon_{N+1} X_{N+1} = Y + \epsilon_{N+1} X_{N+1} \sim S_k\left(\alpha_S, [\epsilon_Y^{\alpha_S} + \epsilon_{N+1}^{\alpha_S}]^{1/\alpha_S}, \beta_S, \mu_S^Y + \epsilon_{N+1} \mu_S\right) \quad (2.94)$$

$$\sim S_k\left(\alpha_S, \left[\sum_{i=1}^N \epsilon_i^{\alpha_S}\right] + \epsilon_{N+1}^{\alpha_S}\right)^{1/\alpha_S}, \beta_S, \sum_{i=1}^N \epsilon_i \mu_S + \epsilon_{N+1} \mu_S \Big), \quad (2.95)$$

$$\sum_{i=1}^{N+1} \epsilon_i X_i \sim S_k\left(\alpha_S, \left[\sum_{i=1}^{N+1} \epsilon_i^{\alpha_S}\right]^{1/\alpha_S}, \beta_S, \sum_{i=1}^{N+1} \epsilon_i \mu_S\right). \quad (2.96)$$

In the special case that all constants ϵ_i are equal, i.e., $\epsilon_i = \epsilon \forall i$ we get

$$\sum_{i=1}^N \epsilon_i X_i \sim S_k\left(\alpha_S, \epsilon N^{1/\alpha_S}, \beta_S, N \epsilon \mu_S\right). \quad (2.97)$$

2.4.3 q -Gaussian Distributions

A q -Gaussian distribution is another generalization of a Gaussian distribution, which we use in conjunction with the concept of superstatistics [16] in Chapter 6. These distributions were introduced by Tsallis when generalizing statistical mechanics [156,157]. We do not cover this “nonextensive statistical mechanics” but only use q -Gaussians as a good description of our data in the context of superstatistics.

The probability density function of a q -Gaussian is given as

$$p(x) = \frac{\sqrt{\beta}}{C_q} e_q(-\beta x^2), \quad (2.98)$$

where $\beta \in (0, \infty)$ and $q \in (-\infty, 3)$ are shape parameters, e_q is the q -exponential defined as

$$e_q(x) = [1 + (1 - q)x]^{1/(1-q)} \quad (2.99)$$

and C_q is the normalization factor, see Fig. 2.15 for examples.

For $q = 1$ the q -Gaussian distribution becomes a Gaussian distribution with standard deviation $\sigma = \beta$.

Connection to superstatistics. Suppose we have a dynamical system, characterized by its variable $x(t)$, that follows a stochastic equation of motion given as

$$\frac{dx}{dt} = -ax(t) + b\xi(t), \quad (2.100)$$

with Gaussian white noise $\xi(t)$, and constants $a > 0$ and $b > 0$. We have previously seen (Section 2.3.2) that this is the Ornstein-Uhlenbeck process and that the variable $x(t)$ is distributed according to a Gaussian distribution.

To extend this to superstatistics [15, 16], we have to allow the constants a and b to change over some long time scale T , which has to be long compared to the intrinsic relaxation of the system $\tau := 1/a \ll T$. To be more specific, let us assume that the expression $\beta := a/b^2$ changes over time and follows a χ^2 distribution:

$$p(\beta) = \frac{1}{\Gamma\left(\frac{n}{2}\right)} \left(\frac{n}{2\beta_0}\right)^{n/2} \beta^{n/2-1} \exp\left(-\frac{n\beta}{2\beta_0}\right), \quad (2.101)$$

with degree n , mean β_0 and Gamma function Γ . Next, assume that the changes of β are much slower than the relaxation time scale, defined by $\tau = 1/a$, during which the system settles down for one fixed β . Then, the conditional probability to find the system in state x at fixed β is

$$p(x|\beta) = \sqrt{\frac{\beta}{2\pi}} \exp\left(-\frac{1}{2}\beta x^2\right), \quad (2.102)$$

and the marginal probability distribution (probability to observe x independent of the value of β) is

$$p(x) : = \int p(x|\beta) p(\beta) d\beta \quad (2.103)$$

$$= \frac{\Gamma\left(\frac{n}{2} + \frac{1}{2}\right)}{\Gamma\left(\frac{n}{2}\right)} \left(\frac{\beta_0}{\pi n}\right)^{1/2} \frac{1}{\left(1 + \frac{\beta_0}{n}x^2\right)^{n/2+1/2}}, \quad (2.104)$$

which is a q -Gaussian and can be re-written as

$$p(x) \sim \frac{1}{\left(1 - \tilde{\beta}(1-q)x^2\right)^{1/(q-1)}}, \quad (2.105)$$

with $q = 1 + 2/(n+1)$ and $\tilde{\beta} = 1/(3-q)\beta_0$. That means a process following Eq. (2.100) with a/b^2 distributed according to a χ^2 (log-normal or inverse χ^2 do also work approximately [16, 17]) distribution will give a q -Gaussian distribution when recording for a long time $t \gg T$.

How do we find out if a recorded time series is based on a superposition of multiple processes with changing parameters a and b ? Following [17], we may extract the important time scales and the

effective damping β as follows. Let $c(\Delta t)$ be the autocorrelation function of our data as a function of time delay Δt . Then, it should display an exponential decay, similar to an Ornstein-Uhlenbeck process:

$$c(\Delta t) \sim \exp(-a\Delta t),$$

which defines the short time scale of the system as $\tau = 1/a$. For the long time scale T , we assume that the recorded data is more heavy-tailed than a Normal distribution, i.e., it has a kurtosis $\kappa > 3$ [166]. Given a time series $x(t)$ with a mean \bar{x} , we compute the local kurtosis as

$$\kappa(\Delta t) = \frac{1}{t_{max} - \Delta t} \int_0^{t_{max} - \Delta t} dt_0 \frac{\langle (x - \bar{x})^4 \rangle_{t_0, \Delta t}}{\langle (x - \bar{x})^2 \rangle_{t_0, \Delta t}^2}, \quad (2.106)$$

where $\langle \dots \rangle_{t_0, \Delta t} = \int_{t_0}^{t_0 + \Delta t} \dots dt$ and then choose T so that $\kappa(T) = 3$, i.e., on average recordings of length T have no excess kurtosis. To be in accordance with the superstatistical approach, we require $\tau \ll T$. Next, we fix this T and extract the effective damping β as

$$\beta(t_0) = \frac{1}{\langle x^2 \rangle_{t_0, T} - \langle x \rangle_{t_0, T}^2}. \quad (2.107)$$

If the distribution of β follows a χ^2 , inverse χ^2 or log-normal distribution, then the superstatistical approach is well justified [15].

2.5 Simulations

Here, we provide a few technical notes on the implementation of numerical procedures.

2.5.1 Ordinary Differential Equations

The nonlinear swing equation (2.44) cannot be solved analytically for all network topologies so that we often use numerical methods to obtain trajectories of the system. In all cases reported here, Mathematica, Versions 9, 10 or 11 were used and the ODE solver *NDSolve* [176] was applied to solve the differential equation. This solver uses a “*LSODA approach, switching between a non-stiff Adams method and a stiff Gear backward differentiation formula method*” [175]. For testing purposes, the results of this solver were compared with explicit Euler or Runge-Kutta written in Mathematica and different languages. The results matched quantitatively so that we expect the solver to have no influence on our results.

2.5.2 Delay Differential Equations

In Chapters 3 and 4 we analyze a delay differential equation, which may for example arise due to signal processing or communication delays [99] or when considering that power intake cannot be switched instantaneously, but many modern devices display a power ramp, see Fig. 2.16. A comprehensive

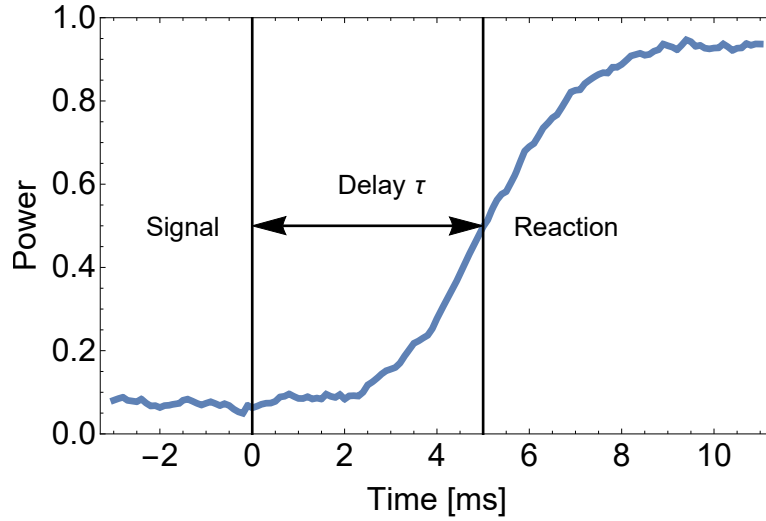


Figure 2.16: Delays arise due to communication delay and ramps. Here we display the potential power consumption of a device that is switched on but only consumes power after a certain delay τ . After the signal is received, the power consumption slowly ramps up from 0% to 100%. The time delay τ depends on the specific device with modern batteries being fast but not instantaneous [51, 181].

introduction to delayed differential equations (DDE) is provided by Roussel [125], which we follow closely here. A more thorough treatment is offered in [41, 57].

Consider a differential equation with one constant delay τ described by the general form

$$\dot{\mathbf{x}}(t) = \mathbf{f}(\mathbf{x}(t), \mathbf{x}(t - \tau)), \quad (2.108)$$

where f is the dynamics of the potentially multi-dimensional state \mathbf{x} . One important difference compared to ordinary differential equations (ODEs) is that ODEs require an *initial condition* $\mathbf{x}(0)$ to be solved while DDEs need an *initial function* or history function $\mathbf{x}(t)$ for $t \in [-\tau, 0]$.

Method of steps. The method of steps provides a straightforward way of solving a DDE. Let us consider the one-dimensional example with one delay $\tau = 1$ given by

$$\dot{x}(t) = x(t - 1). \quad (2.109)$$

Assume that the initial function is $x(t \leq 0) = 1$, i.e., the state of our system has been $x = 1$ for all negatives times, including zero. The left hand side of Eq. (2.109) provides the change of x for all times t . Let us integrate it for the interval $t \in [0, 1]$, obtaining the trajectory for this interval as

$$x_{[0,1]}(t) = x_{[-1,0]}(t) + \int_0^t x_{[-1,0]}(s - 1) ds \quad (2.110)$$

$$= 1 + \int_0^t 1 ds \quad (2.111)$$

$$= 1 + t. \quad (2.112)$$

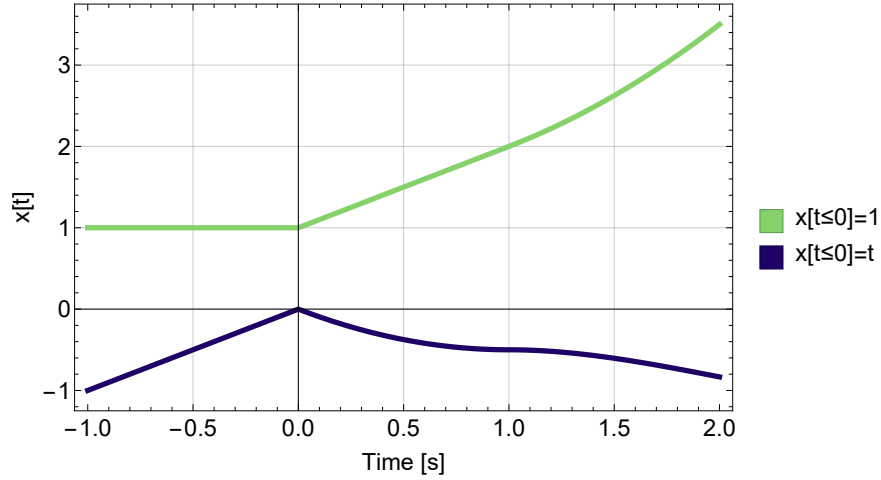


Figure 2.17: Delay differential equations are easily solved by the method of steps for different history functions. The equations $\dot{x}(t) = x(t-1)$ is used with $x(t \leq 0) = 1$ (light green) and $x(t \leq 0) = t$ (dark blue) as history functions.

This solution is then plugged in into Eq. (2.109) once more for the interval $t \in [1, 2]$:

$$x_{[1,2]}(t) = x_{[0,1]}(t=1) + \int_1^t (1 + (s-1))ds \quad (2.113)$$

$$= 2 + \frac{s^2}{2} \Big|_{s=1}^{s=t} \quad (2.114)$$

$$= \frac{3}{2} + \frac{t^2}{2}. \quad (2.115)$$

We display the the trajectory of this (light green) initial function compared to the case of $x(t \leq 0) = t$ (dark blue) in Fig. 2.17. Note that the solution is continuous but not continuously differentiable since for the green curve the first derivative does not exist at $t = 0$. However, the longer the trajectory gets the smoother it becomes: At $t = 1$ the first derivative exists but the second does not and so on.

In general, the solution of Eq. (2.109) for the interval $[t_i, t_i + 1]$ is given as

$$x_{[t_i, t_i+1]}(t) = x_{[t_i-1, t_i]}(t = t_i) + \int_{t_i}^t x_{[t_i-1, t_i]}(s-1)ds. \quad (2.116)$$

For different DDEs, the integral needs to be adjusted by plugging in the left hand side of the dynamical equation into the integral.

Linear stability of DDE. We already discussed linear stability analysis in Section 2.1, which we now extend to the case of delay in the differential equation. First, we approximate the state by the fixed point plus a small perturbation

$$\mathbf{x}_i \approx \mathbf{x}_i^* + \delta \mathbf{x}_i \quad (2.117)$$

and assume again that these perturbations grow or decay exponentially:

$$\frac{d}{dt} \delta \mathbf{x}_i(t) = \delta \mathbf{x}_i(0) \exp(\lambda t). \quad (2.118)$$

Then, we compute the Jacobian matrix as indicated in Eq. (2.13), ignoring all terms that include a delay. Next, we repeat this but only include terms with the delay τ . Thereby, we obtain the non-delayed Jacobian matrix \mathbf{J}_0 and the delayed one \mathbf{J}_τ . With these two matrices, the characteristic equation is given as

$$|\mathbf{J}_0 + e^{-\lambda\tau} \mathbf{J}_\tau - \lambda \mathbf{I}| = 0, \quad (2.119)$$

where \mathbf{I} is the identity matrix. Due to the term $e^{-\lambda\tau}$ this is no longer a polynomial equation in λ but a transcendental equation with infinitely many solutions in general [41, 57].

Numerical computation of eigenvalues. The characteristic equation (2.119) has infinitely many solutions but we are interested whether there are any eigenvalues with a positive real part $Re(\lambda) > 0$ because those would destabilize the system. Here, we describe our procedure, which we developed for Chapter 4.

We initialize our search for eigenvalues by choosing one fixed sampling delay $\tau_{\text{sample}} > 0$ for the characteristic equation (2.119). Then, we numerically obtain solutions of this equation using Newton's method with several thousand different initial guesses in the complex plain. From this list we delete duplicates and end up with about 10-100 unique eigenvalues for a system of 2 nodes. Next, we change the delay by a small amount $\tau = \tau_{\text{sample}} \pm 0.01 s$ and use the eigenvalues previously obtained as initial conditions for this new delay. This procedure is continued until $\tau = 0$ for the lower bound and $\tau = \tau_{\text{max}}$ for the upper bound. It is crucial to sample at non-zero delay because at $\tau = 0$ there are only a finite number of solutions and infinitely many solutions exist as soon as $\tau > 0$. Most of these solutions have a very small real part close to $\tau \approx 0$ and are missed if the sampling delay is chosen to be too small. Also note that we only plot the real parts of the eigenvalues and only those determine whether the system is unstable or not; however, it is crucial for the tracking to keep the imaginary part as well.

Consider a power grid consisting of one consumer and one generator coupled via one transmission line. In Chapters 3 and 4 we modify the power grid equations to include a term with delay of the form

$$\frac{d}{dt} \theta_i(t) = \omega_i(t), \quad (2.120)$$

$$\frac{d}{dt} \omega_i(t) = P_i - \gamma_i \omega_i(t) + \sum_{j=1}^N K_{ij} \sin(\theta_j(t) - \theta_i(t)) - \gamma_{\text{control}} \omega_i(t - \tau). \quad (2.121)$$

We illustrate our eigenvalue sampling approach on this dynamical system in Fig. 2.18.

2.5.3 Stochastic Differential Equations

In Chapters 5 and 6, we apply stochastic processes to investigate the robustness of the grid with respect to power fluctuations. Let us consider a one dimensional equation of motion given by the *Langevin* equation

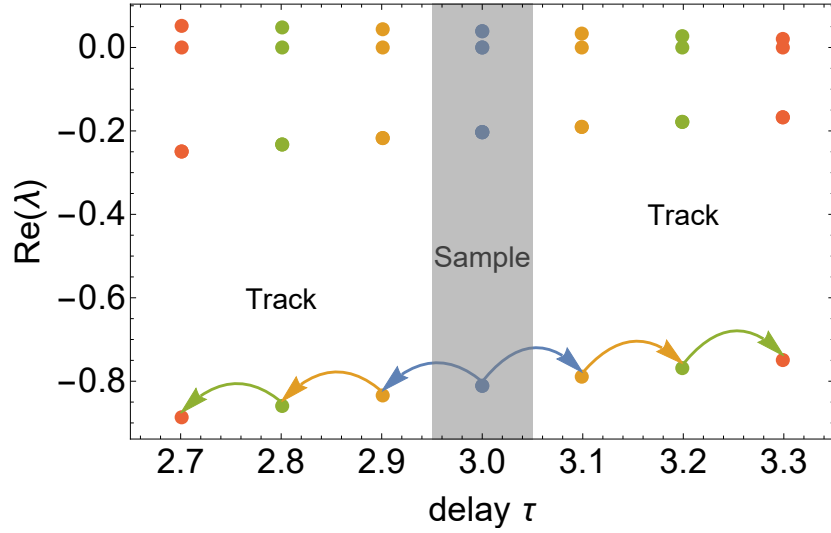


Figure 2.18: Illustration of sampling delay. We start sampling many eigenvalues at $\tau_{\text{sampling}} = 3s$ then these values are used as initial conditions for Newton's method finding the roots of the transcendental characteristic equation. The values are based on a two node power grid system with one generator and one consumer with parameters $P = \pm 0.5/s^2$, $K = 1/s^2$, damping $\gamma = 0.1/s$, control parameter $\gamma_{\text{control}} = 0.25/s$

$$\frac{d}{dt}x(t) = ay(t) + b\xi(t), \quad (2.122)$$

with constant parameters a and b , state $x(t)$ and noise $\xi(t)$. We consider both Gaussian and non-Gaussian noise for $\xi(t)$ but always assume noise sources without temporal correlations. To obtain a specific trajectory based on this equation, we discretize time into intervals of length Δt and compute

$$\begin{aligned} \Delta x &= a \cdot x(t) \cdot \Delta t + Y \cdot \sqrt{\Delta t}, \\ x(t + \Delta t) &= x(t) + \Delta x, \\ t &= t + \Delta t, \end{aligned} \quad (2.123)$$

with Y as our random variable drawn from a previously defined distribution (e.g. Gaussian or α -Lévy-stable distribution) [56]. Note that the noise is scaled with $\sqrt{\Delta t}$ instead of Δt . This way of solving stochastic differential equations is known as the Euler-Maruyama method [73].

Part II

Results - Original Manuscripts

Chapter 3

Decentral Smart Grid Control

Citation

Benjamin Schäfer, Moritz Matthiae, Marc Timme and Dirk Witthaut (2015) Decentral Smart Grid Control, New J. Phys. 17 015002, DOI: <https://doi.org/10.1088/1367-2630/17/1/015002>

© 2015 IOP Publishing Ltd and Deutsche Physikalische Gesellschaft New Journal of Physics, Volume 17, January 2015, published under CC-BY- 3.0

Original Contribution

Conception of the research was done with M. Timme and D. Witthaut. I performed most calculations and simulations, especially in Sections 4 and 5. I generated Figures 3-7 and produced the data for those. I wrote large parts of the introduction and modeling sections. I significantly contributed to the writing of the results section. I revised the manuscript during the revision process, updating texts and figures according to referee suggestions, supported by the co-authors.

New Journal of Physics

The open access journal at the forefront of physics



Published in partnership with: Deutsche Physikalische Gesellschaft and the Institute of Physics



PAPER

Decentral Smart Grid Control

Benjamin Schäfer¹, Moritz Matthiae¹, Marc Timme^{1,2} and Dirk Witthaut^{1,3,4}

¹ Network Dynamics, Max Planck Institute for Dynamics and Self-Organization (MPIDS), D-37077 Göttingen, Germany

² Institute for Nonlinear Dynamics, Faculty of Physics, University of Göttingen, D-37077 Göttingen, Germany

³ Forschungszentrum Jülich, Institute for Energy and Climate Research (IEK-STE), D-52428 Jülich, Germany

⁴ Institute for Theoretical Physics, University of Cologne, D-50937 Köln, Germany

E-mail: timme@nld.ds.mpg.de

OPEN ACCESS

RECEIVED

22 August 2014

ACCEPTED FOR PUBLICATION

19 November 2014

PUBLISHED

9 January 2015

Content from this work may be used under the terms of the [Creative Commons Attribution 3.0 licence](#).

Any further distribution of this work must maintain attribution to the author(s) and the title of the work, journal citation and DOI.



Keywords: Decentral Smart Grid Control, dynamic demand response, delayed coupling, oscillator networks, econophysics, transient stability, frequency-price coupling

Abstract

Stable operation of complex flow and transportation networks requires balanced supply and demand. For the operation of electric power grids—due to their increasing fraction of renewable energy sources—a pressing challenge is to fit the fluctuations in decentralized supply to the distributed and temporally varying demands. To achieve this goal, common *smart grid* concepts suggest to collect consumer demand data, centrally evaluate them given current supply and send price information back to customers for them to decide about usage. Besides restrictions regarding cyber security, privacy protection and large required investments, it remains unclear how such central smart grid options guarantee overall stability. Here we propose a Decentral Smart Grid Control, where the price is directly linked to the local grid frequency at each customer. The grid frequency provides all necessary information about the current power balance such that it is sufficient to match supply and demand without the need for a centralized IT infrastructure. We analyze the performance and the dynamical stability of the power grid with such a control system. Our results suggest that the proposed Decentral Smart Grid Control is feasible independent of effective measurement delays, if frequencies are averaged over sufficiently large time intervals.

1. Introduction

A major challenge in realizing a future sustainable power supply is the volatile character of many renewable sources [1–3]. The power generation of wind turbines and photovoltaics fluctuates strongly on different time scales: in addition to the obvious variations between the seasons and during a single day [4], strong fluctuations occur on much shorter time scales, for instance due to the turbulent character of wind [5]. To match generation and demand in a fully renewable power grid for the current demand characteristics at every point of time, would thus require large storage facilities. Current estimates for the storage capacity range up to 400 TWh for the entire European grid with 100% renewables and no stand-by power plants [4]. In addition to potential environmental effects, as, e.g., the large landscape consumption for pumped hydro storage facilities, this would require massive capital investments.

To reduce these enormous numbers, it has been proposed to regulate the consumer *demand* to match the fluctuating power generation [6]. This is a massive paradigm shift in the operation of power grids, as mainly the generation is regulated in current power grids [7, 8]. In the new system, the price of electric energy shall be adapted to the current generation to provide a stimulus for the consumers to adapt their demand. Most proposals for such a *smart grid* are based on a sophisticated information and communication technology infrastructure. All ‘smart’ power meters communicate with a central computer in order to negotiate the price and control their demand (see, e.g., [9]). However, such a centralized system would also raise questions of cyber security and privacy protection [10, 11]. Even more, it has been shown that interdependent systems, such as this, can become vulnerable to cascading failures [10, 12].

An alternative, decentralized approach has been first proposed already years ago, but received a major interest only recently. The key idea is that the grid frequency provides all information needed to control the grid. The frequency increases in times of excess generation, while it decreases in times of underproduction [13, 14]. In current power grids, the primary control of conventional power plants is already based on the frequency: generation is increased when the frequency decreases and vice versa [15]. In a future, fully renewable grid the consumers could take over this role and regulate their demand autonomously on the basis of the grid frequency. To make this economically favorable, it was proposed that the price of electric energy for each local consumer is a direct function of the local grid frequency [16]. Is such a decentralized approach capable of ensuring stable network dynamics?

Here we analyze systems with prices locally computed as a direct function of local frequency, taking into account averaging time intervals and effective time delays. We demonstrate that the approach holds risks at certain time delays if the averaging interval is short. Intriguingly, for sufficiently large averaging interval, network dynamics is stable, independent of the delays. Our modeling results thus suggest that Decentral Smart Grid Control provides an efficient measure of ensuring grid stability.

The article is structured as follows. First, we introduce a mathematical model for the frequency dynamics of a power grid, describe our concept of a Decentral Smart Grid Control to realize the dynamic demand response (DR) in section 2 and discuss several economic aspects in section 3. The dynamics and stability of a fully interdependent techno-economical system are then analyzed in detail in section 4. We uncover potential systemic risks and show how they can be mastered by a proper implementation of the control.

2. DR via Decentral Smart Grid Control

DR is generally based on a flexible consumer price for electric power which is adapted to the current power generation. In periods of higher demand than generation, prices are high, giving an incentive to the consumers to reduce their consumption. Current approaches for the implementation of DR are mostly based on centralized information and communication infrastructure [8, 9], i.e., all information about production and consumption is collected decentralized, transmitted to one central IT-unit which then sends commands for further consumption and production to the decentralized actors. Such a system would require large financial investments and raises concerns about data protection and system vulnerability [10–12]. However, such an expensive IT-infrastructure may not be needed, as the grid frequency already encodes the necessary information and is accessible everywhere in the grid.

To analyze the essential frequency dynamics of a large-scale power grid and its coupling to pricing information we consider an oscillator model based on the physics of coupled synchronous generators and synchronous motors, which recently attracted a strong interest in physics [17–23]. This model is very similar to the ‘classical model [15] and the structure preserving model [24] from power engineering, which are routinely used to simulate the dynamics of power grids on coarse scales.

The state of each rotatory machine j is characterized by the rotor angle $\theta_j(t)$ relative to the grid reference rotating at $\Omega = 2\pi \times 50$ Hz or $\Omega = 2\pi \times 60$ Hz, respectively, and its angular frequency deviation from the reference $\omega_j = d\theta_j/dt$. Every machine has its moment of inertia M_j and is driven by a mechanical power $P_j^{\text{mech}}(t)$, which is positive for a generator and negative for a consumer. In addition, every machine is driven by the electric power transmitted via the adjacent transmission lines which have a coupling strength K_{ji} . The dynamics of the machine j is then given by the equation of motion as

$$M_j \frac{d^2\theta_j}{dt^2} + \kappa_j \frac{d\theta_j}{dt} = P_j^{\text{mech}}(t) - \sum_{k=1}^N K_{jk} \sin(\theta_k - \theta_j). \quad (1)$$

For a more detailed discussion and short derivation of the equations of motion, see appendix A.

For the sake of simplicity, we assume that all damping constants $\kappa_j = \kappa$ and moments of inertia $M_j = M$ are identical for a while. The overall angular frequency deviation $\langle\omega\rangle := \frac{1}{N} \sum_j \omega_j$ is then determined by the equation of motion

$$M \frac{d}{dt} \langle\omega\rangle + \kappa \langle\omega\rangle = \frac{1}{N} \Delta P, \quad (2)$$

where $\Delta P = \sum_j P_j^{\text{mech}}$ is the total power balance in the grid. Equation (2) can be solved analytically with the result

$$\langle \omega \rangle(t) = \langle \omega \rangle(t_0) e^{-\kappa t/M} + \frac{\Delta P}{N\kappa} (1 - e^{-\kappa t/M}). \quad (3)$$

For $t \rightarrow \infty$, the overall angular frequency deviation $\langle \omega \rangle$ converges to the value $\frac{\Delta P}{N\kappa}$. This relaxation is typically fast; most perturbations are cleared in less than a second [15]. In weakly connected grids inter-area oscillations can last for a minute [3, 26]. Hence, the angular frequency deviation $\langle \omega \rangle$ is directly proportional to the power balance of the entire system. In general, the angular frequency is the same throughout the grid $\omega_j = \langle \omega \rangle$ and can easily be measured, such that it can be used to control the grid without additional communication infrastructure.

The missing step to realize a Decentral Smart Grid Control is to come up with a one-to-one relation between the local grid angular frequency deviation ω_j and the current electricity price $p_j(\omega_j)$. A device that measures the local grid angular frequency and calculates the current price according to this pre-defined function $p_j(\omega_j)$ is cheap and can be implemented in a decentralized way, see [28] for large-scale frequency monitoring. Electric devices with an on-off load characteristic (e.g. washing, refrigeration, thermal heat pumps, electric cars) could automatically shift their consumption to times of high grid frequency, relieving the grid in low frequency times. Ensured by a properly chosen price function $p(\omega)$, this grid service can be economically reasonable for the consumer and also for the electricity provider, because the grid operator would have potentially less costs for primary, secondary and tertiary control. A drastic price increase at low frequencies and cheap electricity at high frequencies might also change the active consumer behavior. The needed technology is readily available, since micro combined heat and power systems or photovoltaic systems, already have a comparable control system included [8, 27].

In particular, we propose a Decentral Smart Grid Control that realizes a dynamic DR in power grids and analyze some of its core economic and dynamic consequences. The mechanical power $P_j^{\text{mech}}(t)$ in the equation of motion (1) is the difference of the generated and consumed power at the j th node of the network. Both generation and consumption depend on the current energy price p , which is described by supply $S(p)$ and demand curves $D(p)$, such that we find

$$P_j^{\text{mech}}(t) = S_j(p_j(t)) - D_j(p_j(t)). \quad (4)$$

A supply function $S(p)$ gives the amounts of goods offered, if this good is traded for a certain price p . Here, this is the amount of power supplied by a generator, if the obtained price is p . Similarly, the demand $D(p)$ gives the amount of power a consumer would like to consume for a given price p . Generally, the supply curve is monotonically increasing with p , while the demand curve is monotonically decreasing. The two curves are exogenous to the model, in fact they are determined by the strategy of the generators, the weather and the preferences of the consumers.

We suggest a Decentral Smart Grid Control that calculates the price on the basis of the local angular frequency deviation ω_j [16]; but measuring and updating the angular frequency in a real grid takes a certain time. Therefore, the price generally depends on a time-averaged angular frequency deviation $\bar{\omega}_j(t)$. Assuming that the angular velocity is measured over an interval of fixed period length T , we define

$$\bar{\omega}_j(t) = \frac{1}{T} \int_{t-T}^t \omega_j(t') dt'. \quad (5)$$

We consider two technical scenarios for the control. First, we consider a control system that adapts only in discrete time steps of length T such that the local prices are given by

$$p_j := p(\bar{\omega}_j(\lfloor t/T \rfloor T)), \quad (6)$$

where $\lfloor \cdot \rfloor$ denotes rounding towards minus infinity. Second, it can take a certain delay time τ until the control system adapts such that the local prices are given by

$$p_j := p(\bar{\omega}_j(t - \tau)). \quad (7)$$

We assume that the price only depends on the frequency and that supply and demand curves are given and keep their form on the time scales (seconds) described in this article. Hence, the design of an appropriate price function $p(\bar{\omega})$ is an important step for the implementation of a DR via Decentral Smart Grid Control.

3. Economic aspects

3.1. Benefits of DR

DR may have huge benefits in future energy systems see, e.g., [7, 8, 25, 29, 30]. Here, we briefly summarize the most important economic aspects, following [7], which hold regardless of the technical implementation: (1)

consumers may reduce their electricity bill by shifting their demand to periods of low prices. (2) In addition, DR may reduce the global costs of the power system as it allows for a more efficient use of the existing infrastructure and avoids costs for additional infrastructure. (3) DR may improve system stability by avoiding dangerous peaks of the demand and thus reduce the probability of power outages. (4) Finally, DR may improve market performance and reduce the price volatility. In addition to these points, DR is particularly important for future power grids because its implementation can potentially allow a higher penetration with renewable energies [31].

3.2. The grid as a market

In the current proposal of a Decentral Smart Grid Control there is no central computer which controls the demand of the consumers and no central exchange to determine the electricity price. The control is realized in a decentralized way using local frequency measurements, thus requiring no long-distance communication. Is this sufficient to provide an efficient market, i.e., to reach an economic equilibrium?

To answer this question we first note that the stable stationary operation of a power grid requires that all machines rotate in synchrony, i.e., the frequency must be the same everywhere

$$\omega_j(t) \stackrel{!}{=} \langle \omega \rangle \quad \text{for all } j \in \{1, \dots, N\}. \quad (8)$$

Otherwise the power flow between two nodes j and k

$$P_{jk}(t) = K_{jk} \sin(\theta_k(t) - \theta_j(t)), \quad (9)$$

would be oscillating and average out over time. The synchronous state must be dynamically stable for small disturbances to be damped out [15, 32] and the grid may self-organize to a synchronous state with steady power flows [18, 22, 33]. Substituting the condition $\omega_j(t) = \langle \omega \rangle$ into the equations of motion (1) shows that the synchronous state is determined by the equation

$$\kappa_j \langle \omega \rangle = S_j(p_j) - D_j(p_j) - \sum_{k=1}^N K_{jk} \sin(\theta_k - \theta_j) \quad \text{for all } j \in \{1, \dots, N\}. \quad (10)$$

Summing up the equations for all j and using $K_{ij} = K_{ji}$ yields

$$\sum_j S_j(p_j) = \sum_j D_j(p_j) + \sum_j \kappa_j \langle \omega \rangle. \quad (11)$$

This shows that a dynamical equilibrium of the grid also implies the economic equilibrium of the market, i.e., the supply equals the demand including transmission losses. Hence, we have to analyze the dynamic stability of the combined techno-economical system to evaluate its stability properties. This will be done in detail in section 4.

For now, we assume that the grid is in equilibrium with $\langle \omega \rangle = 0$ at a price p_Ω . To analyze the stability of this equilibrium, we linearize the supply and demand curves close to the equilibrium:

$$\begin{aligned} S_j(p_j) &= S_j(p_\Omega) + \underbrace{\frac{dS_j}{dp}}_{=: s_j} \Big|_{p_\Omega} (p_j - p_\Omega) \\ D_j(p_j) &= D_j(p_\Omega) + \underbrace{\frac{dD_j}{dp}}_{=: d_j} \Big|_{p_\Omega} (p_j - p_\Omega). \end{aligned} \quad (12)$$

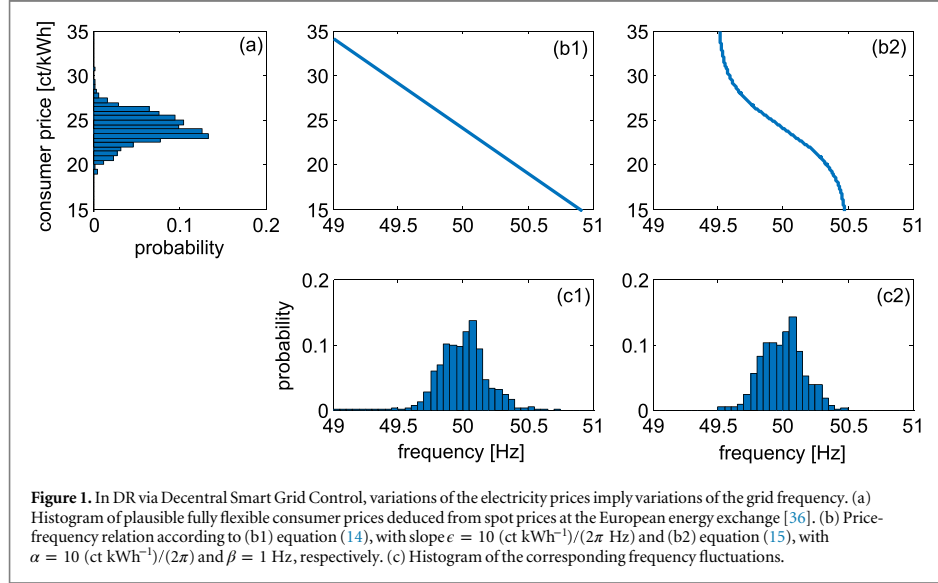
The modeling or measurement of supply and demand curves then reduces to the measurement of the elasticity of supply and demand. Generally, the supply increases with the price while the demand decreases such that $s_j \geq 0$ and $d_j \leq 0$ and thus in particular

$$s_j - d_j > 0 \quad \text{for all } j. \quad (13)$$

Here, we used course-graining, i.e., not every consumer is represented by one demand function but several consumers are aggregated to form one node in the network and hence supply and demand curves are assumed to be smooth.

3.3. Price and frequency fluctuations

The new aspect of our proposal of a Decentral Smart Grid Control is the direct encoding of the electricity price in the grid frequency. Thus, the grid frequency must be allowed to vary in certain boundaries so that fluctuations of



the price are directly related to fluctuations of the frequency. Currently, frequency variations are limited due to technical reasons [34]. In the European grid ± 200 mHz are acceptable in normal operation and up to ± 800 mHz can occur in extreme cases for short times before emergency measures such as load shedding are initiated [35]. This sets the order of magnitude at which the frequency may vary. Accordingly, we consider a frequency range of (50 ± 0.5) Hz.

In figure 1 we analyze the possible variations of the price and the frequency in more detail. Panel (a) shows a histogram of plausible values of the consumer price, if this price is strictly coupled to the variable spot market price for Germany in 2012 [36]. To obtain plausible consumer prices, we add 9 ct kWh⁻¹ for distribution and service, 7 ct kWh⁻¹ fees plus 19% VAT on the total. The variations of the electricity price directly relate to variations of the grid frequency as described above. We consider a linear price curve for all nodes

$$p(\bar{\omega}_j) = p_\Omega - \epsilon \times \bar{\omega}_j, \quad (14)$$

with $p_\Omega = 24.1$ ct kWh⁻¹, as shown in panel (b1). For a slope $\epsilon = 10$ (ct kWh⁻¹)/(2 π Hz), the price curve maps the operational range $(\bar{\omega}_j + \Omega)/2\pi \in [49.5, 50.5]$ Hz to a price interval $p \in [19.1, 29.1]$ ct kWh⁻¹, which covers 98% of the observed fictitious consumer prices. A histogram of the resulting frequency variations is shown in panel (c1). In 2% of all time slots prices outside of this interval were recorded which can even become negative.

To treat such events accordingly, a nonlinear function must be chosen which maps a fixed finite frequency interval to all possible prices, i.e., to the real line. Still, the slope of this function should be bounded around the operational point $\Omega = 50$ Hz. These requirements are satisfied by an inverse sigmoidal function. As a particular example, we here consider the function

$$p(\bar{\omega}_j) = p_\Omega - \frac{\alpha}{2} \tanh^{-1}\left(\frac{\bar{\omega}_j}{\pi\beta}\right), \quad (15)$$

which maps all angular frequency deviations in the interval $\bar{\omega}_j \in (-\pi\beta, +\pi\beta)$ to a price $p \in (-\infty, +\infty)$. The operational range can thus be fixed beforehand, and emergency measures can be specified, if frequencies outside this range are measured. Choosing $\alpha = \beta\epsilon$ yields the same slope of the price curve around the reference frequency as the linear price function (14). Indeed, using $\beta = 1$ Hz the statistics of the observed frequencies in figure 1 hardly change in comparison to the linear price function, see panels (b2) and (c2). The corresponding frequencies change significantly only for extreme price events, which now map to the operational range $(\bar{\omega}_j + \Omega)/2\pi \in [49.5, 50.5]$ Hz as desired. A similar statistic is found for other sigmoidal functions. The precise form of such a nonlinear price function can be designed by the grid operators on the basis of actual market and consumption data.

We note that figure 1 is based on the German spot market prices, which show huge fluctuations compared to other energy markets [39]. Furthermore, one major effect of a comprehensive DR would be to suppress extreme

price fluctuations anyway [7, 14]. Hence, we expect that the fluctuations shown in the figure represent extremes, and that they would be significantly smaller in energy systems with DR and (virtual) storage.

4. Dynamics and stability

Dynamical stability is a basic requirement for power grid operation [3, 15]. For DR via Decentral Smart Grid Control, a stable dynamic equilibrium ensures that the energy system is also in an economic equilibrium as shown above. However, stability properties may become much more involved due to the interdependency of the technical and the economical subsystem. Interdependencies may introduce new systemic risks to dynamical network systems [12, 37].

The interaction of the DR system with the grid depends crucially on their time scales. In contrast to current energy markets, the price can be adapted in almost real time, limited only by the time needed for a frequency measurement. Here, we analyze the dynamical stability of the full techno-economic system and identify new systemic risks for different scenarios and discuss how to master these risks.

4.1. Instantaneous adaption

We first investigate a DR that is fast compared to the grid dynamics. Assuming an instantaneous adaption of the demand, i.e., $T = \tau = 0$ in equations (6) and (7), the effective power $p_j^{\text{mech}}(t)$ in equation (1) becomes a function of the current angular frequency deviation ω_j . In particular, we consider a linear relation of price and angular frequency deviation

$$p_j := p_\Omega - \epsilon \omega_j(t). \quad (16)$$

Linearizing the supply and demand curves around p_Ω as in equation (12) yields

$$M_j \frac{d^2 \theta_j}{dt^2} + \kappa_j \frac{d\theta_j}{dt} = S_j(p_\Omega) - D_j(p_\Omega) - \epsilon (s_j - d_j) \frac{d\theta_j}{dt} - \sum_{k=1}^N K_{jk} \sin(\theta_k - \theta_j). \quad (17)$$

By equation (13), an instantaneous economic response thus increases the *effective* damping constant to

$$\kappa_j^{\text{eff}} = \kappa_j + \epsilon (s_j - d_j) > \kappa_j. \quad (18)$$

Therefore, it always lowers the return times after perturbations, see equation (3).

4.2. Slow adaptation in discrete time steps

A second, more realistic scenario is that the Decentral Smart Grid Control is much slower than the grid dynamics. Here, we consider a discrete time control system, where the price function is the same for all nodes and given by (6). Both supply and demand are updated periodically with periodicity $T \gg \sum_j M_j / \sum_j \kappa_j$. Assuming that the grid is dynamically stable for the given parameters, the angular frequency deviation will relax to

$$\langle \omega \rangle = \frac{\Delta P}{\sum_j \kappa_j} \quad \text{with} \quad \Delta P = \sum_j S_j(p) - D_j(p). \quad (19)$$

On this basis, a new market price p' is calculated. Assuming an affine-linear price function as in equation (14) and using the linearized supply and demand curves (12), we find

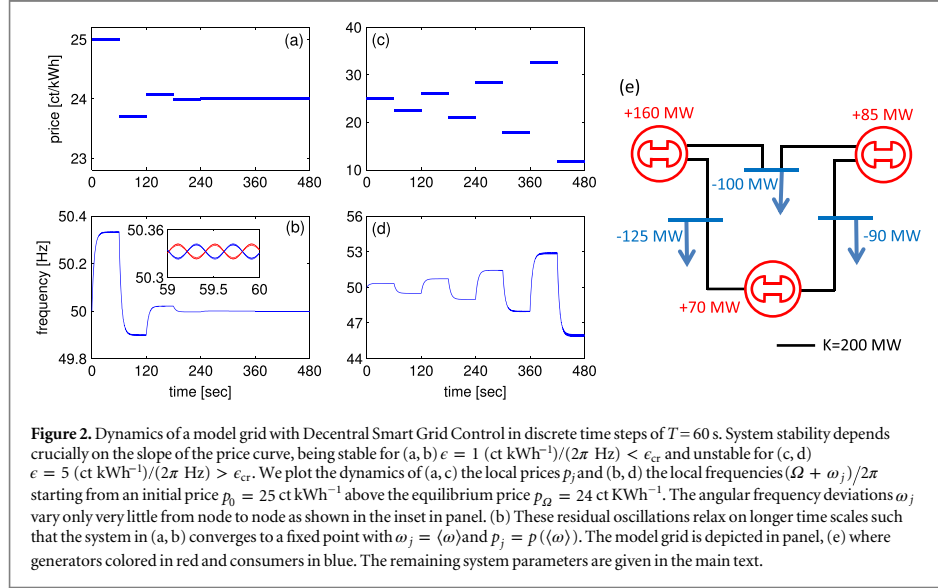
$$p' - p_\Omega = -\epsilon \frac{\sum_j s_j - \sum_j d_j}{\sum_j \kappa_j} (p - p_\Omega). \quad (20)$$

This yields an oscillating dynamics of the market price, which is stable if and only if

$$e < e_{\text{cr}} = \frac{\sum_j \kappa_j}{\sum_j s_j - \sum_j d_j}, \quad (21)$$

setting a strict upper limit for the slope of the price function. The potential instability for $e > e_{\text{cr}}$ is caused by an overreaction of the suppliers and consumers to market incentives. Similar *rebound* effects can generally occur in DR systems [8], such that this problem is not specific to the current proposal.

An example for the possible dynamics of the techno-economical system is shown in figure 2 for a model grid with three generators and three consumers with values inspired by the IEEE 9-bus test grid (see panel (e)). We assume that the price elasticities



$$E_S = \left. \frac{dS_j/dp}{S_j/p} \right|_{p_\Omega} \quad \text{and} \quad E_D = \left. \frac{dD_j/dp}{D_j/p} \right|_{p_\Omega} \quad (22)$$

are the same for all nodes and given by $E_S = +0.3$ and $E_D = -0.3$ in agreement with empirical results [38–40]. The price and subsequently the demand and supply are adapted after a time step of $T = 60$ s. We assume an equilibrium price $p_\Omega = 24 \text{ ct kWh}^{-1}$ and a damping constant $\kappa_j = 0.2/s \times M_j$ with $M_j = 10^4 \text{ kgm}^2 \times \Omega$. All transmission lines have the same transmission capacity $K = 200 \text{ MW}$. For these parameters, the system is stable if and only if $\epsilon < \epsilon_{cr} \approx 3 \text{ (ct/kWh)/(2}\pi \text{ Hz)}$. Otherwise the prices and the grid frequency will diverge after a small perturbation as shown in figure 2.

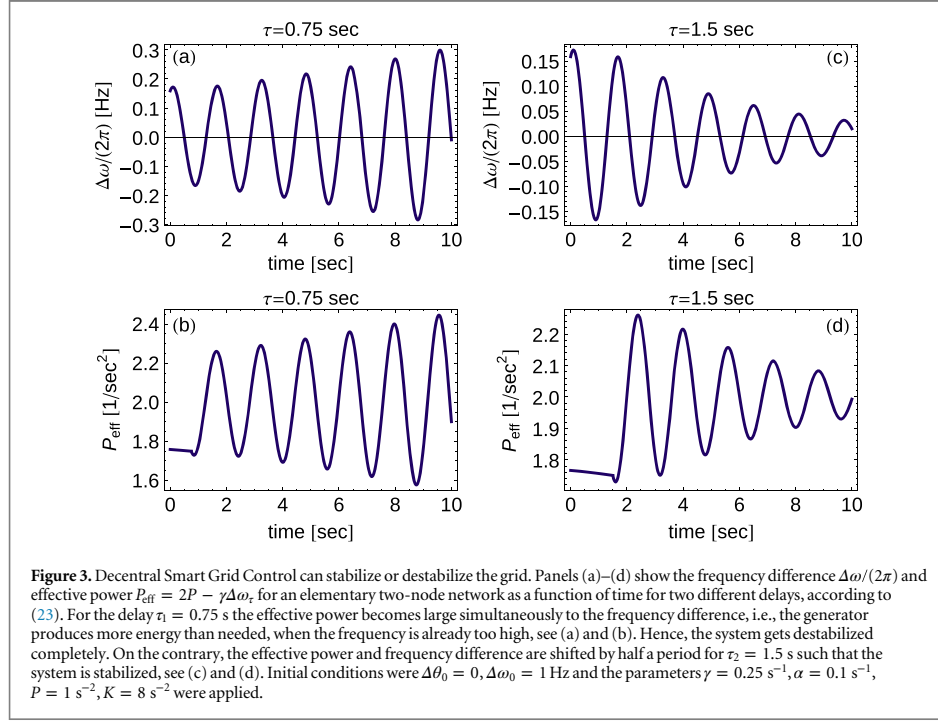
We note that this result can be interpreted as an application of the famous cobweb theorem from microeconomics [41] to Decentral Smart Grid Control. The generalized equilibrium condition (11) can be seen as the intersection of the loss curve $\sum_j \kappa \langle \omega \rangle$ and the net supply curve $\Delta P(\langle \omega \rangle) = \sum_j S_j(p(\langle \omega \rangle)) - D_j(p(\langle \omega \rangle))$. The loss takes the role of an effective demand function with fast relaxation, while the net supply is adapted much slower. The cobweb model then states that the economic system will relax to an equilibrium, if the slope of the loss curve is larger than the slope of the net supply curve, which yields the stability condition (21).

4.3. Delayed adaptation: risks from resonances

New risks may emerge when the Decentral Smart Grid Control acts on similar time scales as the dynamics of the grid such that the two system become truly interdependent. We first consider the case of a delayed feedback, i.e., we consider the price function (7) with $\tau \geq 0$ but without averaging ($T = 0$), i.e., consumers measure their local frequency and try to adapt as fast as possible but need their intrinsic time τ to react. To obtain analytic solutions for the interdependent techno-economical system, we use a very simple system: we linearize the supply and demand curves (12) and consider only two nodes with equal technical and economical parameters, i.e., $M_1 = M_2, \kappa_1 = \kappa_2, s_1 = s_2$ and $d_1 = d_2$. Defining our new variables as the phase difference $\Delta\theta = \theta_1 - \theta_2$ and the angular frequency difference of the two nodes $\Delta\omega = \omega_1 - \omega_2$, the equations of motion read

$$\begin{aligned} \frac{d}{dt} \Delta\theta &= \Delta\omega \\ \frac{d}{dt} \Delta\omega &= 2P - \alpha\Delta\omega - 2K \cdot \sin(\Delta\theta) - \gamma\Delta\omega_\tau, \end{aligned} \quad (23)$$

where we introduced the abbreviations $\alpha = \kappa/M, K = K_{12}/M, \gamma = \epsilon(s_1 - d_1)/M, 2P = (S_1(p_\Omega) - D_1(p_\Omega) - S_2(p_\Omega) + D_2(p_\Omega))/M$ and $\Delta\omega_\tau = \Delta\omega(t - \tau)$. In the following, time is measured in seconds, α and γ in s^{-1} and P and K in s^{-2} . This notation is similar to the one used in [19]. Delayed differential equations need a history function as initial condition, which we chose to be $\Delta\omega(t < 0) = \Delta\omega_0 \cdot (1 + 0.1 \tanh(t/2))$ for our dynamical



simulations. Furthermore, we used standard mathematica routines [42] to solve the ordinary and delayed differential equations.

The delayed adaption of supply and demand can both stabilize and destabilize the grid dynamics as shown in figure 3. The physical reason of this effect can be easily understood. The frequency-adaptive ‘effective’ power $P_{\text{eff}}(t) = 2P - \gamma\Delta\omega_\tau$ in equation (23) can be seen as a resonant driving acting on an oscillating system. Such a driving term will either damp or amplify the oscillations depending on whether the driving is in-phase or out-of-phase. The phase shift of this driving term is directly given by the delay τ , such that the stability of the system depends crucially on the value of τ . To illustrate this result, we compare the dynamics for two different values of τ in figure 3. For $\tau_1 = 0.75$ s the driving is in-phase, the oscillations are amplified and the grid becomes unstable with potentially fatal results, whereas $\tau_2 = 1.5$ s stabilizes the system.

To obtain a global view of the stability and the role of the system parameters we analyze the dynamical stability around the steady-state operation of the grid given by the fixed point

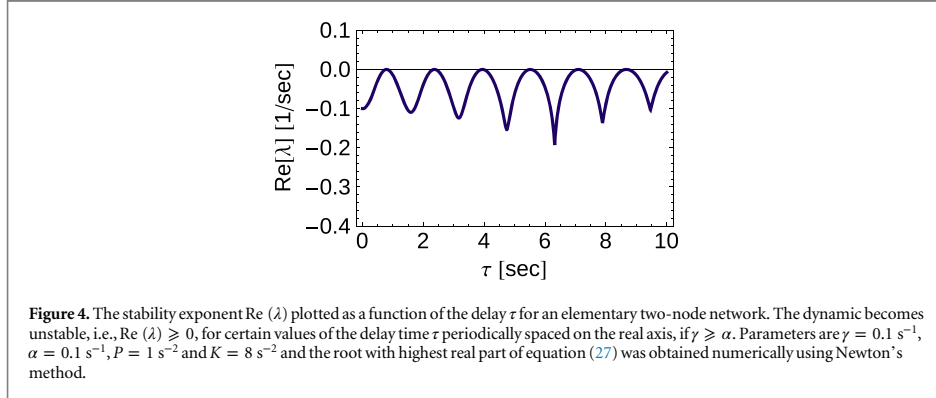
$$\left(\Delta\theta^*, \Delta\omega^*\right) = \left(\arcsin\left(\frac{P}{K}\right), 0\right). \quad (24)$$

A solution exists only if the transmission capacity is larger than the power which has to be transmitted, $K > P$ [32]. The linear stability of a dynamical system is determined by the eigenvalues of the Jacobian matrix. For a delayed system [43–45], we have to calculate the Jacobian of both the non-delayed system, based on equation (23),

$$J_0 = \begin{pmatrix} \frac{\partial}{\partial\Delta\theta} \left(\frac{d}{dt} \Delta\theta \right) & \frac{\partial}{\partial\Delta\omega} \left(\frac{d}{dt} \Delta\theta \right) \\ \frac{\partial}{\partial\Delta\theta} \left(\frac{d}{dt} \Delta\omega \right) & \frac{\partial}{\partial\Delta\omega} \left(\frac{d}{dt} \Delta\omega \right) \end{pmatrix} = \begin{pmatrix} 0 & 1 \\ -2K \cos(\Delta\theta^*) & -\alpha \end{pmatrix}, \quad (25)$$

and the derivatives for the delayed term

$$J_\tau = \begin{pmatrix} \frac{\partial}{\partial\Delta\theta_\tau} \left(\frac{d}{dt} \Delta\theta \right) & \frac{\partial}{\partial\Delta\omega_\tau} \left(\frac{d}{dt} \Delta\theta \right) \\ \frac{\partial}{\partial\Delta\theta_\tau} \left(\frac{d}{dt} \Delta\omega \right) & \frac{\partial}{\partial\Delta\omega_\tau} \left(\frac{d}{dt} \Delta\omega \right) \end{pmatrix} = \begin{pmatrix} 0 & 0 \\ 0 & -\gamma \end{pmatrix}, \quad (26)$$



where we consider exponential solutions, see [45]. The stability eigenvalues λ are then determined by the solution of the characteristic equation

$$\det(J_0 + e^{-\lambda\tau} J_\tau - \lambda \mathbb{1}) = \lambda^2 + \alpha\lambda + 2K \cos(\Delta\theta^*) + \lambda\gamma e^{-\lambda\tau} = 0. \quad (27)$$

Small perturbations induce an oscillatory motion with eigenfrequency $\text{Im}(\lambda)$ and period $2\pi/\text{Im}(\lambda)$. The amplitude grows or decreases exponentially as $e^{\text{Re}(\lambda)t}$ such that $\text{Re}(\lambda) > 0$ is the condition for a dynamic instability. This is possible only if the frequency adaption is strong enough compared to the damping of the system,

$$\text{Re}(\lambda) \geq 0 \quad \text{is possible only if} \quad \gamma \geq \alpha, \quad (28)$$

as shown below. When the delay τ changes, we observe a periodic pattern of stable and unstable parameter values as shown in figures 4 and 5. As explained above, destabilization occurs in the case of an in-phase driving which happens when τ is an integer multiple of the period of the eigenoscillations of the system.

To proof these statements we first note that $\text{Re}(\lambda) < 0$ for $\gamma = 0$ or $\tau = 0$ as long as $\alpha > 0$. We now consider the parameter values where $\text{Re}(\lambda)$ changes its sign such that the system becomes unstable. Decomposing the characteristic equation (27) into real and imaginary parts and setting $\text{Re}(\lambda) = 0$ yields the conditions

$$-\text{Im}(\lambda)^2 + 2K \cos(\Delta\theta^*) + \gamma \text{Im}(\lambda) \sin(\tau \text{Im}(\lambda)) = 0, \quad (29)$$

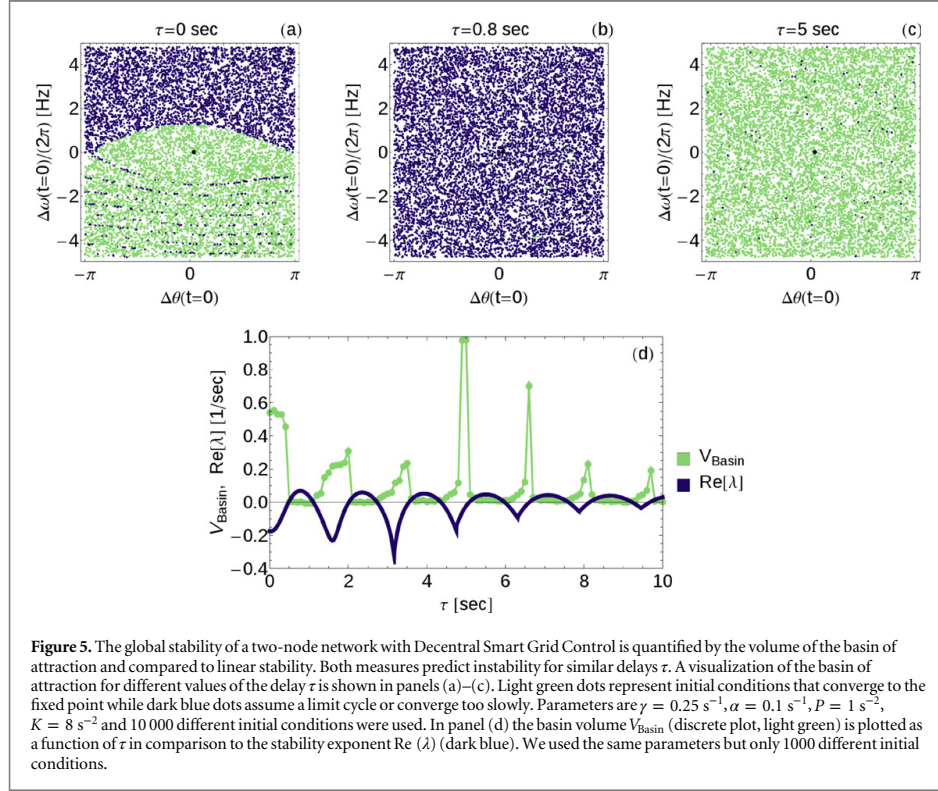
$$\alpha \text{Im}(\lambda) + \gamma \text{Im}(\lambda) \cos(\tau \text{Im}(\lambda)) = 0. \quad (30)$$

The second equation can be solved for τ with the result

$$\tau = \arccos(-\alpha/\gamma) + \frac{2\pi}{\text{Im}(\lambda)}n, \quad n \in \mathbb{N}. \quad (31)$$

One directly sees the periodicity in the delay τ , where the period $2\pi/\text{Im}(\lambda)$ is equal to the period of the eigenoscillations of the system. Furthermore, the $\arccos(-\alpha/\gamma)$ is real only if $\gamma \geq \alpha$, which yields a necessary condition for the destabilization by delay. Note that this statement is equivalent to the one from section 4.2, namely the damping of the system has to be larger than the price influence to always guarantee stability.

In addition to the local stability analysis, we also consider the grid dynamics after a large perturbation. We integrate the equations of motion for a long time period until $t_{\text{max}} = 600 \text{ s}$ with initial conditions randomly drawn from a subset of the phase space $Q = [-\pi, \pi] \times [-30, 30] \text{ Hz}$, see also [46], and evaluate whether the system relaxes to a stable operation, i.e., whether it converges to the fixed point (24), or not. As a criterion for stable operation we assume an angular frequency deviation of $\Delta\omega(t = t_{\text{max}}) \leq 0.1 \text{ Hz}$. The results are visualized in figure 5, panels (a)–(c), where we plot the stability in a color code (light green: stable, dark blue: unstable) as a function of the initial location in phase space for different values of τ . The results confirm the finding of the linear stability analysis. Depending on the value of τ the global stability is altered dramatically. For $\tau = 0.8 \text{ s}$ the fixed point is linearly unstable and the system does not relax for almost all initial conditions. On the contrary, a delay of $\tau = 5 \text{ s}$ leads to an almost perfect stability; the grid converges for almost all initial states. Notably, the regions of initial conditions leading to stable or unstable behavior are not clearly separated because the actual boundary of these regions has a rather complex geometric structure already in the non-delayed case.



The global stability of a fixed point of a dynamical system can be quantified by the volume of its basin of attraction. The ‘basin size’ V_{Basin} can be determined numerically using a Monte Carlo method as the ratio of initial conditions converging to a stable operation to the total number of initial conditions. Figure 5 panel (d) shows how the basin volume depends on the delay time τ in comparison to the linear stability exponent $\text{Re}(\lambda)$. As expected, V_{Basin} tends to zero in the case of linear instability, $\text{Re}(\lambda) \geq 0$. Maxima of V_{Basin} of different height are observed in the stable parameter regions, including an almost perfect stabilization for $\tau \approx 5 \text{ s}$. However, these maxima do not coincide with the minima of $\text{Re}(\lambda)$. As both the linear stability and the basin volume predict similar delays to be problematic for the system, we focus on the computationally easier to handle linear stability in the following.

4.4. Stabilization by averaging

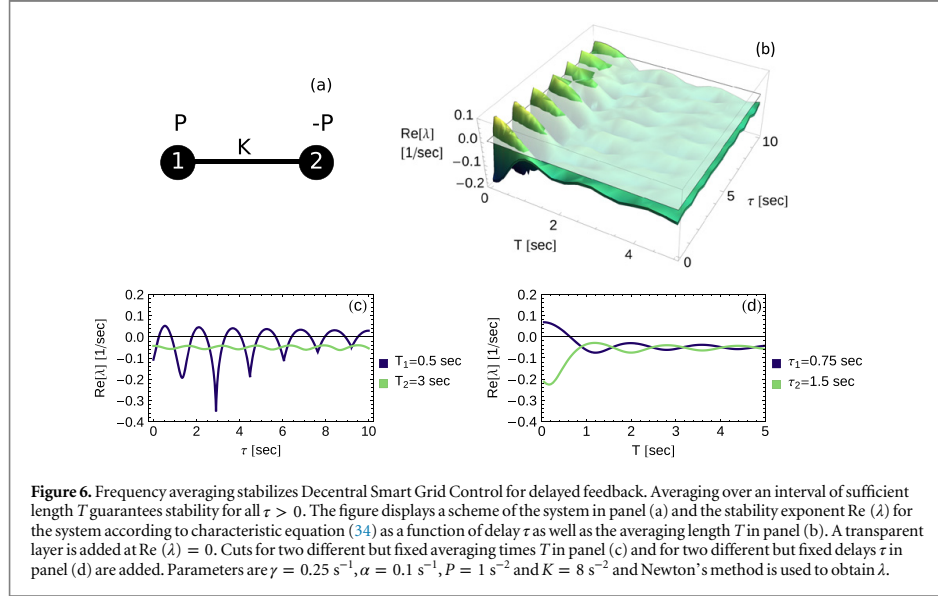
Measuring the local grid frequency will generally take some time in a real-world system. We thus consider the dynamics of the elementary model grid for the price function (7) including both delay $\tau \geq 0$ and averaging over a period $T \geq 0$. The equation of motion for the angular frequency difference $\Delta\omega = d\Delta\theta/dt$ then reads

$$\frac{d}{dt}\Delta\omega = 2P - \alpha\Delta\omega - 2K \sin(\Delta\theta) - \frac{\gamma}{T} \int_{t-T}^t \Delta\omega(t' - \tau) dt'. \quad (32)$$

The integration can be carried out in a straightforward way by using (23) such that we obtain the modified delayed dynamical system

$$\frac{d}{dt}\Delta\omega = 2P - \alpha\Delta\omega - 2K \sin(\Delta\theta) - \frac{\gamma}{T} [\Delta\theta(t - \tau) - \Delta\theta(t - T - \tau)]. \quad (33)$$

To evaluate the stability of the steady state (24), we have to calculate the eigenvalues λ for a system with both the delay τ and the delay $\tilde{T} = T + \tau$. The Jacobian of the non-delayed system is given by (25) as above and for the delay terms only $\frac{\partial}{\partial \Delta\theta_t} \left(\frac{d}{dt}\Delta\omega \right) = -\frac{\gamma}{T}$ and $\frac{\partial}{\partial \Delta\theta_{t-\tilde{T}}} \left(\frac{d}{dt}\Delta\omega \right) = +\frac{\gamma}{T}$ are non-zero. The stability eigenvalues λ are then given by the roots of the characteristic equation [43]



$$p(\lambda) = -\lambda^2 + \alpha\lambda + 2K\sqrt{1 - \frac{P^2}{K^2}} + \frac{\gamma}{T}(e^{-\lambda\tau} - e^{-\lambda(T+\tau)}) = 0. \quad (34)$$

Figure 6 shows the real part of the stability eigenvalue $\text{Re}(\lambda)$ as a function of the delay τ and the averaging time T . Instabilities are observed for certain values of τ , if T is small as discussed above. But for a sufficiently high T , the system stays stable regardless of the time τ . The actual values of the stability exponent $\text{Re}(\lambda)$ for large $T \gg \gamma$ are comparable to the one of the system without any price adaptation.

The results shown here are very interesting: while a delay in adaptation poses a stabilization risk to the grid, averaging the measured signal for a certain time removes the short time fluctuations that could resonantly drive the system and thereby guarantee a stable operation state. Still, the nodes can adapt to changes of the generation on all time scales slower than T , which provides an effective DR management system.

4.5. The role of the network topology

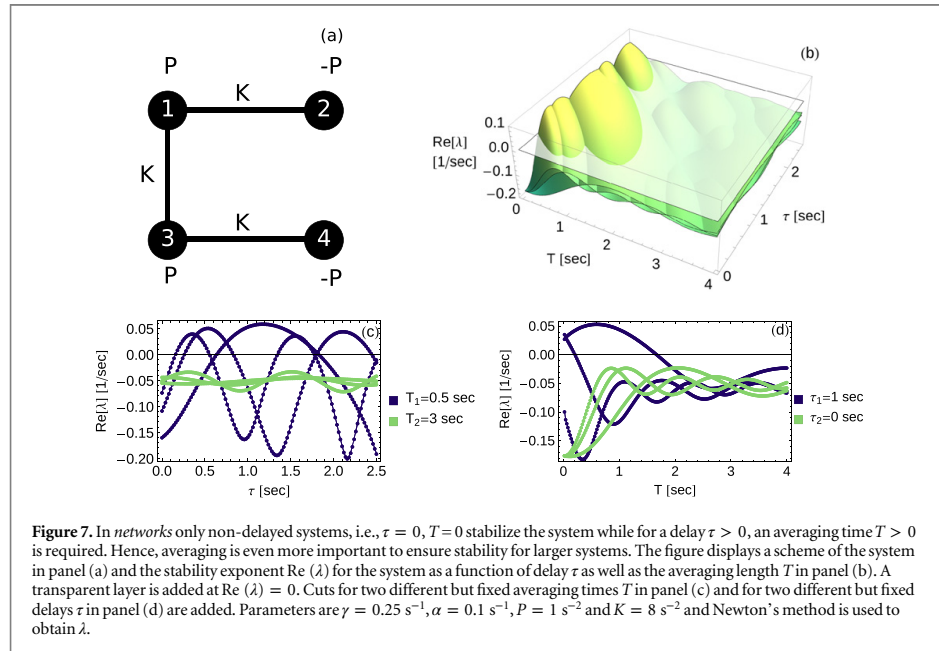
The larger the grid becomes, the more complex behavior it is able to show. Here, we consider a network with four nodes to test our results. Two consumers ($P = (S - D)/M < 0$) are supplied by two generators ($P = (S - D)/M > 0$). Each generator is coupled to a consumer to balance the power production/consumption. In addition, the generators are coupled to each other. As above we assume that all technical and economic parameters are the same for all nodes of the network. The equations of motion can be read in appendix B.

Risks from resonant driving emerge in a grid with delayed response and $T = 0$ as discussed above. The grid becomes unstable in certain regions of parameter space which are periodically spaced on the τ -axis. In a complex network, there are generally many different eigenmodes with different frequencies. The parameter regions where these modes can be excited generally overlap, such that the grid becomes unstable for most values of the delay τ as shown in the dark blue curves of panels (c), (d) in figure 7. Only for a very fast response $\tau \rightarrow 0$ the dynamic is stabilized.

We conclude that either a delayed adaption must be avoided, or alternatively, an averaging over a sufficiently long period T must be introduced as well. Figure 7 panel (b) shows the stability exponents $\text{Re}(\lambda)$ as a function of τ and T for the four-node network. Increasing T to values well above τ restores stability also for 'dangerous' values of τ as shown in the light green curves of panels (c), (d) in the figure.

5. Conclusion and outlook

In summary, we have proposed Decentral Smart Grid Control, a direct and decentralized frequency-price coupling to achieve a reliable DR in the collective network dynamics of power grids. The required information, the grid frequency, is easily accessible from everywhere in the system. As a consequence, DR via Decentral Smart



Grid Control offers a huge potential with both technical and economic benefits, in particular in grids with a large fraction of renewable sources.

First, the load information needs not be collected and evaluated centrally so that additional infrastructure for collection and for sending back central price information, is not required. This removes privacy and data security issues and should drastically lower the costs of hardware required for future power grids. The only technical device required would be a frequency meter at each customer complemented with a simple price function either programmed or implemented in hardware. Second, our results suggest that for sufficiently short feedback delays, as well as for longer delays with sufficient averaging, joint grid and economic stability is guaranteed. Stated simply, such grid would be a stable market: a stable dynamic equilibrium implies economic equilibrium. In contrast, whether joint economic and dynamic stability could be guaranteed in any other, more centralized DR setting, is, to the knowledge of the authors, yet unknown.

Decentral Smart Grid Control does need some modifications of the current system. For instance, the currently implemented strict rules for frequency regulation need to be relaxed to allow for some (small) variability, see section 3.3. Moreover, meters and price response algorithms need to be implemented at the customers' side, which might need convincing arguments. However, such decentralized control might still be much simpler to implement politically as customers need not fear data privacy issues and grid operators would not be required to install massive, network-wide and highly reliable hardware and computing power.

Generally, determining dynamic stability is typically involved for any interdependent socio-technical or techno-economic system, especially when the time scales of the system (here, the grid) and the control are similar. We have uncovered several new systemic risks in potential control options for dynamic DR in smart grids. The above results indicate that essential risks may be mastered by an appropriate design of the control in terms of decentralized and direct frequency-price coupling. This speaks for Decentral rather than Central Smart Grid Control of dynamic DRs.

We recommend to consider Decentral Smart Grid Control as a viable and possibly inexpensive alternative to central measures of DR. Since at least small and possibly unknown delays seem possible, prices should be calculated directly on the basis of a sliding average of the local grid frequency.

Acknowledgments

We thank T Walter and the Easy Smart Grid GmbH for inspiring discussions, T Ketelaer and T Pesch for help with energy market data and references. We gratefully acknowledge support from the Federal Ministry of Education and Research (BMBF grant no. 03SF0472 E [BS, DW, MT]), the Helmholtz Association (grant no. VH-NG-1025 [DW]) and the Max Planck Society [MT].

Appendix A. Swing equation

In the main part, we analyze a coarse-grained oscillator model based on the physics of coupled synchronous generators and synchronous motors, recently derived and numerically evaluated by Filatrella *et al* [17] and extended to complex networks by Rohden *et al* [18]. To achieve the large-scale network reduction, we aggregate coherent synchronous generators. Coherency of two generators means that there is no difference in their rotating angular frequency at any point in time. Together with the associated loads in that area, this coherent group is replaced by a single rotating machine with the index $j \in \{1, \dots, N\}$, which summarizes the physical properties of that group. In the language of network science, one group corresponds to one node of the network. The moment of inertia M_j of that rotating machine and its mechanical power input P_j^{mech} sum up linearly from all generators and loads of the coherent group [15]. In some groups there is more power generated than consumed such that $P_j^{\text{mech}} > 0$. If there is more power consumed than produced, we have $P_j^{\text{mech}} < 0$. The transmission network delivers power from nodes with power excess to nodes with power need.

The state of a coherent group of rotating machines is determined by its angular frequency and the rotor or power angle $\theta_j(t)$ relative to the reference axis rotating at the nominal grid angular frequency $\Omega = 2\pi \times 50$ Hz or $\Omega = 2\pi \times 60$ Hz. Correspondingly, $\omega_j = d\theta_j/dt$ gives the angular frequency deviation from the reference Ω . The dynamic is governed by the *swing equation* [15, 17, 24]

$$M_j \frac{d^2\theta_j}{dt^2} + \kappa_j \frac{d\theta_j}{dt} = P_j^{\text{mech}} - P_j^{\text{el}}, \quad (\text{A.1})$$

where P_j^{el} is the electrical power that is transmitted to or from other rotating machines and κ_j measures the damping, which is mainly provided by damper windings. (Commonly, the symbol D is used for the damping coefficient in the swing equation. In order to avoid confusion with the demand function introduced in the main text, we here use the symbol κ instead.) If the mechanical power at a node j is constantly higher than the corresponding electrical power ($\Delta P_j = P_j^{\text{mech}} - P_j^{\text{el}} > 0$), then the angular frequency deviation ω_j increases until the local mismatch in power ΔP_j dissipates due to damping. Note that all formulae use the angular frequencies while the numbers are divided by 2π for the plots to obtain frequencies.

To analyze the dynamics of the grid beyond the overall angular frequency deviation $\langle \omega \rangle := \frac{1}{N} \sum_j \omega_j$, we must take into account the details of the electrical coupling of the rotating machines along the edges of the transmission grid. The apparent power at the grid node j is given by

$$S_j = V_j \sum_{k=1}^N I_{jk}^*, \quad (\text{A.2})$$

with the complex-valued voltage V_j and the currents

$$I_{jk} = y_{jk} (V_j - V_k), \quad (\text{A.3})$$

where y_{jk} is the admittance of the transmission line between nodes j and k . In power engineering one generally uses the nodal admittance matrix Y , whose elements are defined as

$$Y_{jk} = \begin{cases} -y_{jk} & \text{for } j \neq k \\ \sum_{\ell} y_{j\ell} & j = k. \end{cases} \quad (\text{A.4})$$

The apparent power at node j is then written in the compact form

$$S_j = V_j \sum_{k=1}^N Y_{jk}^* V_k^*. \quad (\text{A.5})$$

We neglect the ohmic resistance of the transmission lines as they are typically much smaller than the shunt admittances [47], hence the admittance $Y_{jk} = iB_{jk}$ is purely imaginary. Furthermore, we assume that the magnitude of the voltage is constant throughout the grid, $|V_j| = V_0$ for all nodes $j \in \{1, \dots, N\}$. Then, the apparent power simplifies to

$$S_j = \sum_{k=1}^N V_0^2 B_{jk} \left[\sin(\theta_k - \theta_j) + i \cos(\theta_k - \theta_j) \right]. \quad (\text{A.6})$$

The electric power P_j^{el} is given by the real part of this expression. Substituting this result into the swing equation (A.1) thus yields the equations of motion

$$M_j \frac{d^2\theta_j}{dt^2} + \kappa_j \frac{d\theta_j}{dt} = P_j^{\text{mech}}(t) - \sum_{k=1}^N V_0^2 B_{jk} \sin(\theta_k - \theta_j). \quad (\text{A.7})$$

The factor $K_{jk} := V_0^2 B_{jk}$ thus gives the maximally transmittable power between nodes k and j . Therefore, we call it the coupling strength. It is zero, if two rotating machines are not coupled along a direct transmission line.

Due to the second order term, equation (A.1) describes an oscillatory system of phase angles. As the phases oscillate, also the local angular frequency deviations $\omega(t) = d\theta_j(t)/dt$ oscillate, a phenomenon well-known in power engineering [15, 21]. In the direct neighborhood of an equilibrium point in state space the oscillations are nearly harmonic and can be decomposed into a set of eigenmodes, corresponding eigenfrequencies and corresponding eigenvectors. The eigenfrequencies depend crucially on the connectivity of the power grid. In a densely connected grid, oscillations are typically fast (> 1 Hz), while the so-called inter-area oscillations in weakly coupled grid are significantly slower. For instance, inter-area oscillations between Turkey and the rest of the European power grid with a period of up to 7 s have recently been observed [26].

We note that this model is derived from the physics of rotating machines [15], or alternatively by assuming frequency-dependent loads [24]. This description includes hydro power as well as power plants based on nuclear and fossil fuel, which dominate today's grid. It is expected that a rising penetration of renewable energy sources will decrease the effective inertia in the future, which may however be compensated by advanced power electronic devices [48]. The future development of these aspects is still under debate and beyond the scope of the present article.

Appendix B. Four node system

In section 4.5 we used a four node system. The equations of motion for this system are

$$\begin{aligned} \frac{d}{dt}\theta_j &= \Delta\omega_j \quad \text{for all } j \in \{1, \dots, 4\} \\ \frac{d}{dt}\Delta\omega_1 &= P_1 - \alpha\Delta\omega_1 + K \cdot \sin(\theta_2 - \theta_1) + K \cdot \sin(\theta_3 - \theta_1) - \frac{\gamma}{T}(\theta_{1\tau} - \theta_{1\bar{T}}) \\ \frac{d}{dt}\Delta\omega_2 &= P_2 - \alpha\Delta\omega_2 + K \cdot \sin(\theta_1 - \theta_2) - \frac{\gamma}{T}(\theta_{2\tau} - \theta_{2\bar{T}}) \\ \frac{d}{dt}\Delta\omega_3 &= P_3 - \alpha\Delta\omega_3 + K \cdot \sin(\theta_1 - \theta_3) + K \cdot \sin(\theta_4 - \theta_3) - \frac{\gamma}{T}(\theta_{3\tau} - \theta_{3\bar{T}}) \\ \frac{d}{dt}\Delta\omega_4 &= P_4 - \alpha\Delta\omega_4 + K \cdot \sin(\theta_3 - \theta_4) - \frac{\gamma}{T}(\theta_{4\tau} - \theta_{4\bar{T}}), \end{aligned} \quad (\text{B.1})$$

with $\theta_{j\tau} = \theta_j(t - \tau)$ and $\theta_{j\bar{T}} = \theta_j(t - T - \tau)$ for all j .

References

- [1] Turner J A 1999 A realizable renewable energy future *Science* **285** 687–9
- [2] Boyle G 2012 *Renewable Energy: Power for a Sustainable Future* (Oxford: Oxford University Press)
- [3] 50Hertz, Amprion, TennET TSO and TransnetBW 2012 *Netzentwicklungsplan Strom*, online at <http://www.netzentwicklungsplan.de> (retrieved 7/8/2014)
- [4] Heide D, von Bremen L, Greiner M, Hoffmann C, Speckmann M and Bofinger S 2010 Seasonal optimal mix of wind and solar power in a future, highly renewable Europe *Renew. Energy* **35** 2483–9
- [5] Milan P, Wächter M and Peinke J 2013 Turbulent character of wind energy *Phys. Rev. Lett.* **110** 138701
- [6] Butler D 2007 Energy efficiency: super savers: meters to manage the future *Nature* **445** 586–8
- [7] Albadi M H and El-Saadany E F 2008 A summary of demand response in electricity markets *Electr. Power Syst. Res.* **78** 1989–96
- [8] Palensky P and Dietrich D 2011 Demand side management: demand response, intelligent energy systems, and smart loads *IEEE Trans. Ind. Inform.* **7** 381–8
- [9] Kok J K, Warmer C J and Kamphuis I G 2005 The powermatcher: multiagent control of electricity demand and supply *Proc. AAMAS' 05 (Utrecht)* pp 75–82
- [10] Ericsson G N 2010 Cyber security and power system communication—essential parts of a smart grid infrastructure *IEEE Trans. Power Deliv.* **25** 1501–7
- [11] Fang X, Misra S, Xue G and Yang D 2012 Smart grid—the new and improved power grid: a survey *IEEE Commun. Surv. Tutorials* **14** 944–80
- [12] Buldyrev S V, Parshani R, Paul G, Stanley H E and Havlin S 2010 Catastrophic cascade of failures in interdependent networks *Nature* **464** 1025–8
- [13] Schweppe F C 1982 Frequency adaptive power-energy re-scheduler *US Patent* 4317049
- [14] Short J A, Infield D G and Freris L L 2007 Stabilization of grid frequency through dynamic demand control *IEEE Trans. Power Syst.* **22** 1284–93
- [15] Machowski J, Bialek J and Bumby J 2008 *Power System Dynamics, Stability and Control* (New York: Wiley)
- [16] Walter T 2014 *VDE Mitgliederinformationen* 2014 64 online at <http://www.vde.com/de/fg/ETG/Pbl/MI/2014-01/Seiten/Homepage.aspx> (retrieved 7/8/2014)

- [17] Filatrella G, Nielsen A H and Pedersen N F 2008 Analysis of a power grid using a Kuramoto-like model *Eur. Phys. J. B* **61** 485–91
- [18] Rohden M, Sorge A, Timme M and Witthaut D 2012 Self-organized synchronization in decentralized power grids *Phys. Rev. Lett.* **109** 064101
- [19] Rohden M, Sorge A, Witthaut D and Timme M 2014 Impact of network topology on synchrony of oscillatory power grids *Chaos* **24** 013123
- [20] Witthaut D and Timme M 2012 Braess's paradox in oscillator networks, desynchronization and power outage *New J. Phys.* **14** 083036
- [21] Dörfler F, Chertkov M and Bullo F 2013 Synchronization in complex oscillator networks and smart grids *Proc. Natl Acad. Sci.* **110** 2005–10
- [22] Motter A E, Myers S A, Anghel M and Nishikawa T 2013 Spontaneous synchrony in power-grid networks *Nat. Phys.* **9** 191–7
- [23] Menck P J, Heitzig J, Kurths J and Schellnhuber H J 2014 How dead ends undermine power grid stability *Nat. Commun.* **5** 3969
- [24] Bergen A R and Hill D J 1981 A structure preserving model for power system stability analysis *Trans. Power App. Syst.* **PAS-100** 25–35
- [25] Strbac G 2008 Demand side management: benefits and challenges *Energy Policy* **36** 4419–26
- [26] Tor O B, Gencoglu C, Tamdir O, Cebeci M E and Güven N 2011 Investigation of necessary transmission enforcements at the Balkan region of ENTSO/E in the sense of inter-area oscillations after interconnection of Turkey *7th Int. Conf. on Electrical and Electronics Engineering (Bursa)* pp 1–7
- [27] For instance, such a system is mandatory for all newly installed devices in Germany since 1.7.2012, see VDE Anwendungsregel VDE-AR-N 4105, online at <http://vde.com/de/fnn/arbeitsgebiete/seiten/n4105.aspx> (retrieved 7/8/2014)
- [28] Zhong Z, Xu C, Billian B J, Zhang L, Tsai S S, Connors R W, Centeno V A, Phadke A G and Liu Y 2005 Power system frequency monitoring network (FNET) implementation *IEEE Trans. Power Syst.* **20** 1914–21
- [29] Borenstein S 2005 The long-run efficiency of real-time electricity pricing *Energy J.* **26** 93–116
- [30] Farhangi H 2010 The path of the smart grid *IEEE Power Energy Mag.* **8** 18–28
- [31] van Renssen S 2014 People power to the rescue *Nat. Clim. Change* **4** 417–9
- [32] Manik D, Witthaut D, Schäfer B, Matthiae M, Sorge A, Rohden M, Katifori E and Timme M 2014 Supply networks: instabilities without overload *Eur. Phys. J. ST* **223** 2527–47
- [33] Subbarao D, Uma R, Saha B and Phanendra M V R 2001 Self-organization on a power system *IEEE Power Eng. Rev.* **21** 59–62
- [34] Kirby B J, Dyer J, Shoureshi R A, Guttromson R and Dagle J 2002 Frequency control concerns in the north american electric power system *Technical Report for the U.S. Department of Energy*, online at <http://dx.doi.org/10.2172/885842> (retrieved 7/8/2014) doi:10.2172/885842
- [35] *Continental Europe Operation Handbook* 2014 European Network of Transmission System Operators for Electricity www.entsoe.eu/publications/system-operations-reports/operation-handbook
- [36] Historical data for the Power Spot Market at the European Energy Exchange (EEX), <http://www.eex.com/en/market-data>
- [37] Bashan A, Berezin Y, Buldyrev S V and Havlin S 2013 The extreme vulnerability of interdependent spatially embedded networks *Nat. Phys.* **9** 667–72
- [38] Green R J and Newbery D M 1992 Competition in the British electricity spot market *JPE* **100** 929–53
- [39] Samyn N 2010 Empirical analysis of price-curves at the EEX *Master Thesis* University of St. Gallen, Switzerland
- [40] Faruqui A and George S S 2002 The value of dynamic pricing in mass markets *TEJ* **15** 45–55
- [41] Ezekiel M 1938 The cobweb theorem *QJE* **52** 255–80
- [42] Wolfram Research Inc. 2012 *Mathematica* Version 9.0 www.wolfram.com/mathematica
- [43] Roussel M R 2005 Delay-differential equations online at people.uleth.ca/~roussel/nld/delay.pdf (retrieved 7/8/2014)
- [44] Forde J and Nelson P 2004 Applications of Sturm sequences to bifurcation analysis of delay differential equation models *J. Math. Anal. Appl.* **300** 273–84
- [45] Driver R D 1977 *Ordinary and Delay Differential Equations* (New York: Springer)
- [46] Menck P J, Heitzig J, Marwan N and Kurths J 2013 How basin stability complements the linear-stability paradigm *Nat. Phys.* **9** 89–92
- [47] van Hertem D, Verboomen J, Purchala K, Belmans R and Kling W L 2006 Usefulness of DC power flow for active power flow analysis with flow controlling devices *8th IEEE Int. Conf. on AC and DC Power Transmission (28–31 March 2006)*
- [48] Trovato V, Tindemans S H and Strbac G 2013 Demand response contribution to effective inertia for system security in the GB 2020 gone green scenario *4th IEEE PES Innovative Smart Grid Technologies Europe (ISGT Europe) (October 6–9, Copenhagen)* pp 1–5



CORRIGENDUM

Corrigendum: Decentral smart grid control (2015 *New J. Phys.* **17** 015002)

OPEN ACCESS

RECEIVED
5 May 2015ACCEPTED FOR PUBLICATION
5 May 2015PUBLISHED
22 May 2015Content from this work
may be used under the
terms of the [Creative
Commons Attribution 3.0
licence](#).Any further distribution of
this work must maintain
attribution to the
author(s) and the title of
the work, journal citation
and DOI.Benjamin Schäfer¹, Moritz Matthiae¹, Marc Timme^{1,2} and Dirk Witthaut^{1,3,4}¹ Network Dynamics, Max Planck Institute for Dynamics and Self-Organization (MPIDS), 37077 Göttingen, Germany² Institute for Nonlinear Dynamics, Faculty of Physics, University of Göttingen, 37077 Göttingen, Germany³ Forschungszentrum Jülich, Institute for Energy and Climate Research (IEK-STE), 52428 Jülich, Germany⁴ Institute for Theoretical Physics, University of Cologne, 50937 Köln, GermanyE-mail: timme@nld.ds.mpg.de

The original manuscript (Schaefer *et al* 2015 *New J. Phys.* **17** 015002) contains three typographical errors that we have corrected below. The scientific results were not affected by the typographical errors and all numerical simulations were carried out using the correct equations.

1. Demand response via decentral smart grid control

Equation (1) should read

$$M_j \frac{d^2 \theta_j}{dt^2} + \kappa_j \frac{d\theta_j}{dt} = P_j^{\text{mech}}(t) + \sum_{k=1}^N K_{jk} \sin(\theta_k - \theta_j), \quad (1)$$

i.e., there is a '+' sign in front of the sum.

4. Dynamics and stability**4.3. Delayed adaptation: risks from resonances**

Equation (31) should read

$$\tau = \frac{\arccos(-\alpha/\gamma)}{\text{Im}(\lambda)} + \frac{2\pi}{\text{Im}(\lambda)} n, \quad n \in \mathbb{N}. \quad (2)$$

This does not change the periodicity of the solution since $\text{Im}(\lambda)$ is constant and not a function of τ .**4.4. Stabilization by averaging**

Finally, equation (34) should read

$$p(\lambda) = \lambda^2 + \alpha\lambda + 2K\sqrt{1 - \frac{P^2}{K^2}} + \frac{\gamma}{T}(e^{-\lambda\tau} - e^{-\lambda(T+\tau)}) = 0. \quad (3)$$

The original equation used an erroneous minus sign.

Chapter 4

Taming Instabilities in Power Grid Networks by Decentralized Control

Citation

Benjamin Schäfer, Carsten Grabow, Sabine Auer, Jürgen Kurths, Dirk Witthaut and Marc Timme (2016), Taming instabilities in power grid networks by decentralized control, *European Physical Journal Special Topics* (2016) 225: 569, DOI: <https://doi.org/10.1140/epjst/e2015-50136-y>
© EDP Sciences, Springer-Verlag 2016. The printed version of the publication is identical in content to the one published by Springer and can be found as arXiv:1508.02217v2.

Original Contribution

Conception of the research was done with all authors. I performed most calculations and simulations, with support by C. Grabow. I generated all figures and produced all data with the exception of the basin stability results in Fig. 3. I wrote large parts of the all text sections, especially the model (II-III) and results (IV) sections. I revised the manuscript during the revision process, updating texts and figures according to referee suggestions.

Taming Instabilities in Power Grid Networks by Decentralized Control

Benjamin Schäfer

Network Dynamics, Max Planck Institute for Dynamics and Self-Organization (MPIDS), 37077 Göttingen, Germany

Carsten Grabow

Potsdam Institute for Climate Impact Research, 14412 Potsdam, Germany

Sabine Auer

*Potsdam Institute for Climate Impact Research, 14412 Potsdam, Germany and
Department of Physics, Humboldt University Berlin, 12489 Berlin, Germany*

Jürgen Kurths

*Potsdam Institute for Climate Impact Research, 14412 Potsdam, Germany
Department of Physics, Humboldt University Berlin, 12489 Berlin, Germany
Institute of Complex Systems and Mathematical Biology, University of Aberdeen, Aberdeen AB24 3FX, UK and
Department of Control Theory, Nizhny Novgorod State University, 606950 Nizhny Novgorod, Russia*

Dirk Witthaut

*Forschungszentrum Jülich, Institute for Energy and Climate Research (IEK-Systems Analysis and Technology Evaluation) and
Institute for Theoretical Physics, University of Cologne, 50937 Köln, Germany*

Marc Timme

*Network Dynamics, Max Planck Institute for Dynamics and Self-Organization (MPIDS), 37077 Göttingen, Germany and
Institute for Nonlinear Dynamics, Faculty of Physics, University of Göttingen, 37077 Göttingen, Germany*

(Dated: 11 February 2016)

Renewables will soon dominate energy production in our electric power system. And yet, how to integrate renewable energy into the grid and the market is still a subject of major debate. Decentral Smart Grid Control (DSGC) was recently proposed as a robust and decentralized approach to balance supply and demand and to guarantee a grid operation that is both economically and dynamically feasible. Here, we analyze the impact of network topology by assessing the stability of essential network motifs using both linear stability analysis and basin volume for delay systems. Our results indicate that if frequency measurements are averaged over sufficiently large time intervals, DSGC enhances the stability of extended power grid systems. We further investigate whether DSGC supports centralized and/or decentralized power production and find it to be applicable to both. However, our results on cycle-like systems suggest that DSGC favors systems with decentralized production. Here, lower line capacities and lower averaging times are required compared to those with centralized production.

PACS numbers: 05.45.Xt: Oscillators, coupled, 89.75.-k: Complex systems, 84.70.+p: High-current and high-voltage technology: power systems; power transmission lines and cables, 88.05.Lg: Cost, trends in renewable energy

I. INTRODUCTION

The ongoing climate change is forcing us to shift our power generation from fossil power plants towards renewable generation¹. In the last years, renewable energy technology development and policy support led to a tremendous increase in the share of Renewable Energy Sources (RES). In 2014, Germany covered 27.8% of its gross electricity consumption with RES². Still, large conventional power plants dominate the power grids: transmission lines connect large plants with regional consumers in a locally star-like topology. With more renewable power sources entering, the grid topologies become more decentralized and more recurrent due to the distributed generation³. In such a scenario, consumers may act as producers and consumers at the same time, so-called *prosumers*⁴ and electricity transport is no longer unidirectional.

A known challenge of many renewable sources is their volatile nature⁵⁻⁷. Fluctuations occur on different time scales, including seasonal, inter-day⁸ and intra-second fluctuations⁹. This requires radical changes in the control and design strategies of electric power grids as well as market innovations to ensure cost effectiveness. Therefore, a need for more flexibility options for power market supply and balancing energy¹⁰ arises because the fluctuating RES cannot guarantee power supply with the certainty conventional plants could. In this regard, it is most important to identify options that are both cost efficient and system stabilizing. So far, the framework of power market design and power grid stability with its long planning horizons does not satisfy the need for sufficient flexibility options¹¹.

Different *smart grid* approaches have been proposed to present ways to match supply and demand in such a fluctuating power grid. However, economic and political feasibility and market integration are often missed out. A key idea of various smart grid concepts is to regulate the consumers' demand¹², a massive paradigm shift compared to the current power grid operation schemes^{13,14}. Many proposals for smart grids are based on sufficient information and communication technology infrastructure, see, e.g.,¹⁵ or¹⁶. However, such a centralized system would raise questions of cyber security and privacy protection^{17,18} and several studies highlight the cost burden these proposals implicate¹⁹.

In contrast, an alternative approach without massive communication between consumers and producers directly utilizes the grid frequency to adjust production and consumption. The frequency increases in times of power excess while it decreases in times of

underproduction^{20,21}. A novel smart grid concept, Decentral Smart Grid Control (DSGC), was introduced in²², based on earlier ideas by²⁰, and its mathematical model proposed and analyzed in²³. Using DSGC prosumers control their momentary demand on the basis of the grid frequency which can easily be measured everywhere with cheap equipment. Ref.²³ demonstrates that DSGC enhances the stability of the power grid dynamics if the frequency measurements are averaged over sufficiently long time intervals. Yet, so far, only very small networks were investigated. Hence, the impact of grid topologies on power grid dynamics with DSGC constitutes a widely open research question.

Here we analyze the impact of network topology by assessing the stability of essential network motifs using both linear stability analysis of delay systems and determining basin volume. Furthermore, we address the question, how grid stability changes when generation is decentralized. The article is structured as follows. First, we present a dynamical model for power grid dynamics and present the concept of Decentral Smart Grid Control (DSGC)²³ to control a power grid in section II. In section III, we briefly summarize linear stability and basin volume measures for such delayed systems. The stability results of DSGC are then presented for a star motif in section IV A where we discuss the destabilizing resonance and rebound effects and how stable grid operation remains possible. Using linear stability analysis, we investigate the effect of decentralized power generation in cyclic and square lattice grid motifs in section IV B. The results suggest that DSGC works successfully for centralized as well as decentralized production, where grids with decentralized production require lower line capacities than centralized ones.

II. COUPLED OSCILLATOR MODEL WITH DECENTRAL SMART GRID CONTROL

To model the frequency dynamics of a large-scale power grid, we consider an oscillator model based on the physics of coupled synchronous generators and synchronous motors, see²⁴⁻³⁰ for details. This model is similar to the "classical model"³¹ and the "structure preserving model"³² from power engineering.

The state of each machine $i \in \{1, \dots, N\}$ is characterized by the rotor angle $\theta_i(t)$ relative to the grid reference rotating at $\Omega = 2\pi \times 50$ Hz or $\Omega = 2\pi \times 60$ Hz, respectively, and its angular frequency deviation $\omega_i = d\theta_i/dt$ from the reference. Each machine is driven by a

mechanical power $P_i(t)$, which is positive for a generator and negative for a consumer. In addition, every machine transmits electric power via the adjacent transmission lines which have a coupling strength K_{ij} . This coupling strength expresses the maximal possible power that may theoretically be transmitted through the power lines. The dynamics of the machine i is then given by the equation of motion as

$$\frac{d^2\theta_i}{dt^2} = P_i - \alpha_i \frac{d\theta_i}{dt} + \sum_{j=1}^N K_{ij} \sin(\theta_j - \theta_i) \quad \forall i \in \{1, \dots, N\}, \quad (1)$$

where α_i is a damping constant. We neglect ohmic loads which should be small compared to shunt admittances³³ for the dynamics we consider. We take the moment of inertia to be identical for all machines and hence eliminate such moments of inertia in the equation of motion for simplicity of presentation. Equation (1) as well as the upcoming equations (5) and (6) are discussed in more detail in²³.

Decentral Smart Grid Control (DSGC) is based on Demand Response that aims to stabilize the power system by encouraging consumers to lower their consumption in times of high load and low production and increase consumption in times of low load but high production. Instead of paying a constant price for electric power, consumers are presented with a linear price-frequency relation $p_i(\frac{d\theta_i}{dt})$

$$p_i(\frac{d\theta_i}{dt}) = p_\Omega - c_1 \cdot \frac{d\theta_i}{dt} \quad (2)$$

to motivate grid-stabilizing behavior. Although consumer reaction might be very complex, we assume a linearized power-price relation $\hat{P}_i(p_i)$

$$\hat{P}_i(p_i) \approx P_i + c_2 \cdot (p_i - p_\Omega) \quad (3)$$

by the consumers close to the stable operational state. Plugging (2) into (3) and defining $\gamma = c_1 \cdot c_2$ leads to a linear response of consumed and produced mechanical power $\hat{P}_i(t)$ as a function of frequency deviation $d\theta_i/dt$:

$$\hat{P}_i(t) = P_i - \gamma_i \frac{d\theta_i}{dt}(t) \quad \forall i \in \{1, \dots, N\}, \quad (4)$$

where γ_i is proportional to the price elasticity of each node i , i.e., measures how much a producer or consumer is willing to adapt their consumption or production, see also²³. In general, such an adaptation will not be instantaneous but will be delayed by a certain time τ

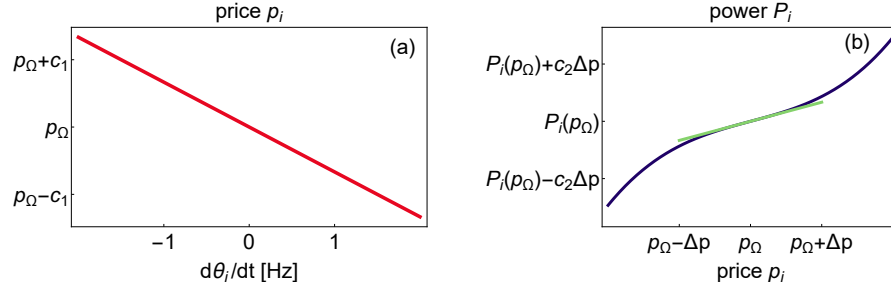


FIG. 1. Using linear relations the power becomes a linear function of the frequency deviation $d\theta_i/dt$. (a): We assume a linear price-frequency relation to motivate consumers to stabilize the grid. For example, if the production is larger than consumption, the power grid frequency increases. Hence, decreasing prices should motivate additional consumption. (b): Although consumers might react non-linearly towards price-changes (dark blue), we assume a linear relationship (light green) close to the operational frequency Ω which corresponds to $d\theta_i/dt = 0$.

by a measurement and the following reaction. We can now substitute the function $\hat{P}_i(t - \tau)$ from (4) for the fixed value P_i in the uncontrolled system (1) and obtain the equation of motion

$$\frac{d^2\theta_i}{dt^2} = P_i - \alpha_i \frac{d\theta_i}{dt} + \sum_{j=1}^N K_{ij} \sin(\theta_j - \theta_i) - \gamma_i \frac{d\theta_i}{dt}(t - \tau) \quad \forall i \in \{1, \dots, N\}, \quad (5)$$

with DSGC including a delayed power adaptation. In²³ it was already shown that such a delayed system poses risks to the stability of the power grid for certain delays τ . Hence, an extension using frequency measurements averaged over time intervals of lengths T were introduced to stabilize the power grid regardless of the specific delay. Such averaging yields

$$\begin{aligned} \frac{d^2\theta_i}{dt^2} &= P_i - \alpha_i \frac{d\theta_i}{dt} + \sum_{j=1}^N K_{ij} \sin(\theta_j - \theta_i) - \frac{\gamma_i}{T} \int_{t-T}^t \frac{d\theta_i}{dt}(t' - \tau) dt' \\ &= P_i - \alpha_i \frac{d\theta_i}{dt} + \sum_{j=1}^N K_{ij} \sin(\theta_j - \theta_i) - \frac{\gamma_i}{T} (\theta_i(t - \tau) - \theta_i(t - \tau - T)) \quad \forall i \in \{1, \dots, N\} \end{aligned} \quad (6)$$

For what follows, we choose homogeneous averaging time T for all machines, as well as similar delays τ for all nodes. In addition, we use homogeneous capacities $K_{ij} = K$ for all lines to simplify the calculations. In the section IV we apply equations (5) and (6) to

different network topologies and evaluate their stability as a function of the delay τ with different averaging times T . We hereby treat the averaging time T as a control parameter that can be chosen when setting up the system, while the delay τ remains as an exogenous parameter introduced by the consumers and producers.

III. ASSESSING ROBUST OPERATION

Here, we discuss how linear stability analysis and measuring basin volume yield information about robust operation, in dependence of delay τ and for different averaging times T . First, we introduce the fixed point of the system, then discuss linear stability analysis of delayed systems and finally point out difficulties when assessing basin volume of a power grid system with delay.

a. Fixed points. To study the stability and the role of the system parameters, we analyze the dynamical stability around the steady-state operation of the grid given by the fixed point

$$\left(\theta_i(t), \frac{d\theta_i}{dt}(t) \right) = (\theta_i^*, \omega_i^*) \quad \forall i \in \{1, \dots, N\}, \quad (8)$$

as obtained by solving

$$\frac{d^2}{dt^2}\theta_i = \frac{d}{dt}\theta_i = 0 \quad \forall i \in \{1, \dots, N\}. \quad (9)$$

Since $\omega_i = d\theta_i/dt$ we directly obtain $\omega_i^* = 0$ for all i . Hence, we only need to determine the angles θ_i^* . A fixed point can only exist, if the grid has a sufficient transmission capacity K_{ij} to transmit the power from the producers to the consumers³⁴. The minimal K_{ij} for which a stable fixed point exists is called critical coupling²⁶.

b. Linear stability. Linear stability of a dynamical system is determined by the eigenvalues of its characteristic equation. For systems without delay this is a polynomial obtained from the Jacobian of the system but for a delayed system it becomes a quasi-polynomial with infinitely many solutions^{35,36}. We obtain the characteristic equation by calculating the Jacobian of both the non-delayed system, based on equation (5) with $\tau = 0$,

$$J_0 = \begin{pmatrix} \frac{\partial}{\partial \theta_i} \left(\frac{d}{dt} \theta_j \right) & \frac{\partial}{\partial \omega_i} \left(\frac{d}{dt} \theta_j \right) \\ \frac{\partial}{\partial \theta_i} \left(\frac{d}{dt} \omega_j \right) & \frac{\partial}{\partial \omega_i} \left(\frac{d}{dt} \omega_j \right) \end{pmatrix} \in \mathbb{R}^{2N \times 2N}, \quad (10)$$

and the derivatives for the delayed terms involving τ ,

$$J_\tau = \begin{pmatrix} \frac{\partial}{\partial \theta_{\tau,i}} \left(\frac{d}{dt} \theta_j \right) & \frac{\partial}{\partial \omega_{\tau,i}} \left(\frac{d}{dt} \theta_j \right) \\ \frac{\partial}{\partial \theta_{\tau,i}} \left(\frac{d}{dt} \omega_j \right) & \frac{\partial}{\partial \omega_{\tau,i}} \left(\frac{d}{dt} \omega_j \right) \end{pmatrix} \in \mathbb{R}^{2N \times 2N}, \quad (11)$$

where we abbreviated $\theta_{\tau,i} = \theta_i(t - \tau)$ and $\omega_{\tau,i} = \frac{d\theta_i}{dt}(t - \tau)$ and $i, j \in \{1, \dots, N\}$. We hereby consider exponentially decaying or growing solutions³⁵. The stability eigenvalues λ are then determined by the solutions of the characteristic equation

$$p(\lambda) = \det(J_0 + e^{-\lambda\tau} J_\tau - \lambda \mathbb{1}) = 0. \quad (12)$$

For the delayed system with averaging, i.e., equation (6), we simply calculate the delayed Jacobian for the two delays τ and $\tilde{T} = T + \tau$. Hence, the characteristic equation is given by

$$p(\lambda) = \det(J_0 + e^{-\lambda\tau} J_\tau + e^{-\lambda\tilde{T}} J_{\tilde{T}} - \lambda \mathbb{1}) = 0. \quad (13)$$

We obtain the symbolic expression for the characteristic equation using Mathematica³⁷ which is then also used to numerically determine roots of the characteristic equation, via Newton's method. Equations (12) and (13) have infinitely many solutions but only a finite number of those can have a positive real part and those determine the instability of the system³⁸.

Our method of finding these eigenvalues works as follows: We start at an arbitrary delay $\tau = \tau_{\text{sampling}} > 0$ and let Mathematica find approximately 10,000 roots by choosing random complex initial conditions for Newton's algorithm. Afterwards, we delete double entries. The obtained eigenvalues are taken as the initial conditions for Newton's algorithm for the next larger delay $\tau = \tau_{\text{sampling}} + 0.01\text{s}$. These eigenvalues then serve as the initial conditions for the next delay step etc. Similarly, we obtain eigenvalues for smaller delays like $\tau = \tau_{\text{sampling}} - 0.01\text{s}$ by using again the eigenvalues from τ_{sampling} as initial conditions.

Linear stability analysis quantifies whether a fixed point is stable to small perturbations and constitutes a fundamental aspect of stability in dynamical system. Assessing the stability of the system with respect to larger perturbations requires further analysis.

c. Basin volume. The global stability of a fixed point of a dynamical system can be quantified by the volume of its basin of attraction. An estimate for the basin volume V_{basin} is determined numerically using a Monte Carlo method as the ratio of initial conditions converging to a stable operation state to the total number of initial conditions, as proposed in³⁹. Note that delayed systems are infinite-dimensional³⁵ and do need an initial function

instead of a single initial condition. We treat this problem by setting the initial function to be identical to the initial condition for all times smaller than zero, i.e.,

$$\theta(t \leq 0) = \theta(t = 0), \quad \omega(t \leq 0) = \omega(t = 0). \quad (14)$$

Thereby, we can effectively choose initial conditions as they completely define the initial function. In the following we take $M = 1000$ randomly chosen initial conditions into account in order to estimate the basin volume's dependence on the delay time τ .

We are mainly interested in how fluctuations or disturbances in the energy generation will influence the system's dynamics. Hence, we first perturb the producer's node phase angle and angular velocity around its component of the fixed point (see fig. 2a for the network topology). In the next series of simulations, we perturb one randomly selected customer node around its component of the fixed point. Perturbations are uniformly chosen at random from the intervals $\Delta\theta_i \in [-\pi, \pi]$ and $\Delta\omega_i \in [-30, 30]$ Hz for the initial angles and initial frequencies respectively, similar to^{29,40}. We run the simulations for a simulation time of $t_{\text{sim}} = 1500\text{s}$. These long and computationally costly simulation times are necessary because we observed that for specific values of delay time τ , e.g., $\tau = 1.4\text{s}$, perturbations may decay relatively quickly toward the fixed point but later still escalate.

Note that we only consider so-called single node basin volumes, i.e., we only perturb the component the a fixed point of one node. In theory, all nodes could be perturbed simultaneously which results in a more complete sample of the phase space. Unfortunately, the total phase space volume grows exponentially with the number of nodes, making it infeasible to sample the full phase space.

IV. RESULTS

We now present results about networks with Decentral Smart Grid Control. First, we present and compare the results of linear stability and basin volume analysis of a four node star motif. This motif constitutes one of the main building blocks of power grids, since, in principle, its effective topology locally resembles a star, the central node being a large power plant that supplies the regional consumers in its vicinity^{6,26}. Hereby, we discuss the destabilizing effects of resonances and the "rebound effect" for large delays. Using basin volume we present how intermediate delays τ benefit the stability. Finally, we consider larger

networks and demonstrate how decentralization enhances stability. The parameters of the swing equation are calculated from standard literature values^{31,40}. In current (European) power plants the initial delays have to be smaller than 2 seconds according to European regulations⁴¹, in practice they will be significantly smaller. However, in future power grids additional communication delays⁴² of the order of several hundred milliseconds might arise in addition to unknown delays caused by demand response and additional power electronics. Hence, we consider a large range of potential delays $\tau \in (0, 5)$ s looking for the boundary of acceptable delays.

A. Stability of the star motif

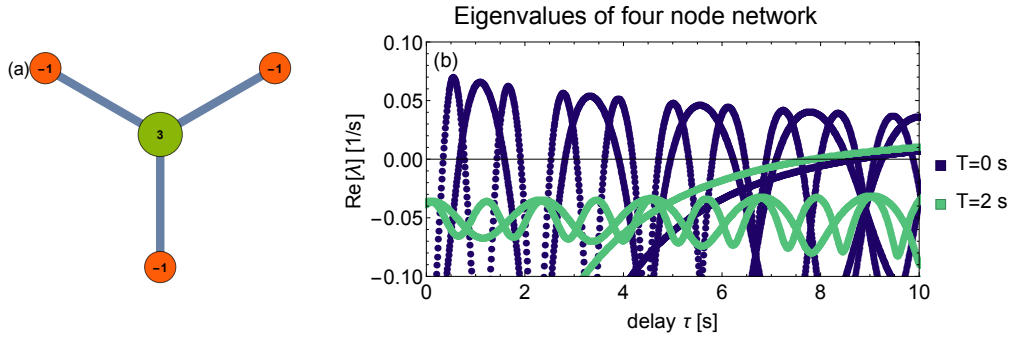


FIG. 2. **Resonances and large delays τ destabilize the four node system.** (a): An elementary building block in a power grid with centralized production is shaped like a star. Shown is a motif whose linear stability and basin volume we study. The network is formed of one producer (green) in the center with power $P_{\text{producer}} = 3/s^2$ and three consumers (red) with power $P_{\text{consumer}} = -1/s^2$ each. (b): Plotted are the eigenvalues with the largest real part as functions of delay τ . For no averaging (dark blue curve), stable and unstable regions exist. For an averaging of $T = 2$ s, the system is stable for all delays below a critical $\tau_c \approx 8$ s. In (6) parameters $\alpha = 0.1/s$, $K = 8/s^2$ and $\gamma = 0.25/s$ were applied.

d. Delays induce destabilizing resonances. Networks with star topology (fig 2a) exhibit stability properties that depend crucially on the delay and the averaging applied (fig. 2b). Without any averaging (fig. 2b dark blue curve), there are delays τ for which the fixed point is linearly unstable, i.e., there are eigenvalues with a positive real part $\text{Re } \lambda \geq 0$. Those

eigenvalues exhibit a periodic behavior with respect to the delay τ . Operating the power grid at a delay τ for which we find a positive real part, e.g., $\tau \approx 1\text{s}$, is equivalent to resonantly driving the power grid away from the fixed point instead of damping it towards stable operation. These destabilizing delays are linked to the eigenfrequency of the oscillators in the power grid. If the delay is half the eigenoscillation duration, then it increases amplitudes of perturbations instead of damping them. This destabilization only occurs for $\alpha < \gamma$ because the resonant driving has to be larger than the intrinsic damping of the system, see also²³. Introducing sufficiently large averaging times into the control cures these instabilities (fig. 2b light green curve); the unstable regions vanish for all delays $\tau < 7\text{s}$.

e. Rebound effect for large delays. For delays larger than a critical delay $\tau > \tau_c \approx 8.7\text{s}$ the system always gets destabilized, i.e., there is an eigenvalue with $\text{Re}(\lambda) > 0$. This rebound effect acts on a longer time scale than the intrinsic oscillations of the power grid system and originates from an over-reaction of the attempted damping as we explain below. The existence of such a rebound effect is independent of averaging T (fig. 2). We determine the critical delay without averaging τ_c to be

$$\tau_c = \frac{\arccos\left(-\frac{\alpha}{\gamma}\right)}{\sqrt{\gamma^2 - \alpha^2}} + \frac{2\pi n}{\sqrt{\gamma^2 - \alpha^2}}, \quad n \in \mathbb{Z}. \quad (15)$$

This result is obtained by the following considerations. We define the sum of all angles as $\Sigma\theta := \sum_{i=1}^N \theta_i$ and obtain its equation of motion by using eq. (5) as

$$\frac{d^2}{dt^2}\Sigma\theta(t) = -\alpha \frac{d}{dt}\Sigma\theta(t) - \gamma \frac{d}{dt}\Sigma\theta(t - \tau). \quad (16)$$

The characteristic equation of this equation reads

$$p(\lambda) = -\alpha - \gamma e^{-\lambda\tau} - \lambda = 0, \quad (17)$$

where we eliminated a zero eigenvalue $\lambda = 0$ which arises due to the possibility to shift all angles by a constant. For $\tau = 0$ the eigenvalue $\lambda = -\alpha - \gamma$ is negative as $\alpha > 0$ and $\gamma > 0$ and hence the system is stable with respect to the sum $\Sigma\theta$. For larger delays $\tau > 0$ we set $\lambda = i \cdot \xi$ to obtain the delays for which the stability changes. We get

$$-\alpha - \gamma e^{-i\xi\tau} - i\xi = 0. \quad (18)$$

Applying complex expansion and separating into real and imaginary parts we obtain

$$-\alpha - \gamma \cos(\xi\tau) = 0 \quad (19)$$

$$\gamma \sin(\xi\tau) - \xi = 0. \quad (20)$$

These equations can be solved for τ and ξ to yield the critical delay as in eq. (15). Note that a critical delay τ_c only exists, if the price adaptation is larger than the intrinsic damping of the system $\gamma > \alpha$. Following straight-forward calculations we can prove that eigenvalues obtained from eq. (17) always destabilize the system, i.e., their real parts are positive for all delays larger than the critical one,

$$\operatorname{Re}(\lambda(\tau)) > 0 \quad \forall \tau > \tau_c. \quad (21)$$

These results hold for all network topologies, since we needed no assumptions regarding the coupling matrix K_{ij} or the power production P_i . Predicting the precise scaling of the critical delay as a function of the averaging time T is not easily possible but an approximation for small ξT is obtained as

$$\tau_c(T) \approx \frac{\sqrt{T^2\gamma^2 - 4} \arctan \left[\frac{(\alpha + \gamma)\sqrt{T^2\gamma^2 - 4}}{(2 + T\gamma)\sqrt{\alpha^2 - \gamma^2}} \right]}{\sqrt{\alpha^2 - \gamma^2}}, \quad (22)$$

which is a decreasing function in T for parameters $\alpha, \gamma, T > 0$. Hence, increasing averaging time T causes the rebound effect to occur for smaller delays τ .

We conclude that the delay τ has to be smaller than a critical value τ_c to ensure stability. This critical value depends only on the intrinsic damping α and the price adaptation γ and decreases for increasing averaging T , while it is valid for all network topologies. Hence, to avoid problems with large delays, we have to enforce all actors of the power grid to react within less than this critical delay τ_c or need to ensure that intrinsic damping is larger than the price adaptation: $\alpha > \gamma$. For the next section, we restrict ourself to the interval $\tau \in [0, 5]$ s to avoid this destabilizing rebound effect.

f. Intermediate delays benefit stability. With the help of linear stability we observed that delays induce destabilizing resonances which can be suppressed by prosumers responding to averaged frequency data. At the same time large delays destabilize the system by introducing a rebound effect. These results are supplemented by information from basin volume analysis. For DSGC with averaging (fig. 3b and c), we demonstrate how intermediate delays τ are beneficial for the stability of the system. The basin volume increases

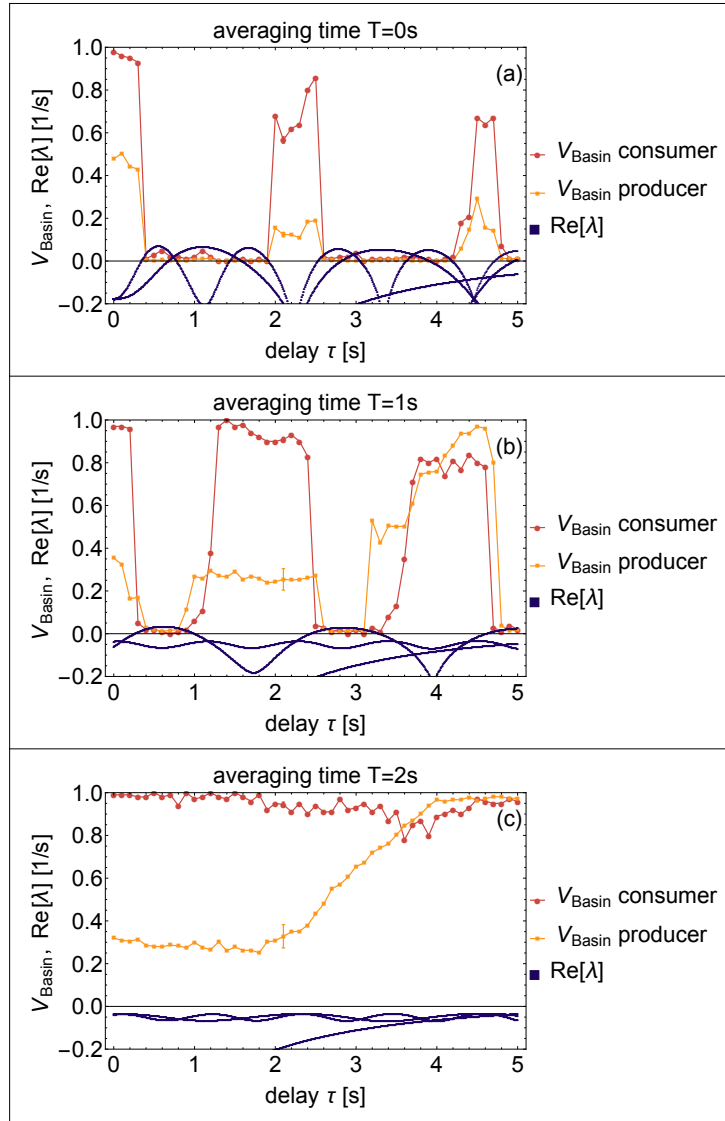


FIG. 3. Stability and basin size for the star topology (see fig. 2). Intermediate delays result in large basin volume if averaging is switched on. Shown are the real parts of the eigenvalues for the 4 node star motif (dark blue) as well as the basin volume of the producer (dark red) and of one consumer (orange) as functions of the delay τ for different averaging times: $T_a = 0\text{s}$, $T_b = 1\text{s}$, $T_c = 2\text{s}$. Parameters $\alpha = 0.1/\text{s}$, $K = 8/\text{s}^2$ and $\gamma = 0.25/\text{s}$ were applied. For delay $\tau = 2.1\text{s}$ simulations were repeated 21 times, averaged and the standard deviation is shown as a typical error bar.

with greater delay $V_{\text{basin}}(\tau > 0) > V_{\text{basin}}(\tau = 0)$ until, for delays $\tau \approx 4\text{s}$, we obtain close to perfect stability with $V_{\text{basin}} \approx 1$ both for an averaging $T_b = 1\text{s}$ and $T_c = 2\text{s}$. In the previous paragraph we demonstrated that high averaging times and large delays always destabilize the power grid. Hence, we observe a trade-off in curing resonances with averaging and avoiding the rebound effect for delays larger than a critical value τ_c . Furthermore, basin volume reveals that disturbances in a consumer node are less likely to destabilize the system than perturbations of the producer (compare dark red and light orange curves in fig. 3). This is intuitively clear as there is only one producer and the topology increases its importance even more.

We conclude that Decentral Smart Grid Control can be applied to the star motif if an averaging time of at least $T = 2\text{s}$ is used or the price elasticity is smaller than the intrinsic damping $\gamma < \alpha$. Additionally, intermediate delays $\tau \approx 4\text{s}$ incorporate the trade-off between curing either destabilizing resonances or rebound effects. They increase the basin volume of the system and thereby benefit the overall stability of the power grid.

B. Effect of decentralized production

In this section we demonstrate that switching from central to decentralized production improves the linear stability in the power grid topologies we investigate for small and intermediate delays. Specifically, we analyze linear stability for moderately sized lattice and cycle networks for different central and decentralized power production.

For a cycle network decentralization enhances stability significantly (fig. 4). For a power line coupling of $K = 8/\text{s}^2$ centralized and decentralized production result in similar stability (fig. 4b and e). However, when choosing the critical coupling of the cycle network, i.e., the minimal coupling needed so that there exists a fixed point²⁶, $K = 4/\text{s}^2$, the cycle with central production cannot be stabilized for all considered delays, while this is possible for decentralized production (fig. 4c and f).

A lattice-like topology for power grids allows stable operation with central power production (fig. 5). Choosing large couplings of $K = 8/\text{s}^2$ (fig. 5b and e) or even $K = 4/\text{s}^2$ (fig. 5c and g), decentralized and centralized production result in very similar stability. Even when operating at the critical coupling of the lattice-like topology $K = 2/\text{s}^2$, the central power production can be stabilized for sufficiently large averaging time $T = 4\text{s}$ (fig. 5d and h).

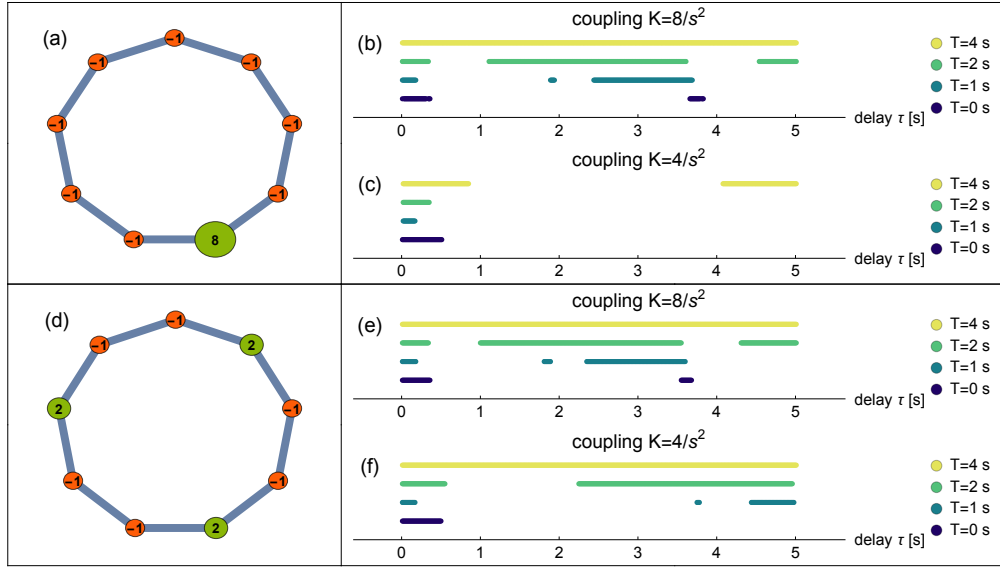


FIG. 4. **Central power production in a circle network requires larger capacity K than in decentralized power grids.** Shown are the ranges of delay τ for which the power grid motifs with central production (a) or decentralized production (d) are linearly stable. Panels (b) and (e) present ranges for a high capacity $K = 8/s^2$, whereas (c) and (f) for $K = 4/s^2$. Overall, the regions of stability tend to become larger, the larger the average time T . Parameters $\alpha = 0.1/s$ and $\gamma = 0.25/s$ were applied.

Note that we chose $\gamma_i = 0.25/s$ for all nodes in the networks. Hence, the large producer with $P_{\text{large}} = 8/s^2$ adapts relatively less compared to the smaller producers with $P_{\text{small}} = 2/s^2$. Nevertheless, the overall adaptation of the whole network is

$$\Delta P = \sum_{i=1}^N \gamma_i \cdot |\Delta\omega|, \quad (23)$$

with $|\Delta\omega|$ being the maximal angular frequency deviation. Hence, the maximal adaptation ΔP is independent of the power distribution.

We conclude that a centralized power production requires larger transmission capacities compared to a decentralized power production to guarantee stable power grid operation. An averaging time of $T \approx 4$ s stabilizes the power grid with Decentral Smart Grid Control for all considered delays. Note that our decentralized production utilized short distances to the consumers. Decentralized power production tends to allow smaller averaging times, thereby

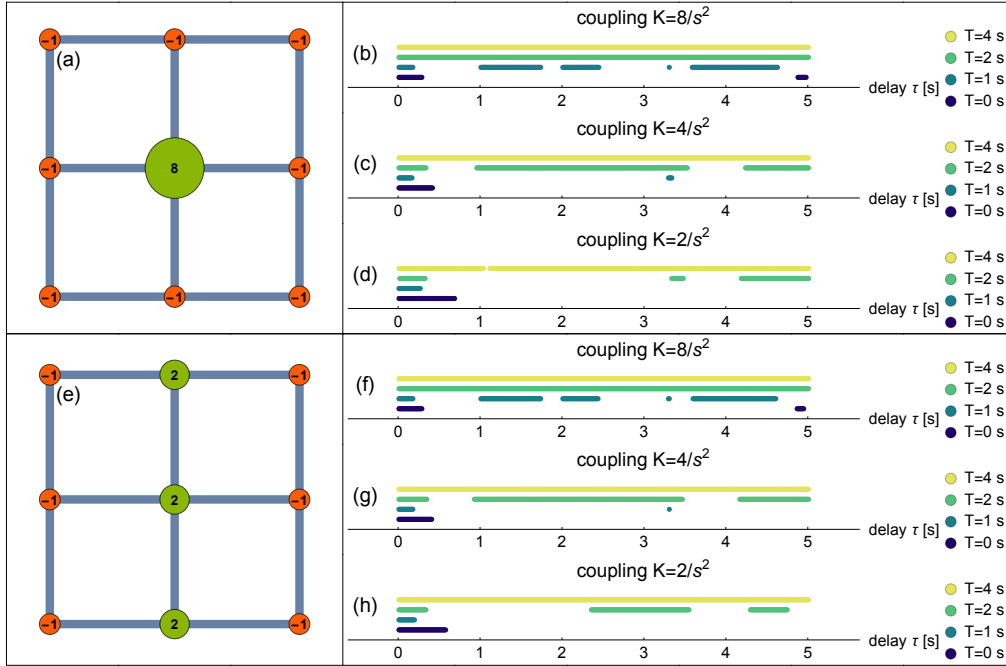


FIG. 5. **Central and decentralized power production in a lattice-like topology lead to similar stability.** In contrast to the cycle network, the lattice-like topology is stable for lower coupling K . Shown are the ranges of delay τ for which the power grid motifs with central production (a) or decentralized production (e) are linearly stable. Panels (b) and (f) present ranges for a high capacity $K = 8/s^2$, (c) and (g) for an intermediate capacity $K = 4/s^2$, finally (d) and (h) for $K = 2/s^2$. Overall, the regions of stability tend to become larger, the larger the average time T . Parameters $\alpha = 0.1/s$ and $\gamma = 0.25/s$ were applied.

offering a greater safe operating space. In addition, a highly connected topology like a lattice outperforms the less connected cycle in terms of stability.

V. SUMMARY AND DISCUSSION

In this article we applied the concept of "Decentral Smart Grid Control" (DSGC), as proposed in²³, to different motifs and small networks. We first determined both the linear stability and the basin volume of a 4-node-star motif in dependence on the delay time τ (see equation 5) and for fixed averaging times T (see equation 6). Linear stability analysis

reveals two destabilizing effects for the power grid: First, resonance catastrophes destabilize the system periodically. This instability can be cured by applying sufficient averaging (fig. 2). Secondly, a rebound effect emerges for large delays and destabilizes the system regardless of averaging. The rebound effect sets an upper limit for the delay $\tau = \tau_c$ and magnitude of adaptation response γ as it has to be smaller than the intrinsic damping of the system α . Basin volume analysis gives further probabilistic insight on how well DSGC tames grid instabilities. For large averaging times T and intermediate delays τ , basin volume approaches unity (fig. 3). Hence, for DSGC exists a trade-off in curing resonances with averaging and larger delays and avoiding the rebound effect for delays larger than a critical value τ_c .

Summarizing the results from linear and basin volume analysis, adaptation has to be smaller than the intrinsic damping of the system ($\gamma < \alpha$) or the demand response time needs to be located in a delay window of safe operation ($\tau < \tau_c$). For values above the critical delay τ_c the system becomes always destabilized, regardless of the averaging time. At the same time, averaging and increasing delay is beneficial for system stability in terms of basin volume. These results have strong implications on how parameters has to be set for real world applications of DSGC.

In the last section of this article, we demonstrated the usefulness of DSGC with centralized as well as with decentralized power production: While it works in both cases, central production requires larger line capacities K . For the lattice-like topology, this effect can be compensated by using longer averaging times. But decentralized power production is clearly advantageous.

Next research steps include considering heterogeneous networks, i.e. the use of different τ , γ , T values for individual nodes, modifying the averaging method, e.g., to a discrete time window and extending the DSGC framework to larger network topologies. In this context, there remain a couple of open questions that will have to be investigated in more detail, namely: What is the reason that we observe delays τ for which $V_{\text{basin}}(\tau) > V_{\text{basin}}(\tau = 0)$, in particular for larger averaging times? Do we need even larger averaging times T when we go to larger networks? How large is the safe operating space to cure instabilities by resonances while avoiding the rebound effect for different networks? These are all widely open questions.

In this article, we have demonstrated that Decentral Smart Grid Control constitutes a promising control concept, in particular for future power grids that will be more decentralized

than the present one.

ACKNOWLEDGMENTS

We thank Dr. Thomas Walter at Easy Smart Grid GmbH for inspiration and valuable discussions. This work was supported by the BMBF, grants No. 03SF0472A (C.G., S.A., J.K.), No. 03SF0472B (D.W.) and No. 03SF0472E (M.T.), by the Helmholtz Association, grant no. VH-NG-1025 (D.W.), by the Max Planck Society (M.T.), by the G ttingen Graduate School for Neurosciences and Molecular Biosciences (DFG Grant GSC 226/2) (B.S.).

REFERENCES

- ¹O. Edenhofer, R. Madruga, Y. Sokona, and K. Seyboth. IPCC Special Report on Renewable Energy Sources and Climate Change Mitigation. 2011.
- ²Bundesministerium f r Wirtschaft und Energie. Erneuerbare Energien im Jahr 2014, 2015.
- ³T. Ackermann, G. Andersson, and L. S der. Distributed Generation: a Definition. *Electric Power Systems Research*, 57(3):195–204, 2001.
- ⁴P. Kotler. The Prosumer Movement: A new Challenge for Marketers. *Advances in Consumer Research*, 13(1):510–513, 1986.
- ⁵J. A. Turner. A Realizable Renewable Energy Future. *Science*, 285(5428):687–689, 1999.
- ⁶50Hertz, Amprion, TenneT TSO, and TransnetBW. Netzentwicklungsplan Strom, 2012.
- ⁷G. Boyle. *Renewable Energy*. Oxford University Press, Oxford, 2004.
- ⁸D. Heide, L. Von Bremen, M. Greiner, C. Hoffmann, M. Speckmann, and S. Bofinger. Seasonal Optimal Mix of Wind and Solar Power in a Future, Highly Renewable Europe. *Renewable Energy*, 35(11):2483–2489, 2010.
- ⁹P. Milan, M. W chter, and J. Peinke. Turbulent Character of Wind Energy. *Physical Review Letters*, 110(13):138701, 2013.
- ¹⁰Bundesministerium f r Wirtschaft und Energie (BMWi). Ein Strommarkt f r die Energiewende, Oktober 2014.
- ¹¹M. Jansen, C. Richts, and N. Gerhardt. Strommarkt-Flexibilisierung - Hemmnisse und L sungskonzepte, Januar 2015.

- ¹²D. Butler. Energy Efficiency: Super Savers: Meters to manage the Future. *Nature*, 445(7128):586–588, 2007.
- ¹³M. H. Albadi and E. F. El-Saadany. A Summary of Demand Response in Electricity Markets. *Electric Power Systems Research*, 78(11):1989–1996, 2008.
- ¹⁴P. Palensky and D. Dietrich. Demand Side Management: Demand Response, Intelligent Energy Systems, and Smart Loads. *Industrial Informatics, IEEE Transactions on*, 7(3):381–388, 2011.
- ¹⁵J. K. Kok, C. J. Warmer, and I.G. Kamphuis. PowerMatcher: Multiagent Control in the Electricity Infrastructure. In *Proceedings of the Fourth International joint Conference on Autonomous Agents and Multiagent Systems*, pages 75–82. ACM, 2005.
- ¹⁶L. Hofmann and M. Sonnenschein. Smart Nord Final Report, 2015.
- ¹⁷G. N. Ericsson. Cyber Security and Power System Communication - Essential Parts of a Smart Grid Infrastructure. *Power Delivery, IEEE Transactions on*, 25(3):1501–1507, 2010.
- ¹⁸X. Fang, S. Misra, G. Xue, and D. Yang. Smart Grids - The new and improved Power Grid: A Survey. *Communications Surveys & Tutorials, IEEE*, 14(4):944–980, 2012.
- ¹⁹Ernst & Young GmbH. Cost-benefit Analysis for the Comprehensive Use of Smart Metering Systems - Final Report - Summary, January 2013.
- ²⁰F. C. Schweppe. Frequency Adaptive, Power-Energy Re-scheduler, February 23 1982. US Patent 4,317,049.
- ²¹J. A. Short, D. G. Infield, and L. L. Freris. Stabilization of Grid Frequency through Dynamic Demand Control. *Power Systems, IEEE Transactions on*, 22(3):1284–1293, 2007.
- ²²T. Walter. Smart Grid neu gedacht: Ein Lösungsvorschlag zur Diskussion in VDE|ETG, 2014.
- ²³B. Schäfer, M. Matthiae, M. Timme, and D. Witthaut. Decentral Smart Grid Control. *New Journal of Physics*, 17(1):015002, 2015.
- ²⁴G. Filatrella, A. H. Nielsen, and N. F. Pedersen. Analysis of a Power Grid using a Kuramoto-like Model. *The European Physical Journal B-Condensed Matter and Complex Systems*, 61(4):485–491, 2008.
- ²⁵D. Witthaut and M. Timme. Braess’s Paradox in Oscillator Networks, Desynchronization and Power Outage. *New Journal of Physics*, 14(8):083036, 2012.

- ²⁶M. Rohden, A. Sorge, D. Witthaut, and M. Timme. Impact of Network Topology on Synchrony of Oscillatory Power Grids. *Chaos: An Interdisciplinary Journal of Nonlinear Science*, 24(1):013123, 2014.
- ²⁷F. Dörfler M., Chertkov F., and Bullo. Synchronization in Complex Oscillator Networks and Smart Grids. *Proceedings of the National Academy of Sciences*, 110(6):2005–2010, 2013.
- ²⁸A. E. Motter, S. A. Myers, M. Anghel, and T. Nishikawa. Spontaneous Synchrony in Power-grid Networks. *Nature Physics*, 9(3):191–197, 2013.
- ²⁹P. J. Menck, J. Heitzig, J. Kurths, and H. J. Schellnhuber. How Dead Ends undermine Power Grid Stability. *Nature Communications*, 5(3969), 2014.
- ³⁰M. Rohden, A. Sorge, M. Timme, and D. Witthaut. Self-organized Synchronization in Decentralized Power Grids. *Physical Review Letters*, 109(6):064101, 2012.
- ³¹J. Machowski, J. Bialek, and J. Bumby. *Power System Dynamics: Stability and Control*. John Wiley & Sons, 2011.
- ³²A. R. Bergen and D. J. Hill. A Structure preserving Model for Power System Stability Analysis. *Power Apparatus and Systems, IEEE Transactions on*, 100(1):25–35, 1981.
- ³³D. Van Hertem, J. Verboomen, K. Purchala, R. Belmans, and W. L. Kling. Usefulness of DC Power Flow for Active Power Flow Analysis with Flow Controlling Devices. In *AC and DC Power Transmission, 2006. ACDC 2006. The 8th IEE International Conference on*, pages 58–62. IET, 2006.
- ³⁴D. Manik, D. Witthaut, B. Schäfer, M. Matthiae, A. Sorge, M. Rohden, E. Katifori, and M. Timme. Supply Networks: Instabilities without Overload. *The European Physical Journal Special Topics*, 223(12):2527–2547, 2014.
- ³⁵R. D. Driver. Introduction to Delay Differential Equations. In *Ordinary and Delay Differential Equations*, pages 225–267. Springer, 1977.
- ³⁶M. R. Roussel. *Delay-Differential Equations*, 2005.
- ³⁷Wolfram Research Inc. *Mathematica*. Champaign, Illinois, 2014.
- ³⁸K. Gu, J. Chen, and V. L. Kharitonov. *Stability of Time-delay Systems*. Springer Science & Business Media, 2003.
- ³⁹P. J. Menck, J. Heitzig, N. Marwan, and J. Kurths. How Basin Stability Complements the Linear-stability Paradigm. *Nature Physics*, 9(2):89–92, 2013.

⁴⁰P. Schultz and J. Heitzig and J. Kurths. Detours around Basin Stability in Power Networks. *New Journal of Physics*, 16(12):125001, 2014.

⁴¹ENTSO-E. Network code on requirements for grid connection applicable to all generators (rfg), March 2013.

⁴²Biju Naduvathuparambil, Matthew Valenti, Ali Feliachi, et al. Communication delays in wide-area measurement systems. In *Southeastern Symposium on System Theory*, volume 34, pages 118–122. Citeseer, 2002.

Chapter 5

Escape Routes, Weak Links, and Desynchronization in Fluctuation-driven Networks

Citation

Benjamin Schäfer, Moritz Matthiae, Xiaozhu Zhang, Martin Rohden, Marc Timme and Dirk Witthaut (2017), Escape Routes, Weak Links, and Desynchronization in Fluctuation-driven Networks, Physical Review E 95, 060203(R), DOI: <https://doi.org/10.1103/PhysRevE.95.060203>

©2017 American Physical Society. Permission to reprint this article in the author's thesis is granted by the American Physical Society.

Original Contribution

Conception of the research was done with M. Timme and D. Witthaut. I performed most analytical calculations, for the first part of the results with support by M. Matthiae, taking into account parts of M. Matthiae's bachelor's thesis. I produced the data for figure 1 and panels a,b in Figure 3. I wrote large parts of the introduction and method sections, as well as the first part of the conclusion. I significantly contributed to the writing of the results section. I revised the manuscript during the revision process, updating texts and figures according to referee suggestions and set up the supplemental material including alternative models and carrying out all simulations. Overall, M. Matthiae and I contributed equally.

PHYSICAL REVIEW E **95**, 060203(R) (2017)**Escape routes, weak links, and desynchronization in fluctuation-driven networks**Benjamin Schäfer,¹ Moritz Matthiae,^{1,2,*} Xiaozhu Zhang,¹ Martin Rohden,^{1,3} Marc Timme,^{1,4,5} and Dirk Witthaut^{2,6}¹*Network Dynamics, Max-Planck-Institute for Dynamics and Self-Organization (MPI DS), 37077 Göttingen, Germany*²*Forschungszentrum Jülich, Institute for Energy and Climate Research—Systems Analysis and Technology Evaluation (IEK-STE), 52428 Jülich, Germany*³*Jacobs University, Department of Physics and Earth Sciences, 28759 Bremen, Germany*⁴*Department of Physics, Technical University of Darmstadt, 64289 Darmstadt, Germany*⁵*Institute for Theoretical Physics, Technical University of Dresden, 01062 Dresden, Germany*⁶*Institute for Theoretical Physics, University of Cologne, 50937 Köln, Germany*

(Received 29 November 2016; revised manuscript received 16 March 2017; published 9 June 2017)

Shifting our electricity generation from fossil fuel to renewable energy sources introduces large fluctuations to the power system. Here, we demonstrate how increased fluctuations, reduced damping, and reduced inertia may undermine the dynamical robustness of power grid networks. Focusing on fundamental noise models, we derive analytic insights into which factors limit the dynamic robustness and how fluctuations may induce a system escape from an operating state. Moreover, we identify weak links in the grid that make it particularly vulnerable to fluctuations. These results thereby not only contribute to a theoretical understanding of how fluctuations act on distributed network dynamics, they may also help designing future renewable energy systems to be more robust.

DOI: [10.1103/PhysRevE.95.060203](https://doi.org/10.1103/PhysRevE.95.060203)

Introduction. The development of a sustainable energy supply is one of the major technical, economical, and societal challenges of the coming decades. To mitigate climate change, the majority of existing fossil-fuel power plants will be replaced by renewable energy sources, in particular wind and solar power [1,2]. This requires a comprehensive reengineering of the electric power grid as well as a better understanding of the operation, dynamics, and stability of complex networked systems [3–6].

The operation of wind turbines and photovoltaics is essentially determined by the weather such that the power generation fluctuates strongly on all time scales [7]. Large storage and backup infrastructures are needed to balance power generation and demand on time scales of hours to months [8]. In addition, the high-frequency fluctuations can be enormous, in particular due to the turbulent character of wind power [9,10]. At the same time, large fossil-fuel plants are closed down such that the effective inertia and damping decreases, making the power grid more vulnerable to instabilities by transients [11].

Here we analyze how high-frequency fluctuations threaten the dynamical robustness of electric power grids. The stable operation of a grid requires all generators and loads to remain phase locked. We analyze the robustness of this phase-locked state, mapping the grid dynamics to an escape problem in a high-dimensional stochastic dynamical system. This analysis reveals essential factors which limit the operability of future power grids. Furthermore, we uncover how the network topology determines the robustness of the grid and identify potential escape routes and vulnerable links in complex networks.

Synchronization and robustness of electric power grids. Consider first the dynamics of coupled synchronous genera-

tors and consumers $j \in \{1, \dots, N\}$. Each unit's dynamics is described by the swing equation [12–14] for the mechanical rotor angle δ_j and the phase velocity ω_j relative to the grid reference frequency $\Omega = 2\pi \times 50$ (or 60) Hz,

$$\dot{\delta}_j = \omega_j, \quad (1)$$

$$\frac{2H_j}{\Omega} \dot{\omega}_j + 2\Omega D_j \omega_j = P_j - P_j^{(\text{el})}, \quad (2)$$

where the right-hand side is the net power acting on the machine. The swing equation is made dimensionless by dividing all terms by the rated power of the machine, which is referred to as the “per unit system” in engineering [12]. The inertia constant H_j then gives the stored kinetic energy at synchronous speed which is proportional to the moment of inertia of the j th machine and D_j is a damping constant. If not mentioned otherwise, we assume a typical value of inertia $H_j = H = 4$ s and a damping constant of $D_j = D = 4 \times 10^{-5} \text{ s}^2$ [15,16].

The input power P_j driving a machine can be subject to strong fluctuations on various time scales induced by renewable resources [9] or consumer behavior [17]. We thus analyze the robustness of the phase-locked state to stochastic fluctuations $\xi_j(t)$, i.e., we set

$$P_j(t) = \bar{P}_j + \xi_j(t). \quad (3)$$

The electric power $P_j^{(\text{el})}$ exchanged over a transmission line is determined by the difference of the voltage phase angle of the two terminal nodes. For a common two-pole machine the voltage phase angle equals the mechanical phase angle such that the transmitted real power reads $K_{ij} \sin(\delta_i - \delta_j)$. The capacity parameter K_{ij} , describing the maximally transmittable power on the transmission line between nodes i and j , is determined by the susceptance B_{ij} of the line and the voltage levels E_i and E_j at the two units as $K_{ij} = B_{ij} E_i E_j$. We note that K gives the physical limit of the transmitted real

*Current address: Department of Micro- and Nanotechnology, Technical University of Denmark, 2800 Kongens Lyngby, Denmark.

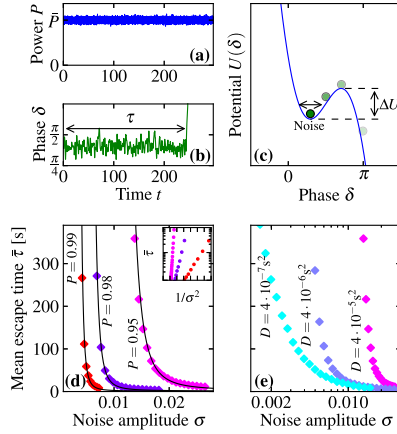
BENJAMIN SCHÄFER *et al.*PHYSICAL REVIEW E **95**, 060203(R) (2017)

FIG. 1. Fluctuating power input may desynchronize a synchronous generator. (a),(b) When the input power P fluctuates, the generator can lose synchrony to the grid after an escape time τ . (c) The generator dynamics corresponds to the motion of a particle in a tilted washboard. The fluctuations can drive the particle over the potential barrier of height ΔU . (d) Kramer's escape rate theory predicts the escape process for Gaussian white noise. Theoretical prediction, Eq. (5), (black lines) perfectly predicts the mean escape times $\bar{\tau}$ for intermediate damping ($D = 4 \times 10^{-5} \text{ s}^2$) as checked by direct numerical simulations (symbols). The averaged escape time crucially decreases with increasing load P of the system. (e) Weaker damping D undermines system robustness, which can become a major problem in future power grids. (Parameters: $H = 4 \text{ s}$, $K = 1$, and $\bar{P} = 0.95$, if not stated otherwise.)

power in the lossless case of our dynamical model. Ohmic losses can lead to an overheating of lines on longer time scales leading to the definition of *thermal capacity*, which includes a security limit by the grid operators [12,18].

In a complex network of lines and generators the total electric power transmitted from machine j is thus given by $P_j^{(\text{el})} = \sum_i K_{ij} \sin(\delta_i - \delta_j)$. Stable operation of the grid requires all units to be in a phase-locked state where $\delta_i - \delta_j$ is fixed. Otherwise, the transmitted electric power $P_j^{(\text{el})}(t)$ would oscillate and average out over time [14,15,19–21]. Throughout this Rapid Communication we assume a heavily loaded grid, where phase differences are comparably large in the stable phase-locked state. Such a situation is yet uncommon, but will become increasingly likely in the future [22]. Other scenarios are analyzed in the Supplemental Material [23], including less heavily loaded transmission lines, inverters without inertia H [24], and higher-order power grid models including voltage dynamics [12,25].

Robustness of a single generator. First, consider a single generator coupled to a large bulk grid. The steady-state operation of the generator is described by a stable phase-locked state, a fixed point of the swing equation with a constant phase difference δ relative to the grid. Fluctuations of the input power P can destabilize the grid as illustrated in Figs. 1(a) and 1(b). As soon as the generator leaves the basin of attraction of the stable phase-locked state after some time τ it rapidly

desynchronizes. Such a serious contingency requires immediate emergency measures to avoid a global network failure.

We analyze desynchronization due to white noise by Kramer's escape rate theory [26–29] as follows: The equation of motion for the generator is equivalent to a driven dissipative particle moving in a tilted washboard potential [30], i.e., $\delta + (\Omega^2 D/H)\delta = (\Omega/2H)[-dU/d\delta + \xi(t)]$ with the effective potential [31]

$$U(\delta) = -\bar{P}\delta - K \cos(\delta). \quad (4)$$

Thus, to escape the basin of attraction around a local minimum of $U(\delta)$ the particle must overcome a potential barrier of height ΔU [see Fig. 1(c)], which is determined by the transmitted power P and the capacity K . For Gaussian white noise $\xi(t)$ with standard deviation σ the mean escape time is given by [27]

$$\bar{\tau} = \frac{2\pi\lambda}{\sqrt{U''(\delta_{\min})|U''(\delta_{\max})|}} \exp\left(\frac{2\gamma\Delta U}{\sigma^2}\right), \quad (5)$$

with effective damping $\gamma = 2D\Omega$ and $2\lambda = \gamma + \sqrt{\gamma^2 + (8H/\Omega)|U''(\delta_{\max})|}$ for intermediate damping and $U''(\delta_{\min})$ and $U''(\delta_{\max})$ being the second derivatives of the potential evaluated at the local minimum and the saddle point of the potential $U(\delta)$, respectively [27]. Numerical simulations averaged over 2000 escape processes for each value of σ show excellent agreement with this prediction [see Fig. 1(d)].

Major concerns about the stability of future power grids arise from the increased transmission needs and lines loads [22] as well as a possible lack of effective inertia and damping when conventional generators are replaced by renewables [11]. Heavily loaded lines are indeed very susceptible to desynchronization as shown in Fig. 1(d). Increasing the load P rapidly decreases the escape time $\bar{\tau}$. Similarly, a decrease of the effective damping factor D implies a rapid decrease of $\bar{\tau}$ [Fig. 1(e)]. In contrast, the inertia H has a minor effect only, as it enters the escape rate (5) only through the nonexponential prefactors [23].

We note that this stability assessment defined by Kramer's escape rate is complementary to existing studies investigating large-scale perturbation in power grids in terms of Lyapunov exponents [32], basin stability [33], or cascading failures [34–36]. Our stochastic approach focuses on small perturbations eventually driving the grid out of synchrony in contrast to singular large disturbing events.

Escape dynamics in phase space. The essential factors in Kramer's formula (5) are the amplitude of the noise σ , the effective damping γ , and the height of the potential barrier ΔU . The theory of random dynamical systems [29] implies that in the limit of weak noise ($\sigma \rightarrow 0$) the system escapes the basin of attraction in the vicinity of a saddle point, where the potential gap to the stable fixed point is smallest. An exemplary escape process in phase space is shown in Fig. 2 for the single generator system. Intriguingly, we observe that at any nonzero noise level $\sigma > 0$, the trajectory leaves the basin near but not exactly at the saddle point (red dot). Only in the limit of small perturbations, i.e., $\sigma \rightarrow 0$, does the system leave the fixed point exactly at the saddle.

The saddle point itself is characterized by a vanishing velocity $d\delta/dt = 0$. However, all simulated trajectories leave the basin with a nonvanishing velocity $d\delta/dt > 0$ (i.e.,

ESCAPE ROUTES, WEAK LINKS, AND ...

PHYSICAL REVIEW E 95, 060203(R) (2017)

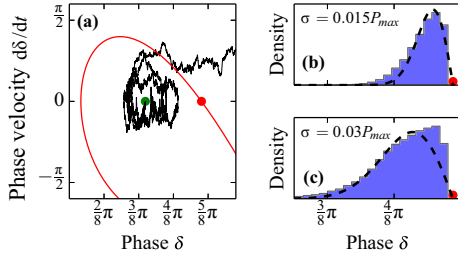


FIG. 2. Where does the system escape? (a) Exemplary escaping process of the basin of attraction in phase space. The state trajectory (thin black line) crosses the boundary of the basin of attraction (red line) in the vicinity of but not at the saddle point (red disk). The stable fixed point is indicated by a green disk. (b),(c) Probability distribution of exit points, i.e., the crossing points of the trajectory and the basin boundary. Numerical results (histogram) compared to the theoretical prediction, Eq. (6) (dashed black line). With increasing noise the distribution becomes broader, i.e., a crossing at some distance from the saddle point (red disk) becomes more probable. (Parameters: $K = 1$ and $\bar{P} = 0.95$ as in Fig. 1.)

“above” the saddle point in the phase space portrait shown in Fig. 2). More precisely, the probability density of the trajectory on the basin boundary in phase space is given by a Weibull function [37]

$$p(\delta) = \mathcal{N}\delta \exp\left(-\frac{\lambda^2\delta^2}{2\sigma^2} - \frac{2\Omega}{H} \frac{|U''(\delta_{\max})|\delta^2}{2\sigma^2}\right), \quad (6)$$

where \mathcal{N} is a normalization constant. This theoretical prediction is equally well confirmed by the numerical simulations as shown in Fig. 2 on the right. With increasing noise amplitude the distribution gets broader, i.e., the escape velocity increases.

Escape via the weakest link. To maintain a stable operation it is essential to know not only under which conditions, but also how power system operation may become unstable. We first consider a simple system of two identical generators coupled to a bulk power grid with transmission lines of different capacity, both being subject to independent and identically distributed Gaussian white noise [see Fig. 3(a)]. Either of the two generators can become unstable, such that the grid can escape the basin of attraction of the stable phase-locked state via two different routes. Scaling of the mean escape time is still described by Kramer’s rate for intermediate damping, when we take into account that the lower potential barrier along both routes determines the escape [see Fig. 3(b)]. The two-dimensional potential is then given as

$$U(\delta_1, \delta_2) = -\bar{P}_1\delta_1 - K_1 \cos(\delta_1) - \bar{P}_2\delta_2 - K_2 \cos(\delta_2). \quad (7)$$

In the limit of weak noise the escape problem is fully determined by the path with the smallest potential barrier ΔU . To illustrate this we vary the capacity K_2 of the transmission line connecting generator 2 to the bulk grid while the capacity K_1 of the other line remains fixed. For $K_2 < K_1$ the robustness is dominated by generator 2, whose connection is weaker. The exponent in Kramer’s formula (5) then crucially depends on the value of K_2 . Indeed, the exponent obtained from the numerical

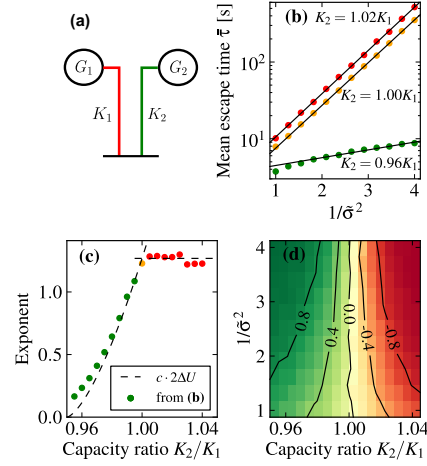


FIG. 3. The easiest escape route determines the escape time $\bar{\tau}$. (a) Two identical generators are coupled to a third node representing the bulk grid via transmission lines with capacity $K_1 = 1$ (constant) and K_2 (variable), respectively. The transmitted power on both lines is $\bar{P}_{1,2} = 0.95$. Power fluctuates on all nodes independently. (b) The mean escape time $\bar{\tau}$ as a function of the noise amplitude σ . Disks represent numerical values; the solid lines are fits to extract the scaling exponent. (c) In this scenario, the exponent in Kramer’s rate is determined by the lowest barrier ΔU , Eq. (7) of the two-dimensional potential landscape, which is determined by $\min\{K_1, K_2\}$, i.e., the weaker of the two transmission line capacities. Thus it increases with K_2 as long as $K_2 \leq K_1$ but depends only on K_1 for $K_2 > K_1$. A comparison of numerical results obtained from exponential fits to the data (disks) and the analytical value of the potential barrier ΔU (with constant c) shows very good agreement. (d) Imbalance of the two escape routes: $p_2 - p_1$ with $p_{1,2}$ being the probability that link 1 or 2 is overloaded first, as a function of K_2/K_1 and the noise amplitude. For weak noise there is a sharp transition at $K_2/K_1 = 1$, which smears out for stronger noise. Panels (b)–(d) use a rescaled noise $\bar{\sigma} = 40\sigma$.

simulations again matches the theoretical predictions well in terms of the potential barrier ΔU [see Fig. 3(c)]. If we increase K_2 beyond K_1 , the other transmission line becomes the Achilles’ heel of the grid. The potential barrier and hence the exponent in Kramer’s formula thus no longer depend on K_2 . Yet, the nonexponential prefactor in the formula (5) increases by increasing K_2 further because the relative transmission line load of the overall system decreases. When the noise becomes stronger, the sharp transition between the two possible escape routes gradually blurs, such that the more strongly connected generator can become unstable too [see Fig. 3(d)].

Robustness of complex power grids. In power grids with a less simple structure, it is essential to understand how the topology determines robustness and to identify possible routes of instability. This enables a precise improvement of the grid and the elimination of weak links. Figure 4(a) shows the stable fixed point in a grid with four generator and eight consumer nodes. The consumer dynamics also follows Eq. (2), but with $P_j < 0$. A fluctuating input can lead to a loss of synchrony and eventually to a system-wide failure. But where does this

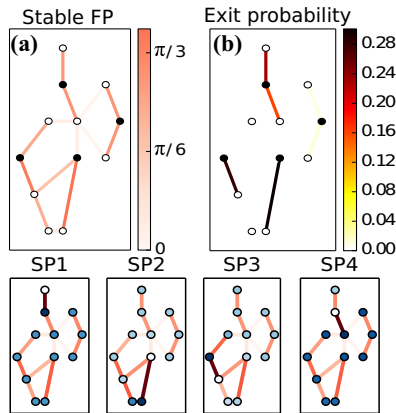
BENJAMIN SCHÄFER *et al.*PHYSICAL REVIEW E **95**, 060203(R) (2017)

FIG. 4. Vulnerable links predicted by the topology of saddle points. Top: (a) The stable phase-locked fixed points in a model power grid with four generators (filled circles) and eight consumers (open circles). Shown is the phase difference $\delta_i - \delta_j$ along the transmission lines. (b) Probability that a transmission line is overloaded first ($|\delta_i(t) - \delta_j(t)|$ crosses $\pi/2$) when the grid becomes unstable due to a fluctuating power input. Four vulnerable transmission lines are identified. Bottom: The vulnerable transmission lines can be traced back to four different saddle points with comparably low potential barrier. All saddle points have exactly one transmission line (darkest line in each plot) with $|\delta_i - \delta_j| > \pi/2$, corresponding to the vulnerable lines identified in (b). The color scale shows the phase differences as in panel (a). The networks consist of four generators (\bullet , $P_j = +2P_0$) and eight consumers (\circ , $P_j = -P_0$); all lines have capacity $K = 24/19 \times P_0$.

instability emerge and which of the transmission lines is most vulnerable?

We simulate the dynamics with all machines subject to independent and identically distributed white noise and record which transmission line becomes overloaded first, i.e., we record for which link (i, j) the phase difference $|\delta_i - \delta_j|$ first crosses $\pi/2$. In this way we identify four transmission lines which are vulnerable. Strikingly, these vulnerable lines are not necessarily the ones which are most heavily loaded in the first place. The loss of synchrony in a complex grid is a collective process, which cannot fully be understood from fundamental properties of single nodes or lines [38,39].

Instead, Kramer's theory tells that the saddle points of the entire dynamical system are decisive: As above, the grid leaves the basin of attraction of the stable phase-locked state in the vicinity of the saddle points. In a complex network, many saddle points may exist. But for the application of Kramer's theory we only need to consider those saddle points with the lowest potential barrier, as escape through all other saddle points is exponentially suppressed. For the system studied here, these saddle points are calculated systematically using a

method introduced in [40]. This method classifies the saddle points by the number of links (i, j) where the phase difference $|\delta_i - \delta_j|$ exceeds $\pi/2$. Typically, the higher this number, the higher is the potential barrier.

For the sample network depicted in Fig. 4 for illustration, this method yields four saddle points with a comparably low potential barrier, all contributing to the escape process (four lower panels). All four saddles have exactly one line where the phase difference $|\delta_i - \delta_j|$ exceeds $\pi/2$. The static analysis thus yields four vulnerable lines which exactly match the lines where overloads have been recorded in the numerical simulations. Even more, Kramer's rate with the respective barrier heights again predicts the exit probabilities (not shown).

Conclusion. In this Rapid Communication we have analyzed how high-frequency fluctuations impact the dynamical robustness of electric power grids. Focusing on Gaussian white noise yielded analytical access, thereby providing deeper insights into the collective dynamics of fluctuation-driven networks. To characterize the robustness of this stochastic system, we derived the scaling of escape times as a function of the grid load, inertia, damping, and the noise amplitude. These analytic results are applicable in the dimensioning of future renewable power grids, where effective inertia and damping must be provided by power electronic devices. Remarkably, the inertia H enters the escape time only algebraically, whereas the damping enters exponentially. While the assumption of Gaussian white noise is common when investigating power grids under uncertainty, we go beyond the typical restriction to case studies [41] by providing analytical insight. Furthermore, we demonstrated how power networks may escape the regime of stable operation. The grid escapes in the vicinity of (saddle) fixed points with a low potential barrier. Interestingly, these can typically be assigned to a single overloaded link, thus revealing the weak links of the grid.

Complementary work on power grid fluctuations [25] addresses the impact of intermittent noise and incorporates features of real wind turbines. Such settings avert the analytic treatment in terms of Kramer's escape theory. The analytic approach presented in this Rapid Communication reveals which factors limit the robustness of power grid operation to fluctuating inputs. The results may thus not only provide efficient methodology to analyze fluctuation-driven oscillatory systems but may also help planning grid extensions to assure dynamic stability and robustness in future highly renewable power systems.

Acknowledgments. We gratefully acknowledge support from the Federal Ministry of Education and Research (BMBF Grant No. 03SF0472A-E), the Helmholtz Association (via the joint initiative "Energy System 2050—A Contribution of the Research Field Energy" and Grant No. VH-NG-1025 to D.W.), the Göttingen Graduate School for Neurosciences and Molecular Biosciences (DFG Grant No. GSC 226/2 to B.S.), and the Max Planck Society (M.T.).

[1] S. M. Amin and B. F. Wollenberg, *IEEE Power Energy Mag.* **3**, 34 (2005).

[2] T. Bruckner *et al.*, in *Climate Change 2014: Mitigation of Climate Change. Contribution of Working Group III to the Fifth*

ESCAPE ROUTES, WEAK LINKS, AND ...

PHYSICAL REVIEW E **95**, 060203(R) (2017)

- Assessment Report of the Intergovernmental Panel on Climate Change*, edited by O. Edenhofer *et al.* (Cambridge University Press, Cambridge, UK, 2014).
- [3] S. H. Strogatz, *Nature (London)* **410**, 268 (2001).
- [4] E. Marris, *Nature (London)* **454**, 570 (2008).
- [5] C. D. Brummitt, P. D. H. Hines, I. Dobson, C. Moore, and R. M. D'Souza, *Proc. Natl. Acad. Sci. USA* **110**, 12159 (2013).
- [6] M. Timme, L. Kocarev, and D. Witthaut, *New J. Phys.* **17**, 110201 (2015).
- [7] R. Sims *et al.*, in *IPCC Special Report on Renewable Energy Sources and Climate Change Mitigation*, edited by O. Edenhofer *et al.* (Cambridge University Press, Cambridge, UK, 2011).
- [8] D. Heide, L. Von Bremen, M. Greiner, C. Hoffmann, M. Speckmann, and S. Bofinger, *Renewable Energy* **35**, 2483 (2010).
- [9] P. Milan, M. Wächter, and J. Peinke, *Phys. Rev. Lett.* **110**, 138701 (2013).
- [10] M. Anvari, G. Lohmann, M. Wächter, P. Milan, E. Lorenz, D. Heinemann, M. R. R. Tabar, and J. Peinke, *New J. Phys.* **18**, 063027 (2016).
- [11] A. Ulbig, T. S. Borsche, and G. Andersson, *IFAC Proc. Vol.* **47**, 7290 (2014).
- [12] J. Machowski, J. Bialek, and J. Bumby, *Power System Dynamics, Stability and Control* (Wiley, New York, 2008).
- [13] G. Filatrella, A. H. Nielsen, and N. F. Pedersen, *Eur. Phys. J. B* **61**, 485 (2008).
- [14] M. Rohden, A. Sorge, M. Timme, and D. Witthaut, *Phys. Rev. Lett.* **109**, 064101 (2012).
- [15] A. E. Motter, S. A. Myers, M. Anghel, and T. Nishikawa, *Nat. Phys.* **9**, 191 (2013).
- [16] T. Nishikawa and A. E. Motter, *New J. Phys.* **17**, 015012 (2015).
- [17] A. J. Wood, B. F. Wollenberg, and G. B. Sheblé, *Power Generation, Operation and Control* (Wiley, New York, 2013).
- [18] P. Kundur, N. J. Balu, and M. G. Lauby, *Power System Stability and Control* (McGraw-Hill, New York, 1994), Vol. 7.
- [19] M. Rohden, A. Sorge, D. Witthaut, and M. Timme, *Chaos* **24**, 013123 (2014).
- [20] F. Dörfler, M. Chertkov, and F. Bullo, *Proc. Natl. Acad. Sci. USA* **110**, 2005 (2013).
- [21] B. Schäfer, M. Matthiae, M. Timme, and D. Witthaut, *New J. Phys.* **17**, 015002 (2015).
- [22] T. Pesch, H.-J. Allelein, and J.-F. Hake, *Eur. Phys. J.: Spec. Top.* **223**, 2561 (2014).
- [23] See Supplemental Material at <http://link.aps.org/supplemental/10.1103/PhysRevE.95.060203> for discussion of robustness of the phenomena reported and a comparison of the escape time across different power grid models.
- [24] J. W. Simpson-Porco, F. Dörfler, and F. Bullo, *IFAC Proc. Vol.* **45**, 264 (2012).
- [25] K. Schmietendorf, O. Kamps, and J. Peinke, [arXiv:1611.08235](https://arxiv.org/abs/1611.08235).
- [26] H. A. Kramers, *Physica* **7**, 284 (1940).
- [27] N. van Kampen, *Stochastic Processes in Physics and Chemistry* (Elsevier, Amsterdam, 1992).
- [28] P. Hänggi, P. Talkner, and M. Borkovec, *Rev. Mod. Phys.* **62**, 251 (1990).
- [29] C. W. Gardiner, *Handbook of Stochastic Methods for Physics, Chemistry, and the Natural Sciences* (Springer, Berlin, 2004).
- [30] H. Risken, *The Fokker-Planck Equation* (Springer, Berlin, 1984).
- [31] D. Manik, D. Witthaut, B. Schäfer, M. Matthiae, A. Sorge, M. Rohden, E. Katifori, and M. Timme, *Eur. Phys. J.: Spec. Top.* **223**, 2527 (2014).
- [32] P. Kundur, J. Paserba, V. Ajjarapu, G. Andersson, A. Bose, C. Canizares, N. Hatziaargyriou, D. Hill, A. Stankovic, C. Taylor *et al.*, *IEEE Trans. Power Syst.* **19**, 1387 (2004).
- [33] P. J. Menck, J. Heitzig, J. Kurths, and H. J. Schellnhuber, *Nat. Commun.* **5**, 3969 (2014).
- [34] F. Hellmann, P. Schultz, C. Grabow, J. Heitzig, and J. Kurths, *Sci. Rep.* **6**, 29654 (2016).
- [35] J.-W. Wang and L.-L. Rong, *Safety Sci.* **49**, 807 (2011).
- [36] D. Witthaut and M. Timme, *Phys. Rev. E* **92**, 032809 (2015).
- [37] Z. Schuss, *Theory and Applications of Stochastic Processes—An Analytical Approach* (Springer, New York, 2010).
- [38] D. Witthaut, M. Rohden, X. Zhang, S. Hallerberg, and M. Timme, *Phys. Rev. Lett.* **116**, 138701 (2016).
- [39] P. Crucitti, V. Latora, and M. Marchiori, *Physica A (Amsterdam)* **338**, 92 (2004).
- [40] D. Manik, M. Timme, and D. Witthaut, [arXiv:1611.09825](https://arxiv.org/abs/1611.09825).
- [41] X. Fang, S. Misra, G. Xue, and D. Yang, *IEEE Commun. Surveys Tutorials* **14**, 944 (2012).

Supplemental Material
accompanying the manuscript
Escape Routes, Weak Links, and Desynchronization in Fluctuation-driven Networks
 by

Benjamin Schäfer,¹ Moritz Matthiae,^{1,2,3} Xiaozhu Zhang,¹
 Martin Rohden,^{1,4} Marc Timme,^{1,5,6} and Dirk Witthaut^{2,7}

¹*Network Dynamics, Max-Planck-Institute for Dynamics and Self-Organization (MPI DS), 37077 Göttingen, Germany*

²*Forschungszentrum Jülich, Institute for Energy and Climate Research - Systems
 Analysis and Technology Evaluation (IEK-STE), 52428 Jülich, Germany*

³*Department of Micro- and Nanotechnology, Technical University of Denmark, 2800 Kongens Lyngby, Denmark*

⁴*Jacobs University, Department of Physics and Earth Sciences, 28759 Bremen, Germany*

⁵*Department of Physics, Technical University of Darmstadt, 64289 Darmstadt, Germany*

⁶*Institute for Theoretical Physics, Technical University of Dresden, 01062 Dresden Germany*

⁷*Institute for Theoretical Physics, University of Cologne, 50937 Köln, Germany*

I. OVERVIEW

Power grids are complex systems and may be described on different levels of detail [1]. A cornerstone model of power system dynamics is the swing equation - a second order differential equation describing the mechanical rotation of synchronous machines. The mechanical phase angle typically equals the voltage phase angle, such that it also determines the power flows in the grid. This model is studied in the main text for heavily loaded lines. In this Supplemental Material we provide additional arguments why this model is appropriate and explore different parameter regimes, in particular less heavily loaded lines and the effects of a decreasing inertia.

Furthermore, we analyze the robustness of different power system models against noise. Wind turbines and photovoltaics are usually connected to a grid via power electronic inverters. Power electronic devices can act as virtual synchronous machines described by the swing equation, otherwise they should be described as first-order Kuramoto oscillators [2–4]. The swing equation is known to describe the short-term dynamical stability of a power system. On longer time scales the assumption of a constant voltage may no longer be satisfied [5]. In this Supplemental Material we study grids without inertia in terms of a first-order model and state the appropriate escape rate formula. In addition, we investigate the effects of voltage variability numerically in terms of the third-order model. For simplicity of presentation, we focus on the scenario of one machine connected to the bulk grid.

II. POWER GRID MODELS

First, we define an effective potential U in terms of the voltage phase δ as

$$U(\delta) = -P \cdot \delta - K \cos(\delta), \quad (1)$$

with effective power produced P and capacity parameter of a line K , which describes the maximal transmittable

power of that line. In terms of this potential, the swing equation, i.e., the equations of motion for the voltage phase δ and its angular velocity ω becomes

$$\begin{aligned} \frac{d}{dt} \delta &= \omega \\ \frac{d}{dt} \omega &= -\frac{\Omega^2 D}{H} \omega + \frac{\Omega}{2H} \left(-\frac{\partial U}{\partial \delta}(\delta) + \xi \right), \end{aligned} \quad (2)$$

with the reference angular velocity $\Omega = 2\pi \cdot 50$ Hz, damping D , inertia H and Gaussian white noise ξ with standard deviation σ . Parameters used (if not stated otherwise) are $D = 4 \cdot 10^{-5} \text{s}^2$, $H = 4 \text{s}$, $P = 0.95$, $K = 1$. In a fully renewable power grid, which is dominated by wind and solar power production, there will be fewer rotating machines than today and the inertia H will be smaller. In the extreme case all rotating machines are replaced by inverters feeding wind and solar power into the grid. However, it has been demonstrated that inverters can be used to act similar to synchronous machines by providing virtual inertia, see e.g. [6, 7]. Again, the dynamics of the inverters is differentially modelled by using the swing equation (2).

Furthermore, we note that the swing equation (2) is also used in coarse grained models [1, 8]. In those models, multiple machines are aggregated into a coherent subgroup. Each node, representing one sub group, is then described as an oscillatory machine with effective power P , damping D and inertia H . The dynamics is again described by the swing equation.

If we model a system without physical or virtual inertia, each node is best described as a Kuramoto oscillator [2–4] with the equation of motion being

$$\frac{d}{dt} \delta = \frac{1}{2D\Omega} \left(-\frac{\partial U}{\partial \delta}(\delta) + \xi \right). \quad (3)$$

In the main text we assumed the voltage amplitude to stay constant even in the scenario of a heavily loaded grid. Here, we consider the third order model [1, 5, 9, 10] which allows the voltage amplitude E to vary over time:

$$\begin{aligned} \frac{d}{dt}\delta &= \omega \\ \frac{d}{dt}\omega &= -\frac{\Omega^2 D}{H}\omega + \frac{\Omega}{2H}(P - EE_0B_0 \sin(\delta) + \xi) \\ \frac{d}{dt}E &= \frac{1}{T_E} \cdot (E_f - E + X(E_0 \cos(\delta) + EB_{11})), \end{aligned} \quad (4)$$

with the voltage time scale $T_E = 1/2$, bulk voltage $E_0 = 1$, $E_f = 1$, $B_0 = 1$, $B_{11} = -\sqrt{1-P^2}$ and the voltage droop X . For $X = 0$ and $E(t=0) = 1$ the voltage remains at the fixed point $E^* = 1$ at all times and reproduces the second order model while for $X > 0$ deviations from the second order model can be observed. Typical parameter values are taken from [9].

III. CALCULATION OF ΔU

In the main text and also in upcoming equations (8) and (11) we use the potential difference ΔU . It is calculated as follows. First, we determine the minimum and maximum of the potential U (1) as

$$\delta_{\min} = \arcsin\left(\frac{P}{K}\right) \quad (5)$$

$$\delta_{\max} = \pi - \arcsin\left(\frac{P}{K}\right) \quad (6)$$

respectively. Plugging these into (1) and calculating $\Delta U = U(\delta_{\max}) - U(\delta_{\min})$ we obtain

$$\Delta U = -P \cdot \left(\pi - 2 \arcsin\left(\frac{P}{K}\right)\right) + 2\sqrt{K^2 - P^2}. \quad (7)$$

IV. MEAN ESCAPE TIME

We simulate the system consisting of one generator coupled to the bulk and extract the scaling of the escape time $\bar{\tau}$, depending on the noise amplitude σ , the inertia H and the voltage droop X for the first, second and third order model. For the sake of consistency and comparability, we define the escape time as that instance when the system passed $\delta_{\text{crit}} = \pi/2$ and did not return to the fixed point. Although this does not correspond exactly to the boundary of the basin of attraction, it enables us to compare these three different models.

A. 2nd Order: Scaling with respect to inertia

Decreasing inertia H in the swing equation (2), decreases the escape time τ and thereby the stability of the system, see fig. S.1. This dependency is well-described in Kramer's escape theory

$$\tau_{2\text{nd}} = \frac{2\pi\lambda}{\sqrt{U''(\delta_{\min})U''(\delta_{\max})}} \exp\left(\frac{2\gamma\Delta U}{\sigma^2}\right) \quad (8)$$

with

$$\gamma = 2D\Omega \quad (9)$$

and

$$2\lambda = \gamma + \sqrt{\gamma^2 + (8H/\Omega)|U''(\delta_{\max})|} \quad (10)$$

as stated in the main manuscript.

B. 2nd Order: Less loaded lines

In the main text we only considered highly loaded lines with $P \approx 0.95K$, i.e., the lines were close to maximum load. In fig. S.2 we display that Kramer's escape theory also holds for less loaded scenarios. We observe a good agreement of the numerical results and the analytical prediction by eq. (8). The noise amplitude σ needs to be increased significantly compared to less loaded scenarios, see, e.g. fig. S.1, to arrive at similar escape times $\bar{\tau}$.

C. First order model

In contrast to the 2nd order model, the 1st order model has only one globally stable fixed point at $\delta^* = \arcsin(P)$ and we observe transitions from δ^* to $\delta^* = n \cdot 2\pi + \delta^*$ with $n \in \mathbb{Z}$. In a real system, the fast change of the angle δ would almost certainly destabilize the system as the power flow along the line given by $F = K \sin(\delta^*)$ would change dramatically during the course of this transition and would most likely violate security regulations [1]. We obtain Kramer's escape rate for the first order model [11] as

$$\tau_{1\text{st}} = \frac{2\pi}{\sqrt{U''(\delta_{\min})U''(\delta_{\max})}} \exp\left(\frac{1}{4D^2\Omega^2} \cdot \frac{2\Delta U}{\sigma^2}\right) \quad (11)$$

and demonstrate perfect agreement of theory and simulations in fig. S.3.

D. Third order model

The fixed point for the angle δ in the third order system is given as $\delta^* = \arcsin\left(\frac{P}{E_0 \cdot E^*}\right)$ [9]. For sufficiently small values of the voltage droop X , the voltage amplitude E tends to the stable fixed point $E^* = 1$. With increasing X this fixed point gets destabilized and the mean escape time $\bar{\tau}$ of the system decreases. This effect might change for larger values of X . Our theory using Kramer's escape rate correctly predicts the stability as long as the voltage changes are sufficiently slow or small, see fig. S.4.

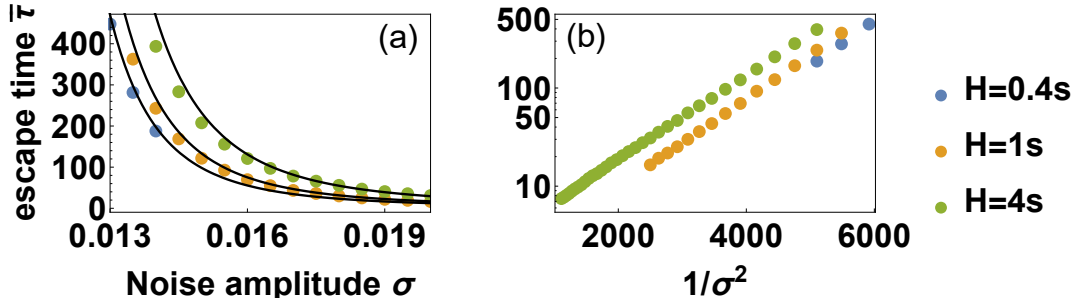


Figure S.1. The mean escape time $\bar{\tau}$ decreases with decreasing inertia. We simulated 2000 trials using $D = 4 \cdot 10^{-5} s^2$, $P = 0.95$ as parameters for one generator coupled to the bulk grid. Kramer's formula (black line) shows an excellent agreement with the numerical results (a). The logarithm of the escape time $\log(\bar{\tau})$ is linear in $1/\sigma^2$ (b), as predicted by eq. (8).

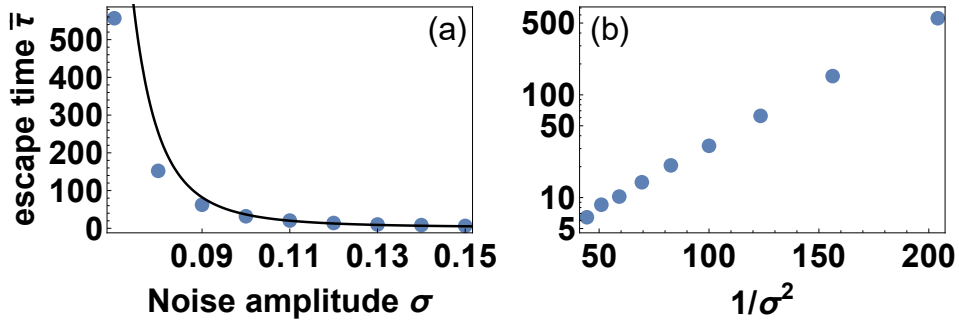


Figure S.2. Kramer's escape theory also describes less loaded scenarios. We simulated 2000 trials using $H = 4s$, $D = 4 \cdot 10^{-5} s^2$ and $P = 0.5$ as parameters for one generator coupled to the bulk grid. Kramer's formula (black line) shows an excellent agreement with the numerical results (a). The logarithm of the escape time $\log(\bar{\tau})$ is linear in $1/\sigma^2$ (b), as predicted by eq. (8). Note that for similar escape times $\bar{\tau}$ the noise amplitude has a much larger absolute value compared to more heavily loaded scenarios.

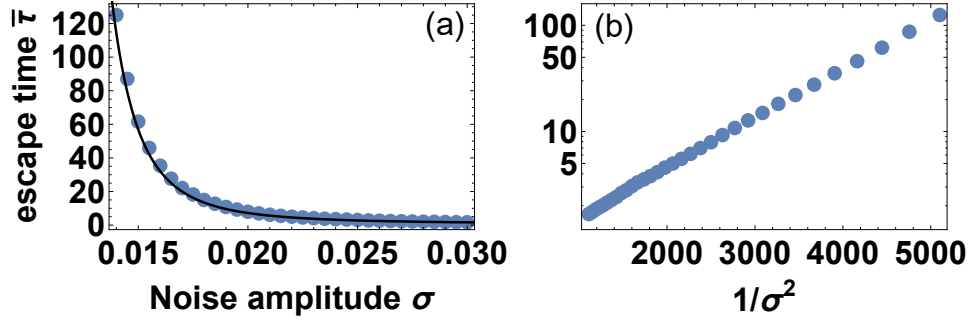


Figure S.3. The mean escape time $\bar{\tau}$ is well predicted for a first order model. The black line is Kramer's escape time for the 1st order model, as given in eq. (11) and is in excellent agreement with the numerical data (a). The logarithm of the escape time $\log(\bar{\tau})$ is linear in $1/\sigma^2$ (b), as predicted by eq. (11). We simulated 2000 trials using $D = 4 \cdot 10^{-5} \text{s}^2$ and $P = 0.95$ as parameters for one generator coupled to the bulk grid.

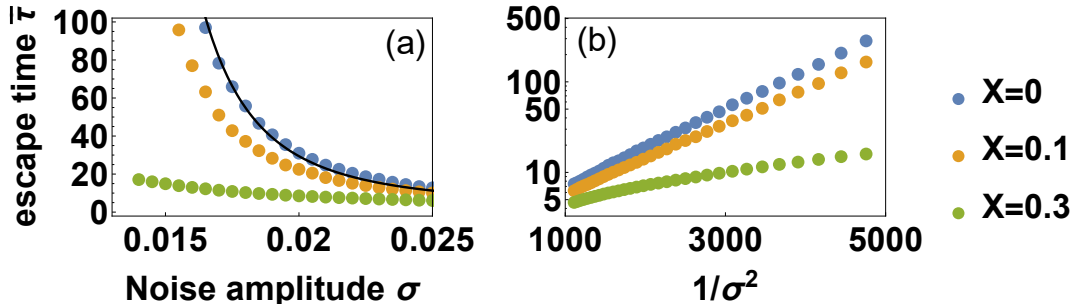


Figure S.4. The mean escape time $\bar{\tau}$ decreases with increasing voltage droop X . We simulated 2000 trials using $D = 4 \cdot 10^{-5} \text{s}^2$, $P = 0.95$, $H = 4 \text{s}$, $\tau_E = 2$, $E_0 = 1$, $E_f = 1$ and $B_{11} = -\sqrt{1 - P^2}$ as parameters for one generator coupled to the bulk grid. The black line is the prediction based on the 2nd order (swing equation) model (a) derived in the main text and in eq. (8). Note that even with voltage coupling $X > 0$, the escape time scales qualitatively with $\tau \sim \exp(c/\sigma^2)$, as in Kramer's theory (b).

-
- [1] J. Machowski, J. Bialek, and J. Bumby, *Power system dynamics, stability and control* (John Wiley & Sons, New York, 2008).
 - [2] M. Calabria, W. Schumacher, J. M. Guerrero, J. C. Vasquez, and X. Zhao, in *2015 IEEE 6th International Symposium on PEDG* (IEEE, 2015), pp. 1–9.
 - [3] J. W. Simpson-Porco, F. Dörfler, and F. Bullo, *IFAC Proceedings Volumes* **45**, 264 (2012).
 - [4] J. W. Simpson-Porco, F. Dörfler, and F. Bullo, *Automatica* **49**, 2603 (2013).
 - [5] S. Auer, K. Kleis, P. Schultz, J. Kurths, and F. Hellmann, *Eur. Phys. J. Special Topics* **225**, 609 (2016).
 - [6] S. D'Arco and J. A. Suul, in *PowerTech (POWERTECH), 2013 IEEE Grenoble* (IEEE, 2013), pp. 1–7.
 - [7] J. Schiffer, D. Goldin, J. Raisch, and T. Sezi, in *Decision and Control (CDC), 2013 IEEE 52nd Annual Conference on* (IEEE, 2013), pp. 2334–2339.
 - [8] A. Ulbig, T. S. Borsche, and G. Andersson, *IFAC Proceedings Volumes* **47**, 7290 (2014).
 - [9] K. Schmietendorf, J. Peinke, R. Friedrich, and O. Kamps, *Eur. Phys. J. Special Topics* **223**, 2577 (2014).
 - [10] J. Ma, Y. Sun, X. Yuan, J. Kurths, and M. Zhan, *PloS one* **11**, e0165943 (2016).
 - [11] N. van Kampen, *Stochastic processes in physics and chemistry* (Elsevier, Amsterdam, 1992).

Chapter 6

Heavy Tails, Superstatistics and Scaling of Power Grid Frequency Fluctuations

Citation

Benjamin Schäfer, Christian Beck, Kazuyuki Aihara, Dirk Witthaut and Marc Timme (2017) Heavy Tails, Superstatistics and Scaling of Power Grid Frequency Fluctuations

© 2017 Benjamin Schäfer, Christian Beck, Kazuyuki Aihara, Dirk Witthaut and Marc Timme

This chapter is the initially submitted version of the article: Benjamin Schäfer, Christian Beck, Kazuyuki Aihara, Dirk Witthaut and Marc Timme (2017) Non-Gaussian Power Grid Frequency Fluctuations Characterized by Lévy-stable Laws and Superstatistics, which is accepted at Nature Energy, DOI: <https://doi.org/10.1038/s41560-017-0058-z>

Original Contribution

Conception of the research was done with support by M. Timme and D. Witthaut as well as by C. Beck and K. Aihara. I performed all calculations and simulations. I retrieved external data sources, produced all numerical data and generated all figures. I set up the Supplementary Information, including all figures. I wrote large parts of all text sections in the main manuscript and the Supplementary Information. I revised the manuscript according to referee suggestions, with the support of all authors.

Heavy Tails, Superstatistics and Scaling of Power Grid Frequency Fluctuations

Benjamin Schäfer,¹ Christian Beck,² Kazuyuki Aihara,³ Dirk Witthaut,^{4,5,*} and Marc Timme^{1,6,7,*}

¹*Network Dynamics, Max Planck Institute for Dynamics and Self-Organization (MPIDS), 37077 Göttingen, Germany*

²*Queen Mary University of London, School of Mathematical Sciences, Mile End Road, London E1 4NS, UK*

³*Institute of Industrial Science, The University of Tokyo, Meguro-ku, Tokyo, Japan*

⁴*Forschungszentrum Jülich, Institute for Energy and Climate Research - Systems Analysis and Technology Evaluation (IEK-STE), 52428 Jülich, Germany*

⁵*Institute for Theoretical Physics, University of Cologne, 50937 Köln, Germany*

⁶*Institute for Theoretical Physics, Technical University of Dresden, 01062 Dresden Germany*

⁷*Center for Advancing Electronics Dresden (cfaed), Technical University of Dresden, 01062 Dresden Germany*

Multiple types of fluctuations impact the collective dynamics of power grids and thus challenge their robust operation. Fluctuations result from processes as different as dynamically changing demands, energy trading, and an increasing share of renewable power feed-in. Here we analyze the fundamental dynamics of these power grid frequency fluctuations. Analyzing frequency time series for a range of power grids, including grids in North America, Japan and Europe, we find a substantial deviation from Gaussianity best described as Lévy-stable and q-Gaussian distributions. We present a coarse framework to analytically characterize the impact of arbitrary noise distributions as well as a superstatistical approach which systematically interprets heavy tails and skewed distributions. We identify energy trading as a significant contribution to today's frequency fluctuations and effective damping of the grid as a controlling factor or enabling to reduce fluctuation risks, with enhanced effects for small power grids.

The Paris conference 2015 set a path to limit climate change to the best of our abilities. To reach this goal, integrating renewable and sustainable energy sources into the electrical power grid is essential [1]. Wind and solar power are the most promising contributors to reach a sustainable energy supply [2], but their integration into the existing electric power system remains an enormous challenge [3–5]. In particular, their power generation varies on all time scales from several days [6] to less than a second [7], displaying highly non-Gaussian fluctuations [8]. This variability must be balanced by storage facilities and backup plants requiring an advanced control of the electric power grid.

The central observable in power grid monitoring, operation and control is the grid frequency f [9]. In case of an excess demand, kinetic energy of large synchronous generators is converted to electric energy, thereby decreasing the frequency. Dedicated power plants measure this decrease and increase their generation to stabilize the grid frequency within seconds to minutes (primary control) [9, 10]. On longer time scales, additional power plants are activated to restore the nominal grid frequency (secondary control). The increase of renewable generation challenges this central control paradigm as generation becomes more volatile and the spinning reserve decreases [11]. How to provide additional effective/virtual inertia is under heavy development [12, 13]. In addition, fluctuating demand [14] and fixed trading intervals [15] already contribute to frequency deviations.

A detailed understanding of the fluctuations of power grid frequency essentially underlies the design of effective

control strategies for the future grids. Many studies for simplicity assume simple Gaussian noise [14, 16–19], while non-Gaussian effects are only rarely studied [20–23]. Gaussian approaches neglect the possibility of heavy tails in the frequency distributions and thus strong deviations from the set frequency posing serious contingencies particularly relevant for security assessment. Even in studies considering non-Gaussian effects, the connection to real data is missing [20], realistic but isolated wind and solar data are only numerically evaluated [22, 23] or the focus is on static power dispatch [14, 19, 21] opposing to real-time dynamics.

It is crucial to understand how collective grid dynamics are driven by the fluctuations originating from varying power demands, fluctuating input generation and trading. While realistic models describing the actual noise input of wind and solar power exist [22, 23], the impact of fluctuations on grid dynamics has been studied for selected specific scenarios, regions or technologies only [24, 25]. Furthermore, a systematic quantitative comparison of differently sized synchronous regions based on their frequency fluctuations is needed. It is important to forecast fluctuation statistics in grids of any size, especially when setting up small isolated systems, e.g., on islands or disconnected microgrids [26].

In this article, we analyze the frequency fluctuations observed in several electric power grids from three continents. We determine and characterize the non-Gaussian nature of these fluctuations existing across grids in both the 60Hz and 50Hz operation regimes. Furthermore, we propose an analytically accessible model successfully describing these data in one consistent framework by systematically incorporating the non-Gaussian nature of fluctuations and verify its predictions. The analysis

* Contributed equally

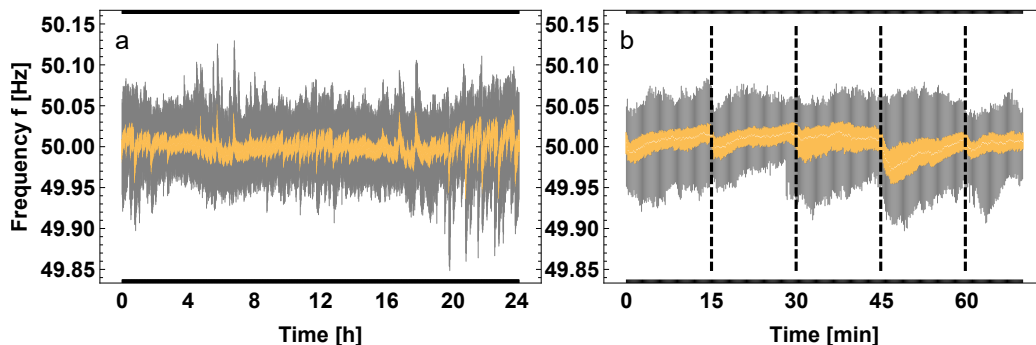


Figure 1. **Fluctuations in frequency around the reference frequency (50Hz)** a: Box plot of the 2015 data by *RTE* describing the Continental European power grid. b: Zoom-in on the first 70 minutes of the frequency measurements, exposing substantial changes in average and degree of fluctuations at 15 minutes trading intervals. Each box contains data of one year for the same time instance (averaged per minute in a). The yellow bars contain the 25% and 75% quartile and the gray bars are the whiskers giving the maximum and minimum values.

yields trading as a key factor for non-Gaussianity. Extracting the effective damping for different synchronous regions via autocorrelation measures, our work highlights that the effective grid damping as well as the size of the grid itself serve as controlling factors to make grid dynamics more robust. Finally, we demonstrate how superstatistics explain heavy tailed and skewed distributions as superimposed Gaussian distributions.

THE STATISTICS OF FREQUENCY FLUCTUATIONS

The bulk frequency of a power grid fluctuates around its nominal frequency of 60 Hz (Most Parts of America, Western Japan, Korea, Philippines) or 50 Hz (Eastern Japan and other countries). To understand and quantify these fluctuations, we analyze data sets for the power grid frequency of the ENTSO-E Continental European (CE) [27, 28], the Nordic [29], Mallorca [30] and Great Britain (GB) [31] grids, the 50 Hz and 60 Hz regions of Japan [32] as well as the Eastern Interconnection (EI) in North America [33], see Supplementary Note 1 for more detailed data breakdown. The data consists of power grid frequency measurements at one location in the given region (two for Continental Europe) at a sampling rate between ten measurements per second and one measurement per five minutes.

Frequency Distributions

A first glance at an average recording of the grid frequency reveals that it coincides extremely well with the nominal grid reference frequency, highlighting the efficiency of today's frequency control, see Fig. 1. Only

rarely do we observe large deviations from the nominal frequency. These large disturbances often occur when a new power dispatch has been settled on by trading (every 15 minutes) introducing jumps and fluctuations of the frequency. The total variance of the frequency fluctuations in a given region thereby depends on the size of the grid – larger grids are more inertial and thus have a smaller variance.

While the central limit theorem suggests that sufficiently long time series approximate Gaussian distributions, we observe that the tails of the distribution are not well described by a Gaussian distribution in all grids. For the Continental European, Nordic, Mallorcan and Japanese grids large deviations from the nominal frequency are more frequent than for a Gaussian distribution of given variance, leading to heavy tails, quantified by an excess kurtosis, see Methods. The grids of Great Britain and the Eastern Interconnection however, are significantly skewed, i.e., they are asymmetric around the reference frequency so that deviations towards lower frequencies are more likely than to higher ones.

Performing a maximum likelihood analysis using a variety of standard probability distributions, we identify Lévy-stable [34] and q -Gaussian distributions [35] as good descriptions for all grids, see Fig. 2 and Supplementary Note 1. Both distributions generalize the central limit theorem to include heavy tails and point to two different microscopic mechanisms underlying the frequency dynamics: q -Gaussians arise when the power fluctuations are Gaussian on short time scales, but with a variance and/or mean changing on longer time scales. In contrast, Lévy-stable distributions arise when the underlying power fluctuations are heavy-tailed or skewed itself. We investigate both settings in more detail below.

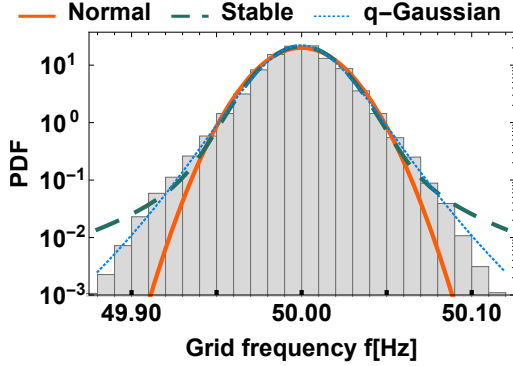


Figure 2. **Non-Gaussian nature of the frequency distribution.** Displayed is the 2015 data set by *50Hertz* describing the Continental European power grid where fitted normal, stable and q-Gaussian distributions are compared with the histogram data using a log scale for the probability density function (PDF). Deviations from a normal distribution become obvious in the tails of the actual data which are more pronounced than expected for a normal distribution. The stability parameter of the stable distribution is $\alpha_S \approx 1.9$ and the deformation parameter of the q-Gaussian distribution is $q \approx 1.2$. Note that the stable distribution uses four, the q-Gaussian three and the Normal distribution two parameters.

Correlation Functions

In addition to the aggregated data, we investigate the autocorrelation of the recorded trajectories, extracting important events and the characteristic time scales during which the system de-correlates. Analyzing the autocorrelation for the Continental European grid reveals pronounced correlation peaks every 15 minutes and especially every 30 and 60 minutes, see Fig. 3. These regular correlation peaks appear in all grids and are easily explained by the trading intervals in most electricity markets [15], which are often 30 or 15 minutes. Furthermore, this is also in line with the observation of large deviations in the frequency trajectories, see Fig. 1, so that trading has an important impact on frequency stability. At the beginning of a new trading interval, the production changes nearly instantaneously and the complex dynamical power grid system needs some time to relax to its new steady operational state.

The autocorrelation of a time series typically decays over a characteristic correlation time that provides information about the underlying process. For the first minutes of each trajectory, we observe an exponential decay

$$c(\Delta t) \sim \exp(-\Delta t/\tau), \quad (1)$$

with a typical correlation time τ , as the expected for elementary stochastic processes without memory such as the Ornstein-Uhlenbeck process [36].

We extract the inverse correlation time $1/\tau$ for each available data set and obtain values within the same or-

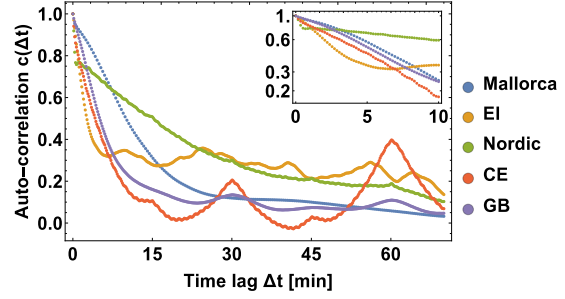


Figure 3. **Decay of the autocorrelation of the frequency dynamics.** Plotted are autocorrelation measures as a function of time lag Δt for the *50Hertz* data set for Central Europe (CE) of 2015, the Great Britain grid (GB) of 2015, the Eastern Interconnection (EI) data for 1 day of 2015 and the Nordic grid data of 2015. After an initial decay of the autocorrelation and peaks emerge every 15 minutes due to trading intervals, especially pronounced for the GB and CE grids, consistent with Fig. 1. Using a log-plot in the inset allows to extract the damping of the grid based on the assumption of exponential decay, Equation (1). Note that the CE, GB and EI grids all display similar decay during the initial 5 minutes. In contrast, the Nordic grid displays a fast decay and then a slower one. The plot uses one full year of data for each region to generate the autocorrelation plots. Especially the trading peaks are typically not visible when only 24h of recordings are considered (as in the case of EI).

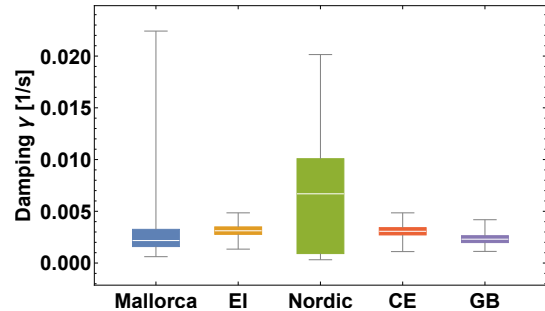


Figure 4. **Damping of different regions.** The box plots display the damping estimates based on the autocorrelation decay fitted by an exponential function, see Equation (1). The data are obtained by evaluating individual days of all years available and splitting the one day of EI into 10 minute trajectories. The box covers the 25% and 75% quartile with the white line being the median while the whiskers give the maximum and minimum values.

der of magnitude for all grids, see Fig. 4. The Japanese data set only has measurements every five minutes, hence we refrain from estimating an autocorrelation. Later, we interpret the inverse correlation time $1/\tau$ as the effective damping in a synchronous region (including primary control). With this in mind it is not surprising that all grids

return similar values for τ as the synchronous machines do not differ significantly in the considered regions.

STOCHASTIC POWER FLUCTUATIONS

The variations of the grid frequency are driven by the fluctuations of power generation and demand. To link the evolution of the grid frequency with the power injections we make use of the well-established *swing equation* [9, 10, 37–42]. Aggregating over the grid, we obtain a Fokker-Planck equation that models the observed frequency fluctuations and allows an analytical description of power grid frequency fluctuations.

Power Grid Dynamics

We analyze frequency dynamics of a power grid on coarse scales. Every node in the grid corresponds to a large generator (power plant) or a coherent subgroup and is characterized by the phase θ_i and the angular velocity $\omega_i = 2\pi(f_i - f_R)$. Here f_i denotes the frequency of the nodes $i = 1 \dots N$ and $f_R = 50\text{Hz}$ or $f_R = 60\text{Hz}$, respectively, is the reference frequency at the grid. The equations of motion of the phase and velocity are then given by

$$\begin{aligned} \frac{d}{dt}\theta_i &= \omega_i, \\ M_i \frac{d}{dt}\omega_i &= P_i + \epsilon_i \xi_i - D_i \omega_i + \sum_{j=1}^N K_{ij} \sin(\theta_j - \theta_i), \end{aligned} \quad (2)$$

where we have at each node i : inertia M_i , voltage angle θ_i , mechanical power P_i , random noise ξ_i with noise amplitude ϵ_i , damping D_i and the coupling matrix K_{ij} is determined by the transmission grid topology.

The power grid must always be at or close to a stable operating state which is given as the equilibrium point of the swing equation (2). The equilibrium point fulfills $\omega_i^* \approx 0$ which is equivalent to all machines working at the reference frequency $f_R = 50\text{Hz}$ or $f_R = 60\text{Hz}$.

At the stable operation point the frequencies at all nodes are equal: $\omega_i = \bar{\omega}$. Deviations are only observed during system-wide failures or transiently after serious contingencies or major topology changes [9, 10]. To obtain the effective equation of motion of the bulk angular velocity $\bar{\omega}$, we assume a homogeneous ratio of damping and inertia throughout the network, $\gamma = D_i/M_i$ [43] as well as symmetric coupling $K_{ij} = K_{ji}$ and assume that the power is balanced $\sum_{i=1}^N P_i = 0$ on average [41]. Setting $M := \sum_i M_i$, the dynamics of the bulk angular velocity $\bar{\omega} := \sum_{i=1}^N M_i \omega_i / M$ is governed by the *Aggregated Swing Equation* as follows (see also [11]):

$$\frac{d}{dt}\bar{\omega} = -\gamma\bar{\omega} + \bar{\epsilon}\bar{\xi}(t). \quad (3)$$

This aggregated swing equation no longer requires precise knowledge of the parameters of a given region but depends crucially on the effective damping γ and the noise $\bar{\epsilon}$, which itself depends on the statistics of the input noise ξ_i , see Methods and Supplementary Note 2. We note that the damping γ integrates contributions from damper windings and primary control actions alike. Finally, both damping γ or the noise amplitude $\bar{\epsilon}$ could easily change over time, e.g., due connection of certain grids or day/night differences. We cover this scenario in the section on superstatistics.

Stochastic Dynamics

The bulk angular velocity $\bar{\omega}$ (and thereby the grid frequency) is not following a deterministic evolution but is influenced by stochastic effects, given by the aggregated power fluctuations $\bar{\xi}$. Hence, we characterize a given grid by the probability distribution function (PDF) of the bulk angular velocity $p(\bar{\omega})$, similar to the frequency distribution plotted in Fig. 2. A wide distribution, i.e. one with high standard deviation, or one with heavy tails, i.e., high kurtosis, displays large deviations more often and is thereby less stable than a narrower distribution.

The central decision when modeling stochastic dynamics is how to describe the noise ξ which is generated from some probability distribution. Explicit choices of noise distributions are covered here and in Supplementary Note 2. Given the distribution of ξ , we then formulate and solve a Fokker-Planck equation [36] to obtain an analytical description of the distribution of $\bar{\omega}$.

Gaussian noise

The simplest noise model assumes ξ_i as independent Gaussian noise based on the often-used central limit theorem. It states that the sum of independent random numbers drawn from any fixed distribution with finite variance approaches a Gaussian distribution if the sample is sufficiently large [36]. The Fokker-Planck equation describing the time-dependent probability density function $p(\bar{\omega}, t)$ follows then as

$$\frac{\partial p}{\partial t} = \gamma \frac{\partial}{\partial \bar{\omega}} (\bar{\omega} p) + \frac{1}{2} \sum_{i=1}^N \frac{\epsilon_i^2}{M^2} \frac{\partial^2 p}{\partial \bar{\omega}^2}, \quad (4)$$

which is the well-known Ornstein-Uhlenbeck process [36]. We are interested in the stationary distribution $p(\bar{\omega})$ of (4) to describe the grid in the steady state, given by

$$p(\bar{\omega}) = \sqrt{\frac{\gamma M^2}{\pi \sum_{i=1}^N \epsilon_i^2}} \exp \left[-\bar{\omega}^2 \frac{\gamma M^2}{\sum_{i=1}^N \epsilon_i^2} \right], \quad (5)$$

see also Methods and Supplementary Note 2 for details.

Crucially, Equation (5) is again a Gaussian distribution of $p(\bar{\omega})$, i.e., a Gaussian distribution for the power feed-in

fluctuations results in a Gaussian frequency distribution. Assuming we know the damping γ , noise amplitudes ϵ_i and the total inertia M , we are able to compute the expected frequency distribution analytically. Furthermore, the Ornstein-Uhlenbeck autocorrelation exactly follows an exponential decay with characteristic time determined by the damping $\tau = 1/\gamma$, i.e., our estimates for the correlation time τ obtained above determine the damping of the grid.

Non-Gaussian noise

Under which conditions do we need to include non-Gaussian effects in the stochastic modeling? When applying the central limit theorem, one explicitly assumes *finite* variance. Hence, to describe deviations from normal distributions including heavy tails and skewed distributions, we need to base the input noise ξ on a non-Gaussian noise generating process [44]. This requires generalized Fokker-Planck equations which are solved for the stochastic system (3) by

$$p(\bar{\omega}, t) = \mathcal{F}^{-1} \left[\exp \left(-\frac{1}{\gamma} \int_0^k \frac{1}{z} \ln \left(\frac{S_z \cdot e^{-\gamma t}}{S_z} \right) dz \right) \right], \quad (6)$$

where S_k is the characteristic function of an arbitrarily distributed and uncorrelated noise generating process and \mathcal{F}^{-1} is the inverse Fourier transform [44].

In the stationary state, the characteristic function of the bulk angular velocity $\bar{\omega}$ is given by

$$F_k = \exp \left[\frac{1}{\gamma} \int_0^k \frac{\ln(S_z)}{z} dz \right]. \quad (7)$$

Lévy-stable noise

Lévy-stable distributions are a particularly good fit for the frequency data and lead to easy-to-analyse analytical results. These distributions include heavy tails and skewed distributions, as often observed in nature [8]. A stable distribution [34] is described by its characteristic function:

$$S_k(\alpha_S, \beta_S, \sigma_S) = \exp \left[-\sigma_S^{\alpha_S} |k|^{\alpha_S} \cdot \left(1 - \operatorname{sgn}(k) i \beta_S \cdot \tan \frac{\pi \alpha_S}{2} \right) \right], \quad (8)$$

with stability parameter $\alpha_S \in (0, 2]$, skewness parameter β_S and scale parameter σ_S . For simplicity, we set the location parameter to zero $\mu_S = 0$.

Using power fluctuations ξ based on a stable distribution $S_k(\sigma_S)$ in the stochastic Equation (3) results in a stable distribution of the power grid frequency. Only the scale parameter of the input distribution σ_S^{in} changes to

the new value σ_S^{out} as follows

$$\sigma_S^{\text{in}} = \frac{1}{\sqrt{2M}} \left[\sum_{i=1}^N \epsilon_i^{\alpha_S} \right]^{1/\alpha_S} \rightarrow \sigma_S^{\text{out}} = \frac{\sigma_S^{\text{in}}}{(\gamma \alpha_S)^{1/\alpha_S}}, \quad (9)$$

while the skewness β_S (asymmetry) and the stability parameter α_S (heavy-tail-ness) are preserved. We emphasize this remarkable and unique property of stable distributions: The input power fluctuations are distributed according to a stable distribution and so is the output frequency. The same happens for Gaussian distributions since they are a subclass of stable distributions. In contrast, we investigate non-stable distributions in the Supplementary Note 2.

Usually, we cannot influence the noise ϵ_i acting on the power grid but by increasing the effective damping γ or the inertia M , the final distribution of frequencies becomes narrower and hence extreme fluctuations of the grid frequency are less likely.

Smaller regions need larger damping

With the previous results, we are able to quantify the intuitive statement that larger regions have more inertia and hence narrower distributions by explicitly comparing the scale parameters (proportional to standard deviations in the case of $\alpha_S = 2$) of two different regions as follows:

$$\sigma_{S2}^{\text{out}} = \sigma_{S1}^{\text{out}} \frac{m_1}{m_2} \left(\frac{\gamma_1 N_1^{\alpha_S - 1}}{\gamma_2 N_2^{\alpha_S - 1}} \right)^{1/\alpha_S}, \quad (10)$$

assuming identical stability parameters α_S and average inertia $m_\mu = M_\mu/N_\mu$ $\mu \in \{1, 2\}$. Equation (10) shows that a small region $N_2 < N_1$ needs larger damping than a larger region $\gamma_2 \stackrel{!}{>} \gamma_1$ or has a broader distribution with $\sigma_{S2}^{\text{out}} > \sigma_{S1}^{\text{out}}$, i.e., a higher risk of large deviations from the stable operational range. The scaling is given by the scale parameter $\sigma_S \sim N^{(\alpha_S - 1)/\alpha_S}$, where the simple square root law is recovered only in the case of Gaussian distributions ($\alpha_S = 2$). Also, it reveals that decreasing inertia proportionally increases the scale parameter.

Furthermore, we calculate the expected noise amplitude by using (9) as

$$\epsilon = \sigma_S^{\text{out}} m (\alpha_S \gamma N^{\alpha_S - 1})^{1/\alpha_S}. \quad (11)$$

Based on pure frequency measurements, every quantity is easily available for each synchronous region: We estimate the output scale parameter σ_S^{out} and stability parameter α_S from the histogram data. We assume that the number of nodes N is directly proportional to the total electricity production of a region per year. Since a process driven by stable noise has no defined autocorrelation function (second moments are not defined), we approximate its autocorrelation with the Ornstein-Uhlenbeck process and thereby derive an estimate for the damping γ . With these

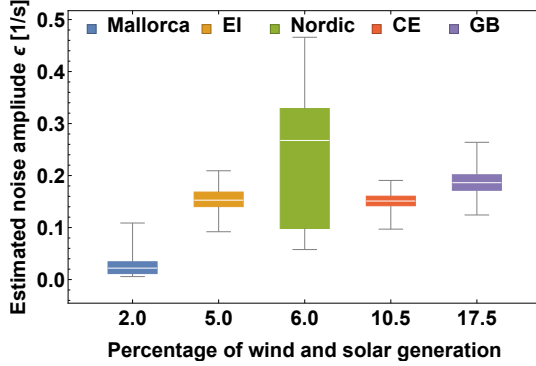


Figure 5. **Noise amplitudes for European and American grids.** The noise amplitude tends to increase with the shares of intermittent renewables. The noise amplitude ϵ for each grid is calculated assuming that it is identical at each node $\epsilon_i = \epsilon$ and assuming homogeneous inertia. The power production is normalized with respect to the Eastern Interconnection (EI) generation for the ENTSO-E grids of Continental Europe (CE), Mallorca, Nordic and Great Britain (GB). Frequency data of all regions and Equation (11) is used to compute the noise amplitude ϵ which we expect to be similar in all regions, providing a self-consistency check of our theory. The box plot is obtained by using different damping, standard deviation estimates, etc. for each day of multiple years. The data for the Nordic grid [29] has large uncertainty due to the two different correlation time scales.

estimates and Equation (11) we plot the noise amplitudes for different regions in Fig. 5.

The estimated noise amplitude tends to increase with increasing share of intermittent renewable generation (wind and solar) in a given region [45, 46]. Nevertheless, this relationship is not very strict and frequency disturbances at trading intervals, see Fig. 1 demonstrate, that at least today trading and demand fluctuations are contributing substantially to frequency fluctuations.

SUPERSTATISTICS

Instead of modeling the underlying stochastic process as non-Gaussian, we may interpret the observed statistic as a superposition of multiple Gaussians, leading to *superstatistics*, explaining heavy tails and skewness [47, 48].

For our superstatistical approach we use Equation (3) with Gaussian noise ξ

$$\frac{d}{dt}\bar{\omega} = -\gamma\bar{\omega} + \bar{\epsilon}\xi(t), \quad (12)$$

which yields a Gaussian distribution, see (5). What changes when the damping γ is not longer constant over time? Both control actions and physical damping contribute to γ and change over time when certain power plants are connected and others are shut down. Similarly, the noise amplitude $\bar{\epsilon}$ of the system depends on

which consumers are currently active, what the time of the day it is, which renewables are connected and more. Hence, it is appropriate to replace our static parameters γ and ϵ by dynamical parameters that change over time with a typical time scale T . When applying superstatistics, we assume that the time scale T is large compared to the intrinsic time scale of the system, which is given by the autocorrelation time scale, namely $T \gg \tau = 1/\gamma$. Then, the stochastic process finds an equilibrium with an approximately Gaussian distribution determined by the current noise and damping. When these parameters change, the frequency distribution becomes a Gaussian distribution with different standard deviation.

In Fig. 6a we demonstrate how just a few Gaussian distributions with different standard deviations give rise to an excess kurtosis and in the Supplementary Note 3 we show how two Gaussian distributions with shifted means result in a skewed distribution.

Extracting time scales from time series

We extract the long time scale T from the data and compare it to the intrinsic short time scale of the system. The short time scale $\tau = 1/\gamma$ is based on the exponential decay of the autocorrelation of the time series of $\bar{\omega}$ yielding a range of $\tau \approx 200..550$ s for all grids. The long time scale T is governed by the idea that the superstatistical ensemble has heavier tails than a normal distribution but that for a given typical time scale T an equilibrium distribution emerges that is approximately Gaussian. Given a time series $x(t)$ with mean \bar{x} , we compute the local kurtosis $\kappa(\Delta t)$ for different time intervals Δt and choose the large time scale T by $\kappa(\Delta t = T) = 3$ [47]. Similarly, we compute the time for which the average skewness is zero to extract the long time scale for the Great Britain or Eastern Interconnection grids, see Methods and Supplementary Note 3 for details and Fig. 6 for an example for Japan.

All synchronous regions return large but different long time scales. We determine the long time scales to be of the order of $T \approx 1..5$ h with small values in Mallorca and the Eastern Interconnections and large values in Continental Europe and Japan, hinting to distinct underlying mechanisms how damping and noise change in each region. Compared to the intrinsic short time scale $\tau \sim 200..550$ s, the long time scale T is larger by at least one order of magnitude. Hence, the superstatistical approach is justified, i.e., it is valid to interpret the heavy tails as a result of superimposing Gaussians.

Finally, we perform another consistency check of the superstatistical approach and extract the distribution of the *effective friction* γ_{eff} [47], see Methods. Based on general results on superstatistics, we expect the effective friction to follow a χ^2 , inverse χ^2 or log-normal distribution, which then leads to an approximate q-Gaussian distribution of the frequency, see Supplementary Note 3 for a derivation. In the case of the Japanese 60Hz region the

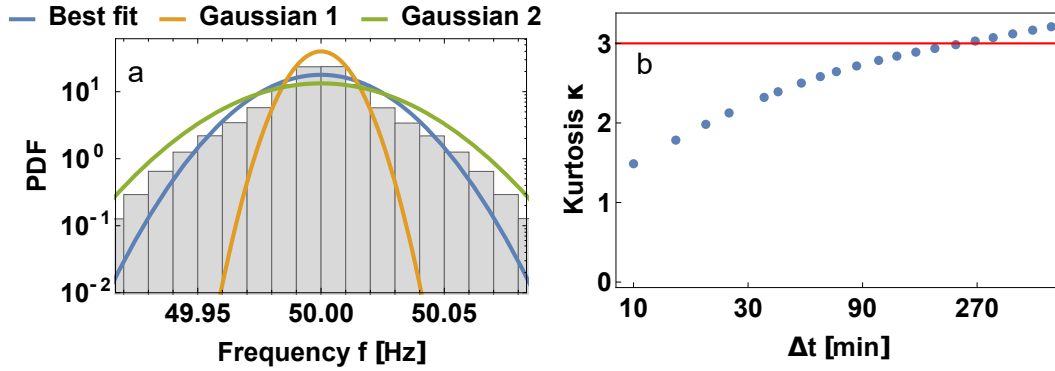


Figure 6. **Superimposed Gaussian distributions leading to heavy tails.** **a:** When the stochastic process follows two different Gaussian distributions (orange and green) and the data is aggregated (gray histogram), resulting in a heavy-tailed distribution which is not Gaussian. Consequently, Gaussian fits (blue curve) tend to underestimate its tails. Assuming such a structure for the real frequency measurements, the frequency recordings are split into trajectories of length Δt each and the kurtosis is computed. **b:** The average kurtosis of the Japanese 60Hz data set in dependence of the length of Δt . For very small Δt the distribution has lighter tails than a Gaussian while using the full data set or large Δt leads to the earlier observed heavy tails. The long time scale T , during which the distribution changes, is determined as $\kappa(\Delta t = T) = 3$.

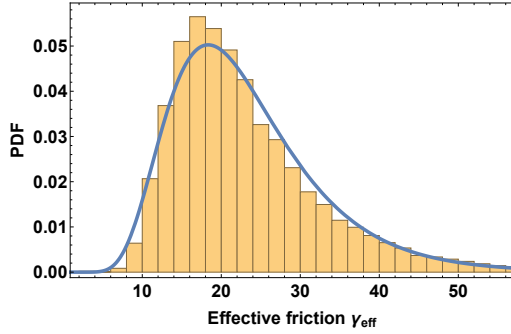


Figure 7. **Self-consistency test of superstatistics.** Plotted is the histogram of the effective friction γ_{eff} based on the Japanese 60Hz frequency measurements which is well-described by a log-normal distribution. Such a distribution of the effective friction γ_{eff} , directly leads to q-Gaussian distributions of the aggregated data, see Supplementary Note 3. Other data sets are also approximated by log-normal distributions, see Supplementary Note 3.

distribution of γ_{eff} is well-described by a log-normal distribution again supporting the superstatistics approach, see Fig. 7.

DISCUSSION

In summary, we have analyzed power grid frequency fluctuations by applying analytical stochastic methods to time series of different synchronous regions across continents including North America, Japan and different European regions. Based on bulk frequency measurements,

we have identified trading as a significant source of fluctuations (Figs. 1 and 3). Although frequency fluctuations and power uncertainty are often modeled as Gaussian distributions [14, 16–19], we pinned down and quantified significant deviations from a Gaussian form, including heavy tails and skewed distributions (Fig. 2).

Obtaining an analytical description of a complex system allows deeper insight into it. Hence, condensing the analysis of frequency fluctuations in power grids via a second order nonlinear dynamics, the swing equation, and neglecting spatial correlations, we derived (generalized) Fokker-Planck equations for the bulk angular velocity $\bar{\omega}$. We obtained precise predictions on how power fluctuations impact the distribution of fluctuations of the grid frequency. Furthermore, our approach identifies, besides grid size, an increasing effective damping as a controlling factor for reducing fluctuation-induced risks. By incorporating smart grid control mechanisms [49] or increasing generator droop control [9], modifying effective damping may therefore reliably reduce the likelihood of large fluctuations in the power grid [50]. Finally, our analytical theory is able to compare differently sized power grids, predicting fluctuations based on the size and inertia of the grid (Equation (10)). Crucially, our mathematical framework goes beyond the simple $N^{-1/2}$ scaling of Gaussian noise. This should enable grid operators to achieve a desired quality of service for the frequency by applying the appropriate effective damping based on the size of their synchronous region especially when facing a decreasing inertia M .

Our results offer two approaches to model power grids under uncertainty: First, an optimization could include the non-Gaussian nature of the distribution by incorporating non-Gaussian noise, e.g. in the form of Lévy-stable

noise. Alternatively, we demonstrated that the distributions are also well explained by a *superstatistics* approach where the non-Gaussian nature of the distributions arises by superimposing different Gaussian distributions. Especially when modeling shorter time scales of one hour or below, a Gaussian approach is supported by our results. Studies aiming to cover time scales of full months or years, however, have to account for changing mean and variance of the assumed Gaussian distribution or explicitly model non-Gaussian distributions, going beyond current Gaussian approaches [14, 16–19].

METHODS

Statistic moments

We quantify the extremity of the tails by the kurtosis κ , i.e., the normalized fourth moment, of the distribution, which we compute to be $\kappa_{\text{CE}} \approx 4$. In contrast, a Gaussian distribution has $\kappa_{\text{Gauss}} = 3$ such that any higher value indicates an increased likelihood of large deviations.

In contrast the skewness β is the normalized third moment of the distribution and a non-zero skewness implies a distribution that is not symmetric around the mean but has more pronounced tails in one direction.

Normally distributed noise

We assumed that the noise ξ at each node is distributed following a Normal distribution, i.e.,

$$\xi \sim N(0, 1) \quad (13)$$

where $N(\mu, \sigma)$ denotes a Normal distribution with mean μ and standard deviation σ . The collective noise $\bar{\xi}$ acting on the bulk frequency is then easily broken down into a normal distribution

$$\bar{\xi} = \sum_{i=1}^N \epsilon_i \xi_i \sim \sqrt{\sum_{i=1}^N \epsilon_i^2} \xi, \quad (14)$$

where $X \sim Y$ denotes that the random variables X and Y follow the same distribution [34].

Fokker-Planck equations

In the main text we made use of a general time-independent solution of a Fokker-Planck equation. Given a general stochastic system whose dynamics is given by

$$\frac{d}{dt}X = a(X) + \sqrt{b(X)}\xi, \quad (15)$$

where ξ is white Gaussian noise based on a Wiener process, its stationary Fokker-Planck equation is given by

$$\frac{d}{dx} [a(x)p(x)] - \frac{1}{2} \frac{d^2}{dx^2} [b(x)p(x)] = 0, \quad (16)$$

which can be solved to give

$$p(x) = \frac{N}{b(x)} \exp \left[2 \int_0^x a(s)/b(s) ds \right]. \quad (17)$$

In the case of $a(x) = -a_0x$ and $b(x) = b_0$ the final distribution is a Gaussian distribution.

Generalized Fokker-Planck equations

Assuming that our system is described by a Langevin equation of the form (15) and is subject to Lévy-stable distributed noise with characteristic function $S_k(\alpha_S, \beta_S, \sigma_S)$ with stability parameter α_S , skewness parameter β_S and scale parameter σ_S , then the generalized Fokker-Planck equation [44] is given by

$$\begin{aligned} \frac{\partial p}{\partial t}(x, t) = & -\frac{\partial}{\partial x} [a(x, t)p(x, t)] \\ & + \sigma_S^{\alpha_S} \frac{\partial^{\alpha_S}}{\partial |x|^{\alpha_S}} [b(x, t)^{\alpha_S} p(x, t)] \\ & + \sigma_S^{\alpha_S} \beta_S \tan\left(\frac{\pi\alpha_S}{2}\right) \frac{\partial^{\alpha_S-1}}{\partial |x|^{\alpha_S-1}} [b(x, t)^{\alpha_S} p(x, t)]. \end{aligned} \quad (18)$$

The fractional derivative of a function $h(x)$ is defined as

$$\frac{\partial^{\alpha_S}}{\partial |x|^{\alpha_S}} h(x) = -\mathcal{F}^{-1} [|k|^{\alpha_S} h_k]. \quad (19)$$

Superstatistics

In the superstatistical approach we have a time series $x(t)$ with a mean \bar{x} and compute the local kurtosis as follows:

$$\kappa(\Delta t) = \frac{1}{t_{max} - \Delta t} \int_0^{t_{max} - \Delta t} dt_0 \frac{\langle (x - \bar{x})^4 \rangle_{t_0, \Delta t}}{\langle (x - \bar{x})^2 \rangle_{t_0, \Delta t}^2}, \quad (20)$$

where $\langle \dots \rangle_{t_0, \Delta t} = \int_{t_0}^{t_0 + \Delta t} \dots dt$. We do so for several values of Δt and choose T so that $\kappa(\Delta t = T) = 3$, i.e., averaging over a time scale T , there is no excess kurtosis.

The effective friction γ_{eff} which is changing over time is then computed as:

$$\gamma_{\text{eff}}(t_0) = \frac{1}{\langle x^2 \rangle_{t_0, T} - \langle x \rangle_{t_0, T}^2}. \quad (21)$$

Following [47] we expect γ_{eff} to follow a log-normal or alternatively a χ^2 or inverse χ^2 distribution as those lead to q-Gaussian distributions of x , see Supplementary Note 3.

-
- [1] Intergovernmental Panel on Climate Change, *Climate Change 2014—Impacts, Adaptation and Vulnerability: Regional Aspects* (Cambridge University Press, 2014).
- [2] M. Z. Jacobson and M. A. Delucchi, *Energy Policy* **39**, 1154 (2011).
- [3] J. A. Turner, *Science* **285**, 687 (1999).
- [4] G. Boyle, *Renewable Energy* (Oxford University Press, Oxford, 2004).
- [5] F. Ueckerdt, R. Brecha, and G. Luderer, *Renewable Energy* **81**, 1 (2015).
- [6] D. Heide, L. V. Bremen, M. Greiner, C. Hoffmann, M. Speckmann, and S. Bofinger, *Renewable Energy* **35**, 2483 (2010).
- [7] P. Milan, M. Wächter, and J. Peinke, *Physical Review Letters* **110**, 138701 (2013).
- [8] J. Peinke, M. Siefert, S. Barth, C. Renner, F. Riess, M. Wächter, and R. Friedrich, in *Advances in Solid State Physics* (Springer, 2004), pp. 363–373.
- [9] J. Machowski, J. Bialek, and J. Bumby, *Power System Dynamics: Stability and Control* (John Wiley & Sons, 2011).
- [10] P. Kundur, N. J. Balu, and M. G. Lauby, *Power system stability and control*, vol. 7 (McGraw-hill New York, 1994).
- [11] A. Ulbig, T. S. Borsche, and G. Andersson, *IFAC Proceedings Volumes* **47**, 7290 (2014).
- [12] G. Delille, B. Francois, and G. Malarange, *IEEE Transactions on Sustainable Energy* **3**, 931 (2012).
- [13] R. Doherty, A. Mullane, G. Nolan, D. J. Burke, A. Bryson, and M. O'Malley, *IEEE transactions on power systems* **25**, 452 (2010).
- [14] A. J. Wood and B. F. Wollenberg, *Power generation, operation, and control* (John Wiley & Sons, 2012).
- [15] N. A. of Sciences Engineering and Medicine, *The Power of Change: Innovation for Development and Deployment of Increasingly Clean Electric Power Technologies* (The National Academies Press, 2016).
- [16] Y. Jin and J. Branke, *IEEE Transactions on evolutionary computation* **9**, 303 (2005).
- [17] H. Zhang and P. Li, *IET Generation, Transmission & Distribution* **4**, 553 (2010).
- [18] M. Matthiae, B. Schäfer, X. Zhang, M. Rohden, M. Timme, and D. Witthaut, *arXiv preprint arXiv:1611.08365* (2016).
- [19] X. Fang, S. Misra, G. Xue, and D. Yang, *Communications Surveys & Tutorials*, *IEEE* **14**, 944 (2012).
- [20] K. Kashima, H. Aoyama, and Y. Ohta, in *2015 54th IEEE Conference on Decision and Control (CDC)* (IEEE, 2015), pp. 1852–1857.
- [21] T. Mühlpfordt, T. Faulwasser, and V. Hagenmeyer, in *2016 IEEE Conference on Control Applications (CCA)* (IEEE, 2016), pp. 70–76.
- [22] M. Anvari, G. Lohmann, M. Wächter, P. Milan, E. Lorenz, D. Heinemann, M. R. R. Tabar, and J. Peinke, *New Journal of Physics* **18**, 063027 (2016).
- [23] K. Schmietendorf, J. Peinke, and O. Kamps, *arXiv preprint arXiv:1611.08235* (2016).
- [24] X. Li, D. Hui, and X. Lai, *IEEE Transactions on Sustainable Energy* **4**, 464 (2013).
- [25] M. Lauby, J. Bian, S. Ekisheva, and M. Varghese, in *2014 North American Power Symposium (NAPS)* (IEEE, 2014), pp. 1–5.
- [26] R. H. Lasseter and P. Paigi, in *2004 IEEE 35th Annual Power Electronics Specialists Conference (PESC)* (IEEE, 2004), vol. 6, pp. 4285–4290.
- [27] 50Hertz Transmission GmbH, *Entso-e netzfrequenz* (2010–2016), URL <http://www.50hertz.com/de/Maerkte/Regelenergie/Regelenergie-Downloadbereich>.
- [28] Réseau de Transport d'Électricité (RTE), *Network frequency* (2014–2016), URL https://clients.rte-france.com/lang/an/visiteurs/vie/vie_frequence.jsp.
- [29] Fingrid, *Nordic power system frequency measurement data* (2015–2016), URL <http://www.fingrid.fi/en/powersystem/Power%20system%20management/Maintaining%20of%20balance%20between%20electricity%20consumption%20and%20production/Frequency%20measurement%20data/Pages/default.aspx>.
- [30] E. Tchuisseu, D. Gomila, D. Brunner, and P. Colet, *arXiv preprint arXiv:1704.01638* (2017).
- [31] National Grid, *Frequency data* (2014–2016), URL <http://www2.nationalgrid.com/Enhanced-Frequency-Response.aspx>.
- [32] Organization for Cross-regional Coordination of Transmission Operators, Japan (OCCTO), *Japanese grid frequency* (2016), URL http://occtonet.occto.or.jp/public/dfw/RP11/OCCTO/SD/LOGIN_login#.
- [33] Power Information Technology Lab, University of Tennessee, Knoxville and Oak Ridge National Laboratory, *FNET/GridEye* (2014), 1 day data set "20140905", contact powerit@utk.edu, URL <http://powerit.utk.edu/fnet.html>.
- [34] G. Samorodnitsky and M. Taqqu, *Stable Non-Gaussian Random Processes. Stochastic Models with Infinite Variance* (Chapman and Hall, 1994).
- [35] C. Tsallis, *Brazilian Journal of Physics* **39**, 337 (2009).
- [36] C. W. Gardiner et al., *Handbook of stochastic methods*, vol. 3 (Springer Berlin, 1985).
- [37] G. Filatrella, A. H. Nielsen, and N. F. Pedersen, *The European Physical Journal B-Condensed Matter and Complex Systems* **61**, 485 (2008).
- [38] M. Rohden, A. Sorge, M. Timme, and D. Witthaut, *Physical Review Letters* **109**, 064101 (2012).
- [39] F. Dörfler, M. Chertkov, and F. Bullo, *Proceedings of the National Academy of Sciences* **110**, 2005 (2013).
- [40] A. E. Motter, S. A. Myers, M. Anghel, and T. Nishikawa, *Nature Physics* **9**, 191 (2013).
- [41] D. Manik, D. Witthaut, B. Schäfer, M. Matthiae, A. Sorge, M. Rohden, E. Katifori, and M. Timme, *The European Physical Journal Special Topics* **223**, 2527 (2014).
- [42] T. Dewenter and A. K. Hartmann, *New Journal of Physics* **17**, 015005 (2015), URL <http://stacks.iop.org/1367-2630/17/i=1/a=015005>.
- [43] M. Weixelbraun, H. Renner, R. Schmaranz, and M. Marketz, in *Electricity Distribution-Part 1, 2009. CIREP 2009. 20th International Conference and Exhibition on (IET, 2009)*, pp. 1–4.
- [44] S. Denisov, W. Horsthemke, and P. Hänggi, *The European Physical Journal B* **68**, 567 (2009).

- [45] ENTSO-E, *Monthly production for a specific year for 2015* (2016), URL <https://www.entsoe.eu/db-query/production/monthly-production-for-a-specific-year>.
- [46] U.S. Department of Energy, *Eia-411: Coordinated bulk power supply and demand program report* (2016), URL <https://www.eia.gov/electricity/data/eia411/>.
- [47] C. Beck and E. Cohen, *Physica A: Statistical mechanics and its applications* **322**, 267 (2003).
- [48] A. V. Chechkin, F. Seno, R. Metzler, and I. M. Sokolov, *Physical Review X* **7**, 021002 (2017).
- [49] B. Schäfer, M. Matthiae, M. Timme, and D. Witthaut, *New Journal of Physics* **17**, 015002 (2015).
- [50] E. Schöll and H. G. Schuster, *Handbook of chaos control* (2008).

ACKNOWLEDGMENTS

We gratefully acknowledge support from the Federal Ministry of Education and Research (BMBF grant no.03SF0472A-E), the Helmholtz Association (via the

joint initiative “Energy System 2050 - A Contribution of the Research Field Energy” and the grant no.VH-NG-1025 to D.W.), the Göttingen Graduate School for Neurosciences and Molecular Biosciences (DFG Grant GSC 226/2) to B.S., the EPSRC via the grant EP/N013492/1 to C.B., the CREST, JST to K.A. and the Max Planck Society to M.T.

Author contributions

B.S. acquired the data, performed the data analysis and formulated stochastic predictions. B.S., D.W. and M.T. designed the research. All authors contributed to discussing the results and writing the paper.

Competing interests

The authors declare no competing financial interests.

SUPPLEMENTARY INFORMATION
accompanying the manuscript
Heavy Tails, Superstatistics and Scaling of Power Grid Frequency Fluctuations
by

Benjamin Schäfer,¹ Christian Beck,² Kazuyuki Aihara,³ Dirk Witthaut,^{4,5} and Marc Timme^{1,6,7}

¹*Network Dynamics, Max Planck Institute for Dynamics and Self-Organization (MPIDS), 37077 Göttingen, Germany*

²*Queen Mary University of London, School of Mathematical Sciences, Mile End Road, London E1 4NS, UK*

³*Institute of Industrial Science, The University of Tokyo, Meguro-ku, Tokyo, Japan*

⁴*Forschungszentrum Jülich, Institute for Energy and Climate Research - Systems
Analysis and Technology Evaluation (IEK-STE), 52428 Jülich, Germany*

⁵*Institute for Theoretical Physics, University of Cologne, 50937 Köln, Germany*

⁶*Institute for Theoretical Physics, Technical University of Dresden, 01062 Dresden Germany*

⁷*Center for Advancing Electronics Dresden (cfaed),
Technical University of Dresden, 01062 Dresden Germany*

SUPPLEMENTARY NOTE 1

Power grid frequency data presentation

We have a closer look at the data sets of power grid frequency measurements. Our available data includes ENTSO-E Continental European (CE) [1, 2], Great Britain (GB) [3], Mallorca [4] and Nordic [5] grids, the 50 Hz and 60 Hz regions of Japan [6] as well as one day of the Eastern Interconnection (EI) [7]. Production data of the regions was taken from [6, 8–10].

Table S.1. The mean frequency is kept close to the reference frequency in all grids while standard deviations differ significantly. We list the estimates for mean, standard deviation (SD), skewness and kurtosis of distributions for different European (Continental Europe (CE), Great Britain (GB), Nordic, Mallorca), Japanese and Eastern Interconnection (EI) data sets and years

Source	year/ region	mean μ [Hz]	standard deviation σ [Hz]	skewness β	kurtosis κ
CE (<i>50Hertz</i>) [1]	2014	49.9995	0.0202	0.047	4.04
	2015	49.9999	0.0200	-0.024	4.10
CE (<i>RTE</i>) [2]	2015	50.0003	0.0202	-0.007	3.89
Nordic (<i>FinGrid</i>) [5]	2015	50.000	0.0434	0.033	3.11
	2016	50.000	0.0456	0.046	3.10
GB (<i>Nationalgrid</i>) [3]	2014	49.9997	0.0545	0.232	3.02
	2015	49.9997	0.0544	0.258	2.91
Japan (<i>OCCTO</i>) 2016 [6]	50 Hz	50.0003	0.0304	0.018	3.17
	60 Hz	60.0025	0.0376	0.000	4.01
Mallorca [4]	2015	49.9999	0.0415	-0.014	4.99
EI (1d) [7]	(2014)	59.9967	0.0175	0.316	2.97

Distribution measures and histograms

As an introduction to the data, we list mean μ , standard deviation σ , skewness β ($\beta^{\text{Gaussian}} = 0$) and kurtosis κ ($\kappa^{\text{Gaussian}} = 3$), i.e., the normalized first four moment of the distributions in Table S.1. Analyzing the figures reveals that all distributions are close to their nominal frequency of 50/60 Hz. Furthermore, all other grids have either a higher kurtosis than expected from a normal distribution (Continental Europe, Nordic, Mallorca, Japan) or are skewed (Great Britain, Eastern Interconnection). Next, we visualize these distributions as histograms compared to their best-fitting normal distribution in Fig. S.1.

For the Continental European (CE) grid we have two data bases, one by the German transmission system operator (TSO) *50Hertz* and the other by the French TSO *RTE*. Although the measurements were taken at different locations of the connected grid, they return close to identical statistics.

Preprocessing of data sets We had to perform some pre-processing especially with the *50Hertz* data set and the data from Mallorca: The original data set [1] contains entries set to 0, 52 or 48 Hz, while the Mallorca data included a few very large and small values. In the case of *50Hertz*, they confirmed measurements problems leading to these small and large values. Hence, we deleted entries larger than 51Hz or smaller than 49 Hz. We associate these large deviations with blackouts or nealy blackouts, which are no longer covered by our theory. However, even after excluding these extreme values, the *50Hertz* data had some very large jumps within 1 second to a larger value by $\Delta f \sim 0.5\text{Hz}$ which we found to be most likely also artifacts. Hence, we decided to scan the data for jumps larger than $\Delta f_{max} = 0.1\text{Hz}$ and delete these if they were isolated, i.e., values before and after this value are at least different by Δf_{max} . This way the statistical measures, e.g. variance and kurtosis, of the *50Hertz* data set approached the *RTE* data set, as expected for the same synchronous region.

When computing the noise amplitude ϵ for different regions in Figure 5, we assumed that the Eastern Interconnection has a total inertia of $M = 1000$ to increase the absolute value of the estimated noise.

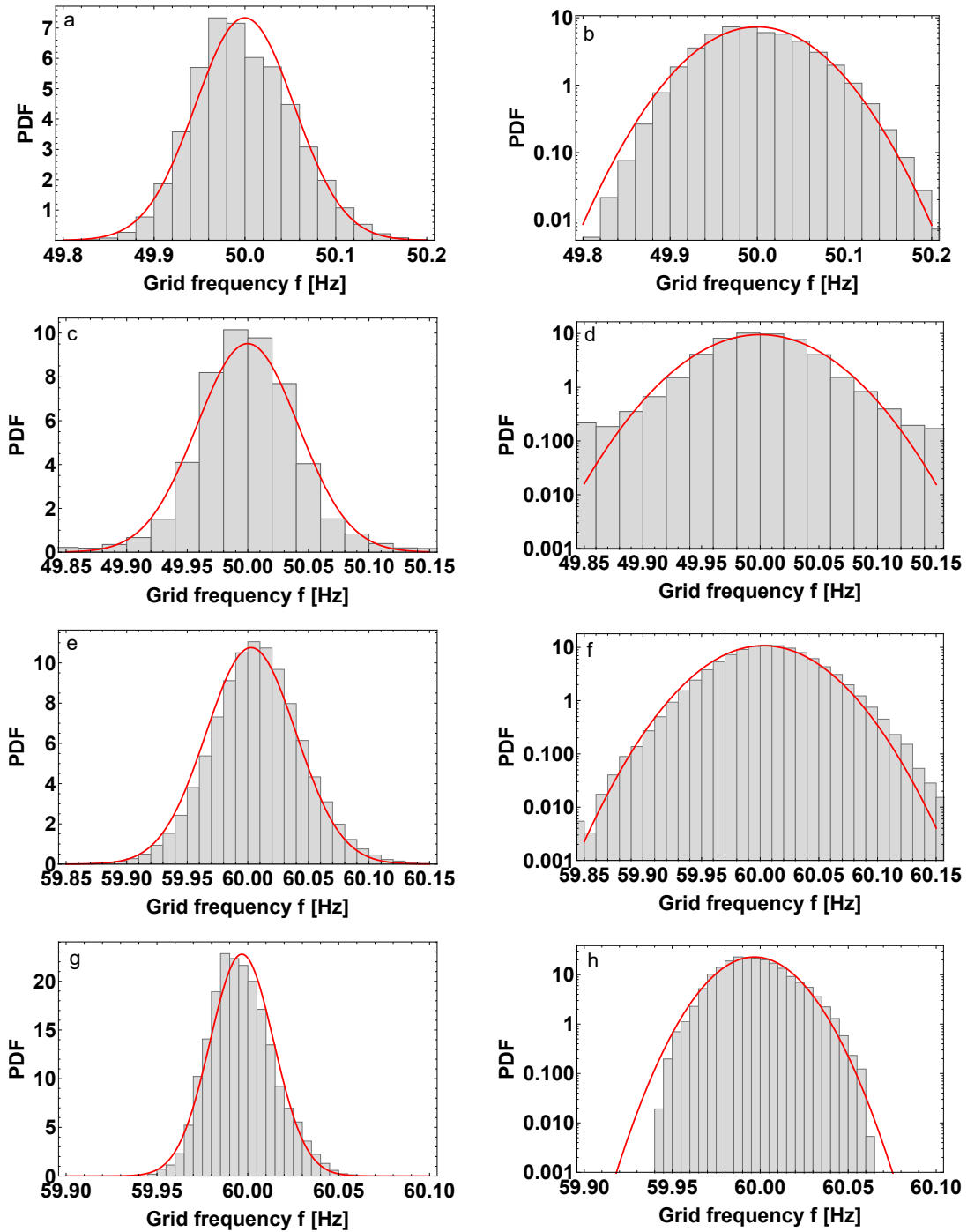


Figure S.1. All data sets show deviations from normal distributions. We plot the histograms for the data of Great Britain (GB), Mallorca, Japan and Eastern Interconnection (EI) together with their estimated normal distribution. **a**: GB with linear scale, **b**: GB with log-scale, **c**: Mallorca region with linear scale, **d**: Mallorca region with log-scale, **e**: Japan 60Hz region with linear scale, **f**: Japan 60Hz region with log-scale, **g**: EI with linear scale, **h**: EI with log-scale. Each histogram is either more heavy-tailed than a Normal distribution or skewed.

Estimated distributions

Noticing deviations from normal distributions both in Table S.1 and Fig. S.1, we perform a maximum likelihood analysis, see e.g. [11], of the available data and thereby determine which standard distribution fits the data best. This is done with the assumption that one well chosen distribution would be able to fit all data sets (with differing parameters for each grid). Given a probability density function $p(x)$ and a data set $Y = \{y_1, y_2, \dots, y_N\}$, we calculate the likelihood that Y is drawn from the distribution p by calculating

$$L_{p,Y} = \prod_{i=1}^N p(y_i). \quad (1)$$

The maximum likelihood estimate is based on comparing at least two different distributions, e.g. $p_1(x)$ and $p_2(x)$ by computing the likelihoods for both distributions. Next, we have a look at the likelihood ratio

$$\frac{L_{p_1,Y}}{L_{p_2,Y}}, \quad (2)$$

which is the most powerful tool to distinguish two distributions [11]. We then accept p_1 over p_2 if the ratio is larger than 1. We use the Mathematica *EstimatedDistribution* [12] routine testing several build-in distributions against the data: *HyperbolicDistribution* $[\lambda, a, b, c, d]$, *StableDistribution* $[a, b, c, d]$, *NormalDistribution* $[a, b]$, *LogNormalDistribution* $[a, b]$, *SkewNormalDistribution* $[a, b, c]$, *LogLogisticDistribution* $[a, b]$, *StudentTDistribution* $[a, b, c]$, *ParetoDistribution* $[a, b, c, d]$, *SechDistribution* $[a, b]$, *ExponentialPowerDistribution* $[a, b, c]$, *JohnsonDistribution* $["SU", a, b, c, d]$ and *TsallisQGaussianDistribution* $[a, b, c]$. As an example, we note down the estimated stable distributions for some grids in Table S.2. Note also that especially the (generalized) hyperbolic and stable distributions use many parameters to fit the distributions.

For the heavy-tail distributions (Continental Europe, Nordic, Japan, Mallorca) normal distributions perform worse than stable distributions which get outperformed by q-Gaussian distributions in terms of likelihood (which get outperformed by a small margin by generalized hyperbolic distributions). However, skewed distributions (Great Britain and Eastern Interconnection) are best fitted by skew normal distributions but can be approximated by stable distributions as these also describe skewed distributions. Hence, we focused mainly on stable and q-Gaussian distributions in the main text.

Table S.2. Estimated stable distributions with *StableDistribution* $[\text{type}, \alpha_S, \beta_S, \mu_S, \sigma_S]$ with stability parameter α_S , skewness parameter β_S , location μ_S and scale parameter σ_S for different regions

Source	year/ region	Stable Distribution
Continental Europe (<i>50Hertz</i>) [1]	2015	<i>StableDistribution</i> [1, 1.898, 0.006, 49.9999, 0.0132]
Great Britain (<i>Nationalgrid</i>) [3]	2015	<i>StableDistribution</i> [1, 1.969, 0.997, 50.0001, 0.0378]
Japan (<i>OCCTO</i>) 2016 [6]	50 Hz	<i>StableDistribution</i> [1, 1.988, 0.237, 50.0003, 0.0213]
	60 Hz	<i>StableDistribution</i> [1, 1.986, 0.387, 60.0025, 0.0263]
Eastern Interconnection(1d) [7]	(2014)	<i>StableDistribution</i> [1, 1.938, 0.999, 59.9969, 0.0121]
Nordic [5]	2015	<i>StableDistribution</i> [1, 1.987, 0.999, 49.9997, 0.0306]
Mallorca [4]	2015	<i>StableDistribution</i> [1, 1.832, 0.509, 50.0000, 0.0238]

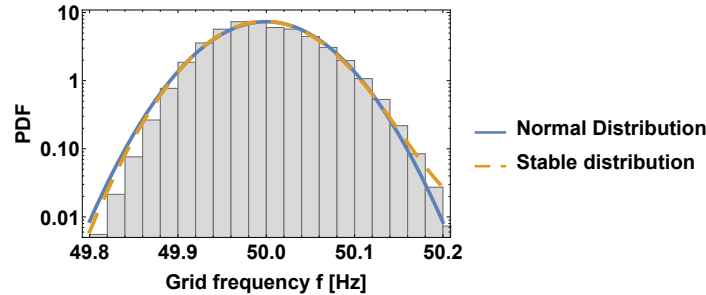


Figure S.2. Stable distributions account for skewed distributions. Plotted is the Log plot of the histogram of the Great Britain 2015 data and its best normal as well as stable distribution fit. The skewed stable distribution is a better description both for low and high frequencies than the normal distribution.

SUPPLEMENTARY NOTE 2

Additional Fokker-Planck results

We extend the Fokker-Planck results obtained in the main text by calculating the standard deviation and noise amplitude assuming Gaussian noise and adding treatment for primary control with deadzones, time-dependent solutions of stable noise input as well as describing how to treat arbitrary distributions. Deadzones arise naturally in power grid control [13] where it is only possible to determine the frequency to a finite precision. Hence, one could argue that the non-Gaussian nature of the observed distribution could be explained by Gaussian noise combined with the nonlinear control.

Ordinary Fokker-Planck equations

Assuming that the power grid is dominated by Gaussian noise, we formulated the Fokker-Planck equation for the bulk angular velocity $\bar{\omega}$ as

$$\frac{\partial p}{\partial t} = \gamma \frac{\partial}{\partial \bar{\omega}} (\bar{\omega} p) + \frac{1}{2} \sum_{i=1}^N \frac{\epsilon_i^2}{M^2} \cdot \frac{\partial^2 p}{\partial \bar{\omega}^2}, \quad (3)$$

which is solved by the probability density function

$$p(\bar{\omega}) = \sqrt{\frac{\gamma M^2}{\pi \sum_{i=1}^N \epsilon_i^2}} \exp \left[-\bar{\omega}^2 \frac{\gamma M^2}{\sum_{i=1}^N \epsilon_i^2} \right], \quad (4)$$

with damping γ , the number of nodes N , noise amplitude ϵ , summed inertia $M = \sum_i M_i$.

Standard deviation predictions The standard deviation of the bulk angular velocity $\bar{\omega}$, assuming that all nodes have the same noise amplitude $\epsilon_i \approx \epsilon$ and unit inertia $M_i = 1 \forall i$, is given by

$$\sigma = \sqrt{\frac{\epsilon^2}{2N\gamma}}. \quad (5)$$

This standard deviation is dependent on the number of nodes N in the grid, i.e., synchronous regions with less production, i.e., with fewer nodes will have a broader distribution and hence higher risk of large fluctuations.

Deadzones The power grid frequency (and angular velocity) cannot be determined to arbitrary precision, giving rise to *deadzones* of control, i.e., for a small interval $\omega = 0 \pm \Delta\omega_D$ there is no (primary) control activated at the swinging machines. Could those deadzones explain the non-Gaussian distributions in the frequency assuming Gaussian noise but nonlinear control? These deadzones are typically of the order $\Delta\omega_D \approx 2\pi (10 \dots 200 \text{ mHz})$ [13, 14], see Fig. S.3 for an illustration where we split the damping γ into intrinsic damping γ_D that arises from damper windings etc. and the (primary) control damping γ_C which is only active outside of the deadzone. Given our solution of the Fokker-Planck equation, we calculate the probability density function for piecewise linear control to be

$$p(\omega) = \frac{\sqrt{\gamma_C}}{2\Delta\omega_D + \sqrt{\pi}} \begin{cases} \exp \left[-\gamma_C (\Delta\omega_D + \omega)^2 \right] & \omega < -\Delta\omega_D, \\ 1 & \text{else,} \\ \exp \left[-\gamma_C (\Delta\omega_D - \omega)^2 \right] & \omega > \Delta\omega_D, \end{cases} \quad (6)$$

where we used $\gamma_D = 0$. Performing a maximum likelihood analysis to estimate the deadzone ω_D , we reach the conclusion that the most likely value for the deadzone parameter is $\omega_D \approx 0$, i.e., we do not need a deadzone to model our real power grid frequency data. Furthermore, stable distributions still outperform Gaussian noise in terms of likelihood even when deadzones are included, see Fig. S.4.

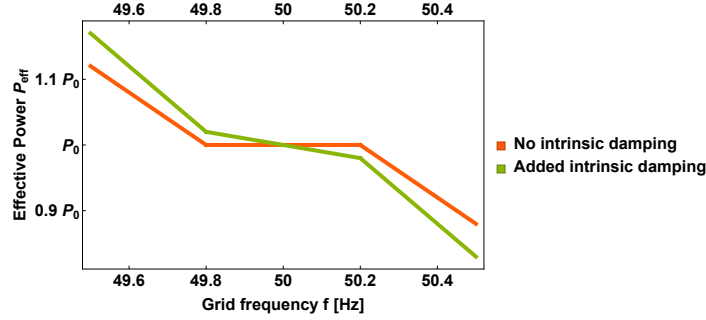


Figure S.3. Deadzones of control lead to piecewise linear power(frequency) functions. We plot the effective power $P_{eff} = P_0 + \text{control}$ as a function of frequency using piecewise linear functions modeling deadzones of primary control $\gamma_C > 0$, with intrinsic damping $\gamma_D > 0$ (green) and without (orange).

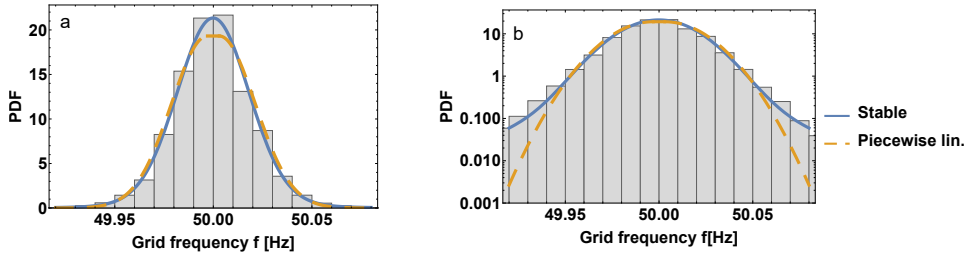


Figure S.4. Stable distributions outperform Gaussian noise with deadzones. We compare stable distributions (blue) with a piecewise linear probability density function modeling deadzones of primary control and the real *50Hertz* 2015 data set (histogram). **a**: We plot the histogram of the real data together with the PDFs of the best-fitting stable distribution and a piecewise linear. **b**: We repeat the plot with a log-scale of the PDF. Parameters are $\Delta\omega_D = 3$ mHz and $N\gamma_C/\epsilon^2 = 1500$. We note that increasing the damping γ_C increases the peak at 50 Hz but also results in flatter tails. Hence, we improve one property at the expense of the other as the piecewise linear distribution tends to have a peak lower than the data (and the stable distribution) and flatter tails.

Generalized Fokker-Planck equation

In the main text we derived the solution of the generalized Fokker-Planck equation as

$$p(x, t) = \mathcal{F}^{-1} \left[\exp \left(-\frac{1}{\gamma} \int_0^k \frac{1}{z} \ln \left(\frac{S_{z \cdot e^{-\gamma t}}}{S_z} \right) dz \right) \right], \quad (7)$$

where S_k is the characteristic function of the (arbitrarily distributed but uncorrelated) noise generating process and

$$\mathcal{F}^{-1} [u_k] = \frac{1}{2\pi} \int_{-\infty}^{\infty} e^{ikx} u_k dk \quad (8)$$

is the inverse Fourier transform [15]. Using the characteristic function of the final distribution F_k and the characteristic function of the input noise distribution S_k , we note the following important relations:

$$F_k = \exp \left[\frac{1}{\gamma} \int_0^k \frac{\ln(S_z)}{z} dz \right], \quad (9)$$

$$S_k = \exp \left[\gamma \cdot k \cdot \frac{\partial}{\partial k} \ln F_k \right]. \quad (10)$$

Time-dependent solution We formulate the time-dependent solution given the quadratic potential $U(x) = \gamma x^2/2$ and assuming stable noise input. We compute

$$\frac{S_z e^{-\gamma t}}{S_z} = \exp[-\sigma_S^{\alpha_S} |z|^{\alpha_S} (e^{-\gamma \alpha_S t} - 1)] \quad (11)$$

and can now compute the final characteristic function

$$F_z(t) = \exp\left[-\frac{1}{\gamma} \int_0^k \frac{1}{z} \ln\left[\frac{S_z e^{-\gamma t}}{S_z}\right] dz\right] \quad (12)$$

$$= \exp\left[\frac{\sigma_S^{\alpha_S}}{\gamma} (e^{-\gamma \alpha_S t} - 1) \int_0^k \frac{|z|^{\alpha_S}}{z} dz\right] \quad (13)$$

$$= \exp\left[-\frac{(1 - e^{-\gamma \alpha_S t})}{\gamma \alpha_S} \sigma_S^{\alpha_S} |z|^{\alpha_S}\right] \quad (14)$$

$$= S_z \left(\alpha_S, 0, \sigma_S \cdot \left(\frac{(1 - e^{-\gamma \alpha_S t})}{\gamma \alpha_S} \right)^{1/\alpha_S} \right). \quad (15)$$

So we get a time-dependent scaling parameter

$$\sigma_S(t) = \sigma_S \cdot \left(\frac{(1 - e^{-\gamma \alpha_S t})}{\gamma \alpha_S} \right)^{1/\alpha_S}, \quad (16)$$

which is zero at the initial condition, consistent with the ansatz in [15]: $\sigma_S(0) = 0$, i.e., the probability density function is a delta function $p(t=0, \bar{\omega}) = \delta(\bar{\omega})$. For $t \rightarrow \infty$, the scaling parameter approaches the value derived in the main text as follows:

$$\sigma_S(t) \rightarrow \sigma_S \cdot \left(\frac{1}{\gamma \alpha_S} \right)^{1/\alpha_S}, \text{ as } t \rightarrow \infty. \quad (17)$$

In this calculation we assumed zero mean and neglected skewness since it does not change.

Generalized hyperbolic distribution The generalized hyperbolic distribution (describing among others, generalized inverse Gamma and StudentT distributions) returned one of the highest likelihoods for the Continental European data and hence is worth special attention. Assuming that the final distribution is given as a generalized hyperbolic distribution, we have

$$F_k = \frac{(\sqrt{\alpha_H H^2 \delta})^\lambda (\sqrt{k^2 + \alpha_H H^2 \delta})^{-\lambda} K_\lambda(\sqrt{k^2 + \alpha_H H^2 \delta})}{K_\lambda(\sqrt{\alpha_H H^2 \delta})}, \quad (18)$$

where K_λ is the modified Bessel function of the second kind, λ and α_H are shape parameters, δ the scale parameter [16] and we set the location parameter μ and skewness parameter β to 0, in accordance to our estimate. Setting the above as our final distribution, we get an initial noise input distribution as

$$S_k = \exp\left(-\frac{k^2 \alpha_H \delta \cdot K_{\lambda+1}(\sqrt{k^2 + \alpha_H H^2 \delta})}{\sqrt{k^2 + \alpha_H H^2 \delta} \cdot K_\lambda(\sqrt{k^2 + \alpha_H H^2 \delta})}\right), \quad (19)$$

which unfortunately is not a well known standard distribution. However, we relate the variances of the input and output distributions assuming $\epsilon_i = \epsilon$ as

$$\left(\frac{\sigma_{F_K}^2}{\sigma_{S_k}^2} \right)_{\text{Hyperbolic}} = \frac{\epsilon^2}{2\gamma N}, \quad (20)$$

which demonstrates how increasing the damping γ or the number of nodes N decreases fluctuations. On the other hand, increasing the noise amplitude ϵ increases the final distribution width. Furthermore, this is exactly the relation of two variances we get when assuming Gaussian noise, see (5) and setting $\sigma_{S_k} = 1$.

Composite distributions Using generalized Fokker-Planck equations, we also treat composite distributions in the case that the power fluctuations are generated by multiple stochastic processes. Suppose that we are aware that our input noise ξ is not generated from a single but from a composite process Z , i.e., $\xi \sim Z$ with the composite noise as a sum of processes $Z = \sum_{i=1}^M X_i$, where any weighting factors in the sum are absorbed in the individual distributions. A sum of different independent processes is also known as a convolution and is easily handled in terms of the characteristic equations of the distributions

$$S_Z = \prod_{i=1}^M X_i, \quad (21)$$

see e.g. [11].

As an example we consider the sum of a normal distribution X and an α -stable distribution Y

$$Z = X + Y, \quad (22)$$

with

$$X \sim N(\mu_N, \sigma_N), \quad (23)$$

$$Y \sim S_{\alpha_S}(\beta_S, \mu_S, \sigma_S), \quad (24)$$

$$S_X(k) = \exp\left[i\mu_N k - \frac{\sigma_N^2 k^2}{2}\right], \quad (25)$$

$$S_Y(k) = \exp\left[i\mu_S k - |\sigma_S k|^{\alpha_S} \left(1 - i\beta_S \text{sign}(k) \tan\left(\frac{\pi\alpha_S}{2}\right)\right)\right]. \quad (26)$$

The composite distribution Z has the characteristic function

$$S_Z(k) = S_X(k) \cdot S_Y(k) = \exp\left[ik(\mu_N + \mu_S) - \frac{\sigma_N^2 k^2}{2} - |\sigma_S k|^{\alpha_S} \left(1 - i\beta_S \text{sign}(k) \tan\left(\frac{\pi\alpha_S}{2}\right)\right)\right]. \quad (27)$$

Note that stable distributions are closed under convolution if they have the same stability parameter α_S . In our example this would only be true for $\alpha_S = 2$ which resembles two normal distributions. Otherwise, the distribution of Z is neither a normal nor a stable distribution. We simplify (27) by setting the skewness parameter to zero $\beta_S = 0$ and assuming both distributions have 0 mean $\mu_N = \mu_S = 0$ as follows

$$S_{Z, \beta=0}(k) = \exp\left[-\frac{\sigma_N^2 k^2}{2} - |\sigma_S k|^{\alpha_S}\right]. \quad (28)$$

We now apply the solution of the generalized Fokker-Planck equation (7) to get the characteristic equation of the final distribution as

$$F(k) = \exp\left[\frac{1}{\gamma} \int_0^k \frac{\ln(S_z)}{z} dz\right] \quad (29)$$

$$= \exp\left[-\frac{\sigma_N^2 k^2}{4\gamma} - \frac{|\sigma_S k|^{\alpha_S}}{\gamma\alpha_S}\right]. \quad (30)$$

The probability density function does not have a closed form but we plot some examples of such a composite distribution in Fig. S.5.

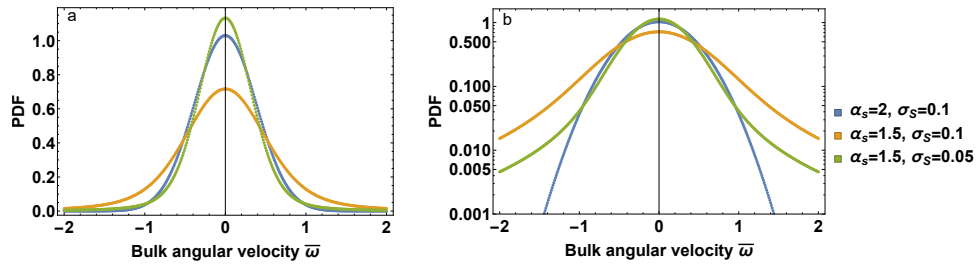


Figure S.5. The generalized Fokker-Planck equation also handles composite distributions. **a:** We depict the final PDF of a power grid with input noise consisting of a (0-mean) normal distribution $N(0, \sigma_N)$ and a (0-mean, 0-skewness) stable distribution $S(\alpha_S, 0, 0, \sigma_S)$. **b:** We repeat this with a log-scale of the PDF. We fix the standard deviation of the normal distribution at $\sigma_N = 0.1$ but test different values for stability parameter α_S and the scale parameter σ_S of the stable distribution. Especially in the Log-Plot we observe clearly the power-law tails of the composite distribution, noting that stable distributions are normal distributions for $\alpha_S = 2$.

SUPPLEMENTARY NOTE 3

Superstatistics

In the main text we introduced the idea of superstatistics as presented in [17–19] where the total distribution is seen as several aggregated Gaussian distributions with changing damping γ and noise amplitude ϵ . We present an illustration of the concept in Fig. S.6 where we combine two Gaussian distributions to form a distribution that is both skewed and heavy-tailed.

To extract the long time scale we need to determine the kurtosis given a certain interval length Δt : For heavy-tailed distributions this Δt is the time interval for which the averaged kurtosis of individual intervals of length Δt is equal to $\kappa = 3$. Similarly, for skewed distributions, such as the Great Britain grid, we determine the long time scale by looking for the longest interval such that the skewness averaged over all intervals equals 0, see Fig. S.7.

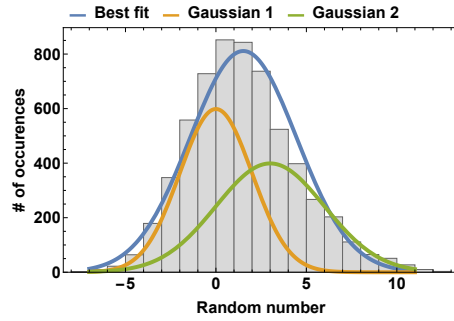


Figure S.6. Few Gaussian distributions give rise to skewed and/or heavy-tailed distributions. We display two Gaussian distributions (green and orange) from which we take 2000 samples each to form a histogram. This histogram is no longer well-described by another Gaussian distribution, as can be seen when comparing histogram and most likely Normal plot (blue). Instead the resulting data is skewed with skewness $\beta \approx 0.45$ and has a kurtosis of $\kappa \approx 3.26$, compared to $\kappa^{\text{Gaussian}} = 3$.

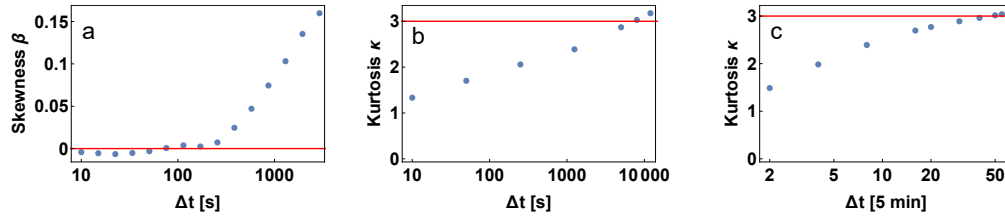


Figure S.7. We determine the long time scale T . **a**: For skewed distributions (Great Britain (GB), Eastern Interconnection (EI)) the long time scale is the time for which the averaged skewness has a minimum. **b-c**: For heavy-tailed distributions (Continental Europe (CE) and Japan 60Hz) the long time scale is the time for which the averaged kurtosis is approximately $\kappa(\Delta t = T) \approx 3$.

Computing effective friction As soon as we computed the long time scale T for a given data set, we extract the distribution of the effective friction γ_{eff} which is changing over time as

$$\gamma_{\text{eff}}(t_0) = \frac{1}{\langle x^2 \rangle_{t_0, T} - \langle x \rangle_{t_0, T}^2}, \quad (31)$$

where $\langle \dots \rangle_{t_0, \Delta t} = \int_{t_0}^{t_0 + \Delta t} \dots dt$. Following [17–19] we expect γ_{eff} to follow a log-normal or alternatively a χ^2 or inverse χ^2 distribution.

In the main text the Japanese data follows a log-normal distribution very well, while we observe larger deviations from the predicted log-normal distribution for the 50Hertz data set, see Fig. S.8.

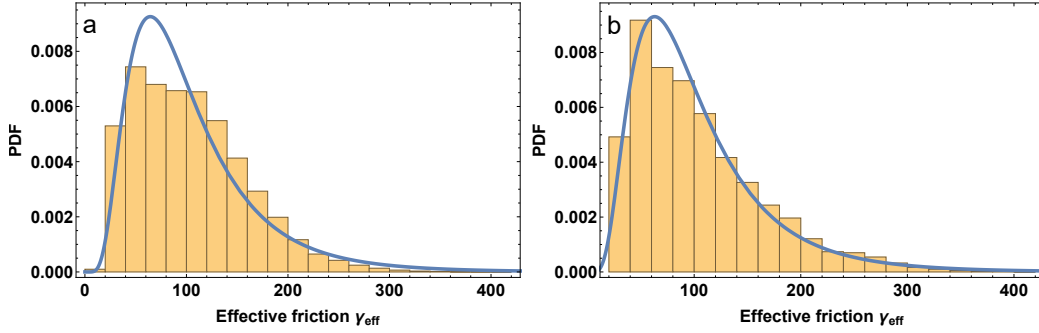


Figure S.8. The variance of Gaussian noise follows approximately a log-normal distribution. Plotted are the histograms of the effective friction γ_{eff} value based on the *50Hertz* 2015 trajectory compared to the best-fitting log-normal distribution. **a:** Full year of 2015. **b:** First million (of 30 mill.) data points only, i.e. approximately 10 days. We notice that the data using a shorter trajectory give the better fit to a log-normal distribution. Most likely this is due to several time scales entering the frequency trajectory. Correlations exist on the half an hour, hour, day, weeks and more time scales. Hence, modeling the varying noise with one long time scale is limited and using the full trajectory reveals this problem.

How to derive q-Gaussians Here we derive how a χ^2 distribution of the effective friction γ_{eff} leads to a q-Gaussian distribution of the frequency, following [17].

Consider the Langevin equation

$$\dot{x} = -\gamma x + \epsilon \xi, \quad (32)$$

with noise amplitude ϵ and damping γ . Now define the effective friction $\gamma_{\text{eff}} = \frac{\gamma}{\epsilon^2}$ and assume that it is following a χ^2 distribution:

$$p(\gamma_{\text{eff}}) = \frac{1}{\Gamma\left(\frac{n}{2}\right)} \left(\frac{n}{2\gamma_0}\right)^{n/2} \gamma_{\text{eff}}^{n/2-1} \exp\left(-\frac{n\gamma_{\text{eff}}}{2\gamma_0}\right), \quad (33)$$

with degree n , mean γ_0 and Gamma function Γ . Next, assume that the changes of γ_{eff} are much slower than the relaxation time scale defined by $1/\gamma$ during which the system settles down for one fixed γ_{eff} . Then, the conditional probability to find the system in state x at fixed γ_{eff} is

$$p(x|\gamma_{\text{eff}}) = \sqrt{\frac{\gamma_{\text{eff}}}{2\pi}} \exp\left(-\frac{1}{2}\gamma_{\text{eff}}x^2\right), \quad (34)$$

and the marginal probability distribution (probability to observe x independent of the value of γ_{eff}) is

$$p(x) := \int p(x|\gamma_{\text{eff}}) p(\gamma_{\text{eff}}) d\gamma_{\text{eff}} \quad (35)$$

$$= \frac{\Gamma\left(\frac{n}{2} + \frac{1}{2}\right)}{\Gamma\left(\frac{n}{2}\right)} \left(\frac{\gamma_0}{\pi n}\right)^{1/2} \frac{1}{\left(1 + \frac{\gamma_0}{n}x^2\right)^{n/2+1/2}}, \quad (36)$$

which is a q-Gaussian and can be re-written as

$$p(x) \sim \frac{1}{\left(1 + \frac{1}{2}\tilde{\gamma}(q-1)x^2\right)^{1/(q-1)}}, \quad (37)$$

with $q = 1 + 2/(n+1)$ and $\tilde{\gamma} = 2/(3-q)\gamma_0$.

Let us review the consequences for our data-driven approach. When we record a χ^2 distribution for the effective friction γ_{eff} , it strongly supports the q-Gaussian modeling of the bulk angular velocity $\bar{\omega}$.

However, we did not fit our distribution of γ_{eff} with a χ^2 distribution but used a log-normal distribution instead. Unfortunately, we cannot derive the q-Gaussian distribution analytically based on a log-normal distribution but we

can compare the predicted PDF or $p(\bar{\omega})$ when convoluting a log-normal distribution with the histogram and the estimated q-Gaussian. Figure S.9 displays this comparison for the 60Hz Japan data which works very well: The q-Gaussian based on the original data and the PDF based on the convolution of the log-normal distribution are close to identical, see also [19] for more discussion on the role of log-normal distributions in superstatistics.

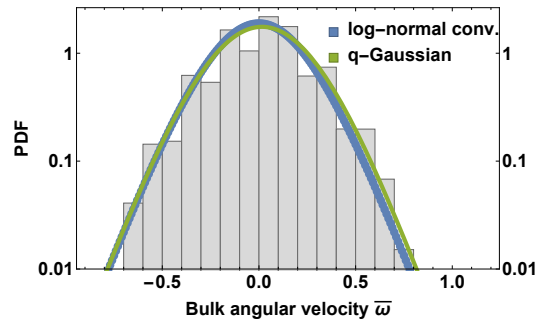


Figure S.9. The log-normal distribution of γ_{eff} predicts nearly the q-Gaussian estimate for the 60Hz Japanese grid. We plot the histogram data of the Japanese 60 Hz region, together with its q-Gaussian estimate. In addition, we compute the expected PDF given that the Gaussian distributions change based on a γ_{eff} following a log-normal distribution. All quantities match very well.

SUPPLEMENTARY NOTE 4

Monte-Carlo simulations

We validate our predicted probability density functions (PDF) based on the Fokker-Planck equation

$$p(\bar{\omega}) = \sqrt{\frac{\gamma M^2}{\pi \sum_{i=1}^N \epsilon_i^2}} \exp\left[-\bar{\omega}^2 \frac{\gamma M^2}{\sum_{i=1}^N \epsilon_i^2}\right] \quad (38)$$

and the generalized Fokker-Planck equation

$$p(x, t) = \mathcal{F}^{-1} \left[\exp\left(-\frac{1}{\gamma} \int_0^k \frac{1}{z} \ln\left(\frac{S_z \cdot e^{-\gamma t}}{S_z}\right) dz\right) \right], \quad (39)$$

by simulating the swing equations on realistic power grid networks which are subject to either Gaussian or stable noise. As topologies we chose the elementary two node system (one producer connected to one consumer), a 10 node, see Fig. S.10 and the Tokyo-Tohoku power grid topology, see Fig. S.11.

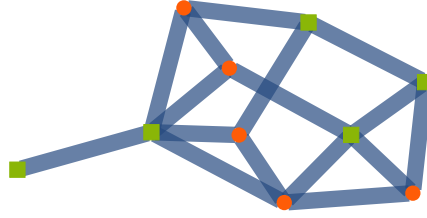


Figure S.10. We test the (generalized) Fokker-Planck predictions with simulations on a toy power grid. Here we show the 10 node system with producers (green) and consumers (red). We set $\gamma = 0.1$, $P^- = -1/s^2$ for consumers and $P^+ = 1/s^2$ for producers with homogeneous coupling of $K = 4/s^2$.

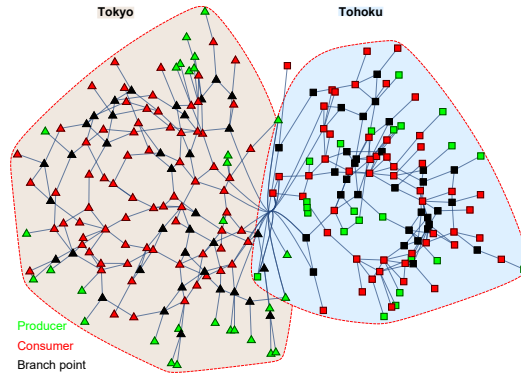


Figure S.11. We test the (generalized) Fokker-Planck predictions with simulations on a realistic power grid. Here we show the joined Tokyo (Triangle) and Tohoku (squares) grid with producers (green), branches (black) and consumers (red) [20]. We set $\gamma = 0.1$ and $P^- = -1/s^2$ for consumers and $P^+ \approx 2.38/s^2$ for producers, with admittance matrix and positions of producers/consumers in the grid given by [20]. For our simulations, we increase the coupling by a factor of $k = 15$.

Swing equation simulations Assuming symmetrical coupling $K_{ij} = K_{ji}$, balanced power $\sum_i P_i = 0$ and homogeneous damping to inertia ration γ we have the following equation of motion

$$\frac{d}{dt}\bar{\omega} = -\gamma\bar{\omega} + \bar{\epsilon}\xi, \quad (40)$$

with mean noise amplitude $\bar{\epsilon}$ and noise ξ . To solve this equation, we discretize time into intervals of length Δt and compute

$$\begin{aligned} \Delta\bar{\omega} &= -\gamma \cdot \bar{\omega}(t) \cdot \Delta t + X \cdot \sqrt{\Delta t}, \\ \bar{\omega}(t + \Delta t) &= \bar{\omega}(t) + \Delta\bar{\omega}, \\ t &= t + \Delta t, \end{aligned} \quad (41)$$

with X as our random variable drawn from a previously defined distribution (normal or stable).

Comparison of data and simulations In order to reproduce the data of the ENTSO-E Great Britain grid, we estimate the stability parameter of the measurements to be as $\alpha_{S,GB} \approx 1.97$, the scale parameter as $\sigma_{S,GB} = 0.2420$ and calculate the damping based on the autocorrelation to be $\gamma_{GB} = 0.00215/s$. We are able to reproduce both our estimate and the original data in the histograms, see Fig. S.12 and in the autocorrelation function, see Fig. S.13.

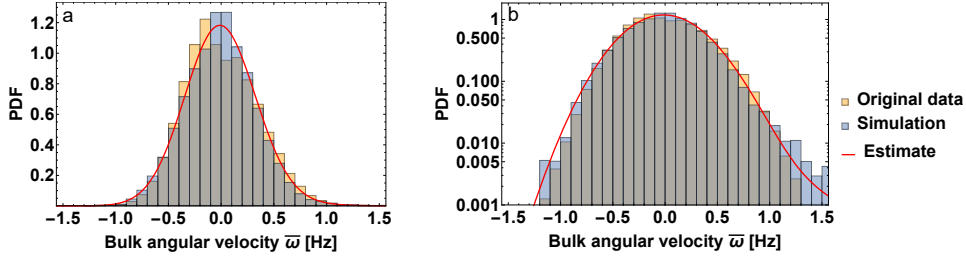


Figure S.12. Simulations reproduce the heavy-tailed ensembles. **a**: We compare the histograms of the original frequency measurements (transformed to angular velocity ω) with simulations and the estimated stable distribution (based on the original data) using the Great Britain 2015 data. **b**: We repeat the plot with a log-scale of the PDF.

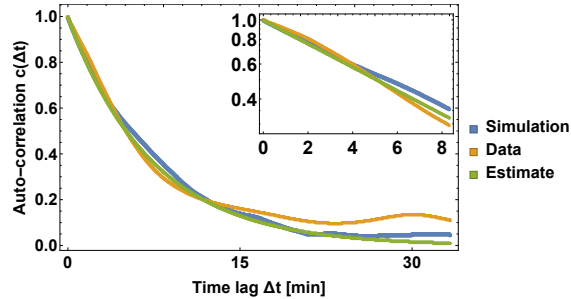


Figure S.13. Simulations reproduce the autocorrelation. We compare the autocorrelation function of the original frequency measurements (transformed to angular velocity ω) with simulations and the estimated exponential decay using the Great Britain 2015 data.

-
- [1] 50Hertz Transmission GmbH. Entso-e netzfrequenz, 2010-2016.
 - [2] Réseau de Transport d'Electricité (RTE). Network frequency, 2014-2016.
 - [3] National Grid. Frequency data, 2014-2016.
 - [4] EB Tehuisseu, D Gomila, D Brunner, and P Colet. Effects of dynamic-demand-control appliances on the power grid frequency. *arXiv preprint arXiv:1704.01638*, 2017.
 - [5] Fingrid. Nordic power system frequency measurement data, 2015-2016.
 - [6] Organization for Cross-regional Coordination of Transmission Operators, Japan (OCCTO). Japanese grid frequency, 2016.
 - [7] Power Information Technology Lab, University of Tennessee, Knoxville and Oak Ridge National Laboratory. FNET/GridEye, 09 2014. 1 day data set "20140905", contact powerit@utk.edu.
 - [8] U.S. Department of Energy. Eia-411: Coordinated bulk power supply and demand program report, 2016.
 - [9] ENTSO-E. Monthly production for a specific year for 2015, 2016.
 - [10] ENTSO-E. Statistical factsheet 2015, 2016.
 - [11] Gerhard Bohm and Günter Zech. *Introduction to statistics and data analysis for physicists*. DESY, 2010.
 - [12] Wolfram Research Inc. Mathematica. Champaign, Illinois, 2014.
 - [13] J. Machowski, J. Bialek, and J. Bumby. *Power System Dynamics: Stability and Control*. John Wiley & Sons, 2011.
 - [14] Math H Bollen and Irene Gu. *Signal processing of power quality disturbances*, volume 30. John Wiley & Sons, 2006.
 - [15] SI Denisov, Werner Horsthemke, and Peter Hänggi. Generalized fokker-planck equation: Derivation and exact solutions. *The European Physical Journal B*, 68(4):567–575, 2009.
 - [16] Matthias Fischer. Generalized hyperbolic distributions. In *International Encyclopedia of Statistical Science*, pages 589–590. Springer, 2011.
 - [17] Christian Beck. Dynamical foundations of nonextensive statistical mechanics. *Physical Review Letters*, 87(18):180601, 2001.
 - [18] Christian Beck and EGD Cohen. Superstatistics. *Physica A: Statistical mechanics and its applications*, 322:267–275, 2003.
 - [19] Christian Beck, Ezechieel GD Cohen, and Harry L Swinney. From time series to superstatistics. *Physical Review E*, 72(5):056133, 2005.
 - [20] Motoki Nagata, Naoya Fujiwara, Gouhei Tanaka, Hideyuki Suzuki, Eiichi Kohda, and Kazuyuki Aihara. Node-wise robustness against fluctuations of power consumption in power grids. *The European Physical Journal Special Topics*, 223(12):2549–2559, 2014.

Chapter 7

Dynamically Induced Cascading Failures in Supply Networks

Citation

Benjamin Schäfer, Dirk Witthaut, Marc Timme and Vito Latora (2017) Dynamically Induced Cascading Failures in Supply Networks

© 2017 Benjamin Schäfer, Dirk Witthaut, Marc Timme and Vito Latora

This chapter is the submitted version of the article: Benjamin Schäfer, Dirk Witthaut, Marc Timme and Vito Latora (2017) Dynamically Induced Cascading Failures in Supply Networks, which is currently under review at Nature Communications. It is also available as a pre-print on arXiv:<https://arxiv.org/abs/1707.08018> where a link to any final version will be provided.

Original Contribution

Conception of the research was done with V. Latora. I performed all calculations and simulations. I produced all numerical data and generated all figures. I set up the Supplemental Material, including all figures. I wrote large parts of all text sections in the main manuscript and the Supplemental Material, with support of all authors.

Dynamically Induced Cascading Failures in Supply Networks

Benjamin Schäfer,¹ Dirk Witthaut,^{2,3} Marc Timme,^{1,4,5} and Vito Latora^{6,7}

¹*Network Dynamics, Max Planck Institute for Dynamics and Self-Organization (MPIDS), 37077 Göttingen, Germany*

²*Forschungszentrum Jülich, Institute for Energy and Climate Research - Systems*

Analysis and Technology Evaluation (IEK-STE), 52428 Jülich, Germany

³*Institute for Theoretical Physics, University of Cologne, 50937 Köln, Germany*

⁴*Institute for Theoretical Physics, Technical University of Dresden, 01062 Dresden Germany*

⁵*Center for Advancing Electronics Dresden (cfaed),*

Technical University of Dresden, 01062 Dresden Germany

⁶*School of Mathematical Sciences, Queen Mary University of London, London E1 4NS, United Kingdom*

⁷*Dipartimento di Fisica ed Astronomia, Università di Catania and INFN, I-95123 Catania, Italy*

Reliable functioning of infrastructure networks is essential for our modern society. Cascading failures are the cause of most large-scale network outages. Although cascading failures often exhibit dynamical transients, the modeling of cascades has so far mainly focused on the analysis of sequences of steady states. In this article, we focus on electrical supply networks and introduce a framework that takes into consideration both the event-based nature of cascades and the details of the network dynamics. We find that transients in the flows of a supply network play a crucial role in the emergence of collective behavior. We show that such dynamically-induced cascades may systematically propagate across a network at a nearly constant propagation speed. This is illustrated using the topologies of the national power grids of Spain, France and Great Britain. We finally propose a forecasting method to identify critical lines and components in advance or during an exceptional situation. Overall, our work highlights the relevance of dynamically induced failures on the synchronization dynamics of national power grids of different European countries and it provides novel methods to predict and limit cascading failures.

Our daily lives heavily depend on the functioning of many natural and man-made networks, ranging from neuronal and gene regulatory networks over communication and transportation networks to electrical power grids [1, 2]. Understanding the robustness of these networks with respect to random failures and to targeted attacks is of utmost importance for preventing system outages with severe implications [3]. Recent examples, as the 2003 blackout in the Northeastern United States [4], the major European blackout in 2006 [5] or the Indian blackout in 2012 [6] have shown that initially local and small events can trigger large area outages of electric supply networks affecting millions of people, with severe economic and political consequences [7]. For this reason, cascading failures have been studied intensively in statistical physics, and different network topologies and non-local effects have been considered and analyzed [8–13]. Complementary studies have employed simplified topologies that admit analytical insights, for instance in terms of percolation theory [14] or minimum coupling [15]. Results have shown, for instance, the robustness of scale-free networks [3, 16, 17], or the vulnerability of multiplex networks [18–20].

Although real-world cascades often include dynamical transients of grid frequency and flow with very well defined spatio-temporal structures, so far models of cascading failures have mainly focused on event-triggered sequences of steady states [8, 10, 11, 21–24] or on purely dynamical descriptions of desynchronization without considering secondary failure of lines [25–29]. In particular, in supply networks such as electric power grids, which are considered as uniquely critical among all infra-

structures [30, 31], the failure of transmission lines during a blackout is determined not only by the network topology and by the static distribution of the electricity flow, but also by the collective transient dynamics of the entire system. Indeed, during the severe outages mentioned above, cascading failures over the electric power grids happened on time scales of dozens of minutes overall, but often started by the failure of a single element [32]. Conversely, sequences of individual line overloads took place on a much shorter time scale of seconds [4, 5], the time scale of systemic instabilities, emphasizing the role of transient dynamics in the emergence of collective behaviors. Notwithstanding the importance of the transients, the causes, triggers and propagation of cascades induced by transient dynamics has been considered only in a few works [9], and still needs to be systematically studied [33].

In this article, we propose a general framework to analyze the impact of transient dynamics on the outcome of cascading failures taking place over a complex network. Namely, we go beyond purely topological or event-based investigations and develop a dynamical model for supply networks that incorporates both the event-based nature of cascades and properties of network dynamics, including transients, which, as we will show, can significantly increase the vulnerability of a network [9]. These transients describe the dynamical response of system variables, such as grid frequency and power flow, when one steady state is lost and the grid changes to a new steady state. Combining microscopic nonlinear dynamics techniques with a macroscopic statistical analysis of the system, we will first show that, even when a supply net-

work seems to be robust because in the large majority of the cases the initial failure of its lines does only have local effects, there exist a few specific lines which can trigger large-scale cascades. We will then analyze the vulnerability of a supply network by looking at the dynamical properties of cascading failures. To identify the critical lines of the network we introduce and analytically derive a flow-based classifier that is shown to outperform measures solely relying on the network topology, local loads or network susceptibilities (line outage distribution factors). Finally, we demonstrate that cascades propagate through the network at a characteristic speed if distance is measured in an appropriate way, using effective distance measures [34].

The article is organized as follows. In Section I we describe a general framework that is commonly adopted to model the real-time dynamics of a power transmission network on coarse scales. In Section II A we discuss the importance of dynamical transients in the development of a cascade of subsequent failures induced by an initial shock to the system, and we introduce our model of cascading failures that properly takes these into account. We then show how the model works on a small synthetic network and when applied to some real case studies considering the real topology of the national power grids of various European countries. In particular, in Section II B we focus on the analysis of the statistical properties of the cascades, while in Section II C we introduce and discuss a method to identify the critical lines of a network, i.e. those lines inducing cascading failures. Finally, in Section II D we investigate the details of how a cascade propagates.

I. MODELING POWER GRIDS

When it comes to model the dynamics of a power transmission network, the *swing equation* is a simple way to deal with the key features of the system as a whole, namely its synchronization properties. Thereby, we avoid dealing directly with a complete dynamical description in terms of complicated power grid simulation software or static power-flow models which are routinely used to simulate specific scenarios on large-scale power grids by power engineers. The swing equation retains the dynamical features of AC power grids, by describing each of the elements of an electric power network as a rotating machine characterized by its angle and its angular velocity at a given time. In practice, a rotating machine either represents a large synchronous generator in a conventional power plant or a coherent subgroup, i.e., a group of strongly coupled small machines and loads which are tightly phase-locked in all cases. The angle of each machine is assumed to be identical to the angle of the complex voltage vector, so that the angle difference of two machines determines the power flow between them to transport, for example, energy from a producer to a consumer.

More formally, let us suppose to have N rotatory machines, each corresponding to a node of a network. Each machine i , with $i = 1, 2, \dots, N$ is characterized by its mechanical rotor angle $\theta_i(t)$ and by its angular velocity $\omega_i := d\theta_i/dt$ relative to the reference frame of $\Omega = 2\pi \cdot (50 \text{ or } 60)$ Hz. Furthermore, machine i either feeds power into the network, acting as an effective generator with power $P_i > 0$, or absorbs power, acting as an effective consumer (corresponding to the aggregate consumers of an urban areas) with power $P_i < 0$. The *swing equation* reads [28, 35, 36]:

$$\begin{aligned} \frac{d}{dt}\theta_i &= \omega_i \\ I_i \frac{d}{dt}\omega_i &= P_i - \gamma_i \omega_i + \sum_{j=1}^N K_{ij} \sin(\theta_j - \theta_i), \end{aligned} \quad (1)$$

where γ_i is the homogeneous damping of an oscillator, I_i is the inertia constant and K_{ij} is a coupling matrix governing the topology of the power grid network, and the strength of the interactions. In the following, we will both consider heterogeneous coupling K_{ij} or we will assume homogeneous coupling $K_{ij} = K a_{ij}$, where a_{ij} are the entries of the unweighted adjacency matrix that describes the connectivity of the network. For simplicity, we assume homogeneous damping $\gamma_i = \gamma$ and inertia $I_i = 1$ for all $i \in 1, \dots, N$. To derive Eq. (1) one has to assume that the voltage amplitude V_i at each nodes is time-independent, that ohmic losses are negligible and that the changes in the angular velocity are small compared to the reference $\omega_i \ll \Omega$, see e.g. [30, 35] for details. All these assumptions are fulfilled as long as we model short time scales on the high-voltage transmission grid [36] which will be sufficient for our study. The coupling matrix K_{ij} is an abbreviation for $K_{ij} = B_{ij} V_i V_j$ where B_{ij} is the susceptance between two nodes [30]. The swing equation is especially well suited to describe short time scales, as they appear in typical large-scale power grid cascades [4, 5, 7], however, we also discuss other models returning qualitatively similar results in Supplementary Note 3.

The desired stable state of operation of the power grid network is characterized by all machines running in synchrony at the reference angular velocity Ω , i.e., $\omega_i = 0 \forall i \in \{1, \dots, N\}$, implying $\sum_i P_i = 0$. Thereby, we determine the fixed point by solving for the angles θ_i^* in:

$$0 = P_i + \sum_{j=1}^N K_{ij} \sin(\theta_j^* - \theta_i^*). \quad (2)$$

The grid in its synchronous state is phase-locked, i.e., all angle differences do not change in time. This is important since the angle difference determines the flow along a line, and fluctuating angle differences would imply fluctuating conducted power which can in turn lead to the shutdown of a plant [30, 36]. Furthermore, transmission system operators demand the frequency to stay within

strict boundaries to ensure stability and constant phase locking [37].

Phase-locking and other synchronization phenomena arise in many different domains and applications, and have attracted the interest of physicists across fields [38]. One of the simplest synchronization models is the *Kuramoto model* which has been used, among other applications, to describe synchronization phenomena in fireflies, chemical reactions and simple neuronal models [39–42]. The swing equation shows similarities with the Kuramoto model, including the sinusoidal form of the coupling function and the existence of a minimal coupling threshold to achieve synchronization [27]. However, the swing equation includes a second derivative due to the inertial forces in the grid. Both equations share the same fixed points but the swing equations display dissipative forces and limit cycles that are not present in the Kuramoto model.

II. RESULTS

A. The dynamics of cascading failures

Failures are common in many interconnected systems, such as communication, transport and supply networks, which are fundamental ingredients of our modern societies. Usually, the *failure* of a single unit, or of a part of a network, is modeled by removing or deactivating a set of nodes or lines (or links) in the corresponding graph [43]. The most elementary damage to a network consists in the removal of a single line, since removing a node is equivalent to deactivate more than one line, namely all those line incident in the node. For this reason, in the following of this work, we concentrate on line failures. In practice, the malfunctioning of a line in a transportation/communication network can either be due to an exogenous or to an endogenous event [44, 45]. In the first case, the line breakdown is caused by something external to the network. Examples are the lightning strike of a transmission line of the electric power grid, or the sagging of a line in the heat of the summer. In the case of endogenous events, instead, a line can fail because of an overload due to an anomalous distributions of the flows over the network. Hence, the failure is an effect of the entire network.

Complex networks are also prone to *cascading failures*. In these events, the failure of a component triggers the successive failures of other parts of the network. In this way, an initial local shock produces a sequence of multiple failures in a domino mechanism which may finally affect a substantial part of the network. Cascading failures occur in transportation systems [46, 47], in computer networks [48], in financial systems [49], but also in supply networks [18]. When, for some either exogenous or endogenous reason, a line of a supply network fails, its load has to be somehow redistributed to the neighboring lines. Although these lines are in general able to handle

their extra traffic, in a few unfortunate cases they will also go overload and will need to redistribute their increased load to their neighbors. This mechanism can lead to a cascade of failures, with a large number of transmission lines affected and malfunctioning at the same time. One particular critical supply network is the electrical power grid displaying for example large-scale cascading failures during the blackout on 14 August 2003, affecting millions of people in North America, and the European blackout that occurred on 4 November 2006. In order

to model cascading failures in power transmission networks, we propose to use the framework of the swing equation in Eq. (1) to evaluate, at each time, the actual power flow along the transmission lines of the network and compare it to the actual available capacity of the lines. Typical studies of network robustness and cascading failures in power grids adopted quasi-static perspectives [8, 10, 11, 21–24, 50] based on fixed-point estimates of the variables describing the node states. Such approach, in the context of the swing equation, is equivalent to the evaluation of the angles $\{\theta_i\}$ as the fixed point solution of Eq. (1) or power flow analysis [30]. In contrast, we use here the swing equation to dynamically update the angles $\theta_i(t)$ as functions of time, and to compute real-time estimates of the flow on each line. The flow on the line (i, j) at time t is obtained as:

$$F_{ij}(t) = K_{ij} \sin(\theta_j(t) - \theta_i(t)). \quad (3)$$

Having the time evolution of the flow along the line (i, j) , we compare it to the capacity C_{ij} of the line, i.e., to the maximum flow that the line can tolerate. There are multiple options how we can define the capacity of a line in the framework of the swing equation. One possibility is the following. The dynamical model of Eq. (1) itself would allow a maximum flow equal to $F_{ij} = K_{ij}$ on the line (i, j) . However, in realistic settings, ohmic losses would induce overheating of the lines which has to be avoided. Hence, we assume that the capacity C_{ij} is set to be a tunable percentage of K_{ij} . In order to prevent damage and keep ground clearance [36, 51], the line (i, j) is then shut down if the flow on it exceeds the value αK_{ij} , where $\alpha \in [0, 1]$ is a control parameter of our model. The overload condition on the line (i, j) at time t finally reads:

$$\text{overload: } |F_{ij}(t)| > C_{ij} = \alpha K_{ij}, \quad (4)$$

Notice that the capacity $C_{ij} = \alpha K_{ij}$ is an absolute capacity, i.e., it is independent from the initial state of the system. This is different from the definition of a relative capacity, $\tilde{C}_{ij} := (1 + \alpha) F_{ij}(0)$, which has been commonly adopted in the literature [9, 21, 52].

Having defined the fixed point of the grid, given by the solution of Eq. (2), and the capacity of each line, we explore the robustness of the network with respect to line failures. We first consider the ideal scenario in which all the elements of the grid are working properly, i.e., all generators are running as scheduled and all the lines are

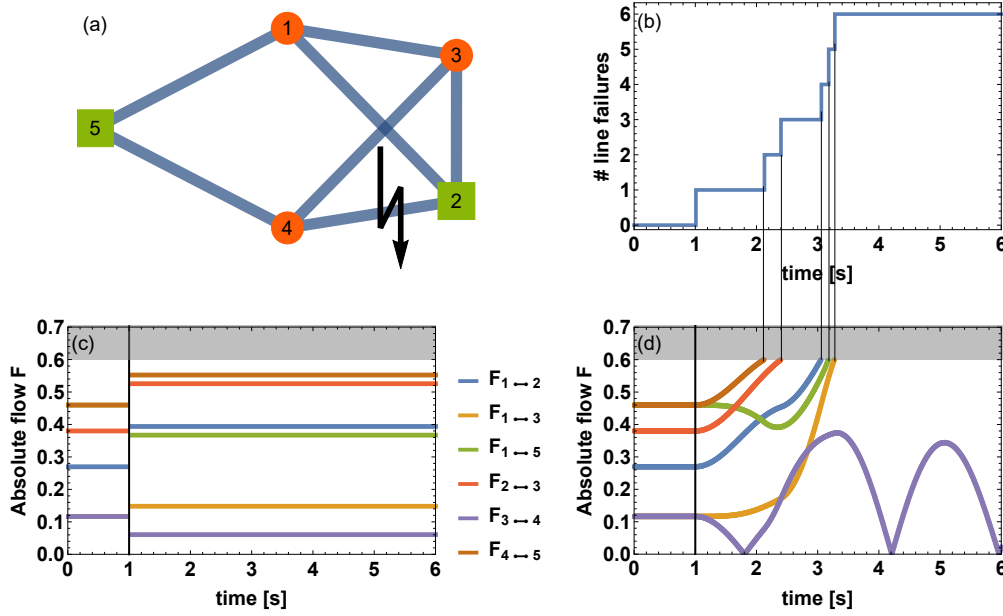


Figure 1. Dynamical overload reveals additional lines failures compared to static flow analysis. (a) A five node power network with two producers $P^+ = 1.5/s^2$ (green squares), three consumers $P^- = -1/s^2$ (red circles), homogeneous coupling $K \approx 1.63/s^2$, and tolerance $\alpha = 0.6$ is analyzed. To trigger a cascade, we remove the line marked with a lightning bolt (2,4) at time $t = 1$ s. (b) We observe a cascading failure with several additional line failures after the initial trigger due to the propagation of overloads. (c) The common quasi-static approach of analyzing fixed point flows would have predicted no additional line failures, since the new fixed point is stable with all flows below the capacity threshold. (d) Conversely, the transient dynamics from the initial to the new fixed point overloads additional lines which then fail when their flows exceed their capacity (gray area).

operational. We say that the grid is $N - 0$ stable [53] if the network has a stable fixed point and the flows on all lines are within the bounds of the security limits, i.e. do not violate the overload condition Eq. (4), where the flows are calculated by inserting the fixed point solution into Eq. (3). Next, we assume the initial failure of a single transmission line. We call the new network in which the corresponding line has been removed the $N - 1$ grid. Since the affected transmission line can be any of the $|E|$ lines of the network, we have $|E|$ different $N - 1$ grids. If the $N - 1$ grid still has a fixed point for all possible $|E|$ different initial failures, and all of these fixed points result in flows within the capacity limits, the grid is said to be $N - 1$ stable [30, 36, 51]. While traditional cascade approaches usually test $N - 0$ or $N - 1$ stability using mainly static flows, our proposal is to investigate cascades by means of dynamically updated flows according to the power grid dynamics of Eq. (3). This allows for a more realistic modeling of real-time overloads and line failures. In practice, this means to solve the swing equation dynamically, update flows and compare to the

capacity rule Eq. (4), removing lines whenever they exceed their capacity. Thereby, our $N - 1$ stability criterion demands not only the stable states to stay within the capacity limits but also includes the transient flows on all lines. See Supplementary Note 1 for details on our procedure and comparison of our framework to other methods.

In order to illustrate how our dynamical model for cascading failures works in practice, we first consider the case of the network with $N = 5$ nodes and $|E| = 7$ lines shown in Fig. 1. We assume that the network has two generators, the two nodes reported as green squares, characterized by a positive power $P^+ = 1.5/s^2$, and three consumers, reported as red circles, with power $P^- = -1/s^2$. For simplicity we have adopted here a modified “per unit system” obtained by replacing real machine parameters with dimensionless multiples with respect to reference values. For instance, here a “per unit” mechanical power $P_{\text{per unit}} = 1/s^2$ corresponds to the real value $P_{\text{real}} = 100\text{MW}$ [30, 36]. Moreover, we assume homogeneous line parameters throughout the grid, namely, we fix the coupling for each couple of nodes i

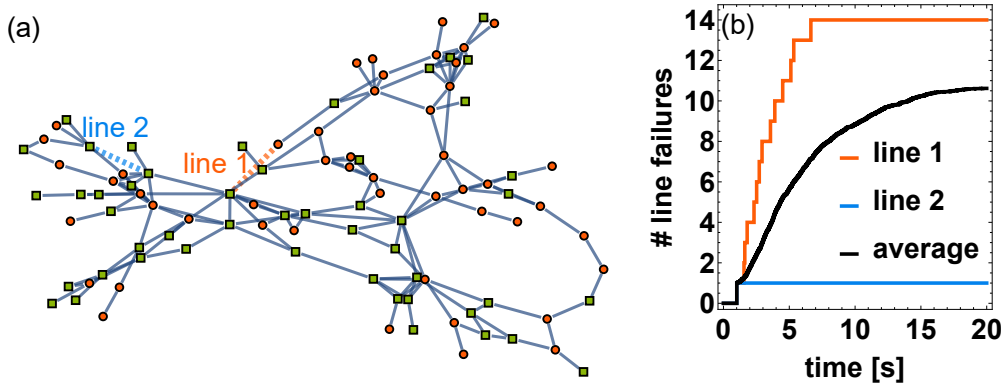


Figure 2. The effect of a cascade of failures strongly depends on the choice of the initially damaged line. (a) The network of the Spanish power grid with distributed producers with $P^+ = 1/s^2$ (green squares) and consumers with $P^- = -1/s^2$ (red circles), homogeneous coupling $K = 5/s^2$, and tolerance $\alpha = 0.52$ is analyzed. Two different trigger lines are selected. (b) The number of line failures as a function of time for the two different trigger lines highlighted in panel (a) and for an average over all the possible initial damages. Some lines do only cause a single line failure, while others affect a substantial amount of the network. On average most line failures do take place within the first ≈ 20 seconds of the cascade.

and j as $K_{ij} = Ka_{ij}$, with $K = 1.63/s^2$. In order to prepare the system in its stable state, we solve Eq. (2) and calculate the corresponding flows at equilibrium. We then fix a threshold value of $\alpha = 0.6$. With such a value of the threshold, none of the flows is in the overload condition of Eq. (4), and the grid is $N - 0$ stable. Next, we perturb the stable steady state of the grid with an initial exogenous perturbation. Namely, we assume that line (2, 4) fails at time $t = 1$, due to an external disturbance. By using again the static approach of Eq. (2) to calculate the new steady state of the system, it is found that all flows have changed but they still are all below the limit of 0.6, as shown in Fig. 1(c). Hence, with respect to a static analysis, the grid is $N - 1$ -stable to the failure of line (2, 4). Despite this, the capacity criterion in Eq. (4) can be violated transiently, and secondary outages emerge dynamically. As Fig. 1(d) shows, this is indeed what happens in the example considered. Approximately one second after the initial failure, the line (4, 5) is overloaded, which causes a secondary failure, leading to additional overloads on other lines and their failure in a cascading process that eventually leads to the disconnection of the entire grid. The whole dynamics of the cascade of failures induced by the initial removal of line (2, 4) is reported in Fig. 1(d).

Dynamical cascades are not limited to small networks as the one considered in this example, but also appear in large networks. In order to show this, we have implemented our model for cascading failures on a network based on the real structure of the Spanish high voltage transmission grid. The network is reported in Fig. 2 and has $N_{\text{Spanish}} = 98$ nodes and $|E|_{\text{Spanish}} = 175$ edges.

We select a set of distributed producers (green squares), each with a positive power $P^+ = 1/s^2$, and consumers (red circles), with negative power $P^- = -1/s^2$. As in the case of the previous example, we adopt a homogeneous coupling, namely we fix $K_{ij} = K \cdot a_{ij}$ with $K = 5/s^2$ for each couple of nodes i and j . We also fix a tolerance value $\alpha = 0.52$, such that none of the flows is in the overload condition of Eq. (4), and the grid is initially $N - 0$ stable. We notice from the effects of cascading failures shown in Fig. 2 that the choice of the trigger line significantly influences the total number of lines damaged during a cascade. For instance, the initial damage of line 1 (dashed red line) causes a large cascade of failures with 14 lines damaged in the first seven seconds, while the initial damage of line 2 (dashed blue line) does not cause any further line failure, as the initial shock is in this case perfectly absorbed by the network. Figure 2 also displays the average number of failing lines as a function of time. Here, we average over all lines of the network considered as initially damaged lines. We notice that the cascading process is relatively fast, with all the failures taking place within the first $T_{\text{Cascade}} = 20$ s. This further supports the adoption of the swing equation, which is indeed mainly used to describe short time scales, while more complex and less tractable models are required to model longer times [36].

B. Statistics of Dynamical Cascades

To better characterize the potential effects of cascading failures in electric power grids, we have studied the

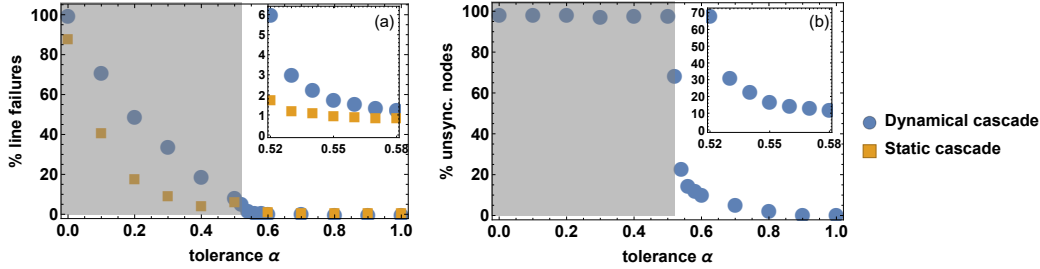


Figure 3. Effects of cascading failures in the Spanish power grid under different levels of tolerance. (a) The percentage of line failures in our model of cascading failures (circles), under different values of tolerance α is compared to the results of a static fixed point flow analysis (squares). The static analysis largely underestimates the actual number of line failures in a dynamical approach. The difference between static and dynamical analysis is especially clear in the inset where we focus on the lowest values of α at which the network is $N-0$ stable. The gray area is $N-0$ unstable, i.e., the network without any external damage already has overloaded lines. (b) Percentage of unsynchronized (damaged) nodes after the cascade as a function of the tolerance α . All analysis has been performed under the same distribution of producers and consumers as in Fig. 2, with homogeneous coupling of $K = 5s^{-2}$.

statistical properties of cascades on the topology of real-world power transmission grids, such as those of Spain and France [54]. In particular, we have considered the two systems under different values of the tolerance parameter α [21], and for various distributions of producers and consumers on the network. As in the examples of the previous section, we have also analyzed all the possible initial damages triggering the cascade. To assess the consequences of a cascade, we have focused on the following two quantities. First, we analyze the number of lines that suffered an overload, and are thus shut down during the cascading failure process. This number is a measure of the total damage suffered by the system in terms of loss of its connectivity. Second, we record the fraction of nodes that have experienced a desynchronization during the cascade, which represents a proxy for the number of consumers affected by a blackout (see Supplementary Note 1 for details on the implementation). In both the cases of affected lines and affected nodes, the numbers we look at are those obtained at the end of the cascading failure process.

Fig. 3 shows the results obtained for the case of the network of the Spanish power transmission grid. The same homogeneous coupling and distribution of producers and consumers is adopted as in Fig. 2. We have considered each of the lines as a possible initial trigger of the cascade, and averaged the final number of line failures and unsynchronized nodes over all realizations of the dynamical process. We have repeated this for multiple values of the tolerance coefficient α . As expected, a larger tolerance results in fewer line failures and fewer unsynchronized nodes, because it makes the overload condition of Eq. (4) more difficult to be satisfied. As we decrease the network tolerance α , the total number of affected lines and unsynchronized nodes after the cascade suddenly

increases at a value $\alpha \approx 0.5$, where we start to observe a propagation of the cascade induced by the initial external damage. Crucially, a dynamical approach, as the one considered in our model, identifies a significantly larger number of line failures (circles) compared to a static approach (squares). This is clearly visible in the inset of the left hand side of Fig. 3, where we zoom to the lowest values of α at which the network is $N-0$ stable. For instance, at $\alpha = 0.52$ our model predicts that an average of six lines of the Spanish power grid are affected by the initial damage of a line of the network through a propagation of failures. Such a vulnerability of the network is completely unnoticeable by a static approach to cascading failures based on the analysis of fixed points. The static approach reveals in fact that on average only another line of the network will be affected. We also note that the increase in the number of unsynchronized nodes for decreasing values of α is much sharper than that for overloaded lines. Below a value of $\alpha \approx 0.5$ the number of unsynchronized nodes jumps to 100%. This transition indicates a loss of the $N-0$ stability of the system, meaning that, already in the unperturbed state several lines are overloaded according to the capacity criterion in Eq. (4) and thus fail. To study only genuine effects of cascades, in the following we restrict ourselves to the case $\alpha > 0.5$, where the grid is $N-0$ stable, but not necessarily $N-1$ stable. Furthermore, to assess the final impact of a cascade on a network, we mainly focus on total number of affected lines [4, 5]. As discussed in Section II A, damages to lines are indeed the most elementary type of network damages.

Furthermore, we have explored the role of centralized versus distributed power production, and that of heterogeneous couplings K_{ij} , and also extended our analysis to other network topologies of European national power

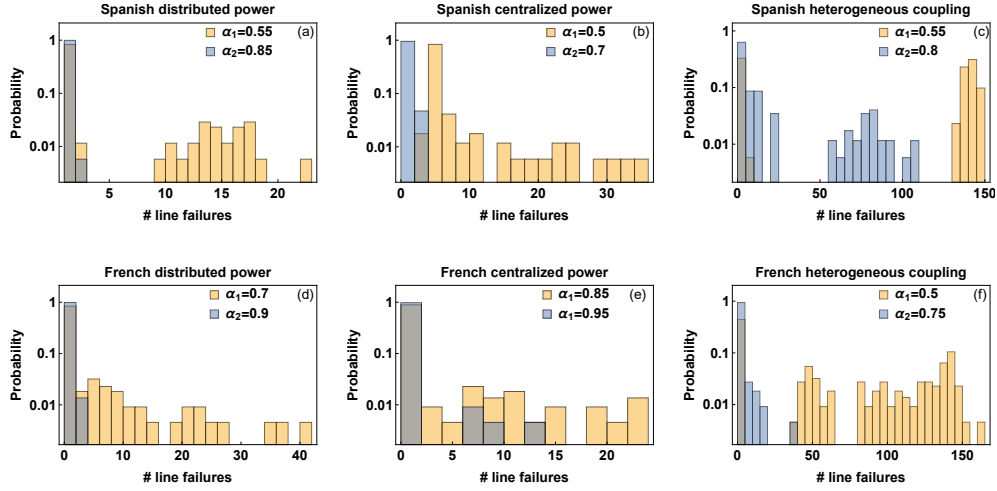


Figure 4. Network damage distributions in the Spanish and French power grids under different power allocations and types of coupling. The histograms shown have been obtained under three different settings. Panels (a) and (d) refer to the case of *distributed power*, i.e., equal number of producers and consumers, each with $P^- = -1/s^2$ and $P^+ = 1/s^2$, and homogeneous coupling with $K = 5/s^2$ for the Spanish and $K = 8/s^2$ for the French grid. Panels (b) and (e) refer to the case of *centralized power*, i.e., consumers with $P^- = -1/s^2$ and fewer but larger producers with $P^+ \approx 6/s^2$, and homogeneous coupling with $K = 10/s^2$ for Spanish and $K = 9/s^2$ for the French grid. Panels (c) and (f) refer to a case of distributed power as in panel (a) and (d), but with *heterogeneous coupling*, so that the fixed point flows on the lines are approximately $F \approx 0.5K$ both for the Spanish and the French grid. For all plots we use two different tolerances α , where the lower one is the smallest simulated value of α so that there are no initially overloaded lines ($N = 0$ stable).

grids, namely those of France and of Great Britain, see Supplementary Note 2. In Fig. 4 we compare the results obtained for the Spanish network topology (three top panels) to those obtained for the French network (three bottom panels). With $N_{\text{French}} = 146$ nodes and $|E|_{\text{French}} = 223$ edges the French power grid is larger in size than the Spanish one considered in the previous figures ($N_{\text{Spanish}} = 98$ and $|E|_{\text{Spanish}} = 175$) and has a smaller clustering coefficient. In each case, we have calculated the total number of line failures at the end of the cascading failure when any possible line of the network is used as the initial trigger of the cascade. We then plot the probability of having a certain number of line failures in the process, so that the histogram reported indicates the size of the largest cascades and how often they occur. Notice that the probability axis uses a log-scale. For each network we have considered both distributed and centralized locations of power producers, and both homogeneous and heterogeneous network couplings. The centralized production is thereby a good approximation to the classical power grid design with few large fossil and nuclear power plants powering the whole grid. In contrast, the distributed production scheme describes well the case in which many small (wind, solar, biofuel, etc.) generators are distributed across the grid [25]. Finally, the choice of heterogeneous coupling is motivated by economic considerations, since maintaining a

transmission network costs money and only those lines that actually carry flow are used in practice. In particular, we have worked under the following three different types of settings:

1. *Distributed power and homogeneous couplings* Equal number of producers and consumers in the network, each of them having respectively $P^+ = 1/s^2$ and $P^- = -1/s^2$. Homogeneous coupling with $K_{ij} = Ka_{ij}$ and $K = 5/s^2$ for the Spanish (as in case of the previous figures) and $K = 8/s^2$ for the French grid. Results shown in panels (a) and (d);
2. *Centralized power and homogeneous couplings* Consumers with $P^- = -1/s^2$ and fewer but larger producers with $P^+ \approx 6/s^2$. Homogeneous coupling with $K = 10/s^2$ for the Spanish and $K = 9/s^2$ for the French grid. Results shown in panels (b) and (e);
3. *Distributed power and heterogeneous coupling* Homogeneous distribution of producers and consumers as in case 1. Heterogeneous distribution of the K_{ij} , so that the fixed point flows on the lines are approximately $F \approx 0.5K$ both for the Spanish and the French grid (see Supplementary Note 1 for details). Results shown in panels (c) and (f).

In each of the above cases, we work in conditions such that no line is overloaded before the initial exogenous damage. We have performed simulations for two values of the tolerance parameter α . For each of the two grids and of the three conditions above, the lowest value $\alpha = \alpha_1$ has been selected to be equal to the minimal tolerance such that each the network is $N - 0$ stable (yellow histograms). In addition, we have considered a second, larger value of the tolerance, α_2 , showing qualitatively different behaviors (blue histograms). As found in other studies [25–27, 29], the (homogeneous) coupling K has to be larger for centralized production compared to distributed small producers to achieve comparable stability.

The first thing to notice from the histograms in Fig. 4(a) is that in most of the cases the initial failure of a line does not cause any cascade at all, or very small ones. This means that the Spanish grid is in most of the cases $N - 1$ stable even in our dynamical model of cascades. Nevertheless, for α_1 , there exist a few lines that, when damaged, trigger a substantial part of the network to be disconnected. This leads to the question whether and how the distribution of producers or the topology of the network impact the size and frequency of the cascade. When comparing distributed (many small producers) in panel (a) to centralized power production (few large producers) in panel (b) we do not observe a significant difference in the statistics of the cascades. The same holds when comparing different network topologies, such as the Spanish and the French grid in panels (d) and (e).

Conversely, allowing heterogeneous couplings introduces notable differences to emerge in panels (c) and (f). To obtain heterogeneous couplings, we have scaled K_{ij} at each line proportional to the flow at the stable operational state (see Supplementary Note 1). Thereby, we try to emulate cost-efficient grid planning which only includes lines when they are used. However, our results show that, under these conditions, the flow on a line with large coupling cannot easily be re-routed in our heterogeneous network when it fails [29]. For certain initially damaged lines, this leads to very large cascades in grids with heterogeneous coupling K_{ij} . For instance, both the Spanish and the French power grid show a peak of probability corresponding to cascades of about 150 line failures when $\alpha = \alpha_1$. But also in the case of $\alpha_2 = 0.8$, which corresponds to a $N - 1$ stable situation under the homogeneous coupling condition, the Spanish grid exhibits cascades involving from 50 to 100 lines in 5% of the cases under heterogeneous couplings, see panel (c). The final number of unsynchronized nodes after the cascade, used as a measure of the network damage follows qualitatively a similar statistics as shown in Fig. 4. Namely, distributed and centralized power productions return similar statistical distributions of damage, while under heterogeneous couplings the system behaves differently. Furthermore, for each network, we have recorded the two extreme situations in which either all nodes or the grid stay synchronized, or the whole grid desynchronizes (see Sup-

plementary Note 2).

The results obtained in this section have important indications for the stability of a power grid. We have shown that a network which is initially stable ($N - 0$ stability), and remains stable even to the initial damage of a line ($N - 1$ stability) according to the standard static analysis of cascades, can display large-scale dynamical cascades when properly modeled. Although these dynamical overload events often have a very low probability, their occurrence cannot be neglected since they may collapse the entire power transmission network with catastrophic consequences. In the examples studied, we have found that some critical lines cause cascades resulting in a loss of up to 85% of the edges (Fig. 4(c)). Hence, it is extremely important to develop methods to identify such critical lines, which is the subject of the next section.

C. Identifying critical lines

The statistical analysis presented in the previous section revealed that the size of the cascades triggered by different line failures is very heterogeneous. Most lines of the networks investigated are not critical, i.e., they are either $N - 1$ stable even in our dynamical model of cascades, or cause only a very small number of secondary outages. However, for heavily loaded grids, as reported in Fig. 4, some highly critical lines emerge. Thereby, the initial failure of a single transmission line causes a global cascade with the desynchronization of the majority of nodes, leading to large blackouts. The key question here is whether it is possible to devise a fast method to identify the critical lines of a network. This might prove to be very useful when it comes to improving the robustness of the network. In this section, we introduce a novel flow-based indicator for the onset of a cascade and demonstrate the effectiveness of its predictions by comparing them to results of the numerical simulation. In particular, we show that our indicator is able to identify the critical links of the network much better than other measures purely based on the topology or steady state of the network, such as the edge betweenness [12, 21, 22].

In order to define a flow-based predictor for the onset of a cascading failure, let us consider the typical time evolution of the flow along a line after the initial removal of the first damaged line (a, b). As illustrated in Fig. 5, we observe flow oscillations after the initial line failure, which are well approximated by a damped sinusoidal function of time. See also Supplementary Note 4 for the time evolutions of the flows for the case of the $N = 5$ node graph introduced in Fig. 1. Now, the steady flows of the network before and after the removal of the trigger line are obtained by solving Eq. (2) for the fixed point angles $\{\theta_i^*\}$, which depend on the node powers $\{P_i\}$ and on the coupling matrix $\{K_{ij}\}$. Thereby, we obtain a set of nonlinear algebraic equations which have at least one solution if the coupling K is larger than the critical cou-

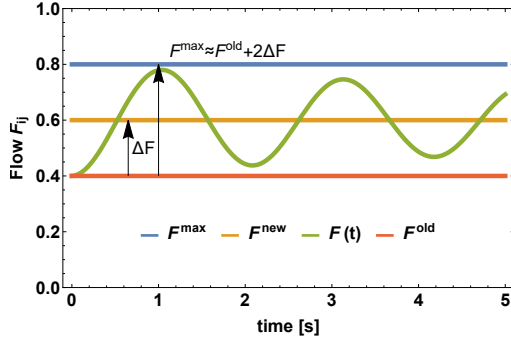


Figure 5. Introducing a flow-based estimator of the onset of a cascade. When cutting an initial line, the flows on a typical edge (i, j) of the network increase from F^{old} (red line) to F^{new} (orange line). Based on numerical observations, the transient flow $F(t)$ from the old to the new fixed point are well approximated as sinusoidal damped oscillation. Knowing the fixed point flows, allows to compute the difference $\Delta F = F^{\text{new}} - F^{\text{old}}$ and estimate the maximum transient flow as $F^{\text{max}} \approx F^{\text{old}} + 2\Delta F$. This estimation is typically slightly larger than the real flow because the latter is damped.

pling [27]. For sufficiently large values of the coupling K there can be multiple fixed points [55]. In each case, we determine a single fixed point with small initial flows by using Newton's method (see Supplementary Note 1 for details). From the values of the fixed point angles $\{\theta^*\}$ we calculate the equilibrium flow along each line, for instance line (i, j) , before and after the removal of the trigger line, from the expression:

$$F_{ij}^* = K \sin(\theta_j^* - \theta_i^*). \quad (5)$$

Let us indicate the initial flow along line (i, j) in the intact network as F_{ij}^{old} , and the new flow after the removal of the trigger line as F_{ij}^{new} , assuming there still is a fixed point. Given enough time, the system settles in the new fixed point and the change of flow on the line is $\Delta F_{ij} = F_{ij}^{\text{new}} - F_{ij}^{\text{old}}$. Based on the oscillatory behavior observed in cascading events, see Fig. 5 for an illustration, we approximate the time-dependent flow on the line close to the new fixed point as:

$$F_{ij}(t) \approx F_{ij}^{\text{new}} - \Delta F_{ij} \cos(\nu_{ij}t) e^{-Dt}, \quad (6)$$

where ν_{ij} is the oscillation frequency specific to the link (i, j) and D is a damping factor. The maximum flow F_{ij}^{max} on the line during the transient phase is then given by:

$$F_{ij}^{\text{max}} \approx F_{ij}^{\text{old}} + 2\Delta F_{ij}. \quad (7)$$

Hence, for our cascade predictor we propose to test whether a line will be overloaded during the transient by computing F_{ij}^{max} from the expression above and by checking whether F_{ij}^{max} is larger than the available capacity C_{ij} of the link. While this provides a good approximation

of the real flows, we need to compute the fixed point of the intact network and that after the initial trigger line is removed. This has to be repeated for each possible initial trigger line, so that we need to compute $|E| + 1$ fixed points, with $|E|$ being the number of edges. A possible way to simplify this procedure is to compute the fixed point flows of the intact grid F_{ij}^{old} only, approximating the fixed point flows after changes of the network topology by the Line Outage Distribution Factor (LODF) [56, 57]. Details on this method can be found in Supplementary Note 1.

After starting the cascade by removing line (a, b) , we define our analytical prediction for the minimal transient tolerance $(\alpha_{ij}^{\text{tr.}(a,b)})_{\min}$ based on the maximum transient flow on line (i, j) given in Eq. (7):

$$(\alpha_{ij}^{\text{tr.}(a,b)})_{\min} = F_{ij}^{\text{max}} \quad (8)$$

such that, if $\alpha > (\alpha_{ij}^{\text{tr.}(a,b)})_{\min}$, then cutting line (a, b) as a trigger will not affect line (i, j) . Finally, we define the minimal tolerance $(\alpha^{\text{tr.}(a,b)})_{\min}$ of the network as that value of α such that there is no secondary failure after the initial failure of the trigger line, i.e., the grid is $N - 1$ secure. We have:

$$(\alpha^{\text{tr.}(a,b)})_{\min} = \max_{(i,j)} (\alpha_{ij}^{\text{tr.}(a,b)})_{\min} = \max_{(i,j)} (F_{ij}^{\text{max}}), \quad (9)$$

where the maximum is taken with respect to all links (i, j) in the network and one trigger link (a, b) . If we set $\alpha \geq (\alpha^{\text{tr.}(a,b)})_{\min}$ then, according to our prediction method, we expect no additional line failures further to the initial damaged line. Let us assume that the network topology is given, for instance that of a real national power grid, and that the tolerance level is preset due to external constraints like security regulations. Then, the calculation of $(\alpha^{\text{tr.}(a,b)})_{\min}$ allows to engineer a resilient grid by trying out different realizations of K_{ij} . When changes of K_{ij} are small, the new fixed point flows are approximated by linear response of the old flows [56] giving us an easy way to design the power grid to fulfill safety requirements.

To measure the quality of our predictor for critical lines and to compare it to alternative predictors, we quantify its performance by evaluating how often it detects critical lines as critical (true positives) with respect to how often it gives false alarms (false positives). In our model for cascading failures, a potential trigger line is classified as truly critical if its removal causes additional secondary failures in the network according to the numerical simulations of the dynamics [29]. Our flow-based prediction is obtained by first calculating the minimal tolerance of the network $(\alpha^{\text{tr.}(a,b)})_{\min}$ based on Eq. (9) and comparing it with the fixed tolerance α of a given simulation. If the obtained minimal tolerance is larger than the value of tolerance used in the numerical simulation, than the

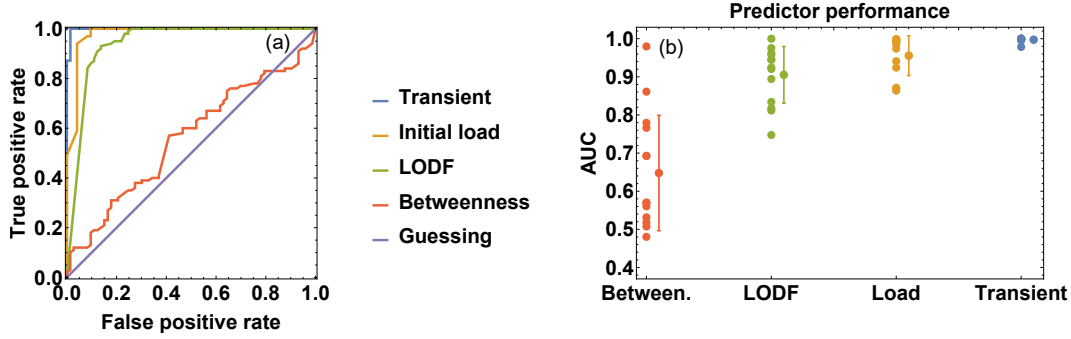


Figure 6. Comparing the predictions of our flow-based indicator of critical lines to other standard measures. Four different predictors are presented to determine whether a given line, if chosen as initially damaged, causes at least one additional line failures. Our dynamical predictor (indicated as Transient) is based on the estimated maximum transient flow (7). The predictor based on the Line Outage Distribution Factor (LODF) [56, 57] uses the same idea but computes the new fixed flows based on a linearization of the flow computation. Predictors based on betweenness and initial load classify a line as critical if it is within the top $\sigma^{th} \times 100\%$ of the edges with highest betweenness/load with threshold $\sigma^{th} \in [0, 1]$. Panel (a) shows the ROC curves obtained for the Spanish grid with heterogeneous coupling and tolerance $\alpha = 0.7$, while in panel (b) the AUC is displayed for all network settings presented in Fig. 4. For each predictor all individual scores are displayed on the left and the mean with error bars based on one standard deviation is shown on the right.

line is classified as critical by our predictor and additional overloads are to be expected. More formally, we use the following prediction rules:

$$\begin{aligned} \left(\alpha^{tr. (a,b)}\right)_{\min} &\geq \alpha + \sigma^{th} \Rightarrow \text{critical}, \\ \left(\alpha^{tr. (a,b)}\right)_{\min} &< \alpha + \sigma^{th} \Rightarrow \text{not critical}. \end{aligned} \quad (10)$$

with a variable threshold $\sigma^{th} \in [-1, 1]$, which allows to tune the sensitivity of the predictor.

Analogously, we define a second predictor based on the Line Outage Distribution Factor (LODF) [56, 57]. In this case, the expected minimal tolerance is obtained by approximating the new flow by the LODF, instead of computing them by solving for the new fixed points (see Supplementary Note 1).

We compare our predictors based on the flow dynamics to the pure topological (or steady-state based) measures that have been used in the classical analysis of cascades on networks. The idea behind such measures is the following. First, we consider the initial load on all potential trigger lines (a, b) : $L^{(a,b)} = F_{ab}(t=0)$, i.e., the flow at time $t = 0$ on the line, when the system is in its steady state. Intuitively, highly loaded lines are expected to be more critical than less loaded ones. Hence, comparing each load $L^{(a,b)}$ to the maximum load on any line in the grid $L_{\max} := \max_{(i,j)} L^{(i,j)}$ leads to the following prediction:

$$\begin{aligned} L^{(a,b)} &\geq (1 - \sigma^{th}) L_{\max} \Rightarrow \text{critical}, \\ L^{(a,b)} &< (1 - \sigma^{th}) L_{\max} \Rightarrow \text{not critical}, \end{aligned} \quad (11)$$

where $\sigma^{th} \in [0, 1]$ is the prediction threshold.

Another quantity that is often used as a measure of the importance of a network edge is the edge betweenness [1, 2]. The betweenness $b^{(a,b)}$ of edge (a, b) is defined as the normalized number of shortest paths passing by the edge. A predictor based on the edge betweenness $b^{(a,b)}$ is then obtained by replacing $L^{(a,b)}$ by $b^{(a,b)}$ in the expressions above.

To evaluate the predictive power of our flow-based cascade predictors and to compare them to the standard topological predictors, we have computed the number of lines that cause a cascade by simulation and compared how often each predictor correctly predicted the cascade thereby deriving the rate of correct cascade predictions (true positive rate) and rate of false alarms (false positive rate). These two quantities are displayed in a Receiver Operator Characteristics (ROC) curve, which reports the true positive rate versus the false positive rate when varying the threshold σ^{th} . The ROC curve would go up straight from point $(0, 0)$ to point $(0, 1)$ in the ideal case in which the predictor is able to detect all real cascade events, while never giving a false positive. Conversely, random guessing corresponds to the bisector. Finally, any realistic predictor starts at the point $(0, 0)$, i.e. never giving an alarm regardless of the setting, and evolves to the point $(1, 1)$, i.e. always giving an alarm. The transition from $(0, 0)$ to $(1, 1)$ is tuned by decreasing the threshold σ^{th} determining when to give an alarm. The ROC curves corresponding to the predictors introduced above are shown in Fig. 6 (a). Notice that a prediction based on the betweenness of the line is only as good as

a random guess. In contrast, using the LODF and the initial load provide much better predictions. Finally, the analytical prediction outperforms any other method, well approximating an ideal predictor.

An alternative way to quantify the quality of a predictor is by evaluating the Area Under Curve (AUC), that is the size of the area under the ROC curve. An ideal predictor would correspond to the maximum possible value $AUC = 1$, while a random guess produces an AUC of 0.5. So the closer the value of AUC for a given predictor is to 1, the better are the obtained predictions. AUC scores have been computed for different networks, settings and parameters. The results for the dynamical flow-based predictor, the predictor based on the LODF, as well as the initial load and betweenness predictors, are shown in Fig. 6(b). The values of the AUC scores reported correspond to all the different settings described in Fig. 4, allowing a more systematic comparison of predictors than that provided by a single ROC curve. Also from this figure it is clear that a prediction of the critical links based on their betweenness is on average only slightly better than random guessing. Furthermore, this result rises concerns on the indiscriminate use of the betweenness as a measure of centrality in complex networks. Especially when the dynamical processes of interest are well known, this must be taken into account in the definition of dynamical centrality measures for complex networks [12, 58, 59]. The LODF and initial load predictors perform relatively better on average, although they still display large standard deviations. This means that, for certain networks and settings they reach an AUC score close to the perfect value of 1, while in some other cases they only reach values of AUC equal to 0.8. Of these two indicators, the initial load predictor results are more reliable. Finally, our dynamical predictor, indicated in figure as “Transient” outperforms all alternative ones, in every single parameter and network realization. The figure indicates that the corresponding AUC scores reach values very close to 1. Moreover, this indicator displays the smallest standard deviation when different networks and parameter settings are considered. In conclusion, this seems to be the best indicator for the criticality of a link. However, the results show that, although the initial load predictor performs worse than our dynamical one, it might still be used when computational resources are scarce as it provides the second best predictions among those considered.

D. Cascade propagation

What we have shown so far is that network cascades, i.e., secondary failures following an initial trigger, can well be caused by transient dynamical effects. We have proposed a model of supply networks that takes this into account, and we have also developed a reliable method to predict whether additional lines can be affected by an initial damage, potentially triggering a cascade of failu-

res. However, knowing whether a cascade develops or not does not answer another important question that is to understand how the cascade evolves over the network, and which nodes and links are affected and when. Intuitively, we expect that network components farther away from the initial failure should be affected later by the cascade. However, we have found that the graph distance between a secondary failure and the initial shock is not a strictly linear function of the arrival time of the cascade (see Supplementary Note 5). A much better correlation between distance from the initial shock and arrival time of the failure is obtained by making use of an *effective distance*, based on the characteristic of the flow from one node to its neighbors. This idea has been first introduced in Ref. [34] in the context of disease spreading, where the effective distance has been shown to be able to capture spreading phenomena better than the standard graph distance. The effective distance between two vertices i and j can be defined in our case as:

$$d_{ij} = 1 - \log \left(\frac{K_{ij}}{\sum_{k=1}^N K_{ik}} \right). \quad (12)$$

Here, we used the coupling matrix K_{ij} as a measure of the flows between nodes [34]. Notice that all couples of nodes not sharing an edge, i.e. such that $K_{ij} = 0$, have infinite effective distance $d_{ij} = \infty$. At each node the cascade spreads to all neighbors but those that are coupled tightly, get affected the most and hence get assigned the smallest distance d_{ij} . Furthermore, the effective distance is an asymmetric measure, since $d_{ij} \neq d_{ji}$ in general. The quantity d_{ij} is a property of two nodes, while the most elementary damage in our cascade model affects edges. Hence, the concept of distance has to be extended from couples of nodes to couples of links. For instance, in the case of an unweighted network it is possible to define the (standard) distance between two edges as the number of hops along a shortest path connecting the two edges. In the case of a weighted graph we make use of the measure of effective distance in Eq. (12) to define a distance between two edges as the minimal path length of all weighted shortest paths between two edges. The distance between two edges can then be obtained based on the definition of distances between nodes $\{d_{ij}\}$. Given the trigger edge (a, b) , the distance from edge (a, b) to edge (i, j) is given by:

$$d_{(a,b) \rightarrow (i,j)} = d_{ab} + \min_{v_1 \in \{a,b\}, v_2 \in \{i,j\}} d_{v_1 v_2} \quad (13)$$

i.e., it is the minimum of the shortest path lengths of the paths $a \rightarrow i$, $a \rightarrow j$, $b \rightarrow i$ and $b \rightarrow j$, plus the effective distance between the two vertices a and b .

Fig. 7 shows that the effective distance is able to capture well the properties of the spatial propagation of the cascade over the network from the location of the initial shock. The figure refers to the case of Spanish grid topology with heterogeneous coupling (see Section IIB). The temporal evolution of one particular cascade event,

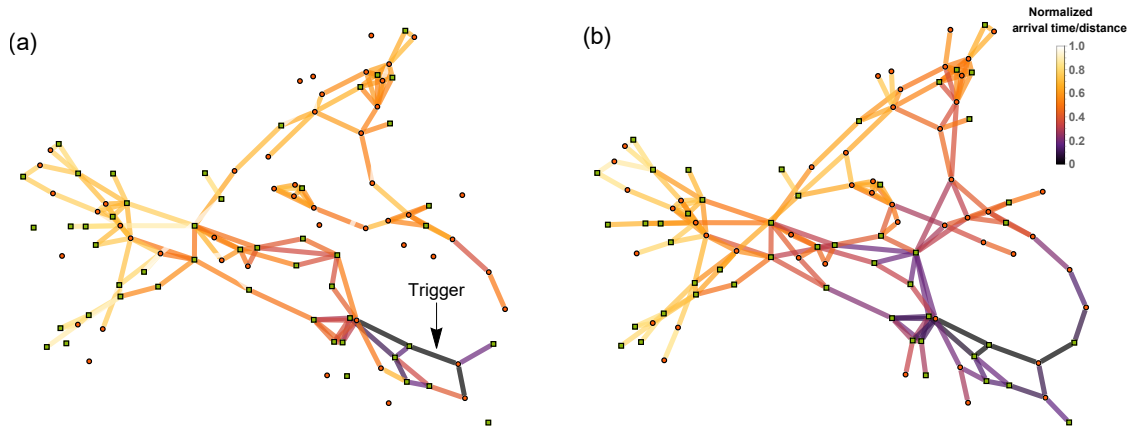


Figure 7. Mapping the propagation of a cascade on the Spanish power grid. (a) The edges of the network are color-coded based on the normalized arrival time of the cascade with respect to a specific initially damaged line, indicated as “Trigger”, and (b) based on their normalized distance with respect to the trigger using the effective distance measure in Eq. (12). In both cases, darker colors indicate shorter distance/early arrival of the cascade. Normalization is carried out using the largest distance/arrival time. Edges that are not plotted are not reached by the cascade at all. The analysis has been performed using the Spanish grid with distributed producers with $P^+ = 1$ (green squares), consumers with $P^- = -1/s^2$ (red circles), heterogeneous coupling and tolerance $\alpha = 0.55$.

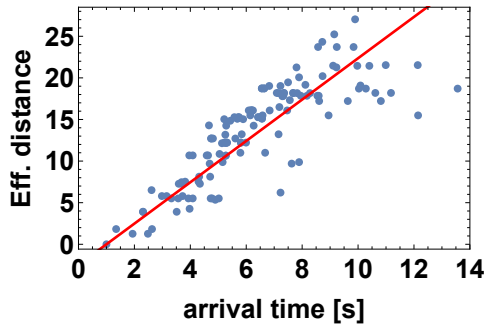


Figure 8. The cascade propagates through the power grid with approximately constant speed if an appropriate measure of distance is defined. Effective distances between the initial trigger and secondary line outages are plotted as a function of time. Each point in the plot corresponds to one edge, while the straight line is the result of a linear fit. Results refer to the Spanish power grid with the same parameters as those used in Fig. 7.

which is started by an initial exogenous damage of the edge marked as “Trigger”, is reported. Network edges are color-coded based on the actual arrival time of the cascade in panel (a), and compared to a color code based instead on their effective distance from the trigger line in panel (b). Edges far away from the trigger line, in terms of effective distance, have brighter colors than edges close to the trigger. Similarly, lines at which the cascade arrives later are brighter than lines affected immediately. The figure clearly indicates that effective distance and ar-

rival time are highly correlated, i.e., the cascade propagates throughout the network reaching earlier those edges that are closer according to the definition of effective distance. The relation between the effective distance of a line from the initial trigger and the time it takes for this line to be affected by the cascade is further investigated in the scatter plot of Fig. 8. The reported fit indicates that the two quantities are related by an approximate linear relationship with regression coefficient $R \approx 0.83$. This means that the cascade propagates with a nearly constant speed through the network when an appropriate measure of distance, such as the effective distance defined above, is adopted [60]. In contrast, a measure of distance solely based on the topology of the network, such as a standard graph distance equal to the number of edges in the shortest path, shows a weaker correlation with the actual arrival time of the cascade (see Supplementary Note 5).

III. DISCUSSION

In this work, we have proposed and studied a model of supply networks highlighting the importance of transient dynamical behavior in the emergence and evolution of cascades of failures. The model takes into account the intrinsic dynamic nature of the system, in contrast to most other studies on supply networks, which are instead based on a static flow analysis. Differently from the existing works on cascading failures in power grids [8–11, 21–24, 50], we have exploited the dynamic nature of the swing equation to describe the temporal

behavior of the system, and we have adopted an absolute flow threshold to model the propagation of a cascade and to identify the critical lines of a network. The differences with respects to the results of a static flow analysis are striking, as $N - 1$ secure power grids, i.e., grids for which the static analysis does not predict any additional failures, can display large dynamical cascades. This result emphasizes the importance of taking dynamical transients into account when analyzing cascades, and should be considered by grid operators when performing a power dispatch, or during grid extensions [5]. Notably, our dynamical model for cascades not only reveals additional failures, but also allows to study the details of the spreading of the cascade over the network. We have investigated such a propagation by using an effective distance measure quantifying the distance of a line (link of the network) from the original failure, which strongly correlates with the time it takes for the cascade to reach this line. This naturally leads to the definition of a propagation speed of the cascade. Being able to measure the speed of the cascade can be highly relevant when designing measures to stop or contain cascades, since the propagation velocity determines how fast actions have to be taken.

While the swing equation is able to capture interesting dynamical effects previously unnoticed, it still constitutes a comparably simple model to describe power grids [36]. Alternative, more elaborated models would involve more variables, e.g., voltages at each node of the network to allow a description of longer time scales [61–64]. In addition, we only focused on the removal of individual lines in our framework, instead of including the shutdown of power plants, i.e., the removal of network nodes. These simplifications are mainly justified by the very same time scale of the dynamical phenomena: All cascades observed in the simulation are very fast, terminating on a time scale of about 10 seconds, which supports the choice of the swing equation [30, 36]. Furthermore, such short time scales are consistent with empirical observations of real cascades in power grids, which were caused in a very short time by overloaded lines. Conversely, power plants (nodes of the network) were usually shut down after the failure of a large fraction of the transmission grid [4, 5, 7]. The same holds for load shedding, i.e., disconnecting consumers. In order to further support our conclusions, we have also performed simulations with a 3rd order model that includes voltage dynamics (see Supplementary Note 3), and we have found qualitatively similar results to those obtained with the swing equation. Overall, our work indicates that a dynamical second order model as the one adopted in our framework is able to capture additional features compared to static flow analyses, while still making analytical approaches possible. This allows to go beyond the methods commonly adopted in the engineering literature, which are often solely based on heavy computer simulations of specific scenarios, e.g. [65].

Furthermore, concerning the delicate issue of pro-

tecting the grid against random failures or targeted attacks, it is crucial to be able to identify critical lines whose removal might be causing large-scale outages. As we have seen, most of the lines of the networks studied in this article cause very small cascades when initially damaged. However, our results have also unveiled the existence in each of these networks of a few critical lines producing large outages, which in certain cases can even affect the entire grid. Within our modeling framework, we have been able to develop an analytical flow predictor that reliably identifies critical lines and outperforms existing topological measures in terms of prediction power. As an alternative to the analytical flow predictor, when a faster assessment of criticality is required, the stable state flows of the intact grid can be used, although they are less reliable. We hope these two indicators can become a useful tool for grid operators to test their current power dispatch strategies against cascading threads.

In a time when our lives depend more than ever on the proper functioning of supply networks, we believe it is crucial to understand their vulnerabilities and design them to be as robust as possible. The results presented in this article represent only a first step in this direction and many interesting questions remain to be investigated and answered within our framework or similar approaches. How is the propagation speed of a cascade linked to the network topology? Which lines are affected by a large cascade, and which parts of the network are able to return to a stable state? What are the best mitigation strategies to contain a cascade or to stop its propagation? All these questions go beyond the scope of this article, whose aim was mainly to provide a first broad analysis of the importance of transients in the emergence and evolution of cascades, but we hope our results will trigger the interest of the research community of physicists, mathematicians and engineers.

ACKNOWLEDGMENTS

B.S. and V. L. acknowledge support from the EPSRC project EP/N013492/1, “Nash equilibria for load balancing in networked power systems”. We gratefully acknowledge support from the Federal Ministry of Education and Research (BMBF grant no.03SF0472A-E), the Helmholtz Association (via the joint initiative “Energy System 2050 - A Contribution of the Research Field Energy” and the grant no.VH-NG-1025 to D.W.), the Göttingen Graduate School for Neurosciences and Molecular Biosciences (DFG Grant GSC 226/2 to B.S.) and the Max Planck Society (to M.T.).

Author contributions

B.S. and V.L. designed the research. B.S. performed most simulations and generated figures. All authors contributed to discussing the results and writing the paper.

- [1] M. Newman, *Networks: An Introduction* (Oxford University Press, Inc., New York, NY, USA, 2010).
- [2] V. Latora, V. Nicosia, and G. Russo, *Complex Networks: Principles, Methods and Applications* (Cambridge University Press, 2017).
- [3] R. Albert, H. Jeong, and A.-L. Barabási, *Nature* **406**, 378 (2000).
- [4] New York Independent System Operator, *Interim report on the august 14, 2003, blackout* (2004), URL https://www.hks.harvard.edu/hepg/Papers/NYISO_blackout_report.8.Jan.04.pdf.
- [5] Bundesnetzagentur für Elektrizität, Telekommunikation und Gas, Tech. Rep., Technical report, German Federal Regulatory Agency for Electricity, Gas, Telecommunications, Postal and Railway Systems, Berlin, Germany (2006).
- [6] Central Electricity Regulatory Commission (CERC), *Report on the grid disturbances on 30th july and 31st july 2012*, URL http://www.cercind.gov.in/2012/orders/Final_Report_Grid_Disturbance.pdf.
- [7] J. W. Bialek, in *Power Tech, 2007 IEEE Lausanne* (IEEE, 2007), pp. 51–56.
- [8] D. Witthaut and M. Timme, *Physical Review E* **92**, 032809 (2015).
- [9] I. Simonsen, L. Buzna, K. Peters, S. Bornholdt, and D. Helbing, *Physical Review Letters* **100**, 218701 (2008).
- [10] M. Rohden, D. Jung, S. Tamrakar, and S. Kettemann, *Physical Review E* **94**, 032209 (2016), URL <http://link.aps.org/doi/10.1103/PhysRevE.94.032209>.
- [11] A. Plietzsch, P. Schultz, J. Heitzig, and J. Kurths, *The European Physical Journal Special Topics* **225**, 551 (2016).
- [12] P. Hines, E. Cotilla-Sanchez, and S. Blumsack, *Chaos: An Interdisciplinary Journal of Nonlinear Science* **20**, 033122 (2010).
- [13] C. D. Brummitt, P. D. H. Hines, I. Dobson, C. Moore, and R. M. D'Souza, *Proceedings of the National Academy of Sciences* **110**, 12159 (2013).
- [14] D. S. Callaway, M. E. Newman, S. H. Strogatz, and D. J. Watts, *Physical Review Letters* **85**, 5468 (2000).
- [15] S. Lozano, L. Buzna, and A. Díaz-Guilera, *The European Physical Journal B* **85**, 1 (2012).
- [16] R. Albert, I. Albert, and G. L. Nakarado, *Physical Review E* **69**, 025103 (2004).
- [17] S. Boccaletti, V. Latora, Y. Moreno, M. Chavez, and D.-U. Hwang, *Physics Reports* **424**, 175 (2006), ISSN 0370-1573.
- [18] S. V. Buldyrev, R. Parshani, G. Paul, H. E. Stanley, and S. Havlin, *Nature* **464**, 1025 (2010).
- [19] S. Boccaletti, G. Bianconi, R. Criado, C. I. Del Genio, J. Gómez-Gardeñes, M. Romance, I. Sendina-Nadal, Z. Wang, and M. Zanin, *Physics Reports* **544**, 1 (2014).
- [20] F. Battiston, V. Nicosia, and V. Latora, *Physical Review E* **89**, 032804 (2014).
- [21] P. Crucitti, V. Latora, and M. Marchiori, *Physica A: Statistical mechanics and its applications* **338**, 92 (2004).
- [22] P. Crucitti, V. Latora, and M. Marchiori, *Physical Review E* **69**, 045104 (2004).
- [23] R. Kinney, P. Crucitti, R. Albert, and V. Latora, *The European Physical Journal B-Condensed Matter and Complex Systems* **46**, 101 (2005).
- [24] C. Ji, Y. Wei, H. Mei, J. Calzada, M. Carey, S. Church, T. Hayes, B. Nugent, G. Stella, M. Wallace, et al., *Nature Energy* **1**, 16052 (2016).
- [25] M. Rohden, A. Sorge, M. Timme, and D. Witthaut, *Physical Review Letters* **109**, 064101 (2012).
- [26] M. Rohden, A. Sorge, D. Witthaut, and M. Timme, *Chaos* **24**, 013123 (2014).
- [27] D. Manik, D. Witthaut, B. Schäfer, M. Matthiae, A. Sorge, M. Rohden, and E. Katifori, *The European Physical Journal Special Topics* **223**, 2527 (2014).
- [28] T. Nishikawa and A. E. Motter, *New Journal of Physics* **17**, 015012 (2015).
- [29] D. Witthaut, M. Rohden, X. Zhang, S. Hallerberg, and M. Timme, *Physical Review Letters* **116**, 138701 (2016).
- [30] P. Kundur, N. J. Balu, and M. G. Lauby, *Power system stability and control*, vol. 7 (McGraw-hill New York, 1994).
- [31] B. Obama, Washington, DC (2013).
- [32] P. Pourbeik, P. S. Kundur, and C. W. Taylor, *IEEE Power and Energy Magazine* **4**, 22 (2006).
- [33] D. Bienstock, in *2011 50th IEEE conference on Decision and control and European control conference (CDC-ECC)* (IEEE, 2011), pp. 2166–2173.
- [34] D. Brockmann and D. Helbing, *Science* **342**, 1337 (2013).
- [35] G. Filatella, A. H. Nielsen, and N. F. Pedersen, *The European Physical Journal B* **61**, 485 (2008).
- [36] J. Machowski, J. Bialek, and J. Bumby, *Power system dynamics, stability and control* (John Wiley & Sons, New York, 2008).
- [37] European Network of Transmission System Operators for Electricity (ENTSO-E), *Statistical factsheet 2014*, <https://www.entsoe.eu/publications/major-publications/Pages/default.aspx>, accessed: 2015-09-01.
- [38] A. Pikovsky, M. Rosenblum, and J. Kurths, *Synchronization: a universal concept in nonlinear sciences* (Cambridge University Press, 2003).
- [39] Y. Kuramoto, in *International Symposium on on Mathematical Problems in Theoretical Physics*, edited by H. Araki (Springer, New York, 1975), Lecture Notes in Physics Vol. 39, p. 420.
- [40] Y. Kuramoto, *Chemical Oscillations, Waves, and Turbulence* (Springer Science & Business Media, 2012).
- [41] S. H. Strogatz, *Physica D: Nonlinear Phenomena* **143**, 1 (2000).
- [42] D. Witthaut, S. Wimberger, R. Burioni, and M. Timme, *Nature Communications* **8** (2017).
- [43] V. Latora and M. Marchiori, *Physical Review E* **71**, 015103 (2005).
- [44] M. Argollo de Menezes and A.-L. Barabási, *Physical Review Letters* **93**, 068701 (2004).
- [45] S. Meloni, J. Gómez-Gardeñes, V. Latora, and Y. Moreno, *Physical Review Letters* **100**, 208701 (2008).
- [46] S. Çolak, A. Lima, and M. C. González, *Nature Communications* **7**, 10793 (2016).
- [47] A. Lima, R. Stanojevic, D. Papagiannaki, P. Rodriguez, and M. C. González, *Journal of The Royal Society Interface* **13**, 20160021 (2016).
- [48] P. Echenique, J. Gómez-Gardeñes, and Y. Moreno, *Europhysics Letters* **71**, 325 (2005).
- [49] D. Petrone and V. Latora, arXiv preprint arXiv:1610.00795 (2016).

- [50] S. Pahwa, C. Scoglio, and A. Scala, *Scientific Reports* **4**, 3694 (2014).
- [51] A. J. Wood, B. F. Wollenberg, and G. B. Sheblé, *Power Generation, Operation and Control* (John Wiley & Sons, New York, 2013).
- [52] A. E. Motter and Y.-C. Lai, *Physical Review E* **66**, 065102 (2002).
- [53] Y. Koç, M. Warnier, P. Van Mieghem, R. E. Kooij, and F. M. Brazier, *Physica A: Statistical Mechanics and its Applications* **415**, 273 (2014).
- [54] V. Rosato, S. Bologna, and F. Tiriticco, *Electric Power Systems Research* **77**, 99 (2007).
- [55] D. Manik, M. Timme, and D. Witthaut, arXiv preprint arXiv:1611.09825 (2016).
- [56] D. Manik, M. Rohden, H. Ronellenfitch, X. Zhang, S. Hallerberg, D. Witthaut, and M. Timme, *Physical Review E* **95**, 012319 (2017).
- [57] H. Ronellenfitch, D. Manik, J. Horsch, T. Brown, and D. Witthaut, *IEEE Transactions on Power Systems* **PP**, 1 (2017), ISSN 0885-8950.
- [58] V. M. E. K. Klemm, M. Á. Serrano and M. S. Miguel, *Scientific Reports* **2**, 292 (2012).
- [59] P. Hines and S. Blumsack, in *Hawaii International Conference on System Sciences, Proceedings of the 41st Annual* (IEEE, 2008), pp. 185–185.
- [60] P. D. Hines, I. Dobson, and P. Rezaei, *IEEE Transactions on Power Systems* **32**, 958 (2017).
- [61] S. Auer, K. Kleis, P. Schultz, J. Kurths, and F. Hellmann, *The European Physical Journal Special Topics* **225**, 609 (2016).
- [62] K. Schmietendorf, J. Peinke, R. Friedrich, and O. Kamps, *The European Physical Journal Special Topics* **223**, 2577 (2014).
- [63] K. Sharafutdinov, M. Matthiae, T. Faulwasser, and D. Witthaut, arXiv preprint arXiv:1706.06396 (2017).
- [64] J. Ma, Y. Sun, X. Yuan, J. Kurths, and M. Zhan, *PLoS one* **11**, e0165943 (2016).
- [65] J. Salmeron, K. Wood, and R. Baldick, *IEEE Transactions on Power Systems* **19**, 905 (2004).

Supplementary Information
accompanying the manuscript
Dynamically Induced Cascading Failures in Supply Networks
by

Benjamin Schäfer,¹ Dirk Witthaut,^{2,3} Marc Timme,^{1,4,5} and Vito Latora^{6,7}

¹*Network Dynamics, Max Planck Institute for Dynamics and Self-Organization (MPIDS), 37077 Göttingen, Germany*

²*Forschungszentrum Jülich, Institute for Energy and Climate Research - Systems*

Analysis and Technology Evaluation (IEK-STE), 52428 Jülich, Germany

³*Institute for Theoretical Physics, University of Cologne, 50937 Köln, Germany*

⁴*Institute for Theoretical Physics, Technical University of Dresden, 01062 Dresden Germany*

⁵*Center for Advancing Electronics Dresden (cfaed),*

Technical University of Dresden, 01062 Dresden Germany

⁶*School of Mathematical Sciences, Queen Mary University of London, London E1 4NS, United Kingdom*

⁷*Dipartimento di Fisica ed Astronomia, Università di Catania and INFN, I-95123 Catania, Italy*

This Supplementary Information follows the general narrative of the main manuscript, adding to it by a detailed description of the applied methods and extending results to different networks and models. This includes a more detailed and technical description of the cascade implementation, plots of further network topologies and formulas to calculate the Line Outage Distribution Factor (LODF). Furthermore, we show that results presented in the main text do not change qualitatively when investigating different grid topologies or different models of the power grid flow. Finally, we investigate the propagation of the cascade using the original graph distance and compare it to the effective graph distance.

SUPPLEMENTARY NOTE 1

Methods

Let us review the methods to analyze cascading failures in more detail. We provide additional technical details which were used to produce the results presented here and in the main text, give definitions for the number of unsynchronized nodes, discuss our choice of test grids and present the computation of Line Outage Distribution Factors (LODF).

Implementation of cascading mechanism

Motivated by the short time scale of cascading failures in the real world [1–3], we model the flows, determined by voltage phase angles, dynamically. To this end, we apply the swing equation [4, 5] given as:

$$\begin{aligned} \frac{d}{dt}\theta_i &= \omega_i \\ \frac{d}{dt}\omega_i &= P_i - \gamma\omega_i + \sum_{j=1}^N K_{ij} \sin(\theta_j - \theta_i). \end{aligned} \quad (\text{SM1})$$

We solve this nonlinear differential equation using computational methods in order to analyze cascades. Each simulation is started at the fixed point, which is defined for a given power network as

$$\begin{aligned} \omega_i^* &= 0 \\ P_i + \sum_{j=1}^N K_{ij} \sin(\theta_j^* - \theta_i^*) &= 0. \end{aligned} \quad (\text{SM2})$$

Due to the nonlinearity, the fixed point angles θ_i^* cannot be expressed in a closed form. Note that the fixed point of this equation is not unique but there exist multiple fixed points [6]. However, as long as the (homogeneous) coupling K is close to the critical coupling $K \sim K_c$ there is only one fixed point, where K_c is the minimal coupling for a fixed point to exist [7]. We determine the fixed point of the power grid using Newton's method. This is done by using an initial guess of $\theta_i^* = 0$ and $\omega_i^* = 0$ for all $i \in \{1, \dots, N\}$. Next, we start the simulation at the fixed point, i.e., set the initial conditions as

$$\begin{aligned} \omega_i(t=0) &= 0, \\ \theta_i(t=0) &= \theta_i^*, \end{aligned}$$

and wait until the trigger time $t_{trigger} = 1s$ to cut one line of the power grid, which we call the trigger line. If cutting the line changes the fixed point, a transient dynamic towards the new fixed point sets in, otherwise the simulation terminates.

We assume that real power grids are never operated at the absolute physical limit but that security margins will cause lines to shut down if they exceed a critical flow [4, 8]. For our algorithm, an additional line fails if the flow along a line defined as

$$F_{ij}(t) = K_{ij} \sin(\theta_j(t) - \theta_i(t)), \quad (\text{SM3})$$

exceeds the capacity of the line C_{ij} which depends on a tolerance parameter α :

$$F_{ij} > C_{ij}(\alpha) = \alpha K_{ij}, \quad (\text{SM4})$$

where the tolerance parameter can be at most one: $\alpha \leq 1$. This procedure is in contrast to other works on cascade that use a threshold dependent on the initial flow in the network [9–11]. However, it seems much more appropriate for power grids where the threshold at which a line has to be shut down does not depend on its initial load but on its physical capacity [12]. Note that the flow is changing over time and gets influenced by additional line failures as flow from other parts of the networks will get re-routed. We continue to track the flow and the failure of overloaded lines using an event-detector in our ODE solver [13] until $t_{max} = 50s$ where in all cases considered the cascade has stopped and no more lines fail.

Unsynchronized nodes

Besides the information which flow F_{ij} exceeded the threshold and hence which lines get overloaded, we also record how many nodes are unsynchronized after the cascade stops. This definition is based on the assumption that a frequency deviation of $\Delta f \sim 20$ mHz is within the stable operation boundaries of the European grid [4, 14] and therefore a node is recorded as unsynchronized if

$$|\omega(t_{\max})| > 2\pi \cdot 0.02 \text{ Hz},$$

i.e., the angular velocity at the end of the simulation $t_{\max} = 50$ s has to be larger than this threshold. If some nodes show a larger deviation from the reference frequency, they would most likely have to be disconnected from the grid, e.g. via load shedding [4]. Thereby, the number of unsynchronized nodes provides a measure for the number of affected consumers. In our case, the comparably strict threshold of $\Delta f = 20$ mHz was chosen to ensure that the system is at a fixed point and not on a limit cycle with small amplitude.

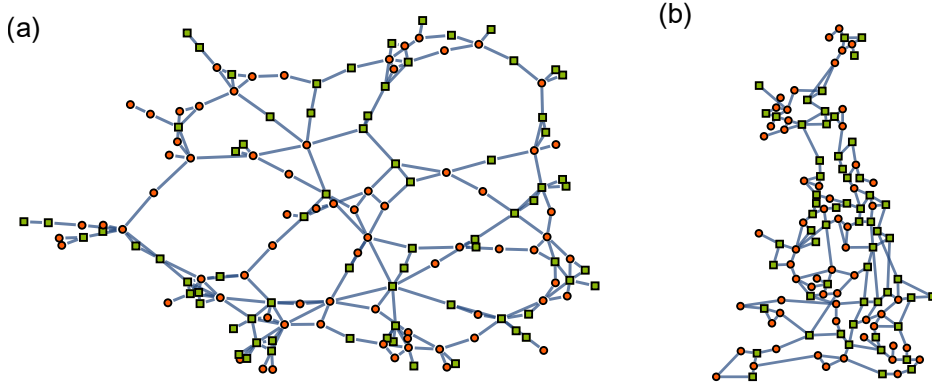
Test grids

Figure SM1. In addition to the Spanish topology presented in the main text, we use the French [15] and Great Britain [16, 17] grid topologies when assessing cascade effects. (a) The French grid topology has weaker clustering than the Spanish grid. (b) The grid of Great Britain has even lower clustering but many 4-cycles. We display both networks using distributed production with consumers (red circles) $P^- = -1/s^2$ and producers (green squares) $P^+ = 1/s^2$.

Dynamical cascades are mainly investigated using the realistic power grid topologies of the Spanish, French [15] and Great Britain [16, 17] high voltage power grids. Results for the number of line failures for the Spanish and French grid are presented in the main text while this Supplementary Information provides the results of the line failures of the British grid and results for the unsynchronized nodes of all grids. The Spanish topology is displayed in the main text while French and Great Britain topologies with randomly distributed production are displayed in Fig. SM1. All grids are considered with distributed small producer nodes with $P^+ = 1$ as well as (centralized) large producer nodes with $P^+ \approx 6$, i.e. each large producer is supplying approximately six consumer nodes. Finally, we also consider heterogeneous coupling where the capacity of each line is chosen so that the line is approximately loaded to 50%.

To construct a heterogeneous coupling matrix K_{ij} , we use an iterative procedure, adapting the capacity to the flow. The grid is initialized with distributed producers and homogeneous coupling $K_{ij}^{\text{old}} = K$ which is $K = 8/s^2$ for the French topology and $K = 5/s^2$ for both the Spanish and Great British topologies. Next, the initial loads on every line (i, j) are computed and the new coupling is set to

$$K_{ij}^{\text{new}} = 0.99K_{ij}^{\text{old}} + 0.01K_{ij}^{\text{old}}F_{ij}^{\text{old}}/0.5. \quad (\text{SM5})$$

Finally, K_{ij}^{old} is set to $K_{ij}^{\text{old}} = K_{ij}^{\text{new}}$ and the next fixed point is computed together with its fixed point flows F_{ij}^{old} . This procedure is iterated a total of 200 times. Thereby, the network approached a state where every line is loaded to about 50% of its physical maximum $F_{ij} \approx 0.5K_{ij}$.

Computing the Line Outage Distribution Factor

To save computation time determining fixed points and hence new steady-state flows, we use the Line Outage Distribution Factor (LODF) [18, 19]. The LODF approximates line flows after the trigger link (a, b) is removed as

$$F_{ab} = 0, \quad (\text{SM6})$$

$$F_{ij}^{\text{new}} \approx F_{ij}^{\text{old}} - F_{ab}^{\text{old}} \frac{\tilde{K}_{ij} (T_{ja} - T_{jb} - T_{ia} + T_{ib})}{1 - \tilde{K}_{ab} (T_{aa} - T_{ab} - T_{ba} + T_{bb})}, \quad (\text{SM7})$$

with a, b the indices of the trigger line and i, j the indices of any other line and auxiliary matrices

$$\tilde{K}_{ij} = K_{ij} \cos(\theta_i^* - \theta_j^*), \quad (\text{SM8})$$

$$A_{ij} = \begin{cases} -\tilde{K}_{ij} & \text{for } i \neq j \\ \sum_l \tilde{K}_{lj} & \text{for } i = j \end{cases}, \quad (\text{SM9})$$

with θ_i^* the fixed point angle of the intact network and the matrix T is as the Moore-Penrose pseudoinverse of A . We use this approximated flow to predict which lines are critical in a network in the main text.

SUPPLEMENTARY NOTE 2

Extended cascade analysis

The main text gave an analysis on the number of line failures of the Spanish and French grid, both displaying mostly uncritical lines with a few highly critical lines. Here, we also review results for the British grid and investigate the number of unsynchronized nodes after the cascade terminates as a measure of how many customers would be affected by a blackout.

Great Britain analysis

So far, we have analyzed the cascade statistics of the Spanish and French power grid topologies which we now complement with the usage of the Great Britain topology as given in Fig. SM1(b). We plot the histograms giving the probability to observe a given number of line failures in Fig. SM2. Compared to the other topologies, the same qualitatively behavior is observed. Most links do cause no or only small cascades, especially for homogeneous coupling. On the contrary, some critical links cause large damage, in particular when applying heterogeneous coupling, see panel (c) with tolerance $\alpha_1 = 0.55$.

Furthermore, the flow-based predictor we derived in the main text, also performs very well on the British topology as is shown in Fig. SM3. Specifically, it outperforms alternative predictors like ones based on the initial load of lines or betweenness measures.

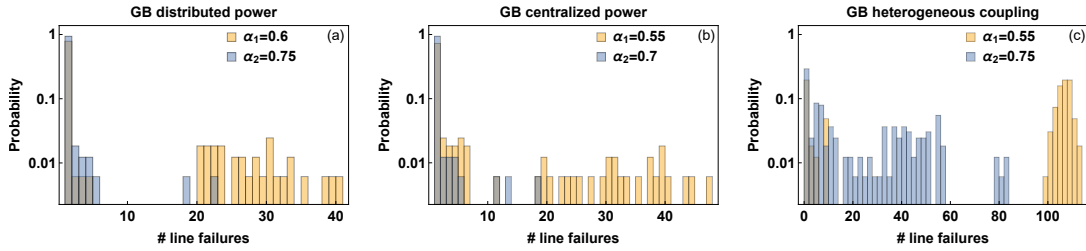


Figure SM2. The power grid topology of Great Britain (GB) returns qualitatively similar results as the grids of Spain and France: Most initially damaged lines result in small or no cascade while there exist some critical lines. (a) Distributed power, i.e., equal number of producers and consumers each with $P^- = -1/s^2$ and $P^+ = 1/s^2$ and homogeneous coupling of $K = 5/s^2$ is used. (b) Centralized power, fewer but larger producers with $P^- = -1/s^2$ and $P^+ \approx 6/s^2$ and homogeneous coupling of $K = 12/s^2$ is investigated. (c) Same power distribution as in (a) with coupling on all lines scaled to have all lines approximately loaded to half their maximum dynamical capacity $F \approx 0.5K$. For all panels we plot two different tolerances α , where the lower one is the smallest simulated value of α so that there are no initially overloaded lines ($N - 1$ stable). Note that the probability axis uses a log-scale. The grid has a total of $N_{GB} = 120$ nodes and $|E|_{GB} = 165$ edges.

Unsynchronized nodes

In the main text we have investigated the statistics of line failures for different grids and noted that most trigger lines cause no additional cascade or very small cascades. Here, we present the corresponding statistics for unsynchronized nodes in Fig. SM4. We note a very similar behavior, i.e., either the whole grid is affected by a line cut, i.e., nearly all nodes lose synchrony, or nothing happens and the grid keeps its steady state. Interestingly, we observe that this all-or-nothing response is more pronounced in the case of homogeneous coupling (distributed and centralized power) while heterogeneous coupling allows for more steps in between. This is opposite to the observations in the main text where we used the number of line failures and homogeneous coupling resulted in a broader distribution. However, one key message is unchanged: Only a few critical edges cause large cascades which we identify in the main text.

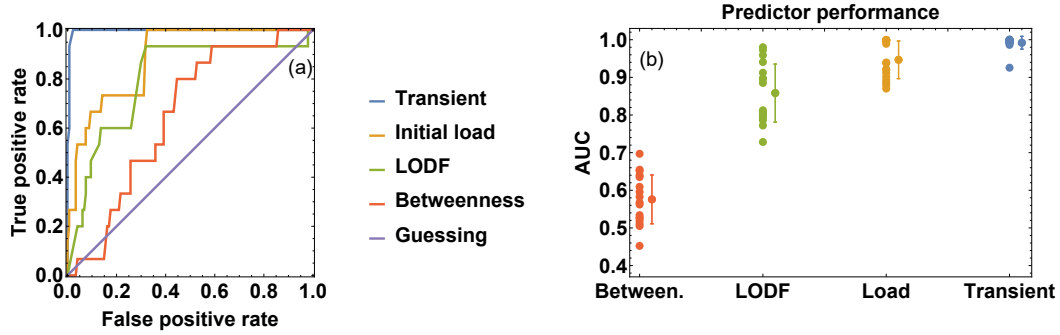


Figure SM3. The analytical flow-based predictor identifies critical lines best, also in the case of British power grid topology. Similar to the main text, four different predictors are presented to judge whether a given line, if chosen as initially damaged, will cause at least one additional line failure. The betweenness and initial load predictor classify a line as critical if it is within the top $x\%$ of the edges with highest betweenness/load with $x \in [0, 100]$. In contrast, the transient predictor exploits the oscillatory behavior to compute maximum transient flows. Finally, the predictor based on the Line Outage Distribution Factor (LODF) [18, 19] uses the same idea but approximates the new fixed flows by the LODF. (a) The predictors are tested against simulations via a Receiver-Operator-Characteristic (ROC) curve recording true positive rate and false positive rate of all predictors for different alarm thresholds. The analysis uses the Great Britain grid with heterogeneous coupling and tolerance $\alpha = 0.6$. (b) The Area Under the Curve (AUC) of each predictor is displayed. This has been computed for the Great Britain Grid with randomized producer positions using distributed and centralized power as well as heterogeneous coupling. For each predictor all individual scores are displayed on the left and the mean with error bars based on one standard deviation is shown on the right. Similar to the main text, the dynamical flow-based predictor outperforms clearly all other predictors.

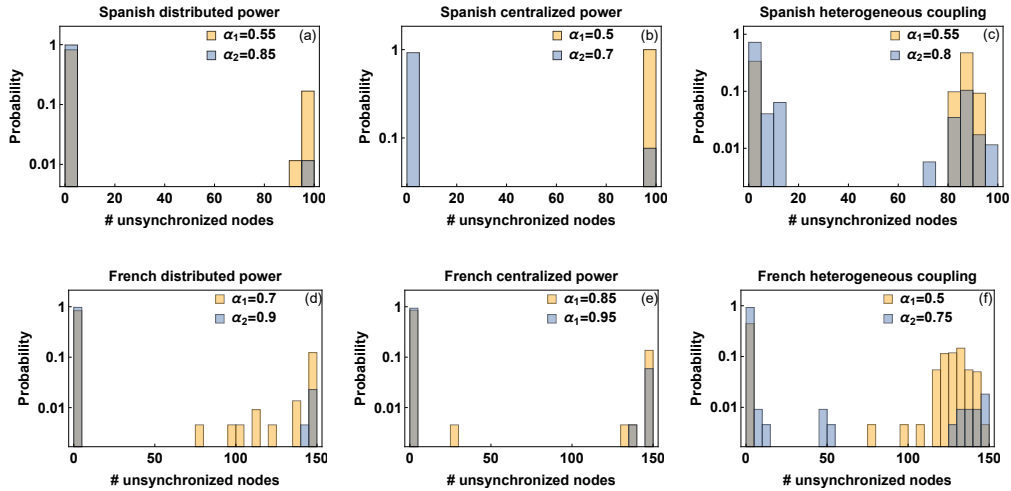


Figure SM4. Nodal desynchronization probability in the Spanish and French power grids under different power distributions and types of coupling. The histograms shown have been obtained under three different settings, see also main text. Panels (a) and (d) refer to the case of *distributed* power, i.e., equal number of producers and consumers, each with $P^- = -1/s^2$ and $P^+ = 1/s^2$, and homogeneous coupling with $K = 5/s^2$ for the Spanish and $K = 8/s^2$ for the French grid. Panels (b) and (e) refer to the case of *centralized* power, i.e., consumers with $P^- = -1/s^2$ and fewer but larger producers with $P^+ \approx 6/s^2$, and homogeneous coupling with $K = 10/s^2$ for Spanish and $K = 9/s^2$ for the French grid. Panels (c) and (f) refer to a case of *distributed* power as in panel (a) and (d), but with heterogeneous coupling, so that the fixed point flows on the lines are approximately $F \approx 0.5K$ both for the Spanish and the French grid. For all plots we use two different tolerances, where the lower one is the smallest simulated value of so that there are no initially overloaded lines ($N = 0$ stable).

SUPPLEMENTARY NOTE 3

Comparison of models

While we have introduced the swing equation and its static flows to assess cascades in the main text, let us consider additional models here in a case study. The swing equation is a simple dynamical model, capturing the essential dynamics of the power grid system [4, 12]. To illustrate this, we compare its cascading behavior with the ones obtained by power flow analysis and 3rd order dynamics. While power flow analysis is often used to assess the static grid behavior in engineering literature [4, 8, 12], the 3rd order model is an extension of the swing equation where the voltage is dependent on time [4, 20–22]. First, we introduce these two models and continue then with a comparison of the cascade using all models.

Power flow equations

The power flow or load flow equations are a common tool to assess steady state power grid flows in the engineering literature [4, 8, 12]. They assume the angular velocity to be zero $\omega = 0$ because only the steady state is analyzed. The power grid network is characterized by the susceptance matrix B_{ij} and the conductance matrix G_{ij} which leads to the following equations

$$\begin{aligned} P_i &= V_i \sum_{j=1}^N (G_{ij} V_j \cos(\theta_i - \theta_j) + B_{ij} V_j \sin(\theta_i - \theta_j)), \\ Q_i &= V_i \sum_{j=1}^N (G_{ij} V_j \sin(\theta_i - \theta_j) - B_{ij} V_j \cos(\theta_i - \theta_j)), \end{aligned} \quad (\text{SM10})$$

where P_i is the active power at each node, Q_i is the reactive power, θ_i is the equilibrium voltage phase angle and V_i is the voltage amplitude. These are the variables the system is solved for at each node. Because only two equations are available at each node, it is necessary to know two additional quantities per node that are fixed. Depending on which quantities are known and which are unknown each node (or bus) is characterized as follows. At the *slack (swing) bus* the voltage amplitude V_i and voltage angle θ_i are specified, while P_i and Q_i are unspecified to compensate power loss in the system. Typically, this would be one of the largest producers which is stabilizing the grid. In addition, there are *voltage-controlled buses (PV)* which are usually generators nodes for which P_i and V_i are fixed while we solve the equations for Q_i and θ_i . Finally, there exist *load buses (PQ)* with constant active power P_i and reactive power Q_i , but unknown voltage amplitude V_i and voltage angle θ_i [8].

Compared to the swing equations presented in the main text, the power flow equations include reactive power Q and ohmic losses by considering conductances G . However, this approach only allows comparison of fixed points since there is no dynamical evolution included.

Third order model equations

The third order model [4, 20–23] is similar to the swing equation but allows the voltage amplitude V_i at each node i to vary over time, in addition to the angle θ_i and the angular velocity ω_i :

$$\begin{aligned} \frac{d}{dt} \theta_i &= \omega_i \\ \frac{d}{dt} \omega_i &= P_i - \gamma \omega_i + \sum_{j=1}^N V_i V_j B_{ij} \sin(\theta_j - \theta_i) \\ \frac{d}{dt} V &= \frac{1}{T_V} \cdot \left(V_f - V_i + X \sum_{j=1}^N V_j \cos(\theta_j - \theta_i) \right), \end{aligned} \quad (\text{SM11})$$

with real power injection P_i , damping γ (see main text) as well as the voltage time scale $T_V = 1/2$, the susceptance matrix B_{ij} including self-coupling terms B_{ii} , voltage set-point $V_f = 1$ and the voltage droop X . For $X = 0$ and $V(t=0) = 1$ the voltage remains at the fixed point $V^* = 1$ at all times and reproduces the second order model while

for $X > 0$ deviations from the second order model can be observed. Typical parameter values are taken from [20]. Note also that the voltage dynamics is typically slower than the angle and angular velocity dynamics, allowing to neglect it for short time scales.

Comparison of cascade effects

After introducing power flow and 3rd order model, let us compare the cascade described using these models with the cascade described using the swing equation.

We implement the cascading algorithm by comparing the sine of the angle difference to our tolerance:

$$|\sin(\theta_i - \theta_j)| > \alpha \Rightarrow \text{line } (i, j) \text{ fails.} \quad (\text{SM12})$$

Alternatively, one could explicitly compute the flows

$$F_{ij} = B_{ij}V_iV_j \sin(\theta_i - \theta_j), \quad (\text{SM13})$$

which then depends on the voltages V_i and V_j , which does not change the results significantly. Using the angles as a criterion on whether a line fails or not, allows for direct comparison with the swing equation which effectively also uses Eq. (SM12) (multiplying both sides with B_{ij}).

We compare the four different models (static and dynamic swing equation, load flow and 3rd order model) using the 5 node sample network introduced in the main text in Fig. SM5. Note that the swing equation, Fig. SM5(c), and the 3rd order power grid model, Fig. SM5(e,f), return qualitatively similar results. The precise nature of the cascade differs and also depends on the parameter choice to extend the swing equation to the third order model. Nevertheless, a dynamical oscillatory transient is observed that leads to overload in both cases. Similarly, the power flow equations, Fig. SM5(d), return qualitatively similar results to the static swing equations, Fig. SM5(b), while the quantitative values differ. Overall, steady state analysis gives largely different results compared to the dynamical models, neglecting transient overloads. Hence, we use the simplest model available to capture the necessary dynamics of the power grid, namely the swing equation.

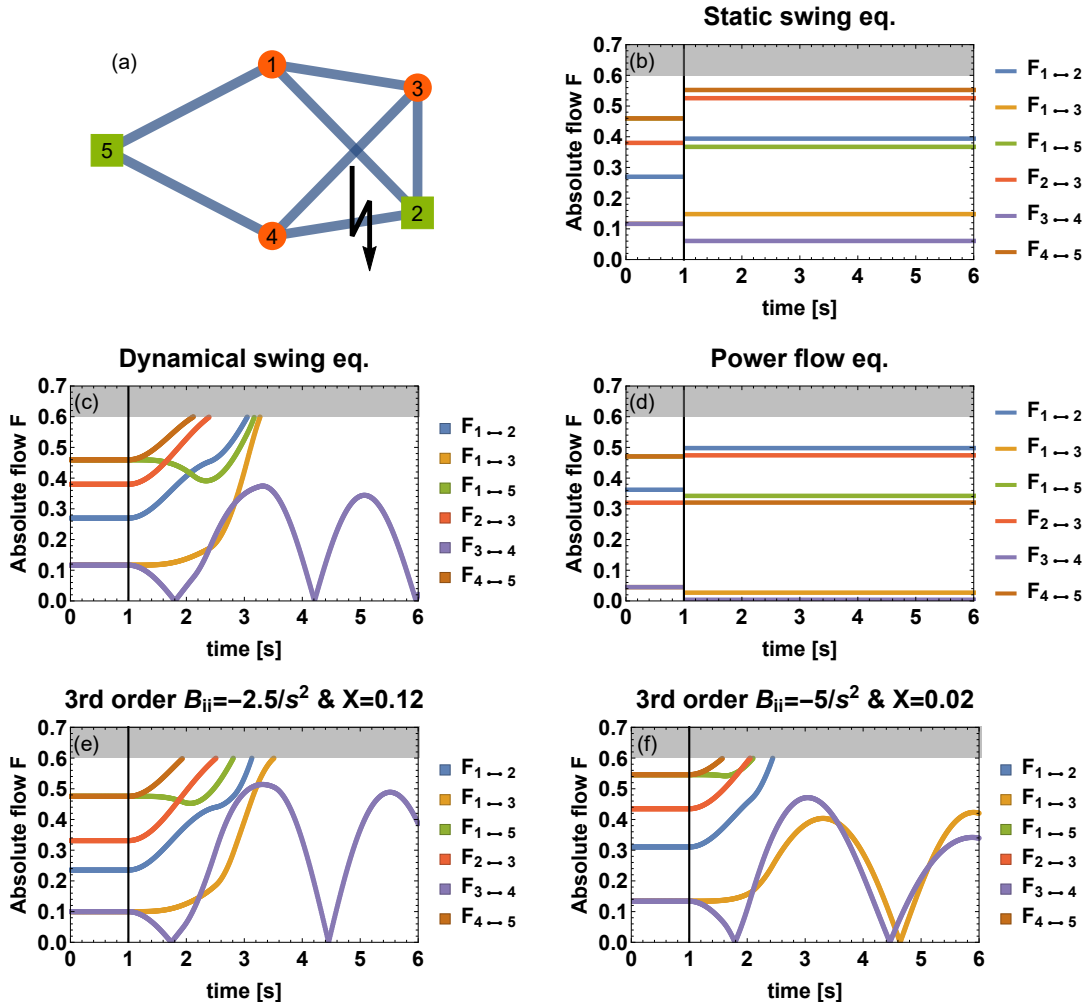


Figure SM5. Power flow and static swing equation as well as 3rd order model and dynamical swing equation return qualitatively similar cascade results. (a) The $N = 5$ node sample system is plotted and used for illustration purposes. (b)-(f) plot the flows in the sample system when the node indicated by the arrow is cut at $t_{\text{trigger}} = 1$ s. A line is assumed to fail when the flow reaches the gray area of $\alpha = 0.6$ which is our tolerance value. (b) The flows are based on the static swing equation (SM2), i.e., the fixed point solution of the swing equation. (c) The dynamical swing equation (SM1) is used for the flow calculation. (d) Flows are based on the power flow Eq. (SM10) with $B_{ii} = -2/s^2$ and $G_{ij} = 4.5/s^2$ for non-diagonal entries with connectivity as seen in (a) and reactive power of the consumers $Q = -9.7/s^2$. (e)-(f) The flows are dynamically updated using the 3rd order model (SM11) with two different values of the self-coupling B_{ii} and voltage droop X . The grid uses two producers $P^+ = 1.5/s^2$ and three consumers $P^- = -1/s^2$ and an susceptance of $B_{ij} \approx 1.63$ for non-diagonal elements. Qualitatively, static swing equation and (static) power flow equations return the same behavior. Similarly, 3rd order models and dynamical swing equation display qualitatively the same behavior.

SUPPLEMENTARY NOTE 4

Predicting cascades

It is crucial to avoid large scale blackouts. However, preventing them requires the identification of critical lines [2, 24]. In the main text, we present a cascade predictor assuming oscillations during the transition from the old to the new fixed point. Here we justify this assumption. Let us consider the 5-node sample system, displayed in SM5(a). We plot the flows of all lines in Fig. SM6, assuming that only the trigger line (marked with a lightning bolt in Fig. SM5(a)) is cut and all other lines are left intact. Thereby, we exclude secondary failures as they are otherwise used in our cascading algorithm. Now, comparing Fig. SM6 with Fig. SM5 (c), where additional lines fail, we note that lines (2,3) and (4,5) get overloaded first because of their respective transient dynamics. However, Fig. SM6 reveals the oscillations around the new fixed point of the flows which is not visible in Fig. SM5 (c) because lines fail when exceeding the maximum flow. Although the oscillations are not perfectly periodic, they are well approximated by damped sinodal functions. Based on these sinodal oscillations, we construct a flow based predictor in the main text, successfully identifying critical links, see also Fig. SM3 for results for the British grid.

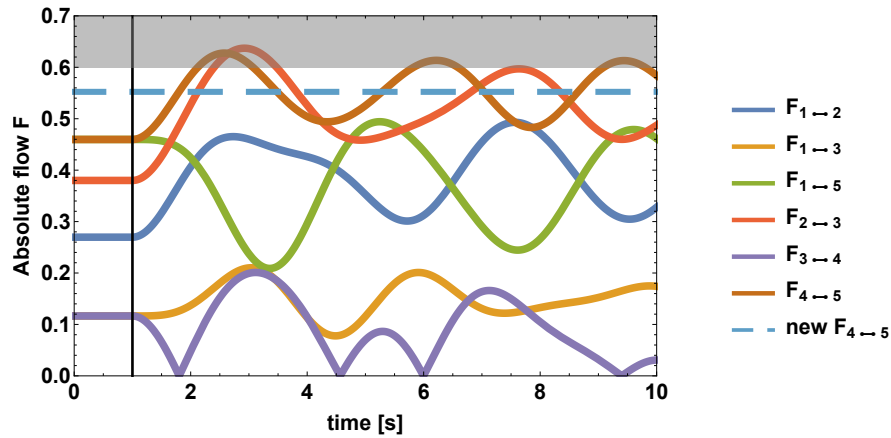


Figure SM6. The flows on all lines oscillate during the transition from the old to the new fixed point. Plotted are the absolute values of the flows of the 5 node sample system when line (2,4) gets cut at time $t = 1$ s and no further line overload is considered. We note that the two largest flows at $t = 2$ seconds ((2,3) and (4,5)) are the first lines that get overloaded in the full cascade algorithm. For illustration purposes, we include the new fixed point flows of (4,5) as a dashed line. We observe oscillations of the flows approximately around their new fixed point flows which inspired the definition of the flow based cascade predictor.

SUPPLEMENTARY NOTE 5

Propagation speed of cascades

Real world cascades often propagate through the power grid on a very fast time scale [1–3]. So, is it possible to observe this propagation in the cascades we simulate using the swing equation? We investigated this in the main text by introducing the effective distance measure, motivated in Ref. [25]. We observe indeed a linear relationship between effective distance and time and thereby a constantly propagating cascade in the network.

To contrast the effective distance, we also show the results when using the (original) graph distance to determine the speed using $d_{ij} = 1/K_{ij}$ and compare the correlation coefficients as well as the speed estimate of both approaches, see Fig. SM7. The linear fit using the naive graph distance [26] does not describe the data as well as it does in the case of effective distance. Furthermore, when averaging over all potential trigger links, the distribution of regression coefficients R is broader and on average at lower values for fits using the original graph distance, i.e., the linear relationship is better achieved using the effective distance measure.

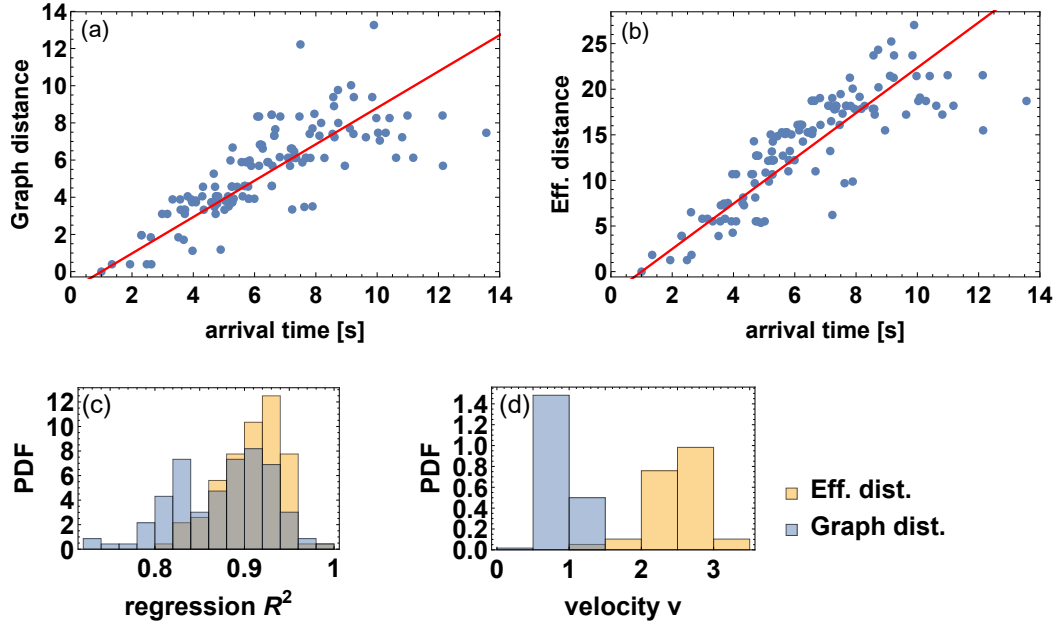


Figure SM7. The effective distance measure describes the constantly propagating cascade with a better linear relationship than the original graph distance. (a,b) Plotted are the distances of line failures with respect to the trigger line as a function of time for the Spanish grid with heterogeneous coupling. Every point in the plot corresponds to one line failure. The red line is a linear fit of the given points. We compare two different distance measures: (a) We use the original graph distance based on the weighted adjacency matrix, using $d_{ij} = 1/K_{ij}$. (b) We calculate the effective distance in the network based on [25]. (c,d) We record the squared regression R^2 and estimated velocity v for all lines with at least 10 line failures. (c) Effective distance provides a significantly better linear relation based on the regression coefficient. (d) The averaged propagation speed is $\bar{v}_{\text{eff.}} \approx 2.55 \text{ links/s}$ for effective distance. We use the Spanish grid with distributed producers $P^+ = 1/s^2$, heterogeneous coupling, as described above, tolerance $\alpha = 0.55$.

[1] Central Electricity Regulatory Commission (CERC), *Report on the grid disturbances on 30th july and 31st july 2012*, URL http://www.cercind.gov.in/2012/orders/Final_Report_Grid_Disturbance.pdf.

- [2] Bundesnetzagentur für Elektrizität, Telekommunikation und Gas, Tech. Rep., Technical report, German Federal Regulatory Agency for Electricity, Gas, Telecommunications, Postal and Railway Systems, Berlin, Germany (2006).
- [3] New York Independent System Operator, *Interim report on the august 14, 2003, blackout* (2004), URL https://www.nysipr.com/harvard/hepg/Papers/NYISO_blackout_report_8_Jan_04.pdf.
- [4] J. Machowski, J. Bialek, and J. Bumby, *Power system dynamics, stability and control* (John Wiley & Sons, New York, 2008).
- [5] G. Filatrella, A. H. Nielsen, and N. F. Pedersen, *The European Physical Journal B* **61**, 485 (2008).
- [6] D. Manik, M. Timme, and D. Witthaut, arXiv preprint arXiv:1611.09825 (2016).
- [7] D. Manik, D. Witthaut, B. Schäfer, M. Matthiae, A. Sorge, M. Rohden, and E. Katifori, *The European Physical Journal Special Topics* **223**, 2527 (2014).
- [8] A. J. Wood, B. F. Wollenberg, and G. B. Sheblé, *Power Generation, Operation and Control* (John Wiley & Sons, New York, 2013).
- [9] P. Crucitti, V. Latora, and M. Marchiori, *Physical Review E* **69**, 045104 (2004).
- [10] D. Witthaut and M. Timme, *Physical Review E* **92**, 032809 (2015).
- [11] I. Simonsen, L. Buzna, K. Peters, S. Bornholdt, and D. Helbing, *Physical Review Letters* **100**, 218701 (2008).
- [12] P. Kundur, N. J. Balu, and M. G. Lauby, *Power system stability and control*, vol. 7 (McGraw-hill New York, 1994).
- [13] Wolfram Research Inc., *Mathematica*, Champaign, Illinois (2017).
- [14] European Network of Transmission System Operators for Electricity (ENTSO-E), *Statistical factsheet 2014*, <https://www.entsoe.eu/publications/major-publications/Pages/default.aspx>, accessed: 2015-09-01.
- [15] V. Rosato, S. Bologna, and F. Tiriticco, *Electric Power Systems Research* **77**, 99 (2007).
- [16] M. Rohden, A. Sorge, M. Timme, and D. Witthaut, *Physical Review Letters* **109**, 064101 (2012).
- [17] M. Rohden, A. Sorge, D. Witthaut, and M. Timme, *Chaos* **24**, 013123 (2014).
- [18] H. Ronellenfitsch, D. Manik, J. Horsch, T. Brown, and D. Witthaut, *IEEE Transactions on Power Systems* **PP**, 1 (2017), ISSN 0885-8950.
- [19] D. Manik, M. Rohden, H. Ronellenfitsch, X. Zhang, S. Hallerberg, D. Witthaut, and M. Timme, *Physical Review E* **95**, 012319 (2017).
- [20] K. Schmietendorf, J. Peinke, R. Friedrich, and O. Kamps, *The European Physical Journal Special Topics* **223**, 2577 (2014).
- [21] S. Auer, K. Kleis, P. Schultz, J. Kurths, and F. Hellmann, *The European Physical Journal Special Topics* **225**, 609 (2016).
- [22] J. Ma, Y. Sun, X. Yuan, J. Kurths, and M. Zhan, *PloS one* **11**, e0165943 (2016).
- [23] K. Sharafutdinov, M. Matthiae, T. Faulwasser, and D. Witthaut, arXiv preprint arXiv:1706.06396 (2017).
- [24] D. Witthaut, M. Rohden, X. Zhang, S. Hallerberg, and M. Timme, *Physical Review Letters* **116**, 138701 (2016).
- [25] D. Brockmann and D. Helbing, *Science* **342**, 1337 (2013).
- [26] M. Newman, *Networks: An Introduction* (Oxford University Press, Inc., New York, NY, USA, 2010).

Part III

Conclusion

Chapter 8

Summary & Discussion

In this thesis, we investigate self-organized dynamics of power grids with respect to their feasibility in future smart grid applications, their resilience to fluctuations and their security in terms of cascading failures. Each of the previous chapters focused on one specific aspect of making self-organized grid operation viable when facing grid re-structuring, fluctuating renewables and random failures. As mentioned in the introduction, power grids show complex behavior on different levels of hierarchy and time scales such that a complete coverage of all questions is beyond the scope of a single PhD thesis. Therefore, we have restricted our analysis by choosing an appropriate model for the high voltage transmission grid and have mostly focused on short time scales.

Overall, we have aimed to answer the following questions: How could self-organized power grid dynamics be implemented? What are the risks and benefits of such a self-organized approach with respect to stability, fluctuations and cascades? Here, we review the advances made in this thesis by splitting the discussion into several parts chosen by topic. First, we review progress made in formulating a decentrally controlled smart grid. Next, we discuss the impact of continuous fluctuations both on the stability of the grid and the power quality. Then, we examine our results on cascading failures in power grids. We close this chapter by considering the limitations of the model and by formulating an outlook of upcoming work and potential technical applications of the presented results.

Decentral Smart Grid Control. Renewable power plants are often smaller than previously used conventional ones and have to be placed at locations with favorable weather conditions, leading to power sources that are spread out more than before. This distributed and also highly fluctuating power generation calls for a new power grid design and a new control scheme to cope with additional fluctuations, see also the next paragraph on *Continuous Perturbations*. A common concept for a new grid design is a *smart grid*, which gathers information from all grid participants and communicates an optimal strategy regarding consumption, generation and control [6,50]. Most smart grid concepts heavily rely on information technology (IT) infrastructure for communication, data storage and transfer. From our point of view, this raises severe privacy and IT security concerns since by monitoring our consumption, a power company effectively monitors most of our activities: They would know when we use our electrical car, when and how much energy we use for heating, warm water, television etc. In addition, relying on IT infrastructure introduces risks due to potential hacking attempts as they

appeared within the past years and months, even hitting large companies and thereby disabling ATMs, forcing hospitals to cancel surgeries [111] or costing the logistics sectors millions of dollars [106]. Furthermore, different smart grid concepts have been proposed, e.g., in [6, 50, 53, 54], but we are not aware of any analysis demonstrating the stability or even feasibility of such a system.

To contrast these existing schemes, we have presented a mathematical formulation in terms of *Decentral Smart Grid Control* in Chapters 3 and 4, based on a concept proposed by T. Walter [163,164]. Similar to other smart grid concepts, it evolves around controlling consumers via demand response, i.e., motivating consumers to adjust their power demand [4,109,155]. However, our proposal does not need any IT infrastructure but relies solely on local frequency information to stabilize the grid. High grid frequencies signal an abundance of power and should thereby encourage additional consumption (and vice versa for low frequency). According to T. Walter [163,164], this could be implemented by locally coupling the electricity price to the frequency. The idea to use the grid frequency to control the power grid has already been proposed earlier, see e.g [140,142]. However, a mathematical formulation of this control concept and a stability analysis was missing.

Therefore, we have derived a mathematical form of the demand control motivated by economic incentives in Chapter 3. To investigate the impact of this demand control on the dynamical stability, we have included it in into an appropriate dynamical model, the swing equation, effectively introducing an additional term, similar to added damping. With this expression, we have analyzed the stability in a systematic way, using both analytical and numerical tools. When reacting instantaneously to the frequency changes, the added control acts like an improved primary control stabilizing the system. Furthermore, the grid is in an economic equilibrium of supply and demand when at the dynamical fixed point. However, introducing a delay in the measurement or reaction of the consumer to a frequency signal has been shown to potentially destabilize the system. Crucially, we have obtained analytical insights both for the stability of an instantaneously controlled system as well as regarding the input of delays, going beyond specific scenarios or simulations, for example, of a single IEEE test grid, as they are often used as standard test cases in engineering literature [95]. In particular, we have illustrated the principles of synchronization delays in Chapter 3, revealing which delays are harmful, and have derived a maximum delay for any power grid system in Chapter 4. Furthermore, one highlight of the numerical results is that by computing the basin of attraction, recently discussed as *basin stability* [92], we have revealed a globally stable fixed point for certain delay conditions, i.e., perfect stability. While explicit simulations have been restricted to comparably small networks of size $N \sim 10$, our analytical results are applicable to any network structure or size and thereby are more useful than additional simulations could be.

Note that our study neglected ohmic losses and voltage dynamics since we have modeled the transmission level, while demand control will also be relevant on the distribution level where these effects become more relevant [86]. Also, we have assumed that the consumer behavior is very simplistic, which could be extended by changing to an agent-based approach or considering a more detailed response to price changes. However, many of these extensions will make an analytical treatment impossible. So far, our work already stimulated additional research on the delays in secondary control [37] or the implementation of electrical cars as control entities in the power grid [12].

Overall, Decentral Smart Grid Control is a simple and concrete smart grid concept that removes

most privacy concerns and potential security issues by design since no communication is necessary. Beyond purely implementing the framework mathematically, we have also investigated its stability. Since it provides additional effective damping for the system, the grid becomes more robust against perturbations, see the next paragraph.

Continuous perturbations. Power grids are subject to fluctuations due to demand variability, power fluctuations of renewable energy generators and trading [82, 83, 105]. In particular, renewable generation poses new risks by introducing jump noise in solar power [9] and heavy tails in wind power [93]. However, a systematic understanding of the impact of these fluctuations on the power grid is not yet established. Important questions include: Can fluctuations desynchronize the grid and under which conditions? How do fluctuations impact the power quality and what are appropriate ways to control the grid in the presence of fluctuations? Which noise distributions are suitable to model uncertainties in power grids?

We answer some of these questions in Chapters 5 and 6. First, we have investigated the impact of fluctuations on the stability in Chapter 5. If the grid is highly loaded and small fluctuations of the power disturb it often enough, it desynchronizes after a finite escape time. To assess the risks of this escape, we have formulated a Fokker-Planck equation for the full power grid system and approximated its solution using Kramer's escape rate. Effectively, we have thereby mapped the power grid problem to a stochastically driven Brownian particle in a tilted washboard potential. By that, we have obtained an analytical expression for the escape rate in small systems, identifying increasing damping and adding transmission capacity as main tools to prevent an escape. Furthermore, we have extended this to networks, where we have identified weak links that are most vulnerable to the desynchronization.

Complementary research includes work by Schmietendorf et al. [136], which also investigates escape rates of the power grid subject to random noise. However, the authors use a more detailed model of the noise based on solar and wind recordings, i.e., the escape process includes heavy tails and time correlation of the noise leading to additional bursts not present in Gaussian noise. Unfortunately, this prevents analytical results but only allows numerical investigations. Hence, the analytical scaling of the escape time as a function of inertia, damping and other power grid parameters is accessible in our simplified framework but not in the more detailed one, which is numerically treated. Nevertheless, the work by Schmietendorf et al. [136] points into the direction of future research. They find that escape rates are dominated by correlation effects of the noise, not necessarily heavy tails of the noise. Therefore, the next step to extend the results provided in Chapter 5 is to formulate the Fokker-Planck equation for correlated Gaussian noise and extract escape times for that. Given that Fokker-Planck equations with correlated noise are much harder to solve, this constitutes an entire new project.

Adding to the desynchronization studies, which constitute extreme events, Chapter 6 investigates the impacts of these fluctuations on the daily power quality, i.e., how much the grid is driven away from its steady operating grid frequency of $f = 50$ Hz or $f = 60$ Hz. Grid operators are quite strict on how much the grid frequency is allowed to vary over time so that fluctuations in Continental Europe are typically much less than $\Delta f = 200$ mHz [45]. However, controlling the system does not necessarily come with the understanding of how fluctuations of renewables and demand impact the power quality. To provide this understanding, we have investigated effects of fluctuations in detail. First, we have collected frequency data of different regions in Europe, the USA and Japan for different

years. Analyzing these data has revealed non-Gaussian effects, rarely considered before [53, 69, 90, 177, 182]. In particular, the frequency distributions are either heavy-tailed or skewed compared to Normal distributions. For a mathematical understanding, we have formulated a Fokker-Planck equation for the bulk (average) frequency of the grid. We have thereby derived the exact scaling of the fluctuations, revealing damping as a key factor in reducing fluctuation risk. Finally, we have also shown how superstatistics [16, 157] may be applied to power grid frequency fluctuations. Superstatistics explain heavy-tailed distributions by a superposition of multiple Gaussian distributions. This complementary approach might prove useful when optimizing flows for microgrids [81] or renewables connected to the full grid [117].

To conclude, effective damping benefits a system subject to fluctuations, both regarding desynchronization and power quality. Thereby, Decentral Smart Grid Control, which provides additional effective damping due the demand control, may be used in the future to counter-act fluctuations.

Discrete Perturbations. Most large-scale blackouts in recent history, regardless whether they took place in North America [101], Europe [26], India [28] or Australia [148], involved a cascade of failures after an initial perturbation of a stressed system. In the reports describing the course of the blackout, each cascade starts after one critical element failed, resulting in a quickly evolving cascade phenomenon that often leads to the blackout of the full grid [19, 25]. To avoid cascades, it is highly desirable to identify critical links that may cause such a large scale blackout and design counter measures stopping or containing cascades before they unpower the whole network. However, existing analysis on cascades in power grids has often used static flow analysis, missing out the dynamical features mentioned above [33, 34, 68, 71, 115, 120, 173].

Therefore, we have investigated the nature of these cascading events including dynamical transients of the power grid frequency and power flows in Chapter 7. This analysis is complementary to the one concerned with continuous perturbations studied in Chapters 5 and 6, which correspond to many small events as they happen every day, while failures constitute extreme events that occur only rarely but could have much more severe implications. In our treatment of cascades, we have developed a combined dynamical and event-based framework, i.e., the failure of a transmission line is modeled as a discrete event while the flows on all lines are updated continuously in time, using a dynamical description of the grid in form of the swing equation. Our framework has revealed additional line failures and in general larger cascades compared to the static flow analysis, stressing the relevance of dynamical effects. Furthermore, we have performed a statistical analysis of cascades on different grid topologies, based on high voltage transmission grids of some European countries including Great Britain and France. We have revealed that most links of the network cause no cascade or only small ones while a few critical links exist, which may cause a complete desynchronization and disconnection of the power grid. As it is crucial to identify these critical links, we have developed a predictor based on the dynamical flows of the network. In identifying critical links it outperforms any alternative predictors based on static flows [120] or the topology [63, 124]. Thereby, we provide a tool for grid operators to predict where to strengthen the grid to avoid weak points. Finally, we have found that observing the propagation of cascades in an appropriate metric, the effective distance [22], implies an almost constant propagation speed of the cascade.

Despite the progress made, there remains at least one large issue, namely how to dynamically

contain or stop cascading failures. The observed propagation speed ($c_{\text{cascade}} \approx 1 \text{ line/s}$) sets a time scale, during which preventive actions have to be taken (tens to hundreds of milliseconds). However, it remains an open question what these actions are. Very recent, unpublished work [178] again highlights the importance of the topic and the necessity to model it dynamically.

In conclusion, we demonstrate the importance of dynamics when investigating cascades in power grids, identify critical links and observe a nearly constant propagation. Compared to other studies on cascades, we use a dynamical treatment of flows [33, 34, 68, 71, 115, 120, 173] and an absolute flow threshold of each line instead of relative ones [97, 144], thereby revealing additional network vulnerabilities and the propagation of the cascades through the network.

Choice of the model and limitations. Most of the analysis presented here has made use of the *swing equation*, a non-linear second order ordinary differential equation. While this equation constitutes a very low detailed approach to power grids, it critically allows analytical methods. In contrast, very sophisticated power system simulation software, like PSS[®]E by Siemens [143] or PowerFactory by DlgSILENT [36], allow a thorough and complete modeling of individual technical elements with all their real parameters. However, these models are typically so complex that the stability analysis is carried out by simulating individual failure scenarios on a few selected grids [11, 30, 127] or alternatively applying brute-force simulations, where every possible failure in the network is tested [177]. Therefore, a reduced model like the swing equation has the great advantage of allowing statements beyond specific scenarios. For example, the swing equation, as introduced in [55, 121], might help to gain analytical insight, see e.g., [89], while still covering realistic effects. In addition, it is often used in engineering literature and text books [76, 86], providing a link between our work and the engineering community. Alternative and more complex models, like “higher-order models” [11, 135], do include voltage effects and consider additional dynamics of the electromagnetic fields in the generator. However, we have not found qualitative differences when comparing effects of the 2nd order and the 3rd order models, see Chapters 5 and 7, justifying the easier approach when possible.

Still, we should mention the limitations of the model. We have assumed nearly constant voltage in most calculations and have neglected ohmic losses. Both assumptions are well justified in high voltage transmission grids [86]. However, they are no longer necessarily valid for lower voltage transmission or distribution grids, where at least ohmic losses are more important due to different line parameters and the lower voltage. Quantitative effects of higher order models [11] might be important for a very realistic system analysis. But more importantly, very specific settings, e.g., the electronic response of solar cells or plug-in electric vehicles, with their individual voltage-current dynamics are not considered in our approach but would require a much more detailed model. Finally, the swing equation assumes a swinging oscillator, in our case a synchronous machine. Inverters however, are important for coupling renewable generation to the power grid and are no synchronous machines. Nevertheless, they may still be operated as if they were such machines [134, 145, 146]. Our modeling approach does not explicitly cover the details of this power electronics nor other effects of directed currents, e.g., when used in high voltage directed current transmission (HVDC) [70].

Outlook and technical applications. What is the impact of the presented results? How may they prove useful in establishing a 100% sustainable electricity supply? Where do we contribute to

the progress of theoretical physics? As a theoretical thesis we mainly intend to highlight opportunities and point out risks of certain power grid design principles instead of discussing, e.g., individual grid extension projects. We thereby provide an essential foundation to build upon when implementing control mechanisms or detecting vulnerable links. Broken down to the different topics covered here, this means:

Implementing self-organized dynamics in power grids, as proposed by Decentral Smart Grid Control in Chapters 3 and 4, was not done so far, but a recent patent [164] suggests the potential application in the near future. Price incentives for power grid control are easiest implemented in islanded grids, e.g., microgrids [81,146]. Within a microgrid the price would then be constant but different connected microgrids could have different prices. This leads to the concept of nodal pricing [141,149], i.e., different prices for different sub-regions of a large synchronous region, e.g., the Continental European grid. However, this is in stark contrast to current grid design and philosophy, at least in large parts of Europe, where electricity is sold for one price in a large region, e.g., all of Germany [44,45,74]. Hence, Decentral Smart Grid Control might be best applied first in (geographical) islands, which have their isolated power grid and where back-up generation currently is supplied via expensive Diesel generators [163] and thereby cost reductions by this flexibility scheme are most significant.

Within the current power grid system, we provide several useful tools, in particular for grid operators and planners. We have identified critical links both in the context of large cascading failures in Chapter 7 and in the context of continuous fluctuations of Chapter 5. While discussing grid extensions [48], critical links should thereby easily be avoided by construction of additional lines or increased transmission capacity. Furthermore, the scaling of fluctuations given in Chapter 6 either allows to set realistic power quality standards, given the parameters of the grid, or alternatively engineer the grid to be able to reach a desired quality, e.g., when setting up a microgrid [81].

From a theoretical perspective, Decentral Smart Grid Control motivates a Kuramoto-like model with a delay-term that is placed in the damping, instead of the coupling as mainly done before [180]. Furthermore, analysis of this model has revealed a fascinating, delay-dependent global attractor in Chapter 4. In addition, we have extended superstatistics for the first time to skewed distributions instead of only applying it to heavy tails [15,16,17]. Moreover, our investigation of cascading failures have demonstrated the propagation of desynchronization through a network of oscillators.

Finally, any prediction should be tested against experimental data, if possible. While the derivation of the scaling of frequency fluctuations in power grids in Chapter 6 has been build based on available data, this is not possible for all topics. For example, our treatment of cascades in Chapter 7 has been motivated by real cascading events [26,28,148] but experiments under realistic conditions seem impossible since a large network would be needed and cascades could easily damage the equipment. Therefore, recording as much data as possible during future cascading failures seems the only viable option. In contrast, results obtained for Decentral Smart Grid Control and its delayed stability analysis presented in Chapters 3 and 4, would be very interesting to investigate in an experimental setup. Currently, we are collaborating with an experimental group using inverter technology [18] to validate some of our theoretical findings. First, we want to experimentally validate the existence of Braess' paradox [171] in power grids. Braess' paradox arises when adding a line, decreases the ability of the grid to stabilize and transfer power. Although this phenomenon is not part of this thesis, its resulting

overloads have to be avoided when planning grids. Next, we aim to implement a demand-response following our proposal of Decentral Smart Grid Control. In particular, it is interesting to operate solar cells or batteries in a test grid using our approach to further test its viability in realistic settings. Especially, the impact of the delay on the stability, which was rarely studied so far [95], seems highly relevant to be tested. In the context of delays, the previously discovered perfect stability, i.e., the ability of the grid to synchronize regardless of its initial conditions, is very interesting to be realized in an experiment. Finally, we will study the impact of fluctuations in an islanded microgrid, verifying results from Chapters 5 and 6.

Overall, we hope that this thesis contributes to the understanding of power grids as complex dynamical systems and will eventually support establishing a 100% sustainable power system.

Acknowledgments

I am very proud of this thesis, which would not have been possible without the support of my family, many dear friends and colleagues.

First, I would like to thank my thesis committee for accompanying me during this task. Thank you, Marc and Dirk for supporting me from the first day of my thesis, responding to my many requests for proof-reading of abstracts, manuscripts and this thesis. Thank you also for the many lessons on science structure, advise and scientific discussions.

I am very thankful for the critical comments and questions raised by Prof. Zippelius during the thesis committee meetings. It was always beneficial to have another view on my results.

Many thanks to Xiaozhu and Debsankha as well as all other CoNDyNet partners and the whole Network Dynamics group for continuous inspiration on several conferences, workshops and personal discussion.

The last two chapters of this thesis arose from very fruitful collaborations abroad. Hence, I would like to thank Vito Latora, Christian Beck (London) and Kazuyuki Aihara (Tokyo) for their hospitality and the stimulating discussions. Traveling during my PhD to experience a different country and working environment was very interesting and fun.

I want to thank the offices of GGNB in general and the PBCS office in particular, as they have been very helpful for any administrative questions, stipends during my thesis, travel grants and on top they offered great courses.

In addition, I want to thank the staff of the Max Planck Institute for Dynamics and Self-Organization, in particular Ayse, Barbara and Monika who assisted with traveling, contracts and more.

I acknowledge financial support by the excellence stipend by GGNB (DFG Grant GSC 226/2) which I received the longest time of my PhD thesis. Furthermore, I thank the JSPS for enabling my stay in Japan.

Finally, as much as I enjoy work, I am very grateful to all my friends and colleagues for all the time spend not worrying about referee reports or plotting issues. In particular, I had much fun saving the world together with Malte, Diemut, Jana and Nina during several board game evenings.

Thanks to all the proof-readers of my thesis that were not mentioned yet, in particular, DschO and Thomas.

Danke an meine Rollenspielrunde, die mich von meinen ersten Tagen in Göttingen durchgehend begleitet hat: Anna, Arne, Roland, Tim, Martin, Marc und Olaf. Es war schön so mit offenen Armen empfangen zu werden.

Ein großer Dank geht an meine Familie, die mich nicht nur finanziell sondern auch moralisch immer unterstützt hat. Danke, dass ihr immer an mich geglaubt habt.

Das Beste zum Schluss: Lieben Dank an Meike, die wissenschaftliche Diskussionen genauso unterstützt hat wie abendliche Zerstreung oder mich zu einem Spaziergang verdonnert hat, damit ich auch einmal pro Tag das Haus verlasse. Unsere gemeinsame Zeit war der perfekte Ruhepol, um Kraft für das Schreiben dieser Arbeit zu sammeln.

Bibliography

- [1] 50Hertz Transmission GmbH. Annual report 2016. http://www.50hertz.com/Portals/3/Content/Dokumente/Medien/Publikationen/2016/50Hertz_GB_Gesamt_E_Web.pdf, 2016.
- [2] 50Hertz Transmission GmbH and Amprion and TenneT TSO and TransnetBW. Netzentwicklungsplan Strom. <http://www.netzentwicklungsplan.de>, 2012.
- [3] Kodjo Agbossou, Mohanlal Kolhe, Jean Hamelin, and Tapan K. Bose. Performance of a stand-alone renewable energy system based on energy storage as hydrogen. *IEEE Transactions on Energy Conversion*, 19(3):633–640, 2004.
- [4] Mohamed H. Albadi and Ehab F. El-Saadany. A Summary of Demand Response in Electricity Markets. *Electric Power Systems Research*, 78(11):1989–1996, 2008.
- [5] Réka Albert, Hawoong Jeong, and Albert-László Barabási. Error and attack tolerance of complex networks. *Nature*, 406(6794):378–382, 2000.
- [6] Massoud Amin and Bruce F. Wollenberg. Toward a smart grid: power delivery for the 21st century. *IEEE Power and Energy Magazine*, 3(5):34, 2005.
- [7] Paul M. Anderson and Aziz A. Fouad. *Power System Control and Stability*. John Wiley & Sons, 2008.
- [8] Marian Anghel, Kenneth A Werley, and Adilson E Motter. Stochastic model for power grid dynamics. In *System Sciences, 2007. HICSS 2007. 40th Annual Hawaii International Conference on*, pages 113–113. IEEE, 2007.
- [9] Mehrnaz Anvari, Gerald Lohmann, Matthias Wächter, Patrick Milan, Elke Lorenz, Detlev Heinemann, Mohammad R. R. Tabar, and Joachim Peinke. Short term fluctuations of wind and solar power systems. *New Journal of Physics*, 18(6):063027, 2016.
- [10] Robert C. Armstrong, Catherine Wolfram, Krijn P. de Jong, Robert Gross, Nathan S. Lewis, Brenda Boardman, Arthur J. Ragauskas, Karen Ehrhardt-Martinez, George Crabtree, and M. V. Ramana. The frontiers of energy. *Nature Energy*, 1(1), 2016.
- [11] Sabine Auer, Kirsten Kleis, Paul Schultz, Jürgen Kurths, and Frank Hellmann. The impact of model detail on power grid resilience measures. *European Physical Journal Special Topics*, 225(3):609–625, 2016.

-
- [12] Sabine Auer, Casper Roos, Jobst Heitzig, Frank Hellmann, and Jürgen Kurths. The contribution of different electric vehicle control strategies to dynamical grid stability. *arXiv preprint arXiv:1708.03531*, 2017.
- [13] Australian Bureau of Statistics. Australian demographic statistics, dec 2016. <http://www.abs.gov.au/ausstats/abs@nsf/mf/3101.0>, 2017.
- [14] Albert-László Barabási and Réka Albert. Emergence of scaling in random networks. *Science*, 286(5439):509–512, 1999.
- [15] Christian Beck. Dynamical foundations of nonextensive statistical mechanics. *Physical Review Letters*, 87(18):180601, 2001.
- [16] Christian Beck and Ezechiele G. D. Cohen. Superstatistics. *Physica A*, 322:267–275, 2003.
- [17] Christian Beck, Ezechiele GD Cohen, and Harry L Swinney. From time series to superstatistics. *Physical Review E*, 72(5):056133, 2005.
- [18] Hans-Peter Beck and Ralf Hesse. Virtual synchronous machine. In *Electrical Power Quality and Utilisation, 2007. EPQU 2007. 9th International Conference on*, pages 1–6. IEEE, 2007.
- [19] Janusz W. Bialek. Why has it happened again? Comparison between the UCTE blackout in 2006 and the blackouts of 2003. In *Power Tech, 2007 IEEE Lausanne*, pages 51–56. IEEE, 2007.
- [20] Alberto Borghetti, Mauro Bosetti, Samuele Grillo, Stefano Massucco, Carlo Alberto Nucci, Mario Paolone, and Federico Silvestro. Short-term scheduling and control of active distribution systems with high penetration of renewable resources. *IEEE Systems Journal*, 4(3):313–322, 2010.
- [21] Godfrey Boyle. *Renewable Energy*. Oxford University Press, Oxford, 2004.
- [22] Dirk Brockmann and Dirk Helbing. The hidden geometry of complex, network-driven contagion phenomena. *Science*, 342(6164):1337–1342, 2013.
- [23] Charles D. Brummitt, Paul D. H. Hines, Ian Dobson, Christopher Moore, and Raissa M. D’Souza. Transdisciplinary electric power grid science. *Proceedings of the National Academy of Sciences*, 110(30):12159, 2013.
- [24] Business Wire. Duration of power outages decreasing due to bge electric system upgrades. <http://www.businesswire.com/news/home/20160525006405/en/Duration-Power-Outages-Decreasing-Due-BGE-Electric>, 2016.
- [25] Sergey V. Buldyrev, Roni Parshani, Gerald Paul, H. Eugene Stanley, and Shlomo Havlin. Catastrophic cascade of failures in interdependent networks. *Nature*, 464(7291):1025–1028, 2010.
- [26] Bundesnetzagentur für Elektrizität, Telekommunikation und Gas. Post und eisenbahnen. bericht über die systemstörung im deutschen und europäischen verbundsystem am 4. Technical report, Technical report, German Federal Regulatory Agency for Electricity, Gas, Telecommunications, Postal and Railway Systems, Berlin, Germany, 2006.

- [27] Mauro Calabria, Walter Schumacher, Josep M Guerrero, Juan C Vasquez, and Xin Zhao. Stability analysis and design of the improved droop controller on a voltage source inverter. In *2015 IEEE 6th International Symposium on PEDG*, pages 1–9. IEEE, 2015.
- [28] Central Electricity Regulatory Commission (CERC). Report on the grid disturbances on 30th july and 31st july 2012. http://www.cercind.gov.in/2012/orders/Final_Report_Grid_Disturbance.pdf.
- [29] Margaret Cheney. *Tesla: Man out of time*. Simon and Schuster, 2011.
- [30] Kristien Clement-Nyns, Edwin Haesen, and Johan Driesen. The impact of charging plug-in hybrid electric vehicles on a residential distribution grid. *IEEE Transactions on Power Systems*, 25(1):371–380, 2010.
- [31] Samuel Cohen and Robert J. Elliott. *Stochastic calculus and applications*. Birkhäuser, 2015.
- [32] Felix Creutzig, Peter Agoston, Jan Christoph Goldschmidt, Gunnar Luderer, Gregory Nemet, and Robert C. Pietzcker. The underestimated potential of solar energy to mitigate climate change. *Nature Energy*, 2:17140, 2017.
- [33] Paolo Crucitti, Vito Latora, and Massimo Marchiori. Model for cascading failures in complex networks. *Physical Review E*, 69(4):045104, 2004.
- [34] Paolo Crucitti, Vito Latora, and Massimo Marchiori. A topological analysis of the italian electric power grid. *Physica A*, 338(1):92–97, 2004.
- [35] Keith Dennis, Ken Colburn, and Jim Lazar. Environmentally beneficial electrification: The dawn of emissions efficiency. *The Electricity Journal*, 29(6):52–58, 2016.
- [36] DIgSILENT GmbH. Powerfactory, 2017.
- [37] Eric D. Dongmo, Pere Colet, and Paul Wofo. Power grid enhanced resilience using proportional and derivative control with delayed feedback. *The European Physical Journal B*, 90(1):6, 2017.
- [38] Florian Dörfler and Francesco Bullo. Synchronization in complex networks of phase oscillators: A survey. *Automatica*, 50(6):1539–1564, 2014.
- [39] Florian Dörfler, Michael Chertkov, and Francesco Bullo. Synchronization in Complex Oscillator Networks and Smart Grids. *Proceedings of the National Academy of Sciences*, 110(6):2005–2010, 2013.
- [40] Florian Dörfler, John W. Simpson-Porco, and Francesco Bullo. Breaking the hierarchy: Distributed control and economic optimality in microgrids. *IEEE Transactions on Control of Network Systems*, 3(3):241–253, 2016.
- [41] Rodney D. Driver. Introduction to Delay Differential Equations. In *Ordinary and Delay Differential Equations*, pages 225–267. Springer, 1977.

- [42] Ottmar Edenhofer, Ramon Pichs-Madruga, Youba Sokona, Kristin Seyboth, Patrick Matschoss, Susanne Kadner, Timm Zwickel, Patrick Eickemeier, Gerrit Hansen, Steffen Schlömer, et al. Ipcc special report on renewable energy sources and climate change mitigation. *Prepared By Working Group III of the Intergovernmental Panel on Climate Change, Cambridge University Press, Cambridge, UK*, 2011.
- [43] Electricité de France. Facts & figures. https://www.edf.fr/sites/default/files/contrib/groupe-edf/espaces-dedies/espace-finance-en/financial-information/publications/facts-figures/f_f_2015_va.pdf, 2016.
- [44] ENTSO-E. Statistical factsheet 2014. <https://www.entsoe.eu/publications/major-publications/Pages/default.aspx>.
- [45] ENTSO-E. Network code on requirements for grid connection applicable to all generators (rfg). <https://www.entsoe.eu/major-projects/network-code-development/requirements-for-generators/>, March 2013.
- [46] ENTSO-E. Regional groups. <https://www.entsoe.eu/about-entso-e/system-operations/regional-groups/Pages/default.aspx>, 2016.
- [47] ENTSO-E. Statistical factsheet 2015. https://www.entsoe.eu/Documents/Publications/Statistics/Factsheet/entsoe_sfs2015_web.pdf, 2016.
- [48] ENTSO-E. Ten year network development plan 2016, 2016.
- [49] Paul Erdős and Alfréd Rényi. On random graphs, i. *Publicationes Mathematicae (Debrecen)*, 6:290–297, 1959.
- [50] Göran N. Ericsson. Cyber Security and Power System Communication - Essential Parts of a Smart Grid Infrastructure. *IEEE Transactions on Power Delivery*, 25(3):1501–1507, 2010.
- [51] Mehdi Etezadi-Amoli, Kent Choma, and Jason Stefani. Rapid-charge electric-vehicle stations. *IEEE Transactions on Power Delivery*, 25(3):1883–1887, 2010.
- [52] Alexander Eydeland and Krzysztof Wolyniec. *Energy and power risk management: New developments in modeling, pricing, and hedging*, volume 206. John Wiley & Sons, 2003.
- [53] Xi Fang, Satyajayant Misra, Guoliang Xue, and Dejun Yang. Smart Grids - The new and improved Power Grid: A Survey. *Communications Surveys & Tutorials, IEEE*, 14(4):944–980, 2012.
- [54] Hassan Farhangi. The path of the smart grid. *IEEE power and energy magazine*, 8(1), 2010.
- [55] Giovanni Filatrella, Arne H. Nielsen, and Niels F. Pedersen. Analysis of a Power Grid using a Kuramoto-like Model. *The European Physical Journal B*, 61(4):485–491, 2008.
- [56] Crispin W. Gardiner. *Handbook of stochastic methods*, volume 3. Springer Berlin, 1985.

- [57] Keqin Gu, Vladimir L. Kharitonov, and Jie Chen. *Stability of Time-delay Systems*. Springer Science & Business Media, 2003.
- [58] Shelby J. Habermann. *Advanced statistics, volume i: description of populations*, 1996.
- [59] Chris Harris. *Electricity markets: pricing, structures and economics*, volume 565. John Wiley & Sons, 2011.
- [60] Benjamin P. Heard, Barry W. Brook, Tom M. L. Wigley, and Corey J. A. Bradshaw. Burden of proof: A comprehensive review of the feasibility of 100% renewable-electricity systems. *Renewable and Sustainable Energy Reviews*, 76:1122–1133, 2017.
- [61] Dominik Heide, Lueder Von Bremen, Martin Greiner, Clemens Hoffmann, Markus Speckmann, and Stefan Bofinger. Seasonal Optimal Mix of Wind and Solar Power in a Future, Highly Renewable Europe. *Renewable Energy*, 35(11):2483–2489, 2010.
- [62] Klaus Heuck, Klaus-Dieter Dettmann, and Detlef Schulz. *Elektrische energievorsorgung: erzeugung, übertragung und verteilung elektrischer energie für studium und praxis*. Springer-Verlag, 2010.
- [63] Paul Hines, Eduardo Cotilla-Sanchez, and Seth Blumsack. Do topological models provide good information about electricity infrastructure vulnerability? *Chaos: An Interdisciplinary Journal of Nonlinear Science*, 20(3):033122, 2010.
- [64] Hannele Holttinen. Impact of hourly wind power variations on the system operation in the nordic countries. *Wind Energy*, 8(2):197–218, 2005.
- [65] Intergovernmental Panel on Climate Change. *Climate Change 2014—Impacts, Adaptation and Vulnerability: Regional Aspects*. Cambridge University Press, 2014.
- [66] Ali Ipakchi and Farrokh Albuyeh. Grid of the future. *IEEE Power and Energy Magazine*, 7(2):52–62, 2009.
- [67] Mark Z. Jacobson and Mark A. Delucchi. Providing all global energy with wind, water, and solar power, part i: Technologies, energy resources, quantities and areas of infrastructure, and materials. *Energy Policy*, 39(3):1154–1169, 2011.
- [68] Chuanyi Ji, Yun Wei, Henry Mei, Jorge Calzada, Matthew Carey, Steve Church, Timothy Hayes, Brian Nugent, Gregory Stella, Matthew Wallace, et al. Large-scale data analysis of power grid resilience across multiple us service regions. *Nature Energy*, 1:16052, 2016.
- [69] Yaochu Jin and Jürgen Branke. Evolutionary optimization in uncertain environments—a survey. *IEEE Transactions on Evolutionary Computation*, 9(3):303–317, 2005.
- [70] Edward W. Kimbark. *Direct current transmission*, volume 1. John Wiley & Sons, 1971.
- [71] Ryan Kinney, Paolo Crucitti, Reka Albert, and Vito Latora. Modeling cascading failures in the north american power grid. *The European Physical Journal B*, 46(1):101–107, 2005.

- [72] Meir Klein, Graham J. Rogers, and Prabha Kundur. A fundamental study of inter-area oscillations in power systems. *IEEE Transactions on Power Systems*, 6(3):914–921, 1991.
- [73] Peter E. Kloeden and Eckhard Platen. Higher-order implicit strong numerical schemes for stochastic differential equations. *Journal of Statistical Physics*, 66(1):283–314, 1992.
- [74] Raimund M. Kovacevic, Georg C. Pflug, and Maria T. Vespucci. *Handbook of risk management in energy production and trading*. Springer, 2013.
- [75] Hendrik A. Kramers. Brownian motion in a field of force and the diffusion model of chemical reactions. *Physica*, 7(4):284–304, 1940.
- [76] Prabha Kundur, Neal J Balu, and Mark G Lauby. *Power system stability and control*, volume 7. McGraw-hill New York, 1994.
- [77] Yoshiki Kuramoto. Self-entrainment of a population of coupled non-linear oscillators. In H. Araki, editor, *International Symposium on on Mathematical Problems in Theoretical Physics*, Lecture Notes in Physics Vol. 39, page 420, New York, 1975. Springer.
- [78] Yoshiki Kuramoto. *Chemical oscillations, waves, and turbulence*, volume 19. Springer Science & Business Media, 2012.
- [79] Darka Labavić, Raluca Suci, Hildegard Meyer-Ortmanns, and Stefan Kettmann. Long-range response to transmission line disturbances in dc electricity grids. *arXiv preprint arXiv:1406.4699*, 2014.
- [80] Lei Lai, Hao T. Zhang, Chun S. Lai, Fang Y. Xu, and Sukumar Mishra. Investigation on july 2012 indian blackout. In *2013 International Conference on Machine Learning and Cybernetics (ICMLC)*, volume 1, pages 92–97. IEEE, 2013.
- [81] Robert H. Lasseter and Paolo Paigi. Microgrid: A conceptual solution. In *2004 IEEE 35th Annual Power Electronics Specialists Conference (PESC)*, volume 6, pages 4285–4290. IEEE, 2004.
- [82] Mark G. Lauby, Jessica J. Bian, Svetlana Ekisheva, and Matthew Varghese. Frequency response assessment of ercot and québec interconnections. In *2014 North American Power Symposium (NAPS)*, pages 1–5. IEEE, 2014.
- [83] Xiangjun Li, Dong Hui, and Xiaokang Lai. Battery energy storage station (bess)-based smoothing control of photovoltaic (pv) and wind power generation fluctuations. *IEEE Transactions on Sustainable Energy*, 4(2):464–473, 2013.
- [84] Henrik Lund. Renewable energy strategies for sustainable development. *Energy*, 32(6):912–919, 2007.
- [85] Jinpeng Ma, Yong Sun, Xiaoming Yuan, Jürgen Kurths, and Meng Zhan. Dynamics and collapse in a power system model with voltage variation: The damping effect. *PloS one*, 11(11):e0165943, 2016.

-
- [86] Jan Machowski, Janusz Bialek, and James Bumby. *Power System Dynamics: Stability and Control*. John Wiley & Sons, 2011.
- [87] Debsankha Manik, Martin Rohden, Henrik Ronellenfitsch, Xiaozhu Zhang, Sarah Hallerberg, Dirk Witthaut, and Marc Timme. Network susceptibilities: theory and applications. *arXiv preprint arXiv:1609.04310*, 2016.
- [88] Debsankha Manik, Marc Timme, and Dirk Witthaut. Cycle flows and multistability in oscillatory networks: an overview. *arXiv preprint arXiv:1611.09825*, 2016.
- [89] Debsankha Manik, Dirk Witthaut, Benjamin Schäfer, Moritz Matthiae, Andreas Sorge, Martin Rohden, Eleni Katifori, and Marc Timme. Supply Networks: Instabilities without Overload. *The European Physical Journal Special Topics*, 223(12):2527–2547, 2014.
- [90] Moritz Matthiae, Benjamin Schäfer, Xiaozhu Zhang, Martin Rohden, Marc Timme, and Dirk Witthaut. Escape routes, weak links, and desynchronization in fluctuation-driven networks. *arXiv preprint arXiv:1611.08365*, 2016.
- [91] Peter J. Menck, Jobst Heitzig, Jürgen Kurths, and Hans Joachim Schellnhuber. How dead ends undermine power grid stability. *Nature Communications*, 5, 2014.
- [92] Peter J. Menck, Jobst Heitzig, Norbert Marwan, and Jürgen Kurths. How Basin Stability Complements the Linear-stability Paradigm. *Nature Physics*, 9(2):89–92, 2013.
- [93] Patrick Milan, Matthias Wächter, and Joachim Peinke. Turbulent Character of Wind Energy. *Physical Review Letters*, 110(13):138701, 2013.
- [94] Patrick Milan, Matthias Wächter, and Joachim Peinke. Stochastic modeling and performance monitoring of wind farm power production. *Journal of Renewable and Sustainable Energy*, 6(3):033119, 2014.
- [95] Federico Milano and Marian Anghel. Impact of time delays on power system stability. *Circuits and Systems I: Regular Papers, IEEE Transactions on*, 59(4):889–900, 2012.
- [96] Ned Mohan and Tore M. Undeland. *Power electronics: converters, applications, and design*. John Wiley & Sons, 2007.
- [97] Adilson E. Motter and Ying-Cheng Lai. Cascade-based attacks on complex networks. *Physical Review E*, 66(6):065102, 2002.
- [98] Adilson E. Motter, Seth A. Myers, Marian Anghel, and Takashi Nishikawa. Spontaneous Synchrony in Power-grid Networks. *Nature Physics*, 9(3):191–197, 2013.
- [99] Biju Naduvathuparambil, Matthew C. Valenti, and Ali Feliachi. Communication delays in wide-area measurement systems. In *Southeastern Symposium on System Theory*, volume 34, pages 118–122. Citeseer, 2002.
- [100] NASA Goddard Space Flight Center. Europe at night. <https://www.flickr.com/photos/gsfrc/12350431693>, February 2014.

- [101] New York Independent System Operator. Interim report on the august 14, 2003, blackout. <https://www.hks.harvard.edu/hepg/Papers/NYISO.blackout.report.8.Jan.04.pdf>, 2004.
- [102] Mark Newman. *Networks: An Introduction*. Oxford University Press, Inc., New York, NY, USA, 2010.
- [103] Takashi Nishikawa and Adilson E. Motter. Comparative analysis of existing models for power-grid synchronization. *New Journal of Physics*, 17(1):015012, 2015.
- [104] Barack H. Obama. Presidential policy directive 21: Critical infrastructure security and resilience. *Washington, DC*, 2013.
- [105] National Academies of Sciences Engineering and Medicine. *The Power of Change: Innovation for Development and Deployment of Increasingly Clean Electric Power Technologies*. The National Academies Press, 2016.
- [106] Oliver Wyman. Digitaler datenklaue bedroht internationale transportketten. howpublished = "<http://www.oliverwyman.de/our-expertise/insights/2017/jun/time-for-transportation-and-logistics-to-up-its-cybersecurity.html>", 2017.
- [107] Opte Project. Image of the internet. <http://www.opte.org>, 2005.
- [108] Sakshi Pahwa, Caterina Scoglio, and Antonio Scala. Abruptness of cascade failures in power grids. *Scientific Reports*, 4:3694, 2014.
- [109] Peter Palensky and Dietmar Dietrich. Demand Side Management: Demand Response, Intelligent Energy Systems, and Smart Loads. *IEEE Transactions on Industrial Informatics*, 7(3):381–388, 2011.
- [110] Joachim Peinke, Malte Siefert, Stephan Barth, Christoph Renner, Falk Riess, Matthias Wächter, and Rudolf Friedrich. Fat tail statistics and beyond. In *Advances in Solid State Physics*, pages 363–373. Springer, 2004.
- [111] Nicole Perloth, Mark Scott, and Sheera Frenkel. Cyberattack Hits Ukraine Then Spreads Internationally. New York Times <https://www.nytimes.com/2017/06/27/technology/ransomware-hackers.html>, June 2017.
- [112] Thomas Petermann. *Gefährdung und Verletzbarkeit moderner Gesellschaften-am Beispiel eines großräumigen und langandauernden Ausfalls der Stromversorgung: Endbericht zum TA-Projekt*. TAB, 2010.
- [113] Helen Pidd. India blackouts leave 700 million without power. the guardian <https://www.theguardian.com/world/2012/jul/31/india-blackout-electricity-power-cuts>, 2012.
- [114] Arkady Pikovsky, Michael Rosenblum, and Jürgen Kurths. *Synchronization: a universal concept in nonlinear sciences*, volume 12. Cambridge university press, 2003.

- [115] Anton Plietzsch, Paul Schultz, Jobst Heitzig, and Jürgen Kurths Kurths. Local vs. global redundancy–trade-offs between resilience against cascading failures and frequency stability. *The European Physical Journal Special Topics*, 225(3):551–568, 2016.
- [116] Morten Grud Rasmussen, Gorm Bruun Andresen, and Martin Greiner. Storage and balancing synergies in a fully or highly renewable pan-european power system. *Energy Policy*, 51:642–651, 2012.
- [117] Yann Riffonneau, Seddik Bacha, Franck Barruel, and Stephane Ploix. Optimal power flow management for grid connected pv systems with batteries. *IEEE Transactions on Sustainable Energy*, 2(3):309–320, 2011.
- [118] Hannes Risken. *The Fokker-Planck Equation*. Springer, Berlin, 1984.
- [119] L. Chris G. Rogers and David Williams. *Diffusions, Markov processes and martingales: Volume 2, Itô calculus*, volume 2. Cambridge university press, 1994.
- [120] Martin Rohden, Daniel Jung, Samyak Tamrakar, and Stefan Kettemann. Cascading failures in ac electricity grids. *Physical Review E*, 94:032209, Sep 2016.
- [121] Martin Rohden, Andreas Sorge, Marc Timme, and Dirk Witthaut. Self-organized Synchronization in Decentralized Power Grids. *Physical Review Letters*, 109(6):064101, 2012.
- [122] Martin Rohden, Andreas Sorge, Dirk Witthaut, and Marc Timme. Impact of network topology on synchrony of oscillatory power grids. *Chaos: An Interdisciplinary Journal of Nonlinear Science*, 24(1):013123, 2014.
- [123] Martin Rohden, Dirk Witthaut, Marc Timme, and Hildegard Meyer-Ortmanns. Curing critical links in oscillator networks as power grid models. *arXiv preprint arXiv:1512.00611*, 2015.
- [124] Vittorio Rosato, Sandro Bologna, and Fabio Tiriticco. Topological properties of high-voltage electrical transmission networks. *Electric Power Systems Research*, 77(2):99–105, 2007.
- [125] Marc R. Roussel. *Delay-Differential Equations*, 2005.
- [126] Matthew N. O. Sadiku. *Elements of electromagnetics*. Oxford university press, 2014.
- [127] Javier Salmeron, Kevin Wood, and Ross Baldick. Analysis of electric grid security under terrorist threat. *IEEE Transactions on Power Systems*, 19(2):905–912, 2004.
- [128] Gennady Samorodnitsky and Murad S. Taqqu. *Stable Non-Gaussian Random Processes. Stochastic Models with Infinite Variance*. Chapman and Hall, 1994.
- [129] Benjamin Schäfer, Christian Beck, Kazuyuki Aihara, Dirk Witthaut, and Marc Timme. Non-gaussian power grid frequency fluctuations characterized by lévy-stable laws and superstatistics. *under review*, 2017.
- [130] Benjamin Schäfer, Carsten Grabow, Sabine Auer, Jürgen Kurths, Dirk Witthaut, and Marc Timme. Taming instabilities in power grid networks by decentralized control. *The European Physical Journal Special Topics*, 225(3):569–582, 2016.

-
- [131] Benjamin Schäfer, Moritz Matthiae, Marc Timme, and Dirk Witthaut. Decentral Smart Grid Control. *New Journal of Physics*, 17(1):015002, 2015.
- [132] Benjamin Schäfer, Moritz Matthiae, Xiaozhu Zhang, Martin Rohden, Marc Timme, and Dirk Witthaut. Escape routes, weak links, and desynchronization in fluctuation-driven networks. *Physical Review E*, 95(6):060203, 2017.
- [133] Benjamin Schäfer, Dirk Witthaut, Marc Timme, and Vito Latora. Dynamically induced cascading failures in supply networks. *arXiv preprint arXiv:1707.08018*, 2017.
- [134] Johannes Schiffer, Darina Goldin, Jorg Raisch, and Tefvik Sezi. Synchronization of droop-controlled microgrids with distributed rotational and electronic generation. In *2013 IEEE 52nd Annual Conference on Decision and Control (CDC)*, pages 2334–2339. IEEE, 2013.
- [135] Katrin Schmietendorf, Joachim Peinke, Rudolf Friedrich, and Oliver Kamps. Self-organized synchronization and voltage stability in networks of synchronous machines. *European Physical Journal Special Topics*, 223(12):2577–2592, 2014.
- [136] Katrin Schmietendorf, Joachim Peinke, and Oliver Kamps. On the stability and quality of power grids subjected to intermittent feed-in. *arXiv preprint arXiv:1611.08235*, 2016.
- [137] Hella Schreier. *Thomas Alva Edison*. Springer-Verlag, 2013.
- [138] Thomas Schröder and Wilhelm Kuckshinrichs. Value of Lost Load: An efficient economic indicator for power supply security? A literature review. *Frontiers in energy research*, 3:55, 2015.
- [139] Paul Schultz, Jobst Heitzig, and Jürgen Kurths. A random growth model for power grids and other spatially embedded infrastructure networks. *arXiv preprint arXiv:1602.02562*, 2016.
- [140] Fred C. Schweppe. Frequency Adaptive, Power-Energy Re-scheduler, #feb# 23 1982. US Patent 4,317,049.
- [141] Fred C. Schweppe, Michael C. Caramanis, Richard D. Tabors, and Roger E. Bohn. *Spot pricing of electricity*. Springer Science & Business Media, 2013.
- [142] Joe Short, David G. Infield, and Leon L. Freris. Stabilization of Grid Frequency through Dynamic Demand Control. *IEEE Transactions on Power Systems*, 22(3):1284–1293, 2007.
- [143] Siemens AG. Power transmission system planning software, 2017.
- [144] Ingve Simonsen, Lubos Buzna, Karsten Peters, Stefan Bornholdt, and Dirk Helbing. Transient dynamics increasing network vulnerability to cascading failures. *Physical Review Letters*, 100(21):218701, 2008.
- [145] John W. Simpson-Porco, Florian Dörfler, and Francesco Bullo. Droop-controlled inverters are kuramoto oscillators. *IFAC Proceedings Volumes*, 45(26):264–269, 2012.
- [146] John W. Simpson-Porco, Florian Dörfler, and Francesco Bullo. Synchronization and power sharing for droop-controlled inverters in islanded microgrids. *Automatica*, 49(9):2603–2611, 2013.

- [147] Ralph Sims, Pedro Mercado, Wolfram Krewitt, Gouri Bhuyan, Damian Flynn, Hannele Holttinen, Gilberto Jannuzzi, Smail Khennas, Yongqian Liu, Lars J Nilsson, Joan Ogden, Kazuhiko Ogimoto, Mark O'Malley, Hugh Outhred, Øystein Ulleberg, and Frans van Hulle. Integration of renewable energy into present and future energy systems. In O. Edenhofer et al., editor, *IPCC Special Report on Renewable Energy Sources and Climate Change Mitigation*. Cambridge University Press, Cambridge, United Kingdom, 2011.
- [148] Michael Slezak. South Australia's blackout explained. the guardian <https://www.theguardian.com/australia-news/2016/sep/29/south-australia-blackout-explained-renewables-not-to-blame>, 2016.
- [149] Paul M. Sotkiewicz and Jesus M. Vignolo. Nodal pricing for distribution networks: efficient pricing for efficiency enhancing dg. *IEEE Transactions on Power Systems*, 21(2):1013–1014, 2006.
- [150] Steven H. Strogatz. *Nonlinear dynamics and chaos: with applications to physics, biology, chemistry, and engineering*. Westview press, 2014.
- [151] Swissgrid. Various grid levels transport electricity. https://www.swissgrid.ch/swissgrid/en/home/grid/transmission_system/grid_levels.html, 2017.
- [152] Pavol Szalai. Edf scientific chief: A 100% renewable energy system is impossible. euractiv <https://www.euractiv.com/section/energy/interview/edf-scientific-chief-a-100-renewable-energy-system-is-technically-impossible-and-economically-unsustainable/>, July 2016.
- [153] Convention on Climate Change (UNFCCC) The 21st Conference of the Parties to the United Nations Framework. The Paris Agreement, 2015.
- [154] Marc Timme, Ljupco Kocarev, and Dirk Witthaut. Focus on networks, energy and the economy. *New Journal of Physics*, 17:110201, 2015.
- [155] Vincenzo Trovato, Simon H. Tindemans, and Goran Strbac. Demand response contribution to effective inertia for system security in the gb 2020 gone green scenario. In *2013 4th IEEE/PES Innovative Smart Grid Technologies Europe (ISGT EUROPE)*, pages 1–5. IEEE, 2013.
- [156] Constantino Tsallis. *Introduction to Nonextensive Statistical Mechanics*, volume 34. Springer, 2009.
- [157] Constantino Tsallis. Nonadditive entropy and nonextensive statistical mechanics-an overview after 20 years. *Brazilian Journal of Physics*, 39(2A):337–356, 2009.
- [158] John A. Turner. A Realizable Renewable Energy Future. *Science*, 285(5428):687–689, 1999.
- [159] Falko Ueckerdt, Robert Brecha, and Gunnar Luderer. Analyzing major challenges of wind and solar variability in power systems. *Renewable Energy*, 81:1–10, 2015.

- [160] Andreas Ulbig, Theodor S. Borsche, and Göran Andersson. Impact of low rotational inertia on power system stability and operation. *IFAC Proceedings Volumes*, 47(3):7290–7297, 2014.
- [161] U.S. Department of Energy. Eia-411: Coordinated bulk power supply and demand program report. <https://www.eia.gov/electricity/data/eia411/>, 2016.
- [162] Nicolaas G. van Kampen. *Stochastic processes in physics and chemistry*. Elsevier, Amsterdam, 1992.
- [163] Thomas Walter. Smart Grid neu gedacht: Ein Lösungsvorschlag zur Diskussion in VDE|ETG. <http://www.vde.com/de/fg/ETG/Pb1/MI/2014-01/Seiten/Homepage.aspx>, 2014.
- [164] Thomas Walter. Method for controlling the ratio between supplied and drawn electric energy in an electric supply network, 2016. EP2875560.
- [165] Duncan J. Watts and Steven H. Strogatz. Collective dynamics of small-world networks. *Nature*, 393(6684):440–442, 1998.
- [166] Peter H. Westfall. Kurtosis as Peakedness, 1905-2014. R.I.P. *The American Statistician*, 68(3):191–195, 2014.
- [167] Wikimedia. New york utility lines in 1890, 1913. public domain, Retrieved 04.07.2017.
- [168] Wikimedia. Map of of european transmission system operators organizations, 2006. by User:Kimdime, Retrieved 04.07.2017, Creative Commons Attribution-Share Alike 3.0.
- [169] Wikimedia. North american electric reliability corporation, 2009. by User:Bouchecl, Retrieved 04.07.2017, Creative Commons Attribution-Share Alike 3.0.
- [170] Dirk Witthaut, Martin Rohden, Xiaozhu Zhang, Sarah Hallerberg, and Marc Timme. Critical links and nonlocal rerouting in complex supply networks. *Physical Review Letters*, 116:138701, 2016.
- [171] Dirk Witthaut and Marc Timme. Braess’s Paradox in Oscillator Networks, Desynchronization and Power Outage. *New Journal of Physics*, 14(8):083036, 2012.
- [172] Dirk Witthaut and Marc Timme. Nonlocal failures in complex supply networks by single link additions. *The European Physical Journal B*, 86(9):1–12, 2013.
- [173] Dirk Witthaut and Marc Timme. Nonlocal effects and countermeasures in cascading failures. *Physical Review E*, 92(3):032809, 2015.
- [174] Jan Wohland, Mark Reyers, Carolin Märker, and Dirk Witthaut. Natural wind variability triggered drop in german redispatch volume and costs from 2015 to 2016. *submitted*, 2017.
- [175] Wolfram Research Inc. Some notes on internal implementation.
- [176] Wolfram Research Inc. Mathematica. Champaign, Illinois, 2017.

-
- [177] Allen J. Wood, Bruce F. Wollenberg, and Gerald B. Sheblé. *Power Generation, Operation and Control*. John Wiley & Sons, New York, 2013.
- [178] Yang Yang and Adilson E. Motter. Cascading failures as continuous phase-space transitions. *Physical Review Letters*, accepted, 2017.
- [179] Yang Yang, Takashi Nishikawa, and Adilson E. Motter. Vulnerability and cosusceptibility determine the size of network cascades. *Physical Review Letters*, 118(4):048301, 2017.
- [180] M. K. Stephen Yeung and Steven H. Strogatz. Time delay in the kuramoto model of coupled oscillators. *Physical Review Letters*, 82(3):648, 1999.
- [181] Karim Zaghib, Martin Dontigny, Abdelbast Guerfi, Patrick Charest, Isadora Rodrigues, Alain Mauger, and Christian M. Julien. Safe and fast-charging li-ion battery with long shelf life for power applications. *Journal of Power Sources*, 196(8):3949–3954, 2011.
- [182] Hui Zhang and Pu Li. Probabilistic analysis for optimal power flow under uncertainty. *IET Generation, Transmission & Distribution*, 4(5):553–561, 2010.

Curriculum Vitae

Personal Information

Name Benjamin Schäfer
 Nationality German
 Date of birth 1990/05/21



Employment

Since October 2014 PhD student at Max-Planck-Institute for Dynamics and Self-Organization (MPI DS) & Georg-August University (GAU) in Göttingen, Germany
 June – August 2016 Visiting scientist at University of Tokyo, Japan (with Kazuyuki Aihara)
 January – March 2016 Visiting scientist at Queen Mary University of London, United Kingdom (with Vito Latora)

Education

Since October 2014 PhD thesis *Self-Organized Dynamics of Power Grids* at GAU and MPI DS in Göttingen, Germany
 June 2013 – May 2014 Diploma thesis at MPI DS, Göttingen & OvGU, Magdeburg, Germany
The neuronal action potential modelled as a first order phase transition
 October 2008 – May 2014 Studied physics at Otto-von-Guericke University (OvGU) Magdeburg, Germany 2014 – Diploma (grade 1.1)
 2008 Allgemeine Hochschulreife (general qualification for university entrance, final grade: 1.4) at Ökumenisches Domgymnasium Magdeburg, Germany

Awards and Scholarships

December 2014- June 2017 Excellence Stipend by the *Göttingen Graduate School for Neurosciences, Biophysics, and Molecular Biosciences*
 June – August 2016 Summer stipend by *Japan Society for the Promotion of Science*
 November 2015 Won stipend by *German Academic Exchange Service* (turned down)
 May 2014 Best Diploma Degree in Magdeburg in Physics 2014
 April 2012 – May 2014 Scholarship of the *Studienstiftung des Deutschen Volkes* (The German Academic Scholarship Foundation supports the top 0.5% of students in Germany)

Skills

Languages German – native
 English – C1 (near native)
 French – A2
 Arabic – A2
 Japanese – A1

Computing	Advanced user of Mathematica and LaTeX Basics in C++, Python and Matlab
Soft skill courses	Voice&Body coaching, Networking for Scientists, Introduction to project management, Introduction to critical reasoning

Teaching

Since 2015	Co-supervising two master students graduating in Mathematics and Physics on the theory of complex systems
Summer term 2015	<i>A Practical Course on Network Science, Seminar on Network Science</i> , combined practical course and seminar on recent network research and its computational implementation for advanced bachelor and master students of mathematics, physics and computer science; approx. 30 participants
Winter term 2014/15	<i>Tutorial: Network Dynamics</i> , introducing concepts of network science to advanced bachelor and master students of mathematics, physics and computer science; approx. 30 participants

Invited Talks

June 2017	<i>Dynamics of decentrally controlled power grids</i> , Dynamic Days Europe 2017
December 2016	<i>Network Dynamics and Decentralized Control</i> , establishing new collaboration, invited by Christian Beck, Queen Mary University of London, United Kingdom
November 2015	<i>Smart-Grid - einfach selbstorganisiert</i> (Smart Grid- simply self-organized), Decentralized self-regulating Grid integration, Congress of the project "PiVo – Optimized charging in Smart Grid", Berlin, Germany
March 2015	<i>Decentral Smart Grid Control</i> , Brussels Spring Workshop: Flexibility for the Electricity Transmission grid, Elia, Brussels, Belgium

Voluntary activities

June 2016	Co-organizer for a Mini-Symposium on power grid research at Dynamic Days 2016 in Corfu, Greece, including 9 speakers
Since 2015	Reviewer activity for <i>New Journal of Physics</i> and <i>Physica A</i>
December 2015	Co-organizer of <i>Physik für Flüchtlinge (Physics for all; helping refugees to perform physics experiments)</i> in Göttingen/Friedland
October 2014	Co-organizer for the <i>Workshop and Symposium on Collective Nonlinear Dynamics and Statistical Physics of Networks</i> in Wittenberg, Germany
June 2009 – June 2012	Elected as student representative

Hobbies

Hiking, Boardgames, Climbing

Publications

B. Schäfer, D. Witthaut, M. Timme and V. Latora, *Dynamically Induced Cascading Failures in Supply Networks*, under review, ArXiv:1707.08018

B. Schäfer, C. Beck, K. Aihara, D. Witthaut, and M. Timme, *Non-Gaussian Power Grid Frequency Fluctuations Characterized by Lévy-stable Laws and Superstatistics*, Nature Energy, accepted

B. Schäfer, M. Matthiae, X. Zhang, M. Rohden, M. Timme and D. Witthaut, *Escape Routes, Weak Links, and Desynchronization in Fluctuation-driven Networks*. Physical Review E **95**, 060203(R), November 2016.

B. Schäfer, C. Grabow, S. Auer, J. Kurths, D. Witthaut and M. Timme, *Taming Instabilities in Power Grid Networks by Decentralized Control*, European Physical Journal Special Topics 225: 569, May 2016

B. Schäfer, M. Matthiae, M. Timme and D. Witthaut, *Decentral Smart Grid Control*, New Journal of Physics 17 015002, January 2015

D. Manik, D. Witthaut, **B. Schäfer**, M. Matthiae, A. Sorge, M. Rohden, E. Katifori and M. Timme, *Supply Networks: Instabilities without Overload*, European Physical Journal Special Topics 223: 2527, October 2014